Fish Population and Behavior Revealed by Instantaneous Continental-Shelf Scale Imaging

by

Deanelle T. Symonds

Submitted to the Department of Mechanical and Ocean Engineering
in partial fulfillment of the requirements for the degree of

Doctor of Philosophy

at the

MASSACHUSETTS INSTITUTE OF TECHNOLOGY

June 2008

Author .....
Department of Mechanical and Ocean Engineering
May 19, 2008

Certified by .....
Nicholas C. Makris
Professor
Thesis Supervisor

Accepted by .....
Lallit Anand
Chairman, Department Committee on Graduate Students

Fish Population and Behavior Revealed by Instantaneous Continental-Shelf Scale Imaging

by

Deanelle T. Symonds

Submitted to the Department of Mechanical and Ocean Engineering
on May 19, 2008, in partial fulfillment of the
requirements for the degree of
Doctor of Philosophy

Abstract

The application of a technique to instantaneously image and continuously monitor the abundance, spatial distribution, and behavior of fish populations over thousands of square kilometers using Ocean Acoustic Waveguide Remote Sensing (OAWRS) is demonstrated with data from its first implementation in a 2003 field experiment off the US Continental Shelf south of Long Island, NY. Conventional methods for monitoring fish populations rely on highly-localized, point measurements made from slow-moving research vessels that survey along widely spaced line transects to cover the vast ocean environments that fish inhabit and so significantly under-sample fish populations in time and space. This leads to incomplete, ambiguous and highly-aliased records of fish abundance and behavior. In contrast, OAWRS surveys at a rate roughly one million times greater than that of conventional fish-finding methods. Within a minute and a half, OAWRS images the ocean environment over more than ten thousand square kilometers, an area similar to the state of Massachusetts. This is possible because OAWRS exploits the natural capacity of the continental-shelf environment to act as a waveguide where sound waves are efficiently propagated over long ranges (tens of kilometers) via trapped modes that suffer only cylindrical spreading loss rather than the spherical spreading loss suffered in the short-range (hundreds of meters), waterborne propagation paths employed by conventional fish-finding sonar (CFFS).

In this thesis, a method is developed for estimating the instantaneous population density and abundance of fish populations from wide-area OAWRS imagery. The OAWRS population density estimates are calibrated with simultaneous local CFFS measurements, and are used to estimate the expected scattering cross section of an individual fish at OAWRS frequencies so that population density may be estimated in regions where CFFS measurements were not made. It is shown that the OAWRS population density estimates have uncertainties of less than 25% at each pixel or spatial resolution cell, for statistically stationary populations. Instantaneous abundance estimates then have much lower uncertainties when OAWRS population density is integrated over tens to hundreds of independent spatial resolution cells by the law of large numbers. A number of discoveries are also documented about the instantaneous

horizontal structural characteristics, temporal evolution, short-term volatile behavior and propagation of information in very large fish shoals containing tens of millions of fish and spanning several kilometers in spatial extent. The OAWRS approach should enable new abilities in the study and assessment of fish populations and their behavioral dynamics.

Thesis Supervisor: Nicholas C. Makris
Title: Professor

Acknowledgments

First and foremost, I would like to thank my advisors, Prof. Nicholas Makris and Prof. Purnima Ratilal, for their support, encouragement, and inspiration. They have been excellent mentors who have guided me with extreme patience throughout my undergraduate and graduate years at MIT. It has been my greatest pleasure to work and learn from such a dynamic duo.

I would like to thank the members of my thesis committee. Dr. Redwood Nero and Dr. Michael Jech have been amazing collaborators; sharing with me not only their knowledge and expertise of marine biology and fisheries science, but also their data—without which this thesis could not have been written. Thank you both for the many memorable moments at sea.

Thanks are also due to the faculty and administration of the Ocean Engineering Department at MIT for their constant support, advice and encouragement throughout my undergraduate and graduate years.

I am forever indebted to my friends and colleagues in the Ocean Acoustics Group and the office mates for the many memories in 5-327. I would like to thank Luis Souza, Irena Veljkovic, Joe and Monica Edwards, Ding Wang, Andrew Poulsen, Hyun Joe Kim, Harish Makundun, and Joe Sikora III. I also want to thank my Northeastern colleagues and collaborators: Ninos Donabed, Saomitro Gupta, Mark Andrews, Roger Gong, and Ameya Galinde. I reserve a special thank you for my labmates and LURS family: Yi-san Lai, Joshua Wilson, Sunwoong Lee, Tianrun Chen, Srinivasan Jagannathan, Alex Tan, Hadi Nia, Ioannis Bertsatos, Michele Zanolin and Geoff Fox.

I would like to thank all of my friends, who have made my time here at MIT unforgettable and have become my family away from home: Ioannis, Iason, Aristos, Panos, Dimitris, Manolis, Tasos, Georgios, Nikos, Spiros, Johnna, Susan, Caro, Tufool, Shawn, Konstantinos, Steve, Naomi, Tom, Whitney, Lynne, Mike, Kerri-Ann, Georgette, Breagin, Julie, Ayanna, et al.

To my family, I'm forever grateful for all the love, support, and patience it took to get me this far. I dedicate my thesis to my two nieces, Mia and Haley. Maybe one

day it'll inspire them to write their own thesis at MIT.

Last, but not least, I'm deeply grateful to Joshua Scofield, who has been my constant source of motivation, inspiration, and sanity through my final year at MIT.

Contents

Chapter 1

Introduction

1.1 Motivation

Fish populations typically comprise a significant percentage of biomass in productive marine ecosystems, and play an essential role in inter-trophic energy transport within complex marine food webs [21, 39]. The dietary importance of fish also extends to human populations since fish account for "roughly 40% of the protein consumed by nearly two-thirds of the world's population" [80]. In addition to their ecological importance, fish play an equally vital role economically. The fishing industry helps to sustain the economies of coastal countries around the world, especially in the developing world, with roughly 60% of the total world catch from waters under the jurisdiction of developing countries alone.[13].

In recent years, there has been substantial evidence that the oceans' wild fish stocks are undergoing rapid decline [28, 72, 25] and exploitation world-wide. In 2005, the UN reported that roughly 52% of the ocean's fish stocks were fully-exploited and approaching their maximum stustainable production limit [43]. In light of the ecological and economic importance of fish populations and their recent decline, it has become increasingly important for marine fisheries to be able to accurately estimate abundance, as well as monitor trends in abundance and behavior for sustainable ocean resource management.

1.2 Historical Background: Acoustic Methods for Monitoring Fish Populations

In the atmosphere, electromagnetic waves have been widely utilized for remote imaging objects and acquiring information about the environment with very fine temporal and spatial resolution. The application of remote-sensing technologies to facilitate ecosystem monitoring and conservation of terrestrial animals have been demonstrated with the use of doppler-weather based radar. Radar-based systems in the atmosphere have been integral in monitoring biodiversity, migratory patterns and abundance distribution of avian populations.

In water, sound waves provide the only efficient means of exploring and investigating ocean environments since these waves can propagate to ranges orders of magnitude beyond the attenuation limits of electromagnetic waves used in the atmosphere. This makes the application of active sonar systems useful for imaging, detecting, and classifying targets of interest, such as seafloor morphology, man-made objects, and marine life in an underwater environment.

Standard acoustic methods [89, 95, 91, 5, 70, 69, 87] used for surveying and monitoring fish populations often produce abundance and behavioral records that are ambiguous, incomplete and have high uncertainty [79, 31, 70, 44, 26, 20]. This is because these methods rely on highly-localized measurements that are restricted to the immediate vicinity (tens to hundreds of meters in range) of slow-moving research vessels [91, 5, 89, 70, 69]. During a typical annual fish survey by the National Oceanographic and Atmospheric Agency (NOAA), such vessels spend rougly 3-4 weeks to survey continental-shelf scale environments via lawn-mower type, line transects that are spaced roughly 30 to 45 km apart. The limited temporal and spatial coverage of conventional systems often lead to a gross undersampling, in time and space, of the vast ocean environments that fish typically occupy.

The application of active sonar techniques to remotely detect, image, and classify aquatic organisms is still less than a century old. The field of fisheries acoustics continues to evolve rapidly with advancements in sonar technology, behavioral ecology,

and data-integration techniques. The very first biological application of acoustics to detect fish in a closed-tank environment was done by Kimura in 1929 [53]. Shortly after Kimura's laboratory experiments, researchers and fishermen demonstrated the utility of echosounder technology to locate wild fish populations and qualitatively visualize vertical distributions, abundance, and fish behavior, [91, 5, 6, 93, 90], with the earliest use of echosounder technology to detect fish occuring in the 1930s, when Ronald Balls used an echosounder fitted on his herring drifter to determine where to set his nets [5, 6]. During the 1940s, researchers in the University of California's Division of War Research (UCDWR) noted a mid-water layer scattering agent, which was later called the "deep scattering layer" [16, 19, 81]. After bathypelagic fish with gas-filled swimbladders were proposed to be the cause of this "deep scattering layer" Marshall [68], the frequency response of these fish was studied to identify resonance [46, 27, 2, 4, 3, 67]. A good historical review of the large literature on the ability of bladder fish to scatter sound can be found in Refs. [46, 27] and [96]. In all the above experiments, the range at which the fish were imaged were still on the order of the local water depths (a few hundred meters or less).

We now follow from Jagannathan et al, "Ocean Acoustic Waveguide Remote Sensing (OAWRS) of Marine Ecosystems" [37], to review long range acoustic techniques to image fish populations. In 1971 when Weston and Revie used a fixed single-beam sonar in a monostatic setting to image underwater returns over long ranges (>10 km) within a narrow angular sector [97]. Weston and Revie observed temporal variations believed to be consistent with fish migrations, but lacked independent data to confirm this. In 1973, Rusby et al. generated synthetic aperture images of the continental shelf environment with a towed, single-beam sidescan sonar (G.L.O.R.I.A.) [36]. Each synthetic aperture image required hours of surveying, which led to high spatio-temporal undersampling and aliasing. They described features as possible fish groups "only when the shape of the groups remain[ed] sufficiently distinctive from run to run," which would bias the analysis towards highly static population distributions. They then guided a fishing vessel to the location of such a feature, where the vessel made a large fish catch. In these and other earlier long range experiments [24, 76],

independent confirmation of fish was not available by simultaneous measurements.

Independent confirmation of long-range acoustic fish detection by simultaneous local measurements appears were first demonstrated by Makris et al in a field experiment conducted on the New Jersey Continental Shelf during April-May, 2003 [32, 66]. This field experiment utilized a long-range, bistatic remote-sensing system to rapidly image wide-areas of the ocean environment, spanning thousands of square kilometers, over 360-degree annular sectors at a minute intervals. In earlier work at very short ranges on the order of the water depth, roughly 300 m, and so with conventional direct-path rather than waveguide propagation and sensing, Isaacs and Schwartzlose used a U.S. Navy mine hunting sonar operating on the southern California continental shelf to detect strong scatterers over 360-degree sectors which they confirmed to be fish with local trawls [50].

Makris et al used a horizontal array that formed simultaneous beams over a 360 degree horizontal azimuth, enabling them to conduct OAWRS surveys of marine life instantaneously over wide areas, tens of thousands of square kilometers [32]. With regular and rapid temporal image updates, they were able to work in a true Eulerian reference frame and map fish distributions without aliasing in space or time. This approach overcame the fundamental problem of sparse spatio-temporal sampling and high aliasing in sidescan (synthetic aperture) and vertical beam sonar surveys of dynamic biological distributions. Tens of thousands of simultaneous measurements by a local, conventional echosounding sonar during the 2003 experiment confirmed the presence of fish within the areas of strong scattering in the long-range imagery. Simultaneous measurements are necessary for confirmation because fish are ubiquitous in continental shelf environments and can easily be found accidentally in a region causing strong acoustic returns. Non-simultaneous correlations can then easily be coincidental or spurious, as can correlations at only a single or very small number of spatial locations. This lesson was learned with geologic features of the sub-bottom, which are also ubiquitous in many continental shelf environments, and often have spurious spatial correlation with acoustic returns caused by other mechanisms [35].

The remote-sensing approach utilized by Makris et al tremendously augments the

areal surveying capacity of conventional fish monitoring techniques since it operates with an areal sampling rate tens of thousands to a million times greater than that of methods currently in practice [32]. The surveying capabilities of OAWRS can now address the long-established need [39, 38, 40, 25] for synoptic-sensing systems to facilitate the assessment of an ecosystem's health and development by providing valuable information about the current state and behavior of key ecosystem components. Continuous monitoring with OAWRS enables the production of unaliased [88] wide-area movies that detail the spatial and temporal distributions of fish population. These wide area movies can reveal behavioral patterns that may enable better modeling and prediction of ecosystem dynamics and future health, including recruitment, productivity, mortality, and sustainability. For example, trends might be revealed in preferred geographic location, horizontal migratory patterns, life-cycle behavior such as spawning, foraging, wintering and group behavioral responses exhibited by variations in shoal morphology. These trends can then be correlated with physical and biological factors including diurnal dynamics, oceanographic or geologic features, such as fronts, currents, bathymetry, variations in climate over time, the location of primary food sources, predators and human activity such as fishing, shipping, oil exploration, and pollution.

1.3 Thesis Organization

In this thesis, we describe the first demonstration of Ocean Acoustic Waveguide Remote Sensing (OAWRS) to instantaneously image and continuously monitor fish populations during Makris et al's 2003 survey on the New Jersey Continental Shelf [32, 66].

First, we present a detailed synopsis of the 2003 field experiment, including relevant background, the experimental design, and the experimental implementation in Chap. 2.

In Chap.3, a full-field, bi-static scattering model, based on a sonar equation approach, is used to analyze the scattered field from groups of fish, as observed by

OAWRS and Conventional Fish-Finding Sonar (CFFS) in 2003. This scattering model is used in conjunction with simultaneous measurements by the low-frequency, bi-static OAWRS system and the high-frequency, conventional echosounding sonar to empirically calibrate for the expected target strength of an individual fish at the OAWRS operating frequencies (400-1400Hz). The empirically-derived target strength is related to the scattering cross-section of the individual fish, and can be used as a scaling factor to convert OAWRS-measured acoustic intensity to actual metrics of areal population density. A classification scheme is developed and presented, as part of the target strength calibration procedure, to address the issues that arise when combining data from independent sonar platforms with significantly different temporal and spatial resolutions. This classification scheme encompass real-world OAWRS-CFFS simultaneous sampling geometries from the 2003 field experiment and is helpful in identifying optimal scenarios which minimize errors in expected target strength estimation at the low, OAWRS operating frequencies. Here, we show that target strength estimation errors, and consequently areal population density errors, are reduced to less than 25% per pixel, or 1 dB per pixel, in areas where both OAWRS and CFFS simultaneously sample large, effectively stationary populations. Such stationary populations are also shown to exhibit statistical and morphological similarity which could be indicative of homogeneity of species composition.

In Chap.4, we demonstrate how the instantaneous areal population density can be estimated from OAWRS imagery by compensating for : (i) the two-way transmission loss, (ii) source power, (iii) the estimated target strength, and (iv) the spatially -varying footprint of the OAWRS system. From OAWRS areal population density imagery, a number of fundamental scientific discoveries have been revealed about the instantaneous horizontal structural characteristics, temporal evolution and propagation of information in very large fish shoals.

Finally, the implications of using the OAWRS approach for surveying fish populations are discussed in Chap. 5, including guidelines and improvements for future surveys that utilize OAWRS and conventional fish-finding methods to study marine populations.

Chapter 2

Main Acoustic Experiment 2003: Co-Registration of Fish Populations with simultaneous measurements of an OAWRS system and a Conventional Fish Finding Sonar

In this chapter, we present the key findings of the Main Acoustic Experiment (MAE03) of the ONR-sponsored Geoclutter Program, conducted from April 28-May 15, 2003 [32, 66]. This field experiment was conducted in an area of the New Jersey continental shelf, approximately 200km south of Long Island, NY, which is also commonly referred to as the Mid-Atlantic Bight and the New Jersey Strataform. During MAE03, a long-range, bistatic remote sensing system was used to instantaneously image and continuously monitor very large fish shoals over a roughly three week period. A US National-Marine-Fisheries-standard echosounder was employed in order to provide simultaneous ground-truth of these shoaling populations identified by strong scattering

regions within the long-range imagery. This high-frequency, conventional fish finding sonar (CFFS) also provided in-situ measurements of the local population density and target strength of individual fish contained within these large shoals. The synoptic measurements by the long-range system and the highly localized measurements by the CFFS system were used to demonstrate that shoaling fish populations are indeed the dominant cause of ambiguous, false returns within long-range, active sonar systems operating in littoral environments. In Sec. 2.1, we provide a detailed description of the design and implementation of the MAE03 field experiment. We describe both the measurement capacities of the long-range, bistatic OAWRS system and the high-frequency CFFS system, in Sec. 2.2 and Sec. 2.3 respectively.

2.1 Main Acoustic Experiment 2003

During April 27-May 2 2001, the Acoustic Reconnaissance Experiement (ARE01) was conducted on the New Jersey Continental Shelf roughly 200 km south of Long Island, NY in the area known as the ONR Strataform site. The primary objective of this first experiment was to investigate the primary physical mechanisms that cause acoustic "clutter" in the output of long-range active sonar systems operating in shallow water environments [65, 35, 82]. The term "clutter" is often used to define any set of unidentified or ambiguous acoustic returns that stand significantly above the diffuse and temporally decaying background reverberation level[65, 35, 82]. Such clutter features can cause a problem in active sonar systems operating in continental shelf environments, since clutter can often be confused with or mask returns from intended targets. During ARE01, a long-range bistatic system rapidly imaged wide areas, spanning thousands of square kilometers, within 50 seconds. Roughly 3000 pings were transmitted during ARE01, with an average of 10 to 100 localized, clutter-like features registered during each wide-area image. This yielded approximately 30,000 clutter-like events that could be confused with an intended target over the course of the entire experiment [65, 35, 82].

Three primary findings of the 2001 reconaissance experiement were:

- A statistical analysis of persistent clutter within areas of fine-resolution geophysical surveys show a random correlation with ubiquituous geological features, such as ancient buried river channels [35, 82, 23].

- Prominent clutter returns were observed to evolve in time and space, making any apparent co-registration with buried river channels spurious and coincidental. The dynamic nature of the clutter returns were also inconsistent with what would be expected from stationary features, such as seafloor and sub-bottom geology. However, limited at-sea time made it impossible to unambiguously explore the dynamicity and spatio-temporal variability in the clutter returns.[65, 35, 82]

- Large fish groups with packing densities on the order of 1 fish/m^2 are commonly observed and known to occupy the ARE01 experimental site [74, 75, 73, 82]. Previously, full-field scattering model has been used to show that such fish groupings can stand above the background reverberation [82, 35]. However, during ARE01, no simultaneous measurements with a local fish-finder or bottom trawl were available to ground-truth the observed clutter returns with fish populations.

The Main Acoustic Experiment, conducted in 2003 in the same geographic location as ARE01, was designed as a follow-up to the 2001 reconnaisance experiment. The MAE03 field experiment was designed to be a controlled experiment that employed two independent, simultaneously-operated sonar systems, in order to:

- Determine the dominant cause of false alarms or clutter in long-range active systems operating in continental shelf environments.

- Determine the spatio-temporal variability scales of prominent OAWRS returns over the 3-week experimental period.

- Correlate and ground-truth prominent OAWRS returns with in-situ measurements by a simultaneously operated CFFS system.

More time was available during MAE03 to repeat tracks in the vicinity of clutter features previously observed during ARE01. For example, multiple tracks were repeated over consecutive days to study both the spatial and temporal evolution of strong scatterers in relation to static geologic features. Meanwhile, the simultaneously operated fish-finding sonar made multiple transects through strong scattering regions identified by the long-range system in order to co-register returns with fish populations. Wide-area movies were generated in order to provide a qualitative co-registration of the temporal and spatial variability of the clutter returns with geology and the CFFS-measured fish populations. Several, moored passive reflectors, with known target strength, were also deployed at each experimental site in order to minimize charting errors and provide ground-truth for full-field, waveguide scattering models[92, 66]. Without apriori knowledge of the target locations, these targets are indistinguishable from clutter arising from environmental scatterers. A schematic illustration of MAE03 experimentalis shown in Fig. 2-1. In the following sections, we discuss the surveying capabilities and the measured data acquired by both the OAWRS and CFFS systems during MAE03.

2.2 The Ocean Acoustic Waveguide Remote Sensing System

A long-range OAWRS system used during MAE03, similar to the bi-static system used during ARE01, was comprised of a moored source array and towed horizontal receiver array, as shown in 2-2. This OAWRS system was used to rapidly insonify continental-shelf scale areas and create real-time wide-area imagery of the ocean environment every 50 seconds. The moored vertical source array, deployed by the UNOL Endeavor, was used to transmit short 1s, linear frequency modulated (LFM) waveforms at three primary operating frequencies: 390-440 Hz (WX1), 875-975 Hz (WMA) and 1250-1400 Hz (WMB). The lowest operating frequency band, WX1, was transmitted alone, while the higher frequency bands (WMA and WMB) were transmitted simultaneously

to investigate frequency-dependence of the scattered returns. The UNOL Oceanus towed the reciver array at a speed of roughly 2m/s along 10km long tracks of varying orientation. The receiver array used for the MAE03 experiment is a 277m, 396-channel nested acoustic array (FORA), divided into five acoustic apertures with a large frequency range from 50-3750Hz. Depth and gyroscopic sensors imbedded into the array which provides heading, pitch, roll and depth of the array. Of the 396 channels, one is dedicated to monitor self-noise and another monitors the output of the receiver's desensitized hydrophone. The source and receiver locations, as well as the time of source transmission are known. Low frequency (hundreds of Hz to a few kHz) active sonars are especially useful for rapidly probing wide areas in the ocean because such sound waves are capable of propagating over long ranges with little attenuation, and so can act as an "underwater" eye for synoptic imaging of wide environments. In the remaining paragraphs, we follow the description of the OAWRS system in Ref. [33, 32].

One of the advantages of the OAWRS system, is that it exploits the natural capacity of the continental shelf to act as a 2-D waveguide, as illustrated in the cartoon schematic in 2-2. A waveguide is a bounded medium that efficiently channels propagating waves [77, 8]. In free space, the intensity (power per unit area) of waves propagating from a point source to a distant receiver is inversely proportional to the square of the range from the source to the receiver. Source power is geometrically spread over spherical areas that increase with the square of this range. In a waveguide, spreading loss is determined by the geometry of the bounded medium. In a one-dimensional tube of constant cross-section, source power no longer spreads as range increases beyond the tube diameter, so that the mean sound intensity over the cross-section stays fixed. As a medium for acoustic waves, the ocean is bounded by the air above and the seafloor below. For ranges much greater than the ocean depth, where OAWRS is particularly useful, loss in mean intensity due to geometric spreading occurs over cylindrical areas, increasing in direct proportion to range if ocean depth is constant or nearly constant, as it typically is. Conventional fish finding sonar operates over ranges less than or on the order of the local ocean depth, and so is

typically governed by the spherical spreading loss encountered in free-space. OAWRS also uses lower frequency waves that suffer far less attenuation from absorption and scattering [61, 82, 35, 11] in the medium than the waves used by CFFS [8, 69].

To form an instantaneous OAWRS image, the vertical source array sends a short broadband transmission of sound out omni-directionally in horizontal azimuth. As they travel, the sound waves reflect from the sea surface and bottom to form standing waves in depth that are called waveguide modes. These are analogous to the normal modes of a vibrating guitar string, where the entire vertical water column of the ocean acts like the plucked string. As the modes propagate horizontally outward from the source, they interact with and scatter from environmental features along the way. Scattered returns from environmental features are then continuously received by a horizontally towed line array. The scattered returns are then charted in horizontal range and bearing by temporal matched filtering and beamforming [61, 35, 17, 52] using the known propagation speeds of acoustic modes in the ocean as determined from local XBT sound speed measurements [66]. A Hanning spatial window function was applied during beamforming to reduce sidelobe leakage, where the first sidelobe level is down 30 dB from the main lobe.

The resulting image is an instantaneous snapshot of the ocean environment over the two-way travel times of the signal returns spanning 360 degrees in azimuth.OAWRS range resolution is fixed at the mean sound speed, c = 1475 m/s, divided by twice the signal bandwidth, or roughly 15 m for the 390-440Hz band before averaging. Theory, modeling, and our field measurements using calibrated targets with known positions show that ranging error of OAWRS is negligible since it is on the order of the 30 m range resolution of our image pixels after averaging [55], and as a consequence of modal propagation, is insensitive to the depth of scatterers or environmental features in the waveguide. OAWRS azimuthal resolution in radians varies as the acoustic wavelength, λ, divided by the projected array length $Lcos\theta$, where L is the full array length and the azimuth angle θ is zero at broadside, which is normal to the array axis. At endfire, parallel to the array axis, the resolution becomes roughly $2\sqrt{\lambda/L}$ radians. The array length,L, varies for each OAWRS operating band and L is: 94.5m

at 390-440Hz, 47.25m at 875-975, and 23.625m at 1250-1400Hz. For each transmission band, the instantaneous 2D OAWRS imagery of acoustic intensity is averaged to a 30-m resolution when mapped into Cartesian space. For the LFM transmission at 390-440 Hz, we spatially average the instantaneous imagery over 2 adjacent, independent 15-m range resolution cells. This reduces the standard deviation per pixel by $sqrt2$. Further reduction of instantaneous fluctuations induced by signal-dependent noise or speckle, transmission scintillation and other random waveguide processes can be achieved by making use of temporal averaging of the 2D acoustic intensity maps over consecutive transmissions. During MAE03, the acoustic intensity images were averaged over five consecutive pings to further reduce the standard deviation per pixel by the square root of the number of independent samples, or $\sqrt{5}$. The temporal window used for the averaging was chosen to be smaller than the time-scales of various ocean processes in order to ensure unaliased imagery by the Nyquist sampling criteria and preserve the instantaneity of each image.

During the 2003 OAWRS experiment, measurements of the mean acoustic intensity after one-way transmission from the source to receiver, as well as two-way returns from the seafloor, show no sign of modal interference structure, such as peaks and nulls from coherent interference. Rather a uniform decay with range is observed, indicating a lack of modal interference, which corresponds to a highly predictable and uniformly mixed acoustic structure over depth. This is expected for a number of reasons. Environmental scatterers such as seafloor inhomogeneities and fish are distributed randomly within the sonar resolution footprint and so decorrelate modes in the acoustic field [82, 64], which then obeys circular complex Gaussian Random field (CCGRF) statistics [61, 45, 59, 60, 18], by the central limit theorem. The intensity of a CCGRF is characterized by signal-dependent noise known as speckle noise [45, 59, 60]. The ocean is also active, with internal waves, eddies and turbulence. These cause small sound-speed changes in time and space that typically cause acoustic modes to decorrelate, which again leads to CCGRF fluctuations at the receiver by the central limit theorem [60, 18]. The one-way acoustic field measurements during our 2003 OAWRS experiment followed CCGRF statistics over time, which is

consistent with the observed lack of modal interference structure in range. These observations and the consequential lack of modal interference structure in depth were verified by simulations where sound speed variations measured during our experiment were input to statistical models for waveguide propagation in the continental shelf [35, 41, 10, 29, 30]. (Even without randomness in the medium, broadband transmissions, such as ours, also lack the delicate modal-interference nulls found in deterministic single frequency transmission.)

An illustrative example of OAWRS 2D acoustic intensity maps are shown in Fig. 2-3. This image shows the diffuse background reverberation level as well as strong scattered returns from the passive reflectors and submerged targets. For each transmission, the signal first measured by the receiver array correspond to the direct arrival from the source to the receiver array. This is shown by the forward scatter region (elliptical region with SPL>90dB re 1uPa) between the source and receiver in Fig. 2-3. The diffuse background reverberation scattered from rough patches in the ocean environment arrive after the direct arrival from the source. In ambient beams, those beams that exhibit no strong scattering occurs after the direct arrival,the mean intensity decays with range due to spreading and absorption in the environment.

The horizontal line-array has left-right ambiguity about the line passing through the source and receiver. For bistatic geometries, ambiguity occurs about an ellipse with a major axis that passes through the source and receiver, while monostatic geometries are ambiguously charted symmetrically about the receiver array axis. In order to break the left-right ambiguity, we can compare the scattering events from images obtained from tracks with different orientations as shown by comparing the two figures in Fig. 2-3. The real scattering regions (T1, T2, R1 and R2 of Fig. 2-3 remains in the same geographic region and is more invariant to array orientation changes. This method to break left-right ambiguity have also been employed in [62, 11, 82, 35, 65].

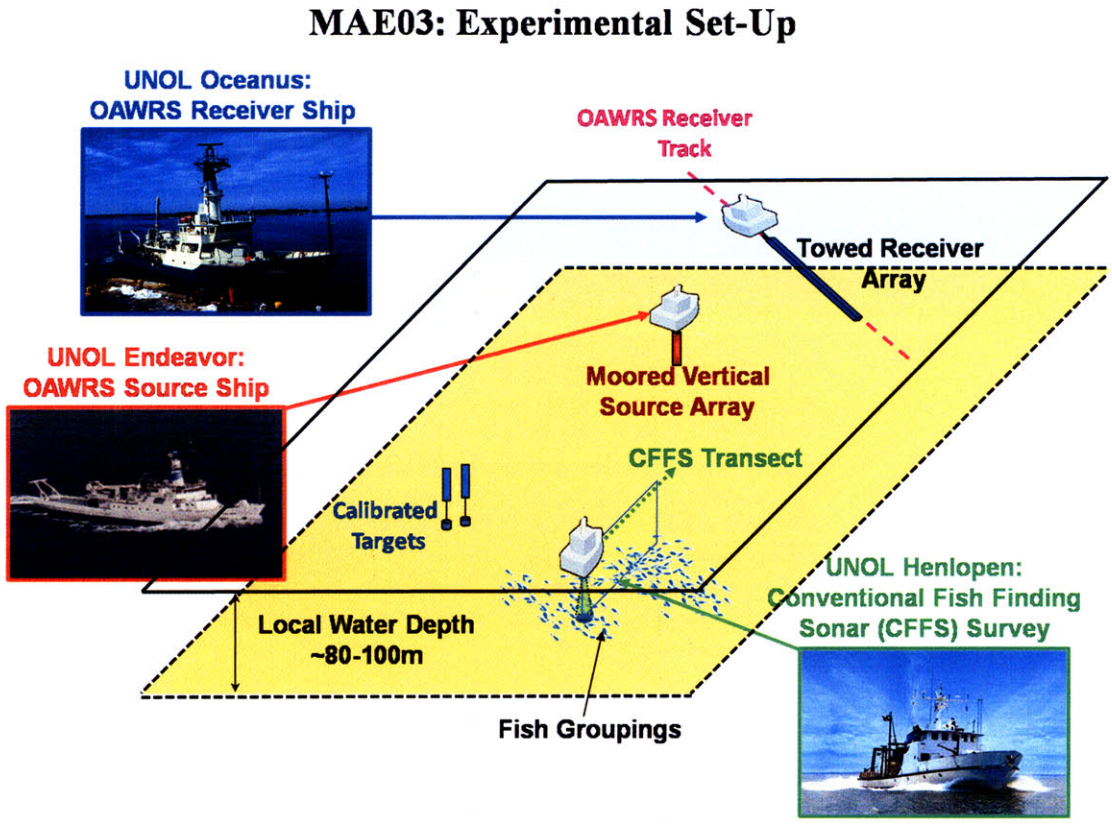

Figure 2-1: During MAE03, a bi-static OAWRS system was used to rapidly image wide-areas with minute updates. The bi-static system was comprised of a moored vertical source array and a horizontal linear receiver array towed along a 10km-long track. Calibrated passive reflectors (targets) were dispersed in the survey region to minimize charting errors and validate waveguide scattering models. A hull-mounted conventional echosounder was simultaneously operated within the OAWRS survey area to provide ground-truth of OAWRS-imaged fish populations, as well as in-situ measurements of local fish density and individual target strength within groupings.

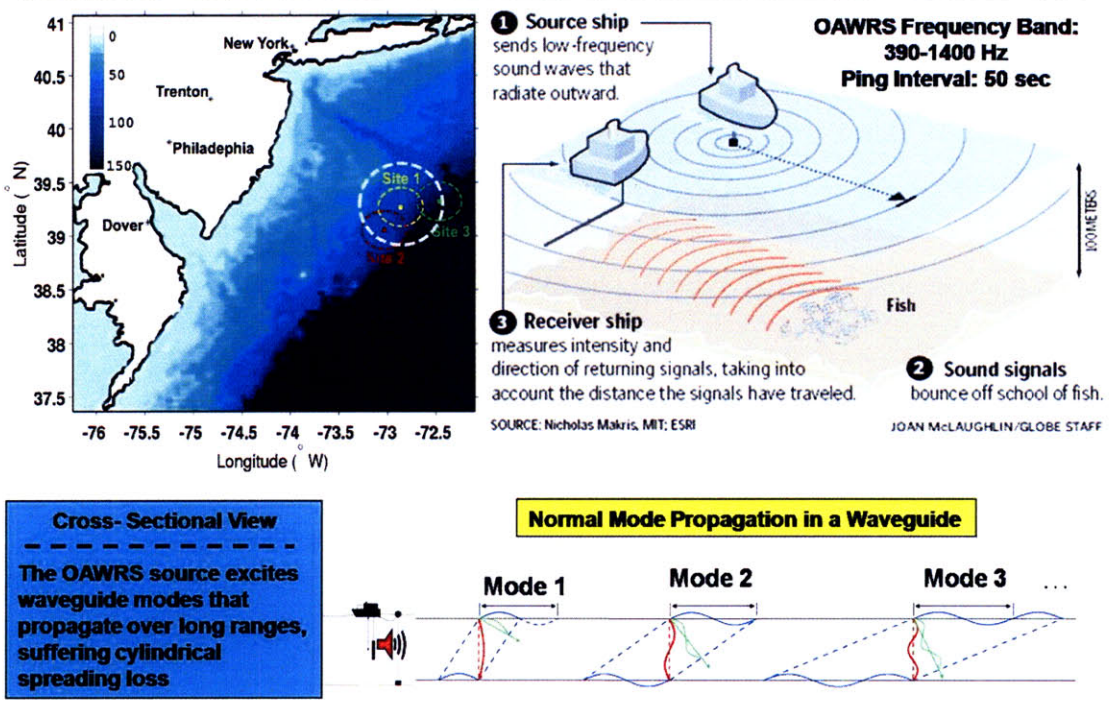

Figure 2-2: The OAWRS system used for the 2003 survey of the New Jersey Continental Shelf was comprised of a moored source and a towed, linear horizontal array. The 2003 OAWRS survey areas are shown in reference to the US East Coast Continental Shelf roughly 200 km south of Long Island, NY. The three OAWRS survey areas for a 40s transmission interval are deliminated by the colored dashed circles (Site 1 = Yellow, Site 2 = Red, Site 3 = Green), with the colored rectangles indicating the location of the moored source at the three sites. For a 80s transmission interval, the survey area can be increased as shown by the white dashed circle. The OAWRS system exploits the natural capacity of the continental shelf to act as a 2-D waveguide. The vertical source array sends a short broadband transmission of sound out omni-directionally in horizontal azimuth. As they travel, the sound waves reflect from the sea surface and bottom to form standing waves in depth that are called waveguide modes. As the modes propagate horizontally outward from the source, they interact with and scatter from environmental features along the way. Scattered returns from environmental features are then continuously received by a horizontally towed line array.

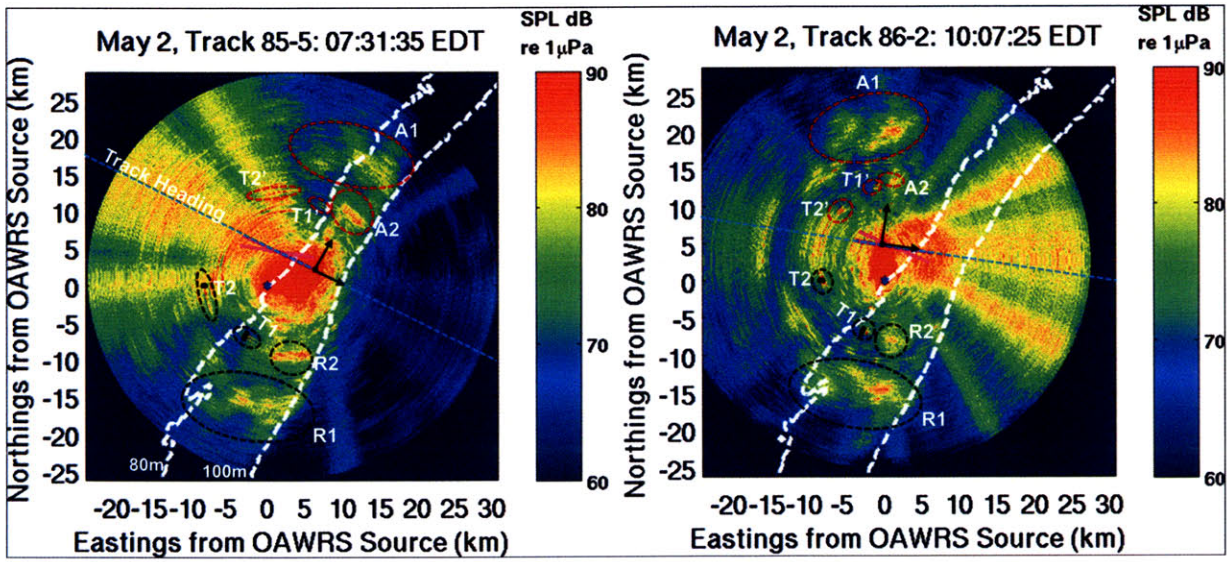

Figure 2-3: An illustrative example of 2D OAWRS acoustic intensity maps from the first and second track on May 2, 2003 at Site 1. These images were created from 1s, broadband (390-440Hz) LFM transmissions. A horizontal line array has left-right ambiguity about the array axis. For a bistatic geometry, such as that shown here, ambiguity occurs about an ellipse with a major asis that passes through the source and receiver. Two prominent and discrete scattering events $>$ 20dB above the diffuse background co-register with the known location of the calibrated targets (black circles denoted by T1 and T2). Note that distortion in the mapping of the ambiguous returns can be seen by the difference in spatial extents between the real targets (T1 and T2) and their ambiguous counterparts (T1' and T2') in both images. Similarly, we also highlight two large regions of prominent scattering (R1 and R2). Comparison of the two images breaks the receiver array's left-right ambiguity. In the second image, we notice that the ambiguous counterparts (A1 and A2) of R1 and R2, shift with the change in receiver orientation. The real scattering region remains in the same vicinity as R1 and R2 in the first figure. The 80 and 100m isobaths are shown for geographic reference to aid in the comparison of the two figures. The origin of both images is the OAWRS Source location (blue star) 39° 16.17'N, 72° 51.78'W. The blue dashed line corresponds to the array heading direction for the current ping, while the magenta line corresponds to the track not in use. The black star corresponds to the receiver location along the track line during the particular transmission. The black arrows indicate the broadside (perpendicular to the array) and endfire (parallel to the array) axes. Ship noise from the receiver ship in the endfire direction can be seen in both figures, while additional noise from other ships (saturated beams off endfire) can be seen clearly in the second figure.

2.3 Conventional Fish Finding Sonar (CFFS) System: EK500

During MAE03, a high-frequency, echosounder was simultaneously operated to measure the scattered intensity from groups of fish. Typical scientific echosounders utilized for fisheries applications operate at frequencies ranging from roughly 20-500kHz and are able to measure the local depth distribution of fish at any instant by echosounding within a narrow, downward-directed beam along the line transect of a slow-moving research vessel [91, 5, 6, 70, 89, 47] .

In US waters, the National Marine fisheries Service often conduct seasonal CFFS surveys in order to monitor abundance and biodiversity trends within productive ecosystems [87]. These surveys often comprise a series of lawn-mower type patterns through large, continental-shelf scale environments over the course of a few weeks to a month. During such surveys, biological samplings by trawls are usually made in conjunction with the hydroacoustic measurements to aid in species identification. The limited areal coverage of the CFFS system, ship-time, and human resources make it impossible to achieve the very high spatial and temporal resolution necessary to accurately estimate abundance indices of wild fish populations. The resulting abundance records are incomplete and aliased in space and time. Statistical methods are often employed to extrapolate abundance in areas where no measurements are available. This can lead to either over- or underestimation of population if sampled populations are nonrepresentative of the fish typically inhabiting a geographic region.

The echosounder used during MAE03 was a SIMRAD EK500, which is comprable to the scientific echosounder sonars utilized by the National Marine Fisheries Service during their annual surveys in US waters. The EK500 sent out a short burst of sounds at two-second intervals to insonify a conical volume of the ocean confined to the immediate area under the tow ship for each single transmission, as illustrated by the schematic in Fig. 2-4. The transmitted pulse propagates through the water and encounters various targets, such as bubbles at the surface and groups of fish, or the seabed. These targets reflect the sound back to the receiver and the backscat-

tered echo can be charted in depth by dividing the two-way travel-time by twice the mean sound speed in the water column. By concatenating the depth profiles from consecutive CFFS transmissions, the in-situ volumetric depth distribution of fish can be plotted along the line transect sampled by the research vessel, as shown in the time-depth profile Fig. 2-4.

For the particular depth profile shown in Fig. 2-4, the fish shoals typically collect in roughly 10m layers one to two meters off the ocean bottom. The continuous, extending shoaling regions are on the order of 1-3 km in along-transect range extent and are roughly homogenously distributed in depth. Many of the larger, continous shoals observed by CFFS during MAE03 are often found extending km-long ranges in homogenously distributed in depth layers between 10-20m approximately 1-5m off the bottom. The smaller groupings, indicated by spikey features in the transect profile, are distributed differently in depth and sometime separated from the continuous shoals. Such groupings could be indicative of a different species of fish to those in more continuous shoals.

Unlike OAWRS, CFFS does not rely on the capacity of the continental environment to behave like an ocean waveguide and, instead, employ waterborne propagation paths that are limited to much shorter ranges, on the order of the local water depth. These waterborne paths suffer much greater geometric spreading losses since they experience free-space, spherical spreading loss as opposed to the cylindrical spreading loss of the trapped wave-guide modes employed by OAWRS. Also, the much higher frequencies utilized by CFFS cause the propagating sound to undergo greater attenuation loss than that of the OAWRS operating frequencies.

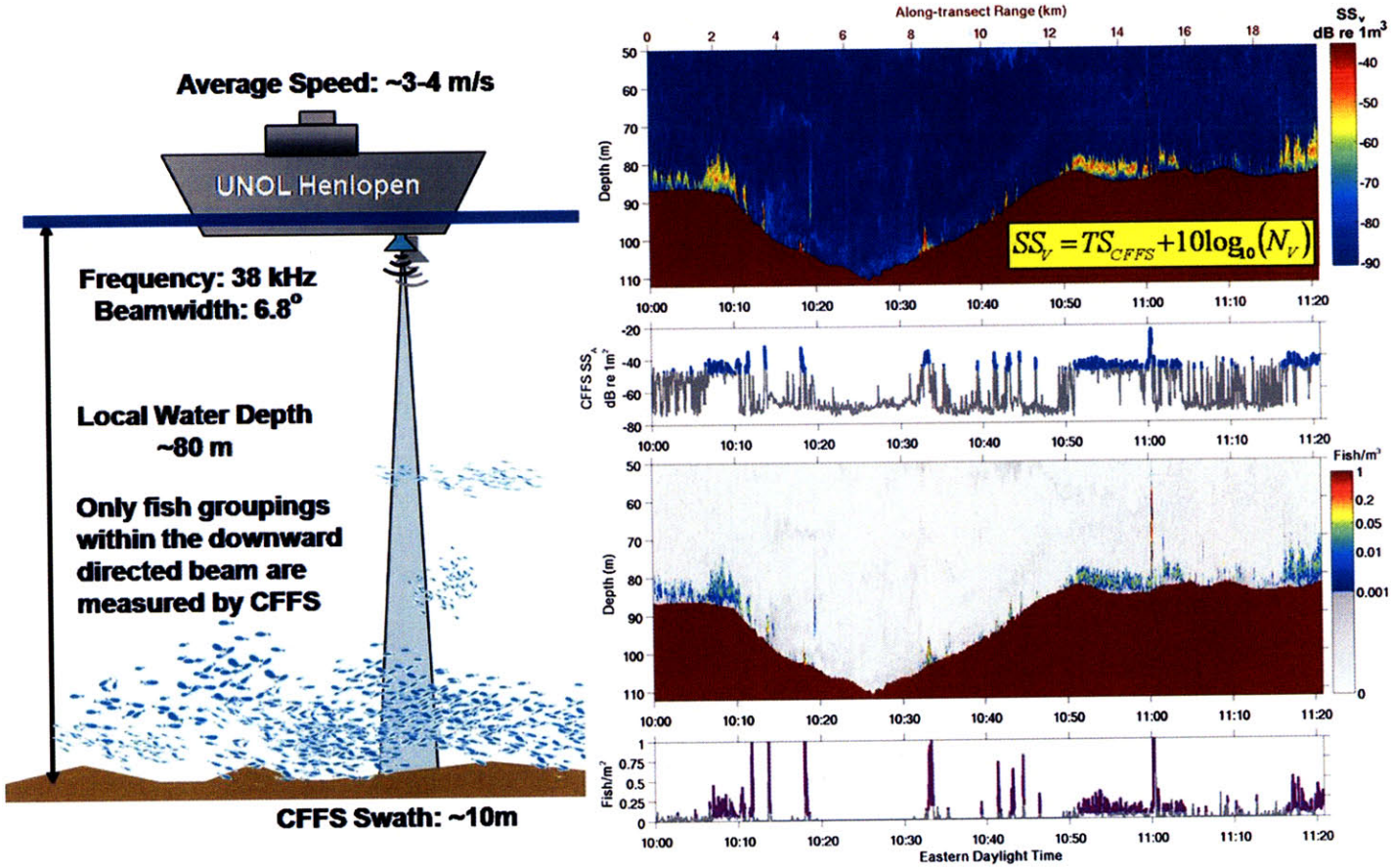

Figure 2-4: The US research vessel UNOL Henlopen simultaneously operated a high-frequency, echosounder through the region 2003 OAWRS survey region. Fish groupings contained within the very narrow, downward-directed beam were measured at 2-sec transmission intervals. The depth of the scatterered returns for each ping can be found by dividing the two-way travel time by twice the mean sound speed in the water column. The scattered intensity can be converted into metrics of volumetric density by compensating for the expected target strength of an individual fishat the CFFS operating frequency. The expected target strength used for this example was TS = -35.3 dB re 1m. The areal scattering strength time series (gray line in B) can be found by integrating the volumetric scattering strength over depth. The blue line in B highlight fish populations shown in A. For this example, typical areal densities are roughly between 0.1-0.25 fish/m^2.

As noted in Ref. [32], CFFS surveys habitats at rates in the vicinity of 0.2 km^2/hour, which are similar to those of capture trawl vessels. The CFFS system deployed during MAE03 had a beamwidth of 6.8° which results in an approximately 100 m^2 circular footprint in typical continental shelf water depths of 80m for each 2s-transmission. The research vessel operated at speeds between 3-5m/s during MAE03 to reduce additional ship noise that could contaminate the imagery generated by the simultaneously operating OAWRS system. During reseach surveys, CFFS tow-ship speeds often travel between 8-12 knots (roughly 4-6m/s). Survey rates can increase by roughly an order of magnitude when standard multi-beam or side-scan technology [70, 26, 24]. Multi-beam and side-scan systems experience difficulties at ranges beyond a few water depths, since they also exploits local, linear, waterborne propagation paths. At ranges an order of magnitude greater than the local water depth, waveguide scattering models need to be used to handle multiple reflection from the ocean boundaries.

The measured CFFS scattered intensity, S_v, can be converted into metrics of volumetric density by dividing the scattered intensity by the expected scattering cross-section of an individual fish at the CFFS operating frequency [89, 95]. Time series of areal population density (purple time series in Fig. 2-4) and areal scattered density (blue time series in Fig. 2-4) can be obtained by integrating the volume density and volumetric scattering density over depth.

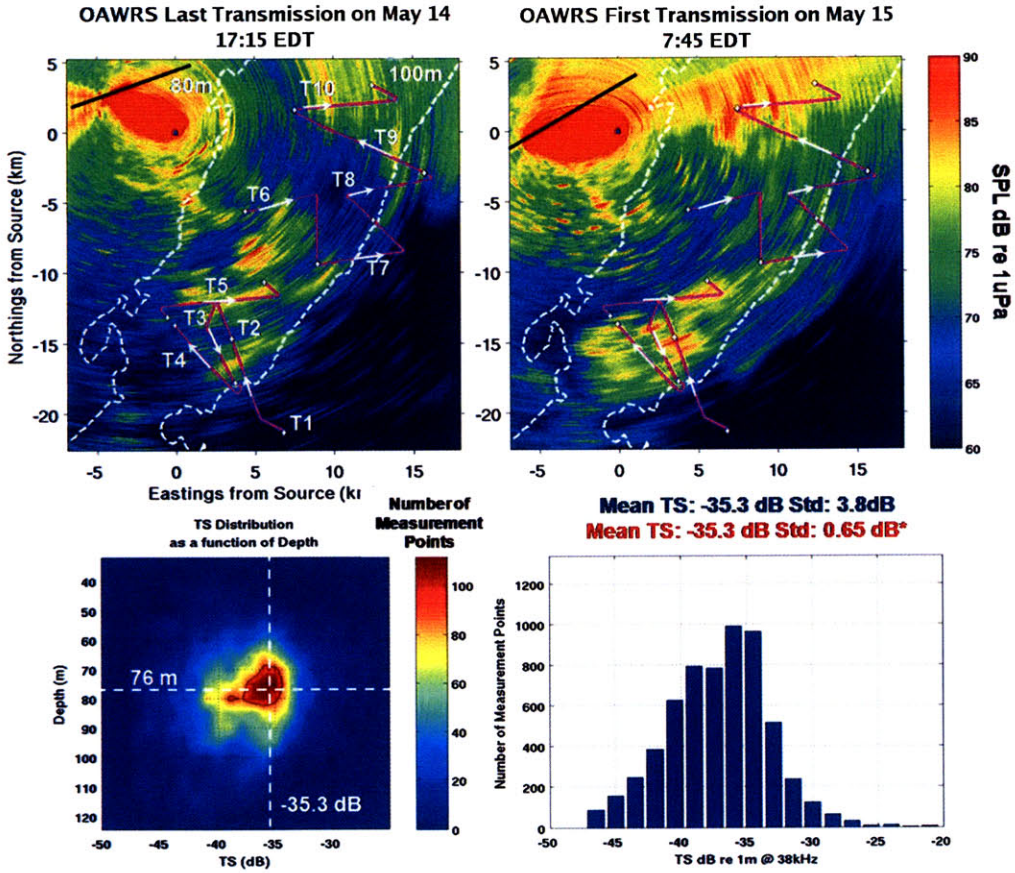

Figure 2-5: Example summarizing CFFS night-time measures of individual target strength at 38 kHz during the night and early morning hours of May 14 and May 15,2003. The overnight CFFS survey transects are overlain onto the last OAWRS 390-440 Hz transmission on May 14 (17:15 EDT) and the first transmission on May 15 (7:45 EDT).

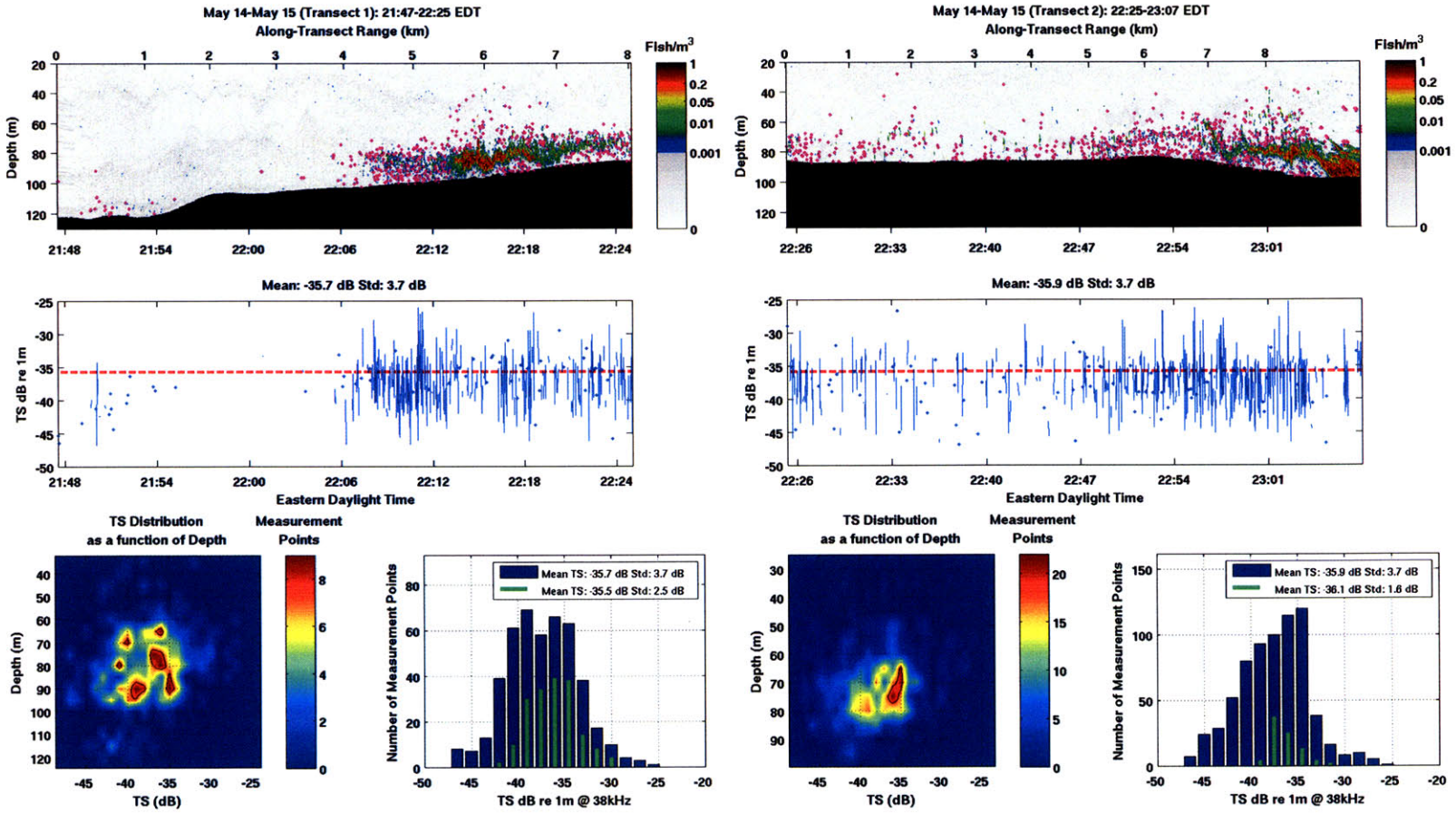

Figure 2-6: Examples of two representative transects taken during the night of May14-May15,2003 where CFFS made measurements of the target strength of an individual fish at 38 kHz. Histograms of the unaveraged (blue) and averaged (green)CFFS target strength corresponding to these transects are presented. Continuous measurements over extended fish groupings are averaged over 20 samples, or over roughly 150 meters, to produce the green histogram.

The EK500 was equipped to measure the target strength, or logrithmic quanitity of the scattering cross-section, of an individual fish. Night-time in-situ measurements of individual target strength were made by the CFFS sonar in the same geographic vicinity of the fish populations imaged by OAWRS during daylight hours. Simultaneous measurements of individual target strength could not be made during the day since most of the fish groupings were tightly consolidated near the bottom. At night, the fish lift off the bottom and are more dispersed throughout the water column. This makes it easier to single scatterers in the vicinity or at the periphery of fish groupings.

2.4 Simultaneous Measurements by CFFS to Ground-Truth Fish Populations Imaged by OAWRS

The OAWRS system operates in an Eulerian reference frame by allowing for the rapidly imaging and monitoring of thousands of square kilometers at minute intervals. In contrast, CFFS operates in a Lagrangian reference frame by making point measurements along the line transect of the slow-moving research vessel. During a single transmission, CFFS is capable of surveying one-millionth of the area surveyed by OAWRS. In order to ground-truth the strong scattering regions in the OAWRS imagery as fish, we co-register fish populations sampled by CFFS at the exact time-space location in the corresponding OAWRS imagery. These exact time-space location where CFFS simultaneously registers fish populations are discussed further in Chap. 3 in the context of empirically calibrating the target strength for an individual fish at OAWRS operating frequencies. On May 14 and May 15, real-time communication between the OAWRS receiver ship and the CFFS ship helped to direct the CFFS survey efforts to regions of large shoaling activity. These days yielded the best co-registration between both systems and demonstrate how a synoptic system like OAWRS can help to direct simultaneously operating in-situ platforms to concentrate localized sampling and at-sea resources to better characterize representative populations within a large geographic vicinity. The limited swath of the CFFS sonar about the line transect

make it easy to graze or miss entire populations as we will show in the following section.

High correlation was found between locations of strong scattering in the OAWRS acoustic intensity imagery and dense clustering of fish found with CFFS. Additionally, regions without strong scattering in the OAWRS imagery were also found to be absent of significant fish populations. Co-registration of returns by both systems were observed repeatedly over the entire experiment at Sites 1 and 2. At Site 3, there were no simultaneous CFFS measurements during the OAWRS survey period. A chronological synopsis of fish activity observations by OAWRS and CFFS during daylight hours during MAE03 is presented in the following section. Overnight CFFS measurements of individual fish target strength at 38kHz are presented and summarized in Chap. 3 as well as in Appendix D.

Fish were also shown to be the dominant physical mechanism of long-range acoustic clutter for low-frequency active sonars operating in littoral environments with very benign bathymetric relief [23, 66, 32]. Fish populations always found within the vicinity (less than 1km) of highly repeatable (repeatable more than 25% of the day) strong scattering regions in the OAWRS imagery. Highly repeatable strong scattering regions imaged by OAWRS were shown to be independent of sub-bottom morphology. This finding is consistent with the conclusion shown earlier by Ratilal et al in Ref. [35]. In contrast, the probability of OAWRS finding strong scatterin regions in CFFS-confirmed, fish-inhabited areas were much higher than the probability of OAWRS measuring strong scattering anywhere in the survey area.

Chapter 3

Method for Empirically Estimating Fish Target Strength for OAWRS system based on simulataneous CFFS measurements during the Main Acoustic Experiment 2003

3.1 Introduction

At-sea trials which employ echosounder technology to qualitatively visualize the in-situ vertical distribution of fish have been in practice as early as 1935 [91, 93, 90, 5, 6]. However, acoustics techniques for quantitatively estimating fish population abundance were not explored until the late 1950s. The earliest attempts at abundance estimation were initially based on simplistic principles of echo-counting, or counting individual echoes from scattered fish [94, 71] and then on echo-integration methods which rely on summing the echo amplitudes from a collective of fish [49]. The earlier development of echo-integration technique was attributed to Ingvar Hoff and was formally detailed by Dragesund and Olsen [15]. In 1966, as an addendum to the

echo-amplitude integration technique, Scherbino and Truskanov [86] suggested that a more correct approach is to integrate the echo-intensity as opposed to the echo amplitude. The integrated echo-intensity could then be scaled by the expected target strength of an individual fish to estimate abundance indices. This modified echo-integration technique remains the fundamental principle behind conventional echo-sounding methods and an established standard for modern hydroacoustic fish stock assessment [89, 69].

In acoustic-biomass estimation, the target strength (TS) of an individual scatterer is necessary to scale measures of acoustic intensity to absolute levels of population abundance [89, 14]. The target strength is the logrithmic quantity of the backscattering cross-section of the intended target and provides a measure of the proportion of the incident energy that is backscattered by the target. In the earliest days, calibration methods were imprecise and the target strength of the fish uncertain. Extensive laboratory and at-sea acoustic experiments (involving suspended, immobilized fish; caged fish in a laboratory tank; and wild fish in their natural environment) have been conducted from the 1970s to the present to directly measure and indirectly estimate the mean target strength of several species of fish and various marine organisms at the higher frequencies that conventional fisheries sonars typically operate (38-400kHz). A comprehensive summary of such published experimental methods and predictive, data-calibrated TS models is detailed in Chapter 6 of [89].

With the advent of dual-beam and split-beam conventional echosounder systems, it is now possible to make in-situ measurements of the individual target strength of fish in their natural environment [89]. The empirical TS values are used by marine fisheries to scale the measures of backscattered intensity obtained during yearly surveys to estimate the abundance of commercially viable species sampled during yearly hydroacoustic surveys [89]. However, these measurements made with conventional echosounders can only sample small ocean volumes at any one instant. The small areal coverage of these systems, limited to a swath along the ship transect (typically 10m) and the slow moving speed of the ship (typically 5-10 knots), make it difficult to track and detect large shoaling populations within the continental-shelf scale areas

they survey. When making in-situ measurements of TS, it is also often difficult to isolate and track single scatterers within densely packed fish populations. Most of the measurements are made during the night when fish are known to disperse throughout the water column. Consequently, it could be problematic to sample scatterers representative of the population when there is a heterogeneous mix of species within populations.

The direct measures of individual TS are used in conjunction with capture trawl data to develop and verify theoretical models for predicting individual target strengths [89, 69, 57]. These models are based on the species-dependent, physiological properties of fish and have been calibrated with data obtained at the high operating frequencies of that conventional echosounders.

Inspite of extensive measures at high frequencies (38-400 kHz), there are few instances of published experimental measures or estimates of TS in the low frequency range (<2kHz). In 1996, Nero and Huster conducted an experiment in the Gulf of Alaska using explosive sources and a horizontal line array to image what was believed to be Pacific Salmon at ranges of 4 km [76]. Experimental data from nine frequency bands between 70 to 1000 Hz were used estimate the target strength of an individual fish and compared with established swimbladder models [57]. During this sea-trial, there was no independent confirmation of the scatterers or calibration of the individual target strength with a simultaneously operated local system. In 2001, Nero and Jech used two independent sonar platforms, a mid-frequency, broadband towed sonar operating in the 1.5-5kHz band and a local high frequency echosounder (12, 38, and 120 Hz), to investigate swim-bladder resonance for pre-spawning Atlantic Herring in the Gulf of Maine [85]. Backscattering data from both systems were combined with in-situ pelagic trawl sampling and compared to Love's length-TS relationship and a low frequency swimbladder model [57, 58].

During April-May of 2003, an OAWRS system operating in the 390-1400 Hz band was used to instantaneously image and continuously monitor fish populations on the New Jersey Continental Shelf approximately 200 km south of Long Island, NY [66]. A conventional echosounder was employed to simultaneously ground-truth significant

fish populations surveyed by OAWRS and to provide local measures of areal density within large shoaling regions and scattered schools.

Since OAWRS is able to insonify areas spanning thousands of square kilometers with minute-to-minute updates, it provides rapid synoptic snapshots of fish 2D spatial distribution, population dynamics and behavior that can be used to efficiently guide the highly-localized survey efforts of a simultaneously operated CFFS system. Hundreds of simultaneous local measurements of areal fish density by CFFS within the OAWRS-imaged populationd were used in conjunction with the long-range acoustic intensity data to empirically estimate the mean TS at the three OAWRS operating frequency bands: 390-440 Hz, 875-975 Hz, and 1250-400 Hz.

In the following chapter, we formulate the TS estimation from the incoherent scattering from a spatial distribution of fish and follow with a discussion of the measured and modelled parameters that are necessary for the TS estimation. Then, a classification scheme of different CFFS-OAWRS sampling scenarios is discussed based on the spatial morphology of the co-incidentally sampled fish populations. Finally, we assess the consistency and discuss the accuracy of the estimated TS using specific examples of real-world sampling scenarios from MAE03 for the three OAWRS operating bands.

3.2 Incoherent scattering from a spatial distribution of fish

The incoherent scattered field from a spatial distribution of small, random inhomogeneities, such as fish, can be modelled using a sonar equation approach. Analogous to the radar equation, the sonar equation is the most widely used analytical tool in applications of active sonar and primarily employed to estimate a target's scattering properties and the limiting range of detection [95, 12, 51, 9, 54, 17] Targets that obey the sonar equation in a waveguide include all acoustically compact scatterers whose physical extents are much smaller than the acoustic wavelength. The use of the sonar equation implicitly assumes that (i) the propagation and scattering effects are inde-

pendent and completely factorable from each other and (ii) that a linear combination of incoherent quantities (target strength, transmission loss, and source level) can approximately account for the sound pressure level at the receiver.It is important to emphasize that the sonar equation is only valid when the propagation and scattering dependencies are approximately separable [82, 63, 64, 95, 12]. For extended targets, in an ocean-waveguide, a full-field scattering model such as those described in Refs. [82, 63, 64, 83] are necessary to accurately describe the scattered field.

3.2.1 The Scattered Field from a Random Distribution of Fish within an OAWRS Resolution Footprint

The scattered field received within an OAWRS resolution footprint is random due to both waveguide fluctuations [60, 41, 10] and randomness in fish distributions, and scattering properties [83]. A statistical approach is then necessary to analyze the OAWRS returns. Note, Ratilal and Makris formally derivethe full-field, 3-D scattering from a random distribution of scatterers within a differential volume in Ref.[64, 83].

Let us first define a coordinate system where the origin is placed at source, the coordinates of the source to be defined by $r_0 = (0, 0)$, the receiver coordinates by $r = (x, y)$, and the coordinates of the centroid of the distribution of scatterers by $r_t = (x_t, y_t)$, as shown in the schematic in Fig. 3-1. Following directly from Appendix 2 in Ref. [83] and assuming propogation loss does not vary significantly over the fish layer, we can write the expected square magnitude of the field scattered from a distribution of fish within an OAWRS resolution footprint centered at horizontal location, r_t, as:

$$\langle|\Phi_s(\mathbf{r}|\mathbf{r_0},\mathbf{f})|^2\rangle = |\mathbf{Q(f)}|^2(4\pi)^4\langle \mathbf{N_A}\frac{|\mathbf{S(f)}|^2}{\mathbf{k^2}}\rangle \int_{\mathbf{\Delta A_t}} \langle|\mathbf{G(r_0}|\mathbf{r_t},\mathbf{f})|^2|\mathbf{G(r_t}|\mathbf{r},\mathbf{f})|^2\rangle \mathbf{dA_t} \tag{3.1}$$

since the mean field will be negligible and scattering from the fish group will be incoherent [64]. In Eq. 3.1, $Q(f)$ is the normalized source spectrum at frequency f,

G is the Green function describing the waveguide propagation to and from r_t,and N_A is the number of fish per unit area within the OAWRS resolution footprint.

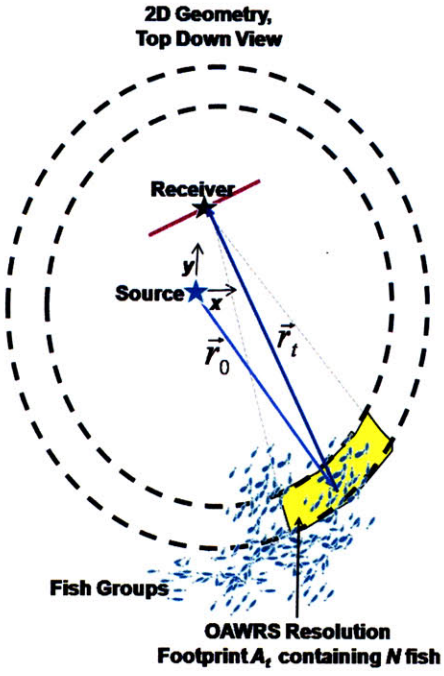

Figure 3-1: A schematic of the 2D, top-down geometry used to model the scattering from a random distribution of fish with an OAWRS resolution footprint.

3.2.2 Generating OAWRS 2D Areal Scattering Strength Maps

The scattering strength is the logrithmic quantity that describes the scattering density at a particular operating frequency. As discussed in Chap. 2, the CFFS system directly measures the volumetric scattering strength at 38 kHz in range and depth along the line transect. The CFFS areal scattering strength can be computed by integrating the volumetric scattering strength over depth for each measurement location along the line transect.

For an OAWRS system, the areal scattering strength within an OAWRS resolution footprint can be expressed by from the logrithimic form of the sonar equation in Eq. 3.1, as

$$SPL = SL - TLA + TS + 10\log_{10}(N_A) \tag{3.2}$$

where SPL is the received sound pressure level at the receiver, SL is the OAWRS source power, TLA is the two-way transmission loss to r_t convolved with the beampattern of the OAWRS receiver array, TS is the target strength of an individual fish at a particular frequency, and N_A is the fish number density within an OAWRS resolution footprint. The OAWRS source power is described by

$$SL = 10\log_{10}(\int_{\Delta f} |Q(f)|^2 df) \tag{3.3}$$

where $Q(f)$ is the normalized source spectrum for a particular OAWRS operating frequency band. The term TLA is written as

$$TLA(f) = 10\log_{10}((4\pi)^4 \int_{\Delta A_t} \langle |G(r_0|r_t, f)|^2 |G(r_t|r, f)|^2 \rangle dA_t) \tag{3.4}$$

.

For the New Jersey Continental Shelf environment, we find that the depth-averaged transmission loss computed at the center frequency of each OAWRS operating band is a good approximation of the broadband transmission loss, as described in Appendix A. Finally, the target strength, TS of an individual fish at a particular frequency, f is given by

$$TS(f) = 10\log_{10}(\frac{\langle |S(f)|^2 \rangle}{k^2}) \tag{3.5}$$

In Eq. 3.2, TS is the target strength for the mean scatter function of an individual fish at the OAWRS operating frequency. From 3.2, we identify the quantity, SS, to be the scattering strength for the OAWRS resolution footprint.

$$SS = TS + 10\log_{10}(N_A) \tag{3.6}$$

In order to generate the instantaneous OAWRS areal scattering strength maps for each OAWRS frequency band, we compensate the measured OAWRS acoustic intensity imagery for the two-way transmission loss, the spatially-varying footprint of the OAWRS system and OAWRS source power. The intermediate steps to generate the OAWRS scattering strength maps are illustrated in Fig. 3-2 (A-E). The sound pressure level is directly measured by the OAWRS system. The transmission loss from the source and receiver were computed numerically using the parabolic equation, a standard method for modelling the Green's function in a range-dependent ocean environment. Known environmental and OAWRS system parameters, including measured sound speed profiles, high-resolution bathymetry, source position, receiver position, receiver heading, frequency, and array dimensions, were used in the propagation modelling. As noted in Ref. [32], the 2003 OAWRS measurements of the mean acoustic intensity after one-way transmission from the source to receiver, as well as two-way returns from the seafloor, show no sign of modal interference structure (i.e. peaks and nulls from coherent interference). Rather a uniform decay with range was observed, indicating a lack of modal interference, which is typically associated with a highly predictable and uniformly mixed acoustic structure over depth. The uniformly mixed acoustic structure over depth makes it possible to approximate the two-way propagation with the depth-averaged transmission loss at the center frequency of the OAWRS operating band to within 1 dB error. The OAWRS source level for all three operating bands were calibrated using data from a desensitized phone on the receiver array. Further discussion of the procedure for generating the OAWRS 2D scattering strength maps can be found in Appendix A.

3.3 OAWRS TS Estimation

The OAWRS target strength empirically estimated for a representative individual fish at various OAWRS operating frequencies from data measured by two independent platforms with different spatial and temporal resolutions.

In order to estimate for the target strength at the OAWRS operating frequencies,

we need to equate the along-transect areal number density measured by CFFS and the areal number density at the same time-space location within the OAWRS 2D imagery. In order to avoid any spurious estimation of the OAWRS target strength in regions absent of fish or insignificant fish populations, we need to first identify time-space locations where both CFFS and OAWRS simultaneously co-register fish populations, as shown in Fig. 3-3.

Fish populations observed by CFFS are distinctly identified in corresponding CFFS echograms as continuous, consolidated groups with trace lengths, or along-transect extents, on the order of tens of meters to a few kilometers. These fish groupings are commonly found to layers ranging from 5 to 35 m thick, roughly 5 to 10 meters above the ocean bottom. In a few instances, fish layers of 10-20 meters thick were also observed suspended in the middle of the water column.

Within consolidated fish groupings, there is often at least an order of magnitude difference in volumetric density between the diffuse background layer and significant fish populations observed by CFFS. The diffuse background level observed by CFFS is often made up of patchy, very low scattering volume densities ($< 0.001 fish/m^2$), which are typically associated with plankton clouds, euphasids, and single fish that are sparsely distributed in the water column. The continuous fish populations in the CFFS echograms are found have corresponding areal densities greater than roughly 0.2 $fish/m^2$, which is consistent with the shoaling density established in Ref. [32]. Following from the shoaling density established in Ref. [32], we choose a critical density threshold of $N_{A_{fish}} >= 0.2 fish/m^2$ to segment continuous CFFS-measured populations for the OAWRS TS estimation.

Once the segments of interest are are identified for the estimation, we can procede by equating the along-transect areal number density measured by CFFS within a particular segment to the corresponding areal number density within the OAWRS 2D imagery. Reviewing from Chap. 2,the areal scattering strength for the CFFS system can be written as,

$$SS_C = TS_C + 10\log_{10}(N_{A_C}) \tag{3.7}$$

where TS_C is the expected target strength at the CFFS operating frequency and n_{A_C} is the areal number density within the CFFS sampled populations. The CFFS scattering strength and target strength are quantities directly measured by the CFFS system. A similar expression for the OAWRS scattering strength is given by Eq. 3.6. The OAWRS scattering strength over the entire OAWRS survey area is computed as discussed previously.

By equating the areal number density, $N_A = N_{A_C}$, the expression for OAWRS TS can be written as,

$$TS = SS - SS_C + TS_C. \tag{3.8}$$

In Fig. 3-3 we observe a large shoaling population simultaneously observed by OAWRS and CFFS. Also highlighted in Fig. 3-3, is the segmented region of interest used for the OAWRS TS estimation (deliminated by the black contour in the OAWRS scattering strength map and the CFFS echogram). Although OAWRS is able to image wide areas within a 50s-interval, the corresponding CFFS measurements during the same time interval are few and confined to a small subset of the OAWRS survey area (red circle in Fig. 3-3). In Eq. 3.8, SS and SS_C are the OAWRS and CFFS areal scattering strength time series vectors that correspond to the CFFS transect within the segment of interest. These time series are constructed by concatenating consecutive CFFS scattering strength measurements and the corresponding OAWRS scattering strength measures within the segment of interest, as demonstrated by Figure 3-4 and (C). The OAWRS TS is estimated within each segment of interest only at time-space locations where CFFS measures fish densities above $N_{A_{fish}} = 0.2$ fish/m^2. These time-space locations are highlighted in color for the the CFFS scattering strength (red), OAWRS scattering strength (blue), and OAWRS target strength (green) time series in Fig. 3-4.

3.4 Classification Scheme for OAWRS TS Estimation

When combining data from independent sonar platforms to assess fish population, the differences in temporal and spatial sampling capabilities need to be considered when calibrating one system with the other(s). During MAE03, the bi-static OAWRS system was able to imaging an area spanning roughly 3600 km^2 , while the CFFS system was only able survey an area spanning roughly 2000 m^2 in the same OAWRS 50s transmission interval. This corresponds to a survey area less than a hundred-thousandth of a percent than that of OAWRS. Due to the contrast in spatial resolution, it is difficult to ensure that both systems simultaneously sample statistically-similar, effectively stationary fish populations.

The OAWRS TS estimation is accurate for sampling scenarios where both systems sample statistically stationary populations. This is an implicit assumption made when equating the number density measured by CFFS to the number density contained within the OAWRS areal resolution footprint, $N_{A_C} = N_A$. If the fish populations are not statistically stationary within either system's resolution window, corrections must be made.

During MAE03, simultaneous measurements from both the conventional and OAWRS systems show excellent co-registration of extended shoaling populations and small scattered schools for identical time-space points along the conventional line transect. Once the segments of interest are identified and the OAWRS TS is estimated by equating the along-transect areal number density measured by CFFS within a particular segment as discussed previously, we can proceed to categorize each sampling scenario into stationary and non-stationary cases with respect to the type of fish grouping observed, such as within a shoaling region or within small, scattered schools. The classification scheme is summarized below.

- **Statistically Stationary Populations within an OAWRS Shoaling Region**

Illustrated in Fig.3-6, is the case where both OAWRS and CFFS observe extended, statistically stationary populations within a large shoaling region. To reduce the variance of the estimated OAWRS TS within Case 1 segments, the estimated OAWRS TS time series is averaged over independent samples. For a stationary process, the variance is reduced in inverse proportion to the the number of independent samples averaged over [60, 45]. For the OAWRS TS estimation, an independent sample is defined by the number of individual points that comprise one temporal coherence length within the OAWRS TS time series. The coherence length per segment is found by taking the auto-correlation of the longest continuous section of the estimated OAWRS TS time series and computing the number of singular estimation points contained within one e-folding length of the auto-correlation function. For example, if a segment has a standard deviation of 5 dB and a temporal coherence length of roughly 4 estimation points, 25 independent samples or 100 individual estimation points are necessary to reduce the segment standard deviation to 1 dB, following Ref. [60].

The extended nature of the CFFS-sampled populations in Case 1 scenarios afford hundreds of continuous ground-truth sample points which allows for the use of stationary averaging to minimize the variance of the OAWRS TS estimate. This makes Case 1 scenarios optimal for OAWRS TS estimation. When available, the estimated OAWRS TS from Case 1 scenarios should be used as a baseline for comparing TS estimates obtained from other sampling scenarios.

- **Statistically Non-Stationary Populations within an OAWRS Shoaling Region**

  The second case corresponds to non-stationary populations contained within a large shoaling region. For such scenarios, CFFS typically observes discrete non-stationary populations extending roughly tens to hundreds of meters in along-transect extent contained within alarge, continuous OAWRS shoaling region. Variance of the OAWRS TS estimate remain high within these regions

since smaller sample sizes prohibit the use of stationary averaging to reduce the variability in OAWRS TS estimate. Three sub-cases of Case 2 sampling are illustrated in Figs. 3-7A-C. In Case 2A, CFFS samples low density regions of the shoal. In Case 2B, CFFS cuts through discrete high density regions within the shoal. In Case 3, CFFS samples in and out of the periphery region of a large shoal.

- **Statistically Non-Stationary Populations within Small Scattered Groups**

  The last case in the classification scheme corresponds to discrete, non-stationary scattered schooling populations that are observed by both CFFS and OAWRS, shown in Figure 3-7D. Similar to Case 2 sampling, variance of the OAWRS TS estimate remain high within these regions since smaller sample sizes prohibit the use of stationary averaging to reduce the variability in OAWRS TS estimate.

3.5 Accuracy of OAWRS TS Estimation

The optimal sampling scenario is when OAWRS and CFFS sample large populations that are statistically stationary and identically distributed as in Case 1, where no correction for the areal mismatch between OAWRS and CFFS resolution footprints is necessary in OAWRS TS estimation. For Case 2 and Case 3 scenarios, the areal resolution mismatch could lead to biases resulting in either an overestimation or an underestimation of the OAWRS TS.

Overestimation of OAWRS TS can arise in Case 2 and Case 3 scenarios when the effective number density averaged over the OAWRS areal footprint is much greater than that measured locally by the CFFS system, or $N_A > N_{A_C}$, as in Fig. 3-9. Overestimation of TS will yield an underestimation of the population contribution if these TS values are extrapolated to other regions where OAWRS data is available but CFFS data is not.

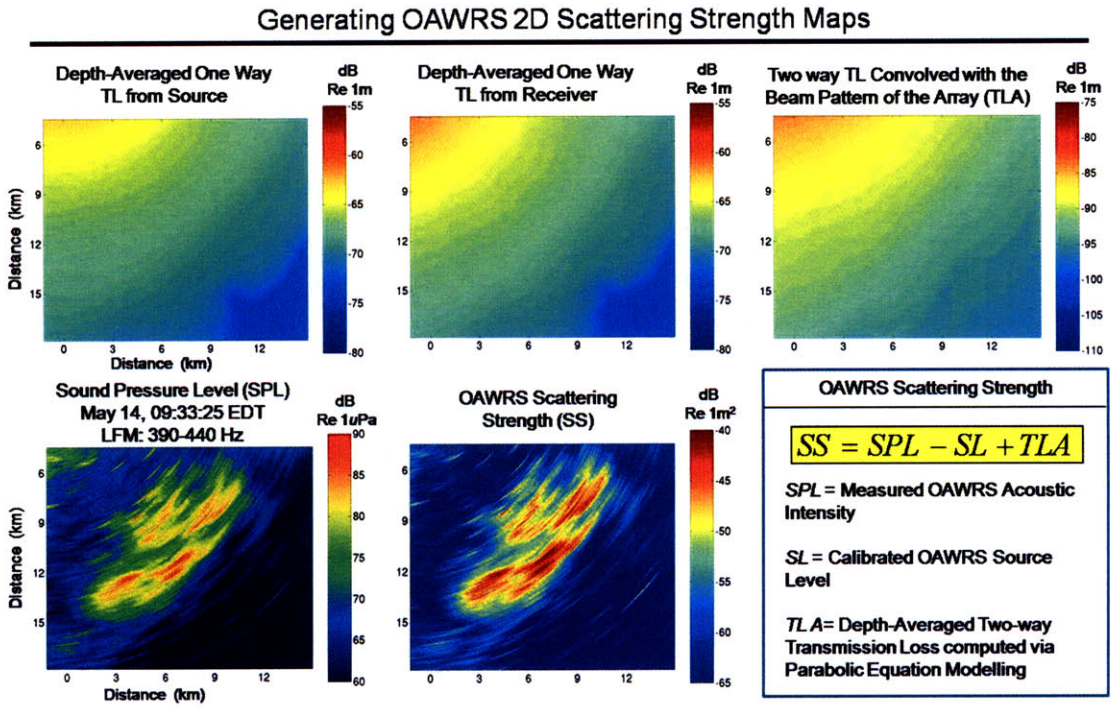

Figure 3-2: Instantaneous OAWRS scattering strength maps (E) can be derived by compensating for the two-way transmission loss from the source and the receiver weighted by the spatially-varying footprint of the OAWRS system (C) and OAWRS Source power. The source level used for this example is 217.9 dB re 1μPa, calibrated from hundreds of independent samples. The center-frequency, depth-averaged one-way transmission loss maps from the OAWRS source array (A) and the receiver (B) prior to weighting by the beam pattern of the OAWRS array are also shown. The one-way transmission loss maps were computed via parabolic equation modelling, using a center frequency of 415Hz, and were averaged over the entire water column.

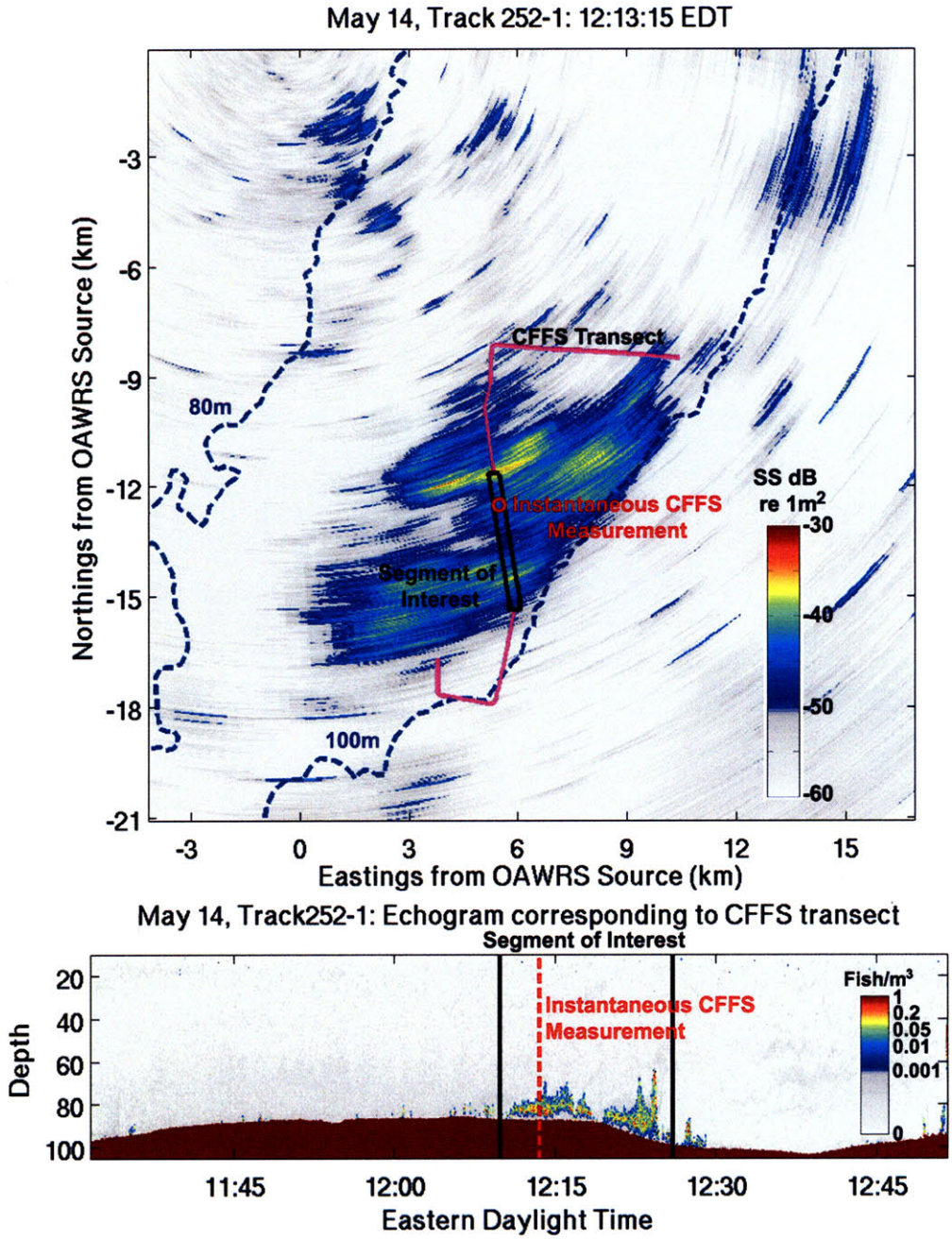

Figure 3-3: The OAWRS target strength is estimated in regions where both CFFS and OAWRS simultaneously co-register fish populations. Regions absent of fish or insignificant fish populations are excluded to avoid spurious estimation. The black rectangular region in the OAWRS scattering strength image corresponds to the segment of interest. The corresponding segment within the CFFS echogram of volumetric fish density is bounded by the two solid black lines. For this particular OAWRS scattering strength image, the red circle corresponds to the exact time-space instant surveyed by CFFS during the OAWRS transmission.The same time-space location is also indicated in the echogram by the dashed red line.

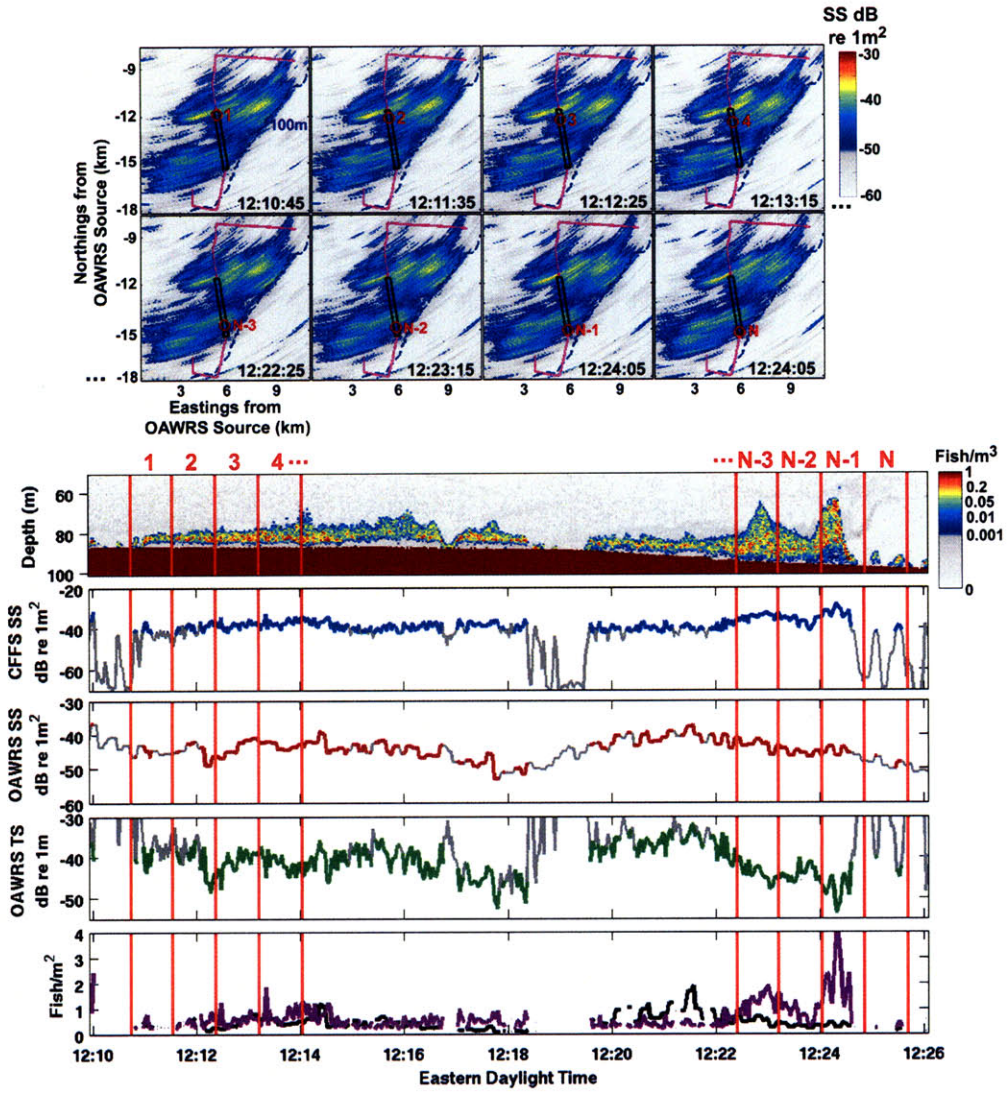

Figure 3-4: The CFFS scattering strength time series contains all measures of CFFS scattering strength within a particular segment of interest. The OAWRS scattering strength time series is constructed by concatenating the OAWRS scattering strength measurements corresponding to the exact time-space locations measured by CFFS within each consecutive OAWRS transmission interval (i.e. intervals 1 through N shown in the corresponding OAWRS scattering strength images). The OAWRS TS is estimated only in locations where CFFS measures fish densities greater than 0.2 fish/m^2 . The time instants in which CFFS measures fish densities greater than 0.2 fish/m^2 are highlighted for the time series of CFFS scattering strength (blue), OAWRS scattering strength (red), and the OAWRS TS time series (green). The OAWRS TS time series is computed using the OAWRS and CFFS scattering strength time series, as well as the mean TS measured by CFFS at 38 kHz. For this particular day, the mean CFFS TS was -35.3 dB re 1m. The CFFS fish density along the segment transect is also shown in the purple time series, while the OAWRS fish density is also plotted in black by assuming a mean OAWRS TS of -40 dB re 1m.

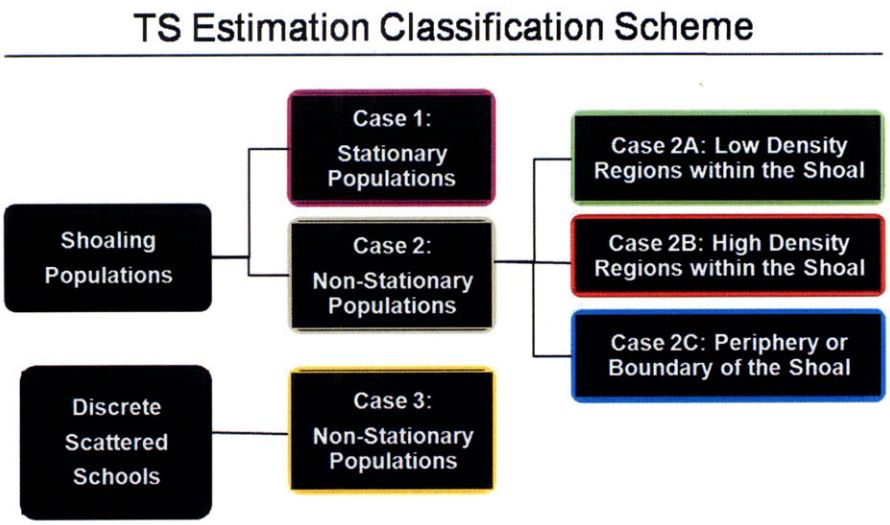

Figure 3-5: Classification Scheme for OAWRS Target Strength Estimation

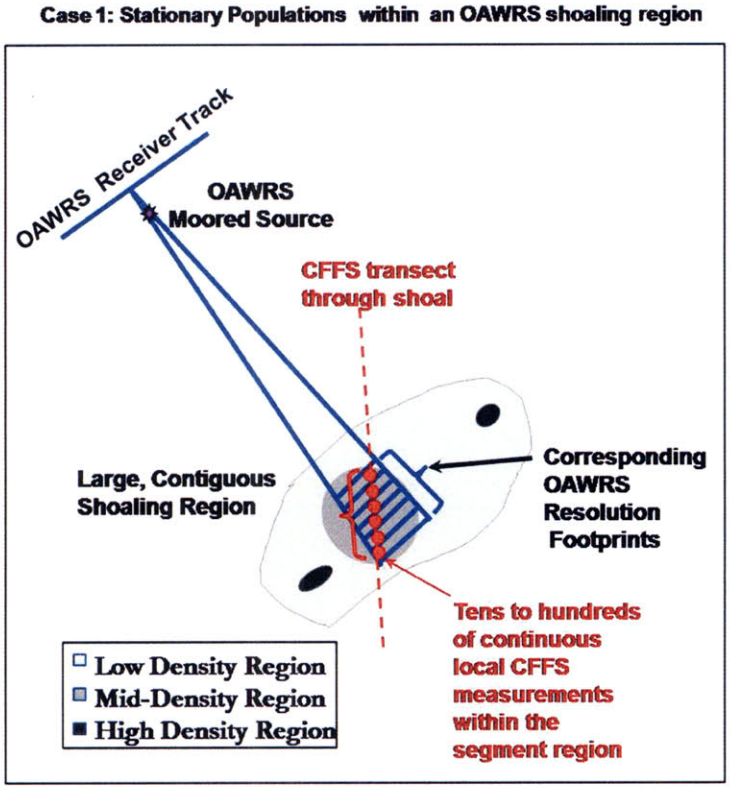

Figure 3-6: Case 1: Statistically stationary populations within an OAWRS shoaling region.

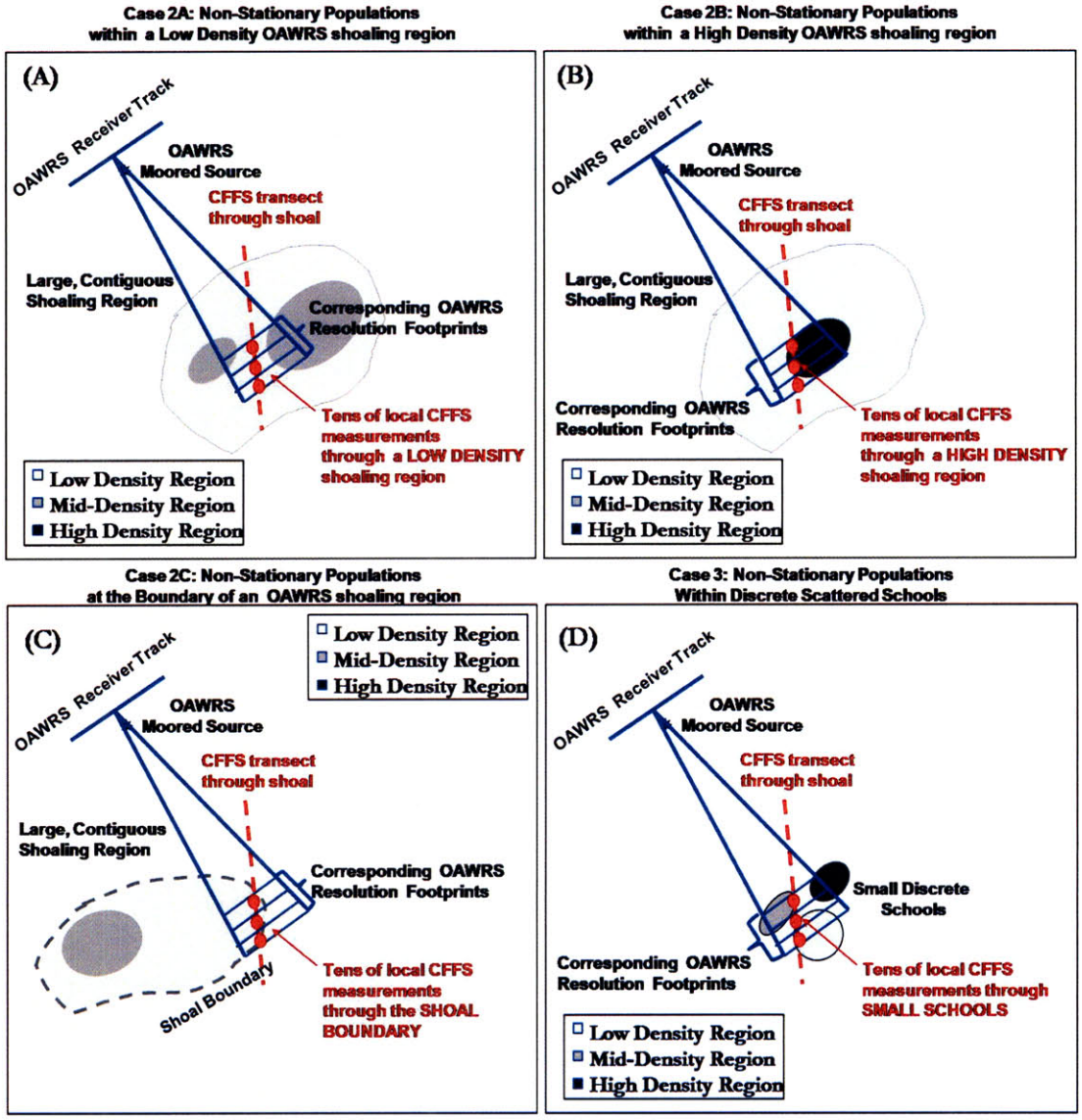

Figure 3-7: Schematic of non-stationary populations within low density regions of an OAWRS shoaling region (A),within high density regions of an OAWRS shoaling region (B), at the boundary of an OAWRS shoaling region (C), and within discrete, scattered schools (D).

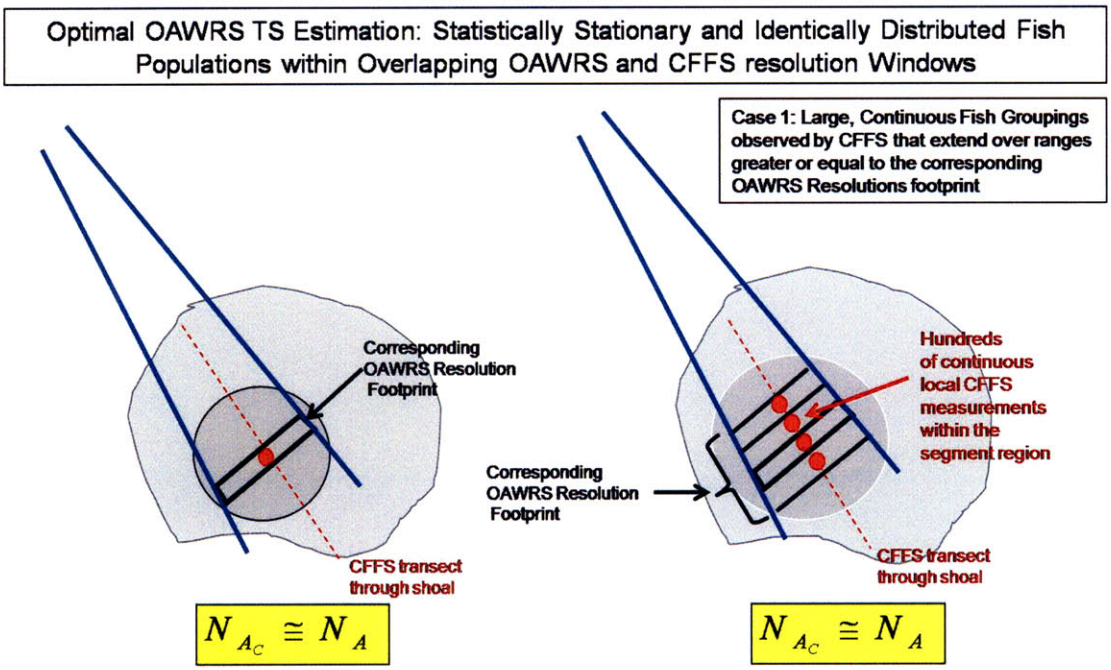

Figure 3-8: The optimal CFFS-OAWRS sampling scenario occurs when CFFS and OAWRS simultaneously sample statistically stationary, identically-distributed fish populations and results in most accurate estimate of OAWRS TS. This typically occurs during Case 1 sampling scenarios.

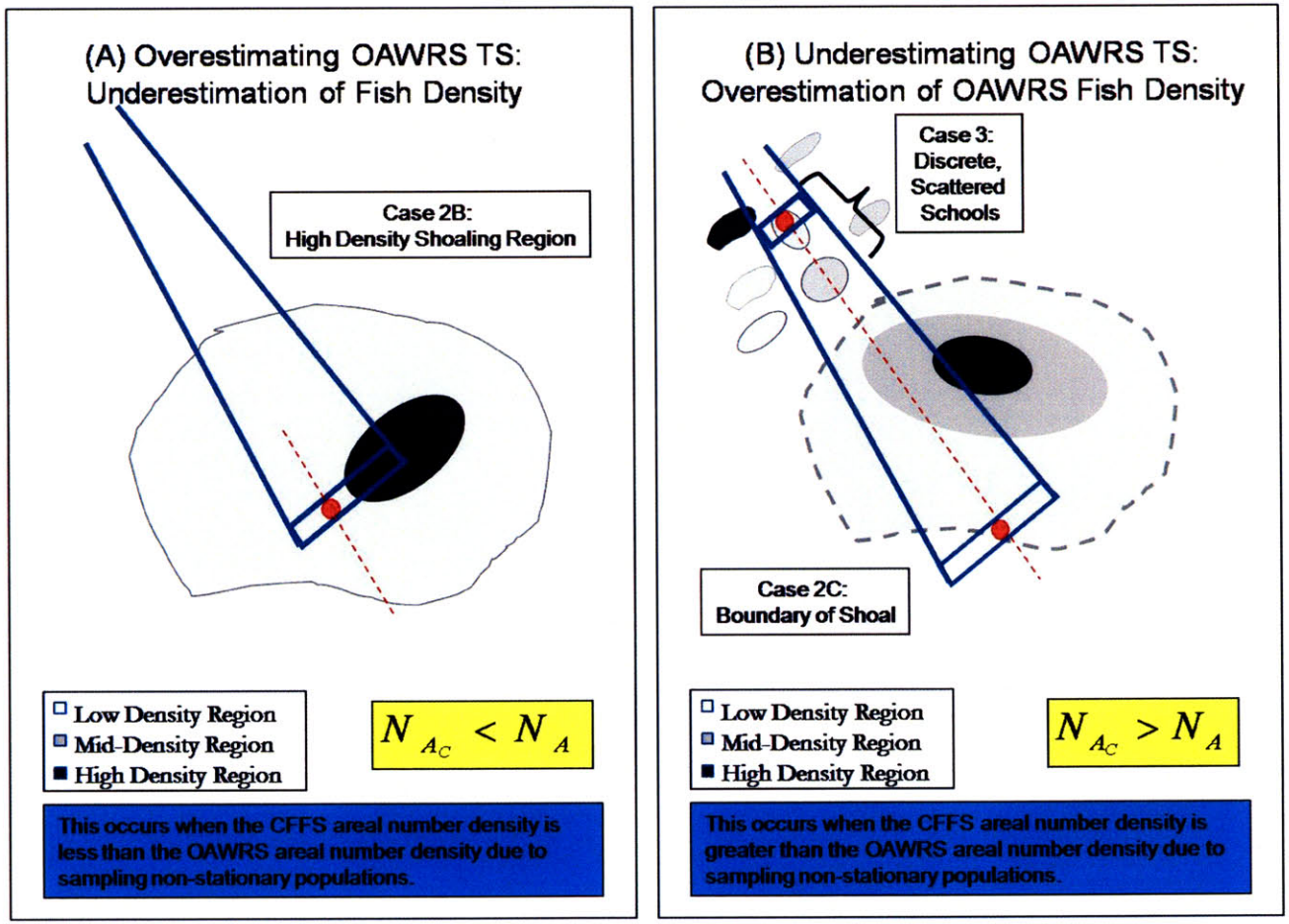

Figure 3-9: Typical CFFS-OAWRS Sampling Scenarios that lead to an Underestimation (Case 3 and Case 2C) and Overestimation of OAWRS TS (Case 2B).

An underestimation of OAWRS TS often arises when the fish populations sampled by the CFFS system do not fully occupy the corresponding OAWRS areal resolution cell. For such sampling scenarios, the CFFS-sampled population density is greater than OAWRS population density density results. Scenarios leading to an underestimation of OAWRS TS are illustrated in Fig. 3-9. For populations measured at the boundary of the large shoals (Case 2C) and small, scattered schools (Case 3), where the corresponding OAWRS footprints are expected to be much larger than the actual area occupied by the fish population, an order of magnitude overestimation of areal fish population density can occur. For such sampling scenarios, it is necessary to apply corrections as described Appendix D.

Since these corrections are highly dependent on the spatially-varying OAWRS footprint, CFFS sampling geometry, and the along transect extent of the CFFS-measured population, it is difficult to apply a universal correction to the data. These corrections can be applied on a case-by-case basis, but are most helpful when trying to set lower bounds for the expected OAWRS TS and gauging consistency with the baseline TS established by Case 1 scenarios.

3.6 Results

During MAE03, OAWRS linear frequency modulated signals of 1s duration were transmitted for three different frequency bands spanning roughly 400 to 1400 Hz were transmitted. The 390-440 Hz, or WX1, band was used as the primary waveform throughout the duration of the 2003 experiment. It was transmitted on 13 of the 15 experimental days. Most of the OAWRS-CFFS time-space coregistrations of fish were measured using this frequency band were from Site 2. Simultaneous measurements by OAWRS and CFFS from 4 experimental days (May 7, 8, 14 and May 15) at Site 2 were used to estimate OAWRS TS at 415 Hz.

In addition to the primary waveform, OAWRS also simultaneously transmitted two waveforms in the 875-975 Hz (WMA) and 1250-1400 Hz (WMB) band on 5 experimental days (April 29; May 4, 9,14 and 15). OAWRS TS estimation was done

for these higher frequency bands on two days, May 9 and May 15, at Site 2 where CFFS co-registered significant fish populations within the OAWRS imagery.

In this section, OAWRS TS estimation for the 2003 experiment are summarized. Here, we present the analysis of the OAWRS target strength estimation data at 415 Hz for Case 1 scenarios. Detailed analyses of the other cases from MAE03 can be found in Appendix B. In Appendix B, we show the (i) OAWRS 2D scattering strength maps to highlight the horizontal morphology of the segment populations, (ii) corresponding range-depth profiles of the volumetric fish density measured by CFFS along the segment transect, and (iii) time series of CFFS Scattering Strength, OAWRS Scattering Strength, and the estimated OAWRS TS. Tables summarizing the OAWRS resolution parameters, the CFFS characterization of the fish populations and the means and standard deviations of the OAWRS Estimation variables for each segment are presented in Appendix B and C as well.

During MAE03, Case 1 sampling scenarios typically occur when both the OAWRS and CFFS observe groupings that continuously extend over several hundred meters to a few kilometers within a contiguous OAWRS shoaling region. For such cases, the spatial continuity of the populations within the CFFS sampled segment affords tens to hundreds of identical time-space co-registration points for the OAWRS TS estimation. These large sample sizes enable variance reduction by stationary averaging of OAWRS TS.

Very large fish shoals, spanning several kilometers were imaged by OAWRS on May 14 and May 15. CFFS was able to make multiple transects through these large, contiguous populations with the guidance from OAWRS imagery to produce hundreds of continuous time-space co-registration points for the OAWRS TS estimation. The OAWRS TS estimates for 6 specific examples are plotted in Fig. 3-10 and summarized in Table 3.1, where details of variance reduction are found.

The expected OAWRS TS, found by a global average over all estimation points contained within each segment, is computed to be -40 dB re $1m^2$ at the 415 Hz. Prior to stationary averaging, the standard deviation of the six segments range between roughly 1 to 5 dB. Stationary averaging is implemented in order to further reduce

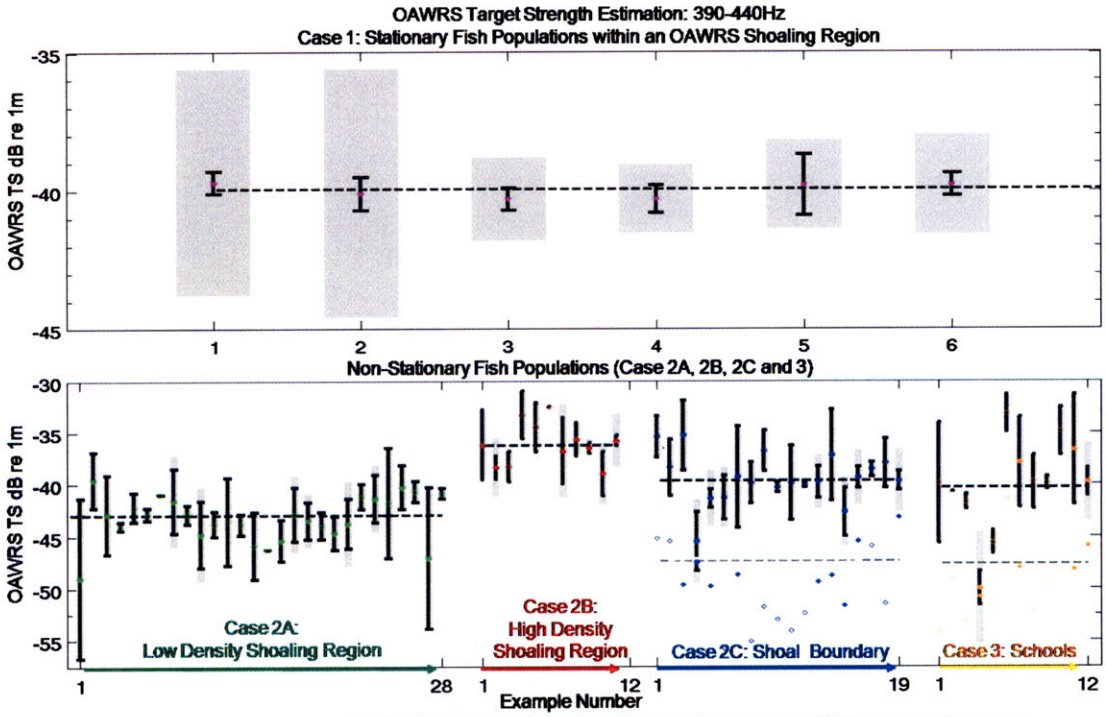

Case 1	Case 2A	Case 2B	Case 2C	Case 3
Mean: -40 dB	Mean: -42.9 dB	Mean: -36.2	Corrected Mean: -39.7 dB	Corrected Mean: -40.3 dB
—	—	—	Uncorrected Mean: -47.4 dB	Uncorrected Mean: -47.6 dB

Figure 3-10: Summary of OAWRS TS Estimation at 415 Hz for available OAWRS-CFFS sampling scenarios.For each case, the mean estimated OAWRS TS per example segment is plotted (colored circles). The gray shaded regions indicate +/- one standard deviation from the mean prior to stationary averaging, while the black error bars indicate +/- one standard deviation from the mean TS after applying stationary averaging. Note, for Case 2C and Case 3, +/- one standard deviation are shown from the mean estimated OAWRS target strength after correcting for the areal resolution mismatch between CFFS and OAWRS. The overall mean OAWRS TS for each case (black dashed lines) combines the data from each example segment for each sampling scenario. For Case 2C and Case 3, the uncorrected mean per example (blue and orange diamonds) and the uncorrected mean per case (gray dashed lines) are also shown.

the variance in each segment. For all segments, the standard deviation is reduced to roughly 1 dB or less.

Example	Day	Track	Segment	Time (EDT)	Number of Estimation Points	Coherence Length (Estimation Points)	Independent Samples (Coherent Cells)	$< TS_O >$ dB re $1m^2$	σ_{TS_O} dB (before averaging)	σ_{TS_O} dB (after averaging)
1	14-May	252-1	H	12:17	343	4	85	-39.7	4.1	0.4
2	14-May	251-2	C	14:03	416	7	59	-40.1	4.5	0.6
3	15-May	252-2	A	10:08	24	2	12	-40.3	1.5	0.4
4	15-May	252-2	Q	11:19	12	2	6	-40.3	1.2	0.5
5	15-May	254-1	E	12:20	10	4	2	-39.8	1.6	1.1
6	15-May	254-1	G	13:19	35	2	17	39.8	1.8	0.4

Table 3.1: Table summarizing the estimated OAWRS TS and standard deviation, as well as the standard deviation per segment after applying stationary averaging over independent coherent cells. Stationary averaging can reduced the sample standard deviation by the square root of the number of samples of independent samples or coherence cells. The number of independent coherent cells per segment is calculated by dividing the number of time-space measurements (column 5) by the coherence length of the OAWRS TS time series (column 9). For most examples, the standard deviation is reduced to less than 1 dB after stationary averaging.

The horizontal shoal morphology, as imaged by the OAWRS system, for each of the 6 segments described in Table 3-1 is shown in Figs. 3-11to 3-13. These very large shoals instantaneously imaged by OAWRS can extend tens of kilometers in range and cross-range extent. It takes the CFFS system many minutes to traverse the segment,so the segment transect (rectangular region) is shown on a representative OAWRS scattering strength image. The CFFS range-depth profile of volumetric fish density measured along corresponding segment transect is also shown for comparison. The fish populations within each Case 1 segment typically extend in 10-30m depth layers off the ocean bottom and exhibit statistical stationarity of the fish populations over hundreds of meters to kilometer scales. This stationarity is consistent with that observed in the corresponding OAWRS imagery.

By examining the OAWRS scattering strength images and the corresponding OAWRS TS time series in Figs. 3-11-3-13, examples, we observe consistency between mean OAWRS TS on the same day through the same OAWRS shoaling region. For instance, in Example 1 and 2 (Segments H and C in Fig. 3-11 respectively) CFFS makes multiple transects through the same shoal imaged by OAWRS, and exhibit one of the most favorable sampling scenarios for estimating OAWRS TS. These segments also comprise two independent samplings of the same shoal showing high statistical stationarity. More specifically, these segments are separated by a roughly two hour interval and follow non-overlapping spatial trajectories, yet we find statistical stationarity in the corresponding range-depth profile of volumetric density measured by CFFS, as well as in the time series of CFFS scattering strength, OAWRS scattering strength, and OAWRS estimated TS. This also means that the estimated OAWRS TS time series have effectively the same means and standard deviations. This large shoal imaged on May 14 extends over tens of OAWRS resolution cells in range and cross-range such that the segments sampled by CFFS are well contained within the OAWRS shoaling region. The large spatial area occupied by the entire shoal as shown by the OAWRS 2D scattering maps, the consistency within the corresponding time series, and the similarity of volumetric population distribution as measured by CFFS suggest that those populations sampled in Example 1 and Example 2 are similarly

distributed fish species comprising the same shoal.

On May 15, a large consolidated shoal was imaged by OAWRS in roughly the same geographic vicinity of that on the previous day. During the second and third track on May 15 (roughly 10:00-12:30 EDT), CFFS zig-zags through this large shoal. Three independent samplings of this particular shoal were made at approximately 10:08 EDT, 11:20 EDT, and 12:21 EDT through non-overlapping CFFS trajectories, as shown in Example 3 and 4 of Fig. 3-12 and Example 5 of Fig. 3-13. As on May 14, we find statistical stationarity in the corresponding range-depth profile of volumetric density measured by CFFS, as well as in the time series of CFFS scattering strength, OAWRS scattering strength, and OAWRS estimated TS, for all three independent samplings of the large shoal. Later in the day, at approximately 13:20 EDT, CFFS transects through a northern shoal roughly 6km to the east of the OAWRS source, as shown in Example 6 of Fig. 3-13 (Segment G). From the corresponding CFFS echogram of this segment, we observe a statistical stationarity of the fish population over hundreds of meters and roughly uniformly distribution of volumetric density over depth in corresponding CFFS echogram. This stationarity is also consistent with that observed in the corresponding in the time series of CFFS scattering strength, OAWRS scattering strength, and OAWRS estimated TS.

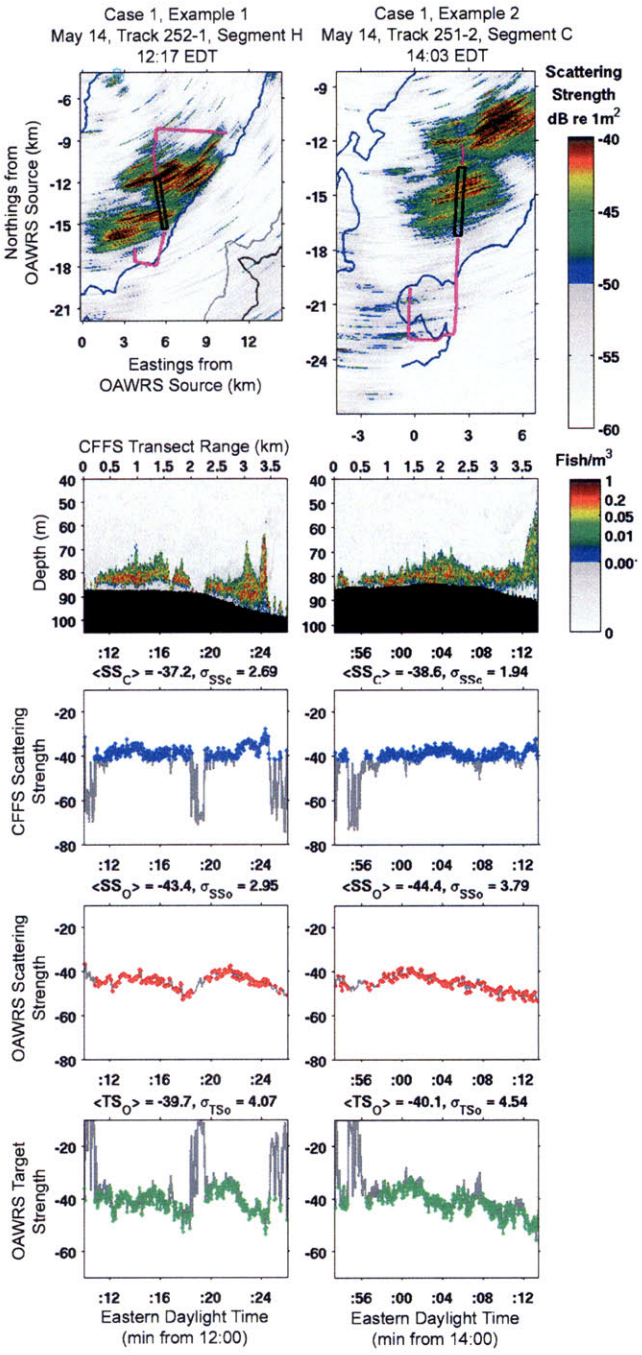

Figure 3-11: Site 2, Case1, May 14, Example segments 1 and 2.The OAWRS TS is estimated in locations where CFFS measures fish densities greater than 0.2fish/m^2, highlighted in color for each time series. The CFFS segment (rectangular contour) is overlain onto a representative OAWRS scattering strength image. The range-depth profiles of CFFS volumetric density for each segment is also shown.

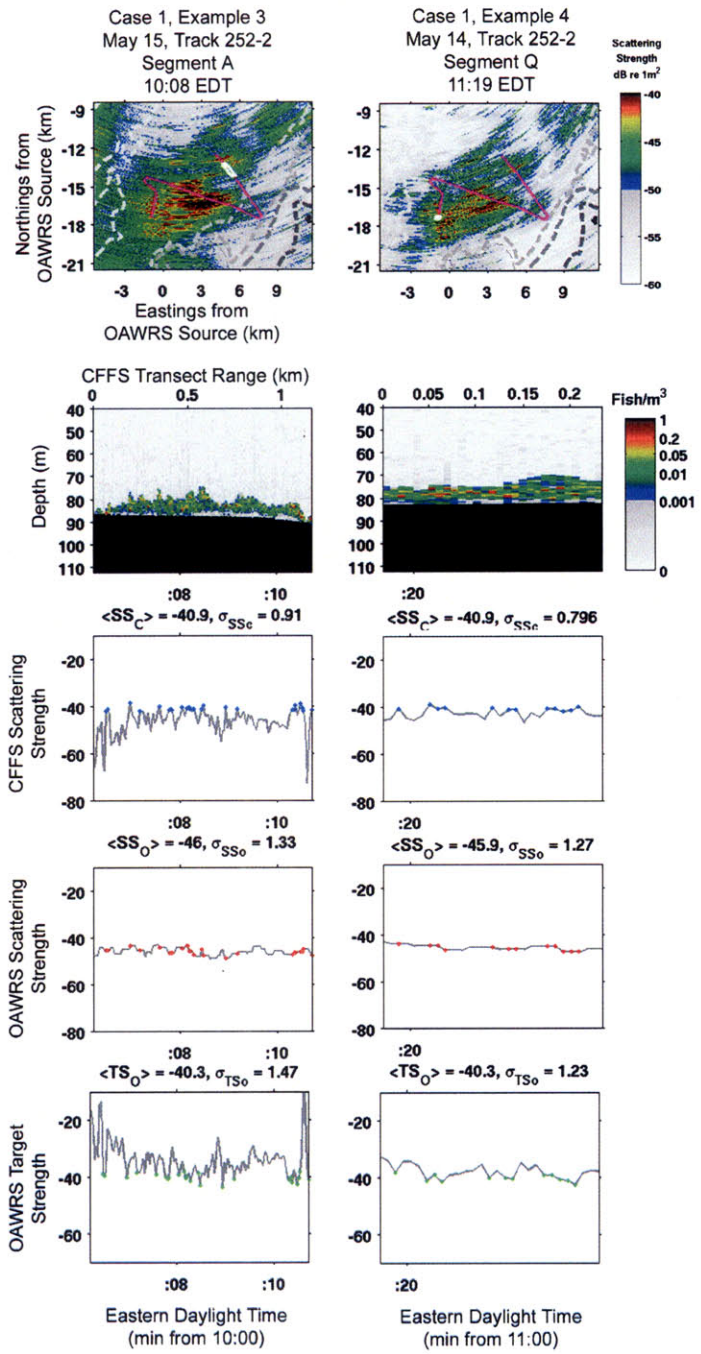

Figure 3-12: Site 2, Case1, May 15 Track 252-1, Example segments 3 and 4. The OAWRS TS is estimated in locations where CFFS measures fish densities greater than 0.2fish/m^2, highlighted in color for each time series. The CFFS segment (rectangular contour) is overlain onto a representative OAWRS scattering strength image. The range-depth profiles of CFFS volumetric density for each segment is also shown.

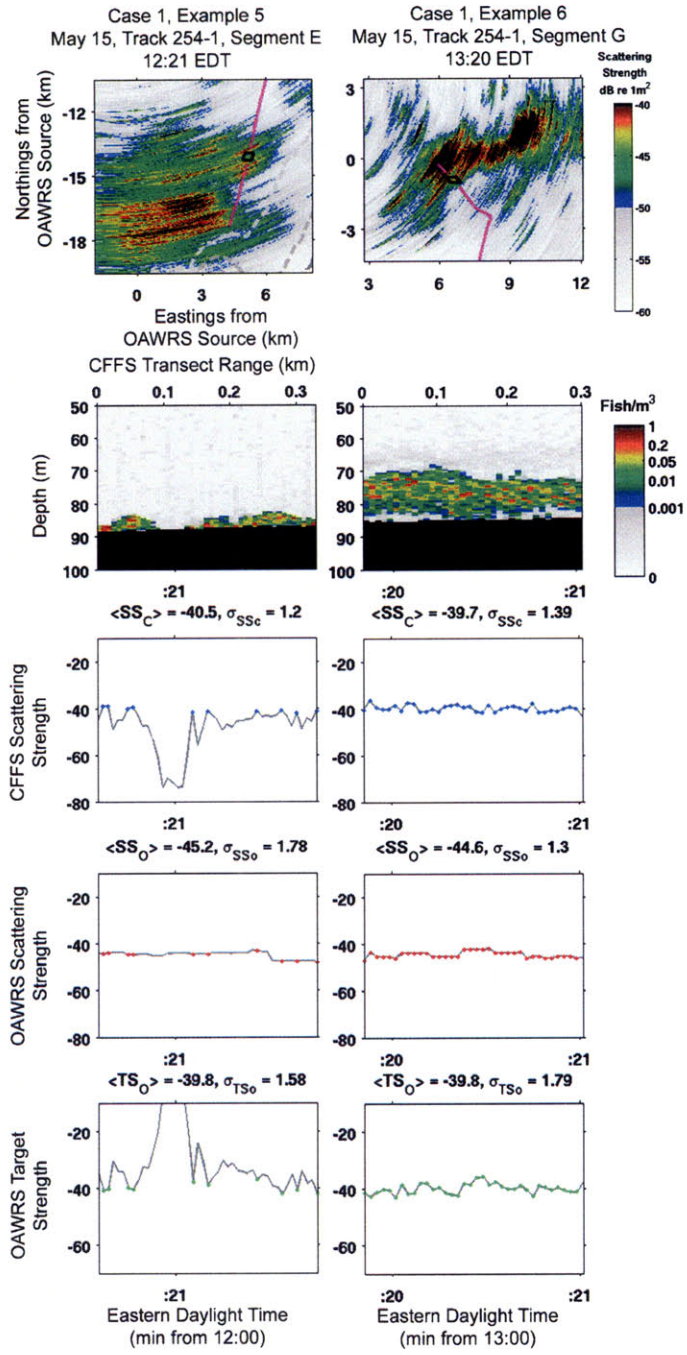

Figure 3-13: Site 2, Case1, May 15 Track 254-1, Example segments 5 and 6. The OAWRS TS is estimated in locations where CFFS measures fish densities greater than 0.2fish/m^2, highlighted in color for each time series. The CFFS segment (rectangular contour) is overlain onto a representative OAWRS scattering strength image. The range-depth profiles of CFFS volumetric density for each segment is also shown.

During MAE 03, there were 28 segments from four experiment days at Site 2 in which CFFS observed discrete, clumpy fish populations extending rougly tens of meters through low density, patchy regions of large, continuous OAWRS shoals (Case 2A). These OAWRS shoaling regions exhibit 2D horizontal contiguity over kilometer scales as previously observed in the Case 1 examples. The OAWRS estimation for the Case 2A examples are plotted and summarized in Fig. 3-10 (green data points). The mean estimated OAWRS target strength per segment are consistently lower than the calculated Case 1 global mean TS (-40 dB re $1m^2$ at 415 Hz). The estimated OAWRS TS per segment are combined to compute a global mean for the Case 2A segments . The global mean for the Case 2A segments is found to be roughly -43 dB re $1m^2$ at the center frequency of 415 Hz. Since the fish groupings measured by CFFS in Case 2A sampling scenarios are continuous over short distances (tens of meters), there are a lower number of identical time-space co-registration points to compute the OAWRS TS estimation. This low number of estimation points also yields a lower number of independent coherent cells within each segment. Most of the segments contain 1-2 independent coherent cells, which are insufficient to significantly reduce the variability per segment. For these segments, the standard deviation remains before (gray envelope) and after stationary averaging (black error bars) per segment in Fig. 3-10 (green data points).

Case 2B sampling scenarios occur when CFFS transects through dense populations centers of large, contiguous shoals. For the Case 2B examples, the global mean OAWRS TS is found to be roughly -36 dB re $1m^2$. The mean estimated OAWRS TS per segment is shown to be consistently between 2-4 dB higher than the Case 1 mean of -40 dB in Fig. 3-10 (red data points). This is likely an overestimate in TS due to the scenario shown in Fig.3-9A. As with the Case 2A sampling scenarios, the limited number of continuous time-space corregistration points lead to an insufficient number of independent coherent cells to reduce the variability within each segment, and so the standard deviation per segment remained relatively unchanged after stationary averaging.

For large, contiguous OAWRS shoals, the last case examined corresponds to sam-

pling scenarios where CFFS traverses through the boundary or periphery region of larger, kilometer scale shoals, or Case 2C. Like the other Case 2 examples, CFFS measures small, singular groupings or a series of discrete clumps tens to a hundred meters in extent, resting in 5-10m layers off the ocean bottom. The mean estimated OAWRS TS per individual segments are typically between 5 to 15 dB lower than the Case 1 mean of -40 dB. When combining the estimated OAWRS TS values per segment, the global mean for the Case 2C examples is roughly -47 dB re $1m^2$ (gray dashed line in Fig. 3-10, blue diamonds), which is likely an underestimate of the kind shown in Fig.3-9B.

Finally, the last case examined corresponds to the sampling scenario where both OAWRS and CFFS simultaneously measure small, scattered populations or schools, or Case 3. These populations typically are observed as discrete, clumps of fish with along-transect range extens of tens of meters in the corresponding CFFS range-depth profiles. The small Case 3 populations can occur as compact, scattered schools or as satellite schooling populations comprising the background population surrounding larger shoals. The mean estimated OAWRS TS per individual segments for Case 3 scenarios is typically between 6-15dB lower than the Case 1 mean of -40 dB. When combining the estimated OAWRS TS values per segment, the global mean for the Case 3 examples is roughly -48 dB re $1m^2$ (gray dashed line in Fig. 3-10, orange diamond data points). This is likely another instance of an underestimate of the kind described in Fig.3-9B.

When the fish do not fully occupy the OAWRS areal footprint, vacancies within OAWRS footprint become important and can bias the OAWRS TS estimation by lowering the effective population density. This is due to the areal mismatch between both CFFS and OAWRS. A correction factor can be determined as the ratio of the expected area occupied by the CFFS-sampled fish population to the area occupied by the corresponding OAWRS resolution footprints. Careful analysis of CFFS and OAWRS imagery is necessary to determine this correction factor. After applying the correction factor, the corrected mean for the Case 2C and Case 3 scenarios are within less than 1 dB of the calibrated mean found in the Case 1 scenarios. The correction

factors for each Case 2C and Case 3 scenarios are described by the accompanying tables in Appendix B.

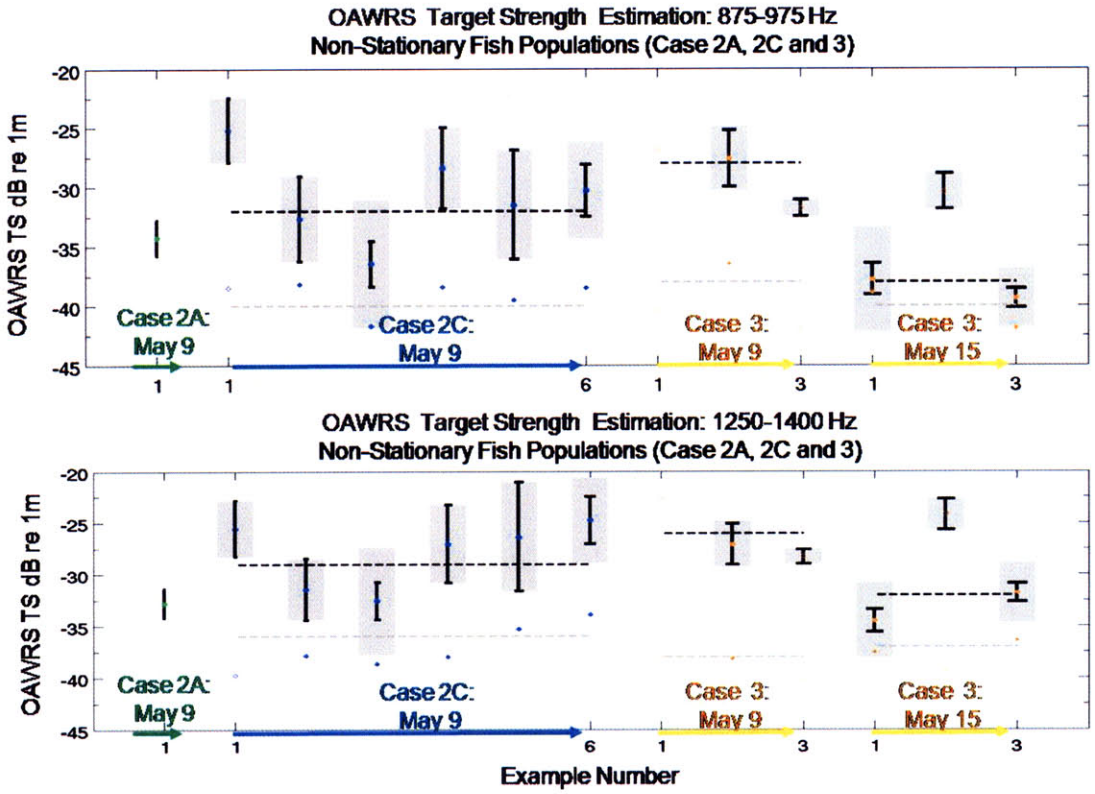

Frequency Band	Case 2A	Case 2C	Case 3	
			May 9	May 15
875-975 Hz	Mean: -34.4 dB	Corrected Mean: -31.9 dB	Corrected Mean: -28.2 dB	Corrected Mean: -38.1 dB
	—	Uncorrected Mean: -39.5 dB	Uncorrected Mean: -37.9 dB	Uncorrected Mean: -40.3 dB
1250-1400 Hz	Mean: 32.9 dB	Corrected Mean: -28.6 dB	Corrected Mean: -26.5 dB	Corrected Mean: -32.5 dB
	—	Uncorrected Mean: -36.5 dB	Uncorrected Mean: -38.1 dB	Uncorrected Mean: -36.5 dB

Figure 3-14: Summary of the OAWRS TS Estimation at 925 Hz and 1325 Hz for available OAWRS-CFFS sampling scenarios.

Unlike the measurements at the lower frequency band (415 Hz), there were only four tracks from 2 days that afforded co-registration with OAWRS imaged fish populations at the higer frequencies of 925 Hz and 1325 Hz. On May 9, there was one

instance where CFFS traverses through the diffuse, patchy region of a shoal, 6 instances where CFFS traverses through the periphery of a large shoal, and 3 instances where CFFS traverses through small, scattered fish schools. On May 15, there were only 3 instances in which CFFS traverses through small scattered schools. The results at these higher frequencies are presented in Fig. 3-14.

From Fig. 3-15, we note that the optimal scenario for estimating the OAWRS target strength corresponds to the Case 1 scenario. When we include all the data at 415Hz for each of the sampling scenarios, the mean OAWRS target strength is -39.7 dB re 1m with a standard deviation of 5 dB. This includes the corrected data for the Case 2C and Case 3 scenarios. The variability in the estimated OAWRS target strength can be reduced significantly when we restrict the analysis to Case 1 scenarios. To generate the red histogram in Fig. 3-15, we combine data from all Case 1 scenarios in Figs. 3-11 through 3-13. We apply stationary averaging over one coherent length per segment, as described in Table 3-1. This yields a total of roughly 180 independent Case 1 samples. The resulting histogram of the estimates per independent Case 1 sample is shown by the black histogram in Fig. 3-15. The mean after stationary averaging of the Case 1 scenarios is similar to the mean computed with all of the 415 Hz data. However, the standard deviation is reduced to 0.3 dB or less than a 10% error in estimated OAWRS TS. At the higher frequencies, the variability remains high due to insufficient samples to employ stationary averaging. By including data from non-stationary sampling scenarios, we introduce additional noise and variability into the OAWRS target strength estimation. For future experiments, sampling scenarios at-sea should be designed to concentrate on collecting data from multiple transects through large shoaling regions. Errors in estimated OAWRS target strength are smallest within large extended, stationary shoaling regions simultaneously sampled by CFFS and OAWRS.

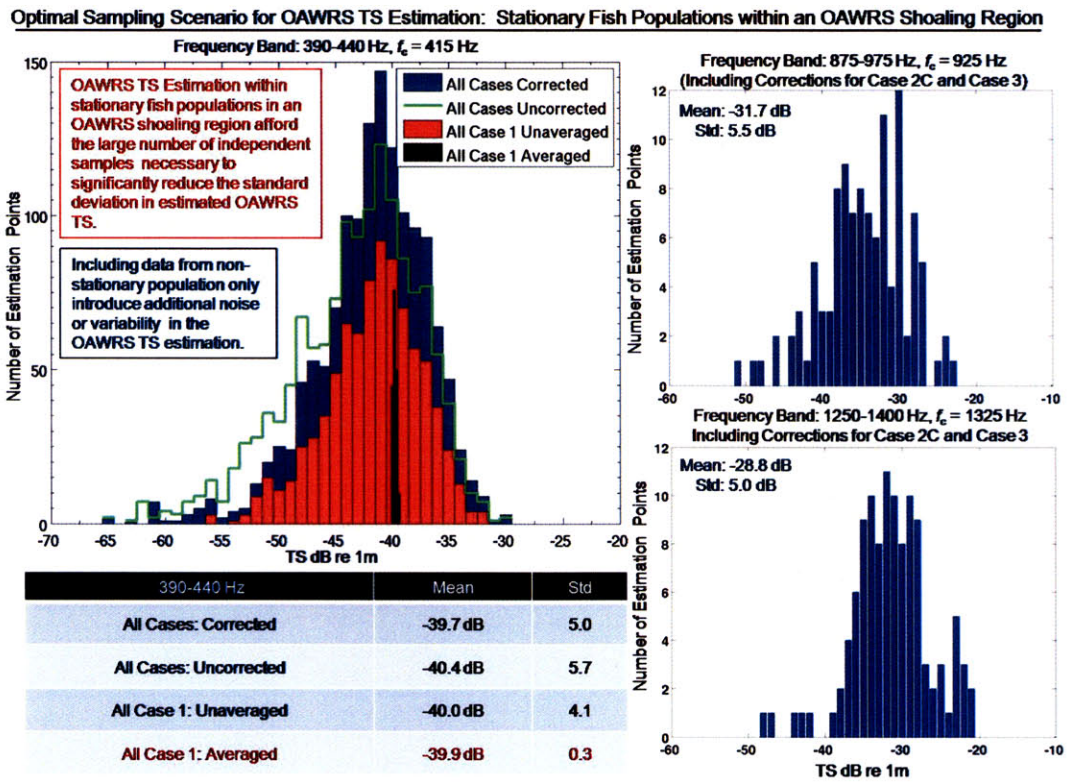

Figure 3-15: Case 1 scenarios afford the optimal scenario for estimating the OAWRS target strength. Including data from other sampling scenarios can only introduce variability, or additional noise, in the estimation. For the corrected and uncorrected 415 Hz histogram corresponding to all cases (blue and green respectively), there were 1400 individual co-registration points (roughly 400 independent samples) where OAWRS TS was estimated. For the 415 Hz Case 1 unaveraged histogram (red), there were approximately 800 individual co-registration points containing roughly 180 independent samples. The statistics for the 415 Hz Case 1 averaged histogram (black) was computed from 180 independent samples. For the 925 and 1325 data set, there were roughly 180 individual co-registration points (roughly 60 independent samples) where the OAWRS TS was computed.

Chapter 4

Fish Population and Behavior Revealed by Instantaneous Continental-Shelf Scale Imaging

We will now review work from N.C.Makris, P. Ratilal, D. Symonds, S. Jagannathan, S. Lee, R. Nero, "Fish population and behavior revealed by instantaneous continental-shelf scale imaging," Science, Volume 311, 660-663 (February 3,2006). As mentioned previously, continental shelf environments have been monitored with highly localized line-transect methods from slow-moving research vessels. These methods significantly undersample fish populations in time and space, leaving an incomplete and ambiguous record of abundance and behavior. We have shown previously in Chap.2 and Chap.3, that fish populations in continental shelf environments can be instantaneously imaged over thousands of square kilometers and continuously monitored by a remote sensing technique in which the ocean acts as an acoustic waveguide. Once we estimate the OAWRS target strength, we can directly estimate the OAWRS 2D areal population density distribution (Fig. 4-1) from the OAWRS scattering strength maps.

For an OAWRS 2D areal density image, the shoals are automatically segmented using a density threshold of 0.2 fish/m^2, of the fish shoaling density. Once the shoals are segmented, the area can be numerically computed by the area bounded by the shoal contours and the population can be determined by integrating the density over

the shoal area. Additionally, the center of density can be computed per ping and the velocity of the centroid can be tracked as a function of time. The relative speed is computed by tracking the difference in speed between two or more shoal centroids.

Using the OAWRS 2D areal density maps and such morphological and dynamics information, we will show how this novel remote-sensing technique can be used to reveal information about the instantaneous horizontal structural characteristics and behavior of very large fish shoals, containing tens of millions of fish and stretching for many kilometers.

The synoptic spatial sampling and fine temporal resolution of OAWRS makes it possible to continuously monitor fish population dynamics, behavior, and abundance, with minute-to-minute updates over thousands of square kilometers, producing records without aliasing [88, 33] in time and space. Key observations by OAWRS in 2003 include (i) instantaneous horizontal structural characteristics, (ii) temporal evolution, and (iii) the propagation of information in very large fish shoals, containing tens of millions of fish and extending for many kilometers. All of these observations were made from distances that were typically greater than 10 km from the shoal boundaries and with sound that was at least three orders of magnitude less intense than conventional fish-finding sonar.

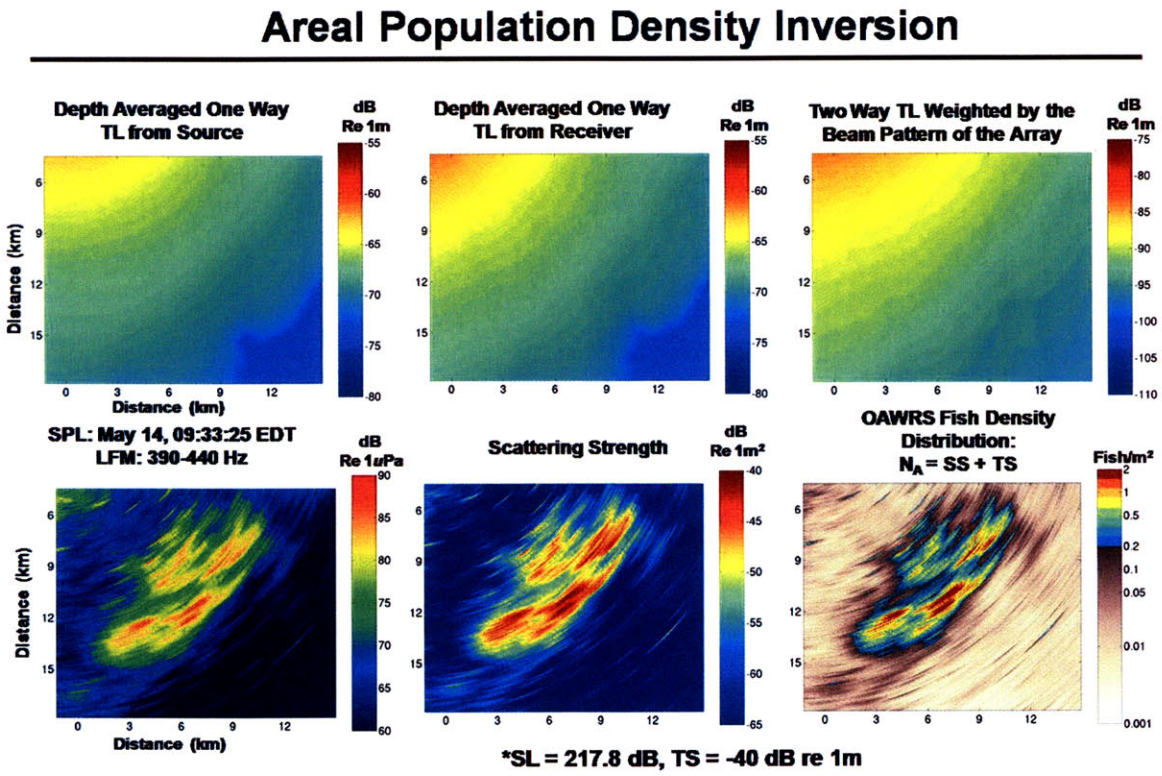

Figure 4-1: Areal fish density maps can be generated by scaling the OAWRS Scattering Strength by the calibrated target strength from an individual fish. The calibrated OAWRS target strength at 415Hz for this example is -40 dB re 1m.

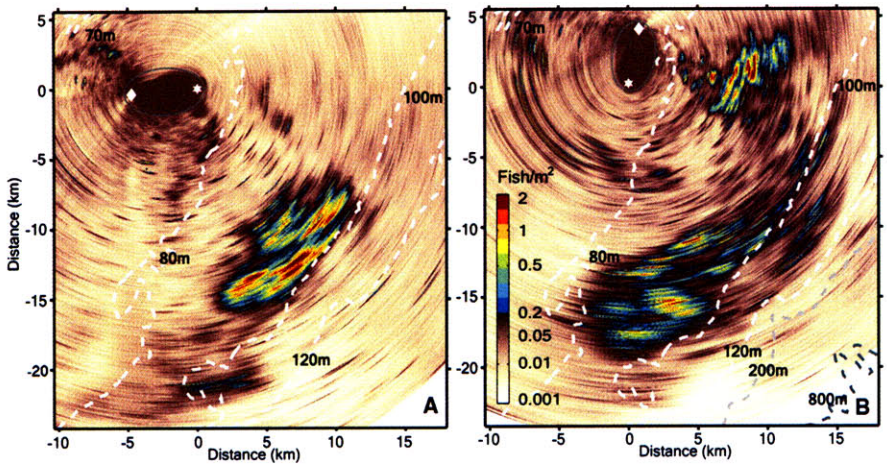

Figure 4-2: Two instantaneous areal density images of fish shoals near the continental shelf edge obtained by ocean acoustic waveguide remote sensing (OAWRS) at (A) 09:32 EDT, 14 May 2003, and (B) 08:38 EDT, 15 May 2003, each acquired within 40 s. nuA is shown in color. The moored source (the white star) is the coordinate origin in all figures at 39.0563N, 73.0365W. The towed horizontal receiving array (the white diamond) has 2.6 azimuthal resolution at array broadside. The range resolution is 30 m after averaging. The forward propagation of sound masks imaging inside the gray ellipse surrounding the source and receiver. The positive vertical axis points north. Depth contours are indicated by dashed lines. In (A) and (B), the continental shelf edge begins at roughly the 100-m contour.

Typical realizations of the instantaneous horizontal structure of very large fish shoals, comprising perhaps the largest massing of animals ever instantaneously imaged in nature, are shown in A and B of Fig. 4-2. We found population centers of various size, interconnected by a network of "fish bridges" at various scales. These made the shoal shown in Fig. 4-2A a contiguous entity that stretched for over 10 km. A similar situation is seen in the very large southern and smaller northern shoal of Fig. 4-2B. All shoals exhibit large internal vacuoles and hourglass patterns previously observed only in fish groups that were many orders of magnitude smaller in area [44, 79, 78] . The shoals are often very sharply bounded on the seaward side by a specific bathymetric contour of the continental shelf edge, as in Fig. 4-2A. This geophysical boundary apparently organizes the shoal horizontally as a social entity and may also be a navigational landmark for distant migrations [84, 56]. Although

we found all large shoals between roughly the 80- to 100-m bathymetric contour, fish assemblages changed dramatically over time in any given region, as shown in Fig. 4-2 from one morning (A) to the next (B). The overall background population, for example, increases significantly from Fig. 4-2 A to B, with a dense distribution of very small groups of fish appearing between the very large southern shoal and the smaller northern one. Under some circumstances, these may provide the building blocks for the fish bridges that bind a shoal together. Annual trawl surveys conducted earlier in the season and historically [87], as well as our visual and behavioral observations at sea, indicate that Atlantic herring, scup, hake, and black sea bass are likely species candidates in the large shoals. An detailed analysis of the 2003 annual spring data is discussed further in the Appendix section of this thesis.

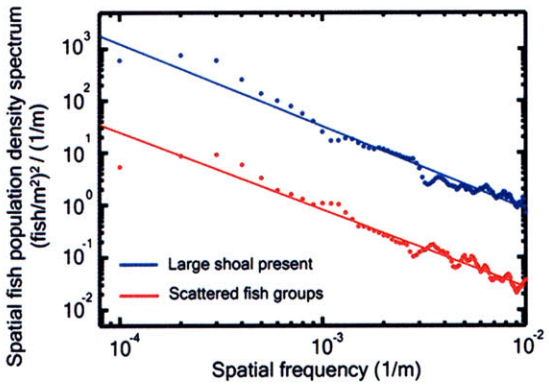

Figure 4-3: Spatial frequency spectra, based on scores of instantaneous OAWRS images of ν_A, for cases where a large shoal is present and only small scattered fish groups are present. A consistent spectral power law of spatial frequency to the -1.46 is observed

The instantaneous horizontal spatial distribution of fish over wide areas follows a fractal or power-law spectral process, as quantitatively shown in Fig. 4-3. To generate the spatial power spectrum, the 2-D Fourier transform of an instantaneous OAWRS areal fish density image was computed. Squared magnitudes of 2-D transforms of 10 consecutive OAWRS images, over an 8 minute period, were combined by standard periodigram averaging to obtain an estimate of the 2-D spectrum of areal population density. This estimated spectrum corresponds to the Fourier transform of the 2-

D autocorrelation function of areal fish population density, normalized so that the correlation at zero-spatial lag, which is the integral of the 2-D spectrum, is the second statistical moment of areal population density. Apart from expected asymmetries arising from variations in the range and cross-range resolution of our imaging system, the resulting 2-D spectra showed uniform azimuthal dependence in wavenumber which was repeatable throughout all our observations of the shoals and scattered fish groups regardless of their orientation with respect to our measurement system. The radial wavenumber dependence of the spectrum was then estimated by averaging within a roughly 20° azimuthal wavenumber spread where the resolution of our imaging system is highest. Two periods were chosen, one at 16:19 EST of May 14 with a very large shoal present and the other at 21:30 EST of May 9 with only small scattered groups present. The 2-D spectrum was then multiplied by radial wavenumber and normalized so that the 1-D integral over spatial frequency, or radial wavenumber, of either curve plotted in Fig. 4-3 yields the mean of the square of areal fish density over the survey area. The power laws shown were obtained by least squares fits. These results are very stable. They were repeated 4 times at uniform intervals: on May 14 from 9:34 EST to 17:02 EST, leading a mean power law of -1.55 with a 0.04 standard deviation, and on May 9, from 17:10 EST to 17:50 EST leading to a mean power law of -1.46 with a 0.03 standard deviation.

Instantaneous structural similarity then exists at all scales observed, from tens of meters to tens of kilometers, and suggests that similar underlying behavioral mechanisms may be responsible for structures at all scales. This supports the qualitative argument for a fractal process in [44] but not the disjoint clustering of population centers that is perhaps implied there. The power law is invariant to the size of the largest fish group present, and so remains constant if an area contains a very large shoal or only much smaller scattered groups of fish, as shown in Fig. 4-3. Our observations that very large shoals are structurally similar to much smaller fish groups must be a consequence of the power law. Knowledge of this power law now enables more accurate statistical predictions of the instantaneous spatial distribution of fish populations over wide areas.

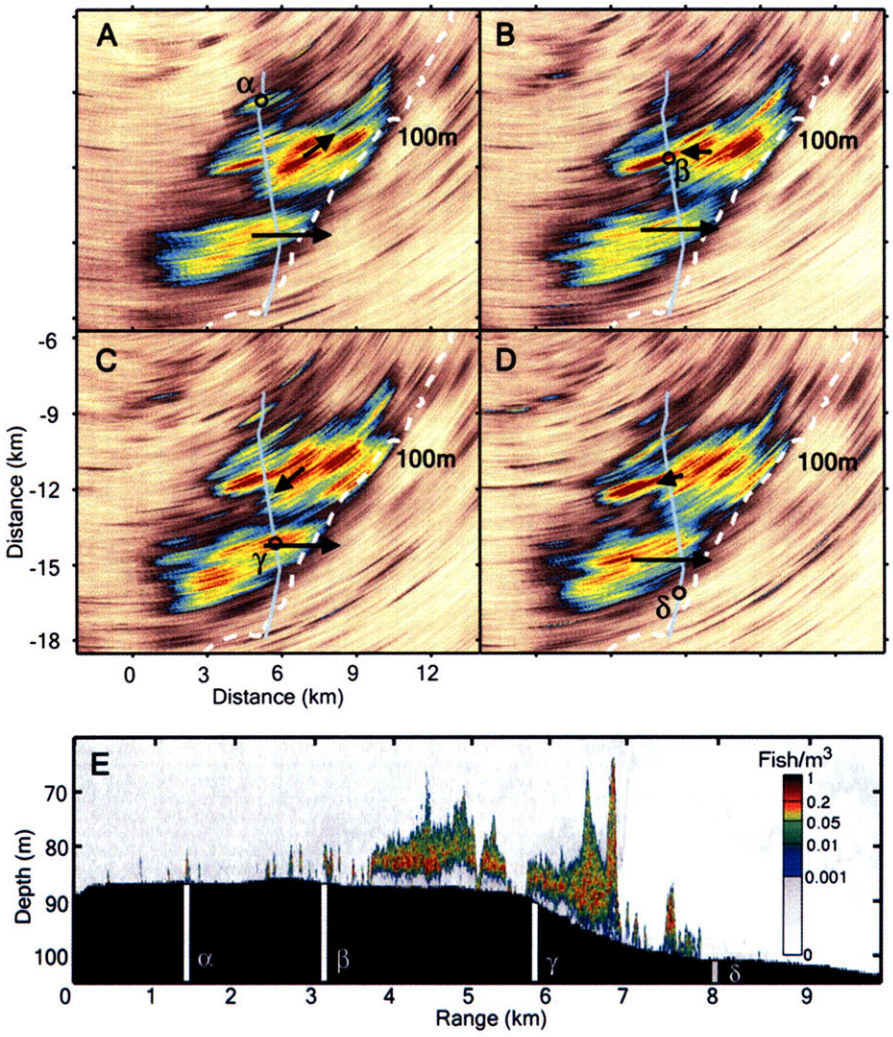

Figure 4-4: A comparison of OAWRS with conventional fish-finding sonar (CFFS). (A to D) A sequence of instantaneous OAWRS areal density (fish/m^2) images taken roughly 10 min apart, starting at 11:59:05 EDT on 14 May 2003, is shown. The corresponding CFFS transect is overlain in light blue, with the CFFS position for the given OAWRS image indicated by a circle. The white dashed line is the 100-m depth contour. (E) Range-depth profile of fish volumetric density (fish/m^3) measured by CFFS along the transect shown in (A) to (D). White bars (in the lower black region below the sea floor) correspond to typical time-space points α, β, and γ, where both systems co-register dense fish groups [(A) to (C)]; the gray bar corresponds to point δ in (D), where neither system registers dense fish groups.

Simultaneous measurements from both the conventional and the waveguide remote-sensing systems show excellent agreement in fish population density at identical time-space points along the conventional line transect (light blue line in Fig. 4-4, A to D), but only the waveguide technology senses two-dimensional (2D) horizontal structure and temporal change. Both systems reveal dense populations of fish at time-space points α, β, and γ, and neither system registers fish at δ beyond the shoal's seaward edge. The sharp and extensive 2D horizontal boundary of the shoal seen with the waveguide technology along the shelf edge in Figs. 4-2A and 4-4, A to D, is too transitory to be inferred from or practically measured with conventional line-transect methods, even from a series of transects. Nor can the conventional system detect or recognize the network of interconnecting bridges between population centers that waveguide technology has shown to be part of the fundamental structure of shoals. For example, the large but transitory bridge connecting the northern and southern wings of the shoal in Fig. 4-4, A to D, gives it a classic hourglass pattern, never previously observed over such a large scale. This is missed by the conventional line-transect method (Fig. 4-4E), which provides no evidence that fish in the γ group are actually well connected to those previously imaged in the β group or occasionally in the α group as well.

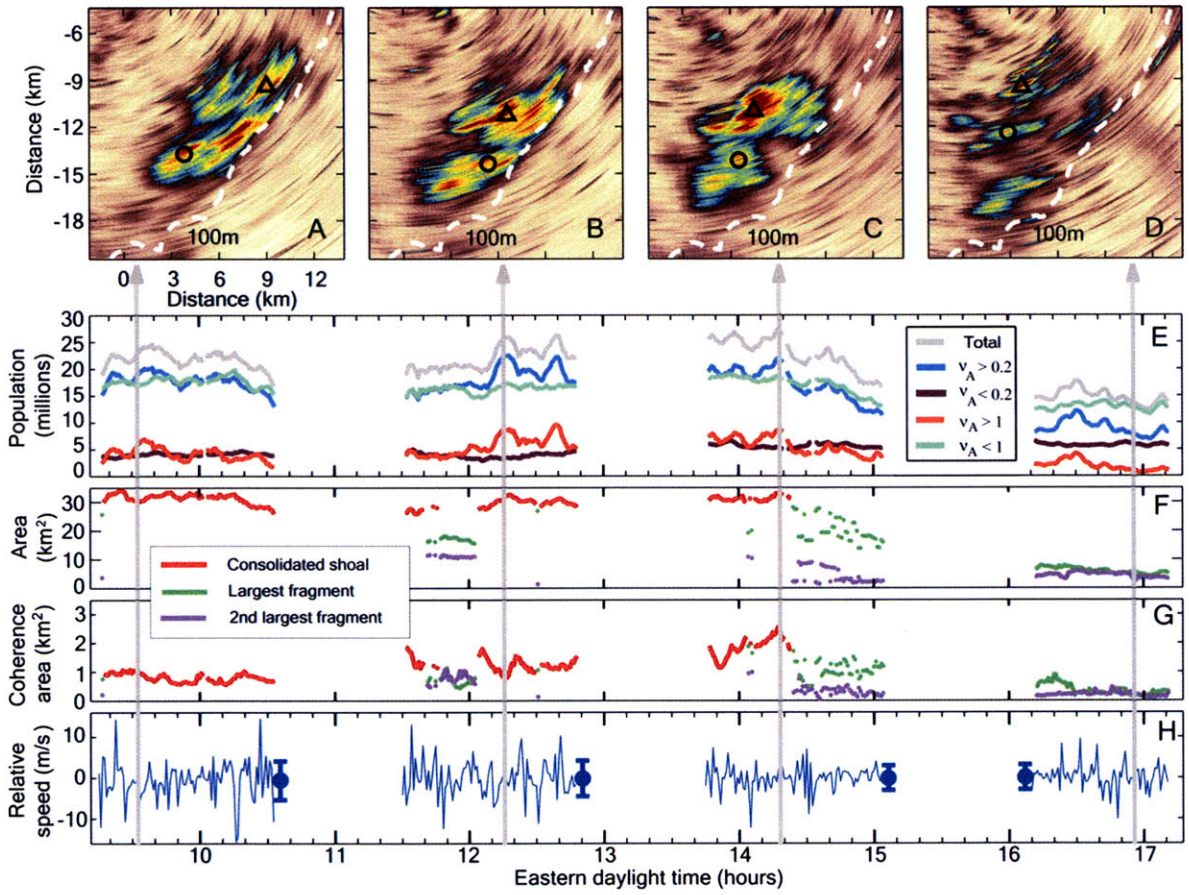

Figure 4-5: Evolution of a fish shoal from morning to evening from OAWRS imagery and a time series on 14 May 2003. (A to D) Four instantaneous OAWRS images or snapshots illustrating morning consolidation and afternoon fragmentation of the shoal. The color bar is the same as in 4-2. Vertical arrows indicate snapshot times. (E) A time series of population within the area shown in (A) to (D) for nuA within each of the thresholds specified. Gaps in the time series are due to towed-array turns. (F) Area occupied by a consolidated shoal or its two largest fragments for $\nu_A > \nu_{shoal} = 0.2 fish/m^2$. (G) The internal coherence area is the area within 1/e of the 2D autocorrelation peak of instantaneous OAWRS fish density within the shoal or fragment. The centroids of two particular population centers within the shoal are indicated by the circle and the triangle in (A) to (D). (H) Relative speeds between the centroids of the two population centers shown in (A) to (D), with mean (blue circle) and standard deviation (bars) shown for each track.

We noticed a daily pattern in shoal behavior that involved considerable horizontal migration and thus differed substantially from the day-to-night vertical migrations previously observed with downward-directed sonar in line transects [1, 7]. The pattern, observed consistently on days where we could monitor large shoals over all daylight hours, began with the horizontal consolidation of shoals in the morning, typically organized by a sharp seaward edge extending for kilometers along a bathymetric contour of the continental shelf edge. Rapid fragmentation and dispersal followed by mid-afternoon, well before sunset when vertical migration began, as shown in Fig. 4-5, A to D, between 14:20 and 15:00 eastern daylight time (EDT). Fragmentation predictably began with faulting at the bridges between population centers. The bridges were apparently not sufficiently strong to withstand the internal or external pressures to diverge that acted on the shoal's internal population centers.

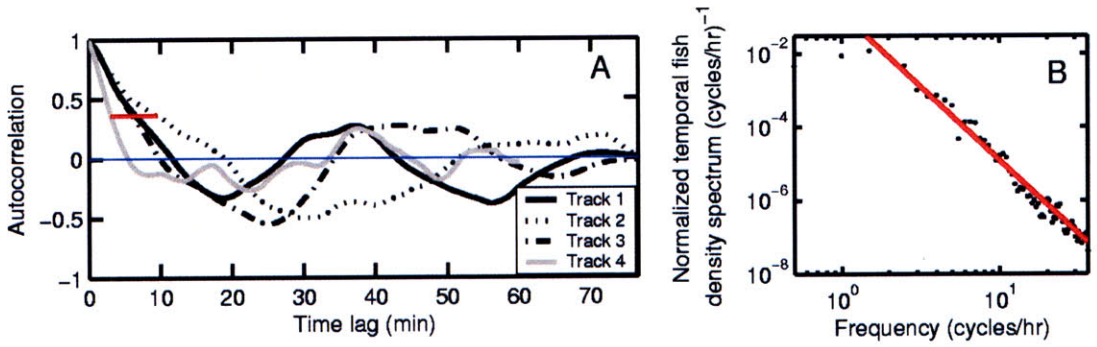

Figure 4-6: Autocorrelation function of the population time series, with red horizontal line indicating the e-folding times (A) and Frequency power spectrum with the frequency to the -2 dependence for the shoal population time series (blue curve in Fig. 4-5

To describe this behavior quantitatively, time series of changing fish population (Fig. 4-5E) were computed at very high sample rates (50-s intervals) from imagery acquired with the waveguide technology over the hundreds of square kilometers immediately encompassing the shoal. We find that total fish population (gray curve of Fig. 4-5E) decomposes into the sum of a temporally stable (brown curve of Fig. 4-5E) and a temporally unstable (blue curve of Fig. 4-5E) time series. The same

areal fish density (ν_A) threshold (0.2 fish/m2) that separates the temporally stable from the unstable population is also extremely effective in spatially segmenting large shoals from smaller background groups in our instantaneous wide-area images (Figs. 4-2; 4-4, A to D; and 4-5, A to D). The stable component comprises the widely scattered fish groups that would form the observable background scene in the absence of a large shoal. The temporally unstable component effectively characterizes the dramatically dynamic spatial-temporal fluctuations of the large shoal. We believe that fluctuations in total population are primarily due to convergences and divergences in ν_A values above and below another threshold [minimum detectable fish density (ν_0) = 0.01 fish/m2] where seafloor scattering mechanisms begin to become important and mask fish imaging [61, 35, 60, 64, 82] . They may also arise from fish groups entering and leaving the survey box.

Time series enable us to introduce the concept of an autocorrelation [45] time scale to quantitatively characterize major temporal fluctuations in shoal population. This time scale was computed by taking the autocorrelation function of the total population time series for each track on May 14. The time scale corresponds to the e-folding length from the peak of the autocorrelation function at zero-time lag. We find that the autocorrelation time scale ranges between 5 and 10 minutes. Note that the time scales of major population change are much longer than the OAWRS 50-second transmission interval; making the OAWRS system capable of capturing such fluctuations without temporal aliasing.

Shoal population (blue curve in Fig. 4-5E) can fluctuate dramatically in these short time scales, by 20% or a few million fish. These fluctuations are consistent with the roughly 1 m/s speed at which fish in a shoal typically swim [48, 34, 24], as seen from the corresponding areal changes in Fig. 4-5F. The frequency spectrum of shoal population (Fig. 4-6B) shows no remarkable periodicity, but like the spatial spectrum follows a consistent power-law process that now enables quantitative statistical predictions of temporal behavior over wide areas and short time scales.

Shoal fragmentation and dispersal also occur very rapidly, as shown in Fig. 4-5E, where total population plummets in a 30-min period beginning at 14:20 EDT. More

than 10 million fish disperse to below the ν_0 threshold or leave the survey box. The remaining shoal fragments contain less than half the original shoal population. This and other remotely observed depopulation events were episodic, with peak dispersal rates reaching up to 0.5 million fish/min. Indeed, very large fish shoals were often lost from the view of our conventional line-transect survey system but not from the simultaneous view of our remote-sensing system based on waveguide technology.

Structural similarity can be reexamined in a time-space context by comparing time series of a shoal's outer area (Fig. 4-5F) to its characteristic internal area of coherence (Fig. 4-5G), which is the area within which population density is relatively constant. The coherence area of Fig. 4-5G is found by taking the 2-D fish density autocorrelation function of a particular shoal or shoal segment and computing the area bound by the contour within one e-folding length from the peak at zero-lag.This coherence area is a quantitative way of describing the extent of concentrated centers within the shoal. It is also the area within which the population density should not vary significantly and can be used to determine the number independent cells or populations within a shoal.

The ratio of the shoal's outer area to its internal coherence area gives an estimate of the number of "degrees of freedom", the independent coherence cells [45, 10, 41, 82, 60] or primary population centers within the shoal or within its largest shoal fragment. The fact that this ratio remains relatively constant over time even after the shoal undergoes severe fragmentation and dispersal is further evidence of structural similarity at all spatial scales, even during such dramatic events, which is consistent with fish assembly and reassembly models [22]. Fluctuations in the shoal's outer area tend to span only a small percentage of the total area. This is true for the inner area only during periods when the shoal is not undergoing fragmentation. Otherwise, the inner area fluctuates rapidly, reflecting an internal turbulence that probably initiates fragmentation in shoals.

The waveguide technology has also revealed the internal motion and migration patterns within very large fish shoals, during time spans ranging from less than 1 min to days, as shown in the imagery sequence of Fig. 4-4, A to D. Fundamental

questions that depend on knowing "the degree of coordination in the movements" between fish populations that were previously "nearly impossible to detect" [70] can now be addressed. We show that even when very large shoals are highly consolidated, densely packed, and structurally similar to small groups of fish, they do not exhibit synchronized motion over short time scales, as much smaller groups often do [79, 78]. The many interconnected population centers within a very large shoal have centroids that undergo local positional oscillations in the horizontal, over time scales on the order of minutes, which have no correlation with each other. This is illustrated by the image sequence of Fig. 4-4, A to D, where velocity vectors for two centroids within the very large shoal are effectively uncorrelated in time and space.

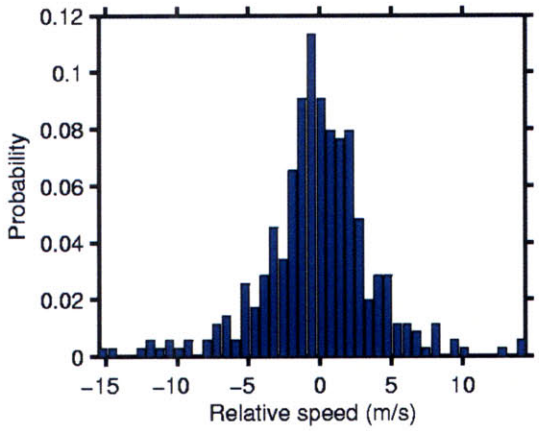

Figure 4-7: Histogram of all relative speeds between shoal centers.

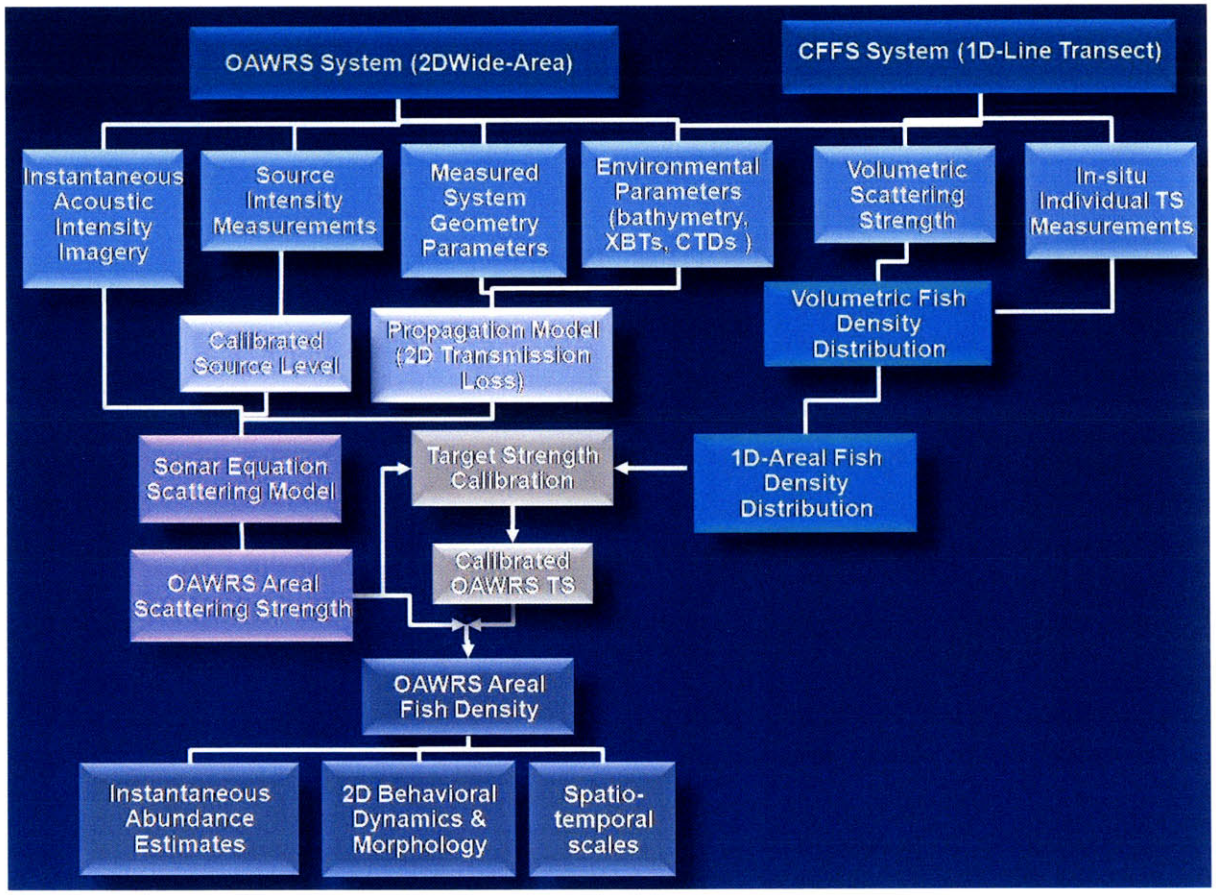

Figure 4-8: Flow chart of the post-processing analysis for the 2003 survey of the New Jersey Continental Shelf. This flowchart summarizes the measuring capabilities of the OAWRS and CFFS systems and how the measurements from both systems were used to estimate fish population and reveal fish behavior over continental-shelf scale areas.

Chapter 5

Conclusion

In this thesis, we reviewed the first demonstration of OAWRS to instantaneously image and continuously monitor population and behavior of shoaling fish populations during April- May 2003 off the US Continental Shelf south of Long Island, NY. With a single transmission, OAWRS is able to survey an area with diameter of roughly 60 km in less than 40 s and 120 km in less than 80 s depending on the ping repetition rate. This single-ping areal coverage is on the order of a typical US east coast state such as Connecticut or New Jersey. It is effectively instantaneous because the entire region is surveyed within a time scale much smaller than the time it takes fish to traverse a single OAWRS resolution cell.

With proper calibration within statistically stationary populations, OAWRS can make very accurate population density estimates. For example, over regions where fish populations are statistically stationary in measured OAWRS scattering strength and measured CFFS scattering strength, OAWRS 2003 instantaneous population density estimates had uncertainties of less than 1 dB (or 25%) at each pixel or spatial resolution cell [32, 33]. These population density estimates depend on the expected scattering cross section of an individual fish, which is empirically calibrated for using thousands of local measurements of population density by CFFS. Given stationary samples, instantaneous abundance estimates should have uncertainties of much less than 25% by the law of large numbers [42, 32, 33]. This should hold within larger shoaling regions where OAWRS population density is integrated over tens to hun-

dreds of independent OAWRS resolution cells or samples of a roughly homogenous or stationary population. Large shoaling regions often make the dominant contribution to total population and estimation error, but this error becomes easier to model through the central limit theorem [42, 32, 33].

Appendix A

Materials and Methods for Generating OAWRS 2D Scattering Strength Maps

In this section, we detail the procedure for computing the 2D areal maps of two-way transmission loss and OAWRS scattering strength as shown in the illustrative example in Fig. 3-2. We briefly discuss the source level calibration used to obtain daily estimates of the expected intensity for the different OAWRS operating bands, as well as spatio-temporal averaging of the OAWRS measured acoustic intensity to further reduce fluctuations in the data for the OAWRS target strength calibration. for in source power modelled parameters and actual measurement data to obtain the calibrated OAWRS TS.

A.1 TL Modelling at OAWRS operating frequencies

In this section, we present an illustrative example for modelling the range-dependent, waveguide Green's funtion in the New Jersey Continental Shelf environment. For this illustrative example, we describe the environmental and source-receiver geom-

etry parameters that are inputs to the parabolic equation modelling. Additionally, we show that the one-way transmission loss from the source and to the receiver can be approximated by the depth-averaged, center-frequency one-way transmission loss for this particular environment since the measured sound speed structure during MAE03 did not support significant channeling. For other environments where upper-water column channeling could be an issue, the choice of depth-averaging layer and frequency-averaging band can contribute significantly to the accurate modelling of the transmission loss.

Environmental and OAWRS Geometry Parameters

A number of environmental and OAWRS geometry inputs are necessary to model the transmission loss. These parameters were either measured simultaneously during the OAWRS 2003 survey or come from historical measurements. Previous geophysical surveys in the vicinity of the 2003 survey area provide characterization of the bathymetry, sub-bottom morphology, and sediment composition **??**. Typical water depths range between 70-100m at primary OAWRS survey sites (Site 1 and 2), as shown in Fig. A-1. Although the water depths at Site 3 were roughly twice that at Site 1 and 2, only one experimental day was dedicated surveying this location. The seafloor has an extremely benign slope, typically less than 1°, as can be seen in Fig. 4 of [82]. Historical bottom core samples identify the bottom sediment composition as a mixture of sand and silt with density of 1.9g/cm^3, attenuation coeffiecient of 0.8 dB/λ and mean sound speed of 1700 m/s [82].

During the OAWRS 2003 survey, XBT's on the receiver ship were used to measure the sound speed profiles at the beginning and end of each track. The measured sound speed profiles were averaged to compute a daily mean sound speed structure, as shown in Fig. A-2. Daily measures of OAWRS source depth, receiver depth and receiver array orientation were recorded throughout the 2003 field experiment. The source depth was recorded at the beginning of each day during morning deployment. Adjustments to the source depth were also recorded. The source depths used for the modelling were taken from p. 43 of Ref(Cruise Report). Pressure sensors embedded

in the OAWRS receiver array depth recorded the receiver depth at the center of the array for each OAWRS transmission. The mean receiver depth for each OAWRS frequency band was used for the transmission loss modelling since the depth variations were typically less than 3m over an entire experimental day, as illustrated in Fig. A-3 and Fig. A-4. Gyroscope sensors, also embedded in the receiver array, recorded the array heading for each transmission and array orientation fluctuations were found to vary between 1-2° during the duration of an OAWRS track. The exact array heading per transmission is used when weighting the two-way transmission loss maps by the beam-pattern of the OAWRS receiver array.

Areal Transmission Loss Maps at OAWRS operating frequencies

In this section, we present various scenarios for computing the one-way transmission loss from the OAWRS source array and from the OAWRS reveiver array at the three OAWRS operating frequency bands: 390-440Hz, 875-975Hz, and 1250-1400Hz. The center-frequncy, transmission loss profile computed with the average, measured sound speed profile is compared with the: (i) broad-band transmission loss computed with the mean sound speed profile one-way transmission loss and (ii) the average transmission loss computed using Monte Carlo simulations that have varying sound speed profiles as a function of range (every 250 m). The Monte Carlo simulation approach is similar to that used by Andrews et al in [29] when modelling the one-way transmission loss to estimate the expected source intensity. The center-frequency, one-way, depth-averaged transmission loss computed using the mean sound speed profile for each experimental day was found to be a good approximation (to within 1dB) to the broad-band, transmission loss averaged over the water column computed via Monte Carlo simulations. The one-way transmission loss from the source and receiver positions are computed over the 360-degree radials (with the angular separation between radials equal to the broadside resolution of the array), spanning the area surveyed by OAWRS, for each transmission. The two-way transmission loss is then weighted by the beampattern of the array to account for the spatially-varying OAWRS resolution footprint.

A.2 OAWRS SL Calibration

The temporally and spatially varying nature of the ocean environment causes acoustically transmitted signals to get randomized. A statistical approach that incorporates fluctuations in the source transmission due to medium uncertainties is necessary to accurately model the scattered field from the ocean environment.

Although daily measurements of the on-axis source level were made at-sea during routine transmissions at 400 Hz and 950 Hz [66], there were no measurements of the source level at the highest transmission band (1250-1400). Additionally, the at-sea measurements were taken roughly once or twice per experiment day and were not taken frequent enough to quantify fluctuation trends in source intensity and accurately estimate the average source intensity for each waveform transmitted on each experiment day.

To verify the sparse measures of SL and to obtain source levels for the highest frequency band, broadband measurements of the acoustic intensity of the direct arrival by a desensitized phone on the receiving array were used to calibrate for the expected source level at each transmitted frequency band per experiment day. The match filtered data are compared to the expected TL output from a parabolic equation model that accounts for bathymetric variations. A maximum likelihood estimator is implemeted to provide a global inversion of the data for the expected source level for each experimental day [29]. Roughly 200-600 independent measurements of the direct arrival were used to compute the daily average of the source intensity.

A.3 OAWRS Measurementsof Acoustic Intensity

First, the endfire noise from the OAWRS receiver ship, as well as ship noise from other vessels operating in the vicinity are removed from the OAWRS instantaneous acoustic intensity maps. Then the instantaneous acoustic maps are incoherently averaged in time over five consecutive single ping transmissions to reduce the variability over time. Each individual acoustic intensity map generated from the 390-440 Hz transmission

band (1-5 in the sequence) is also spatially average in range over two adjacent range cells, yielding a pixel resolution equal to 30m. The standard deviation per spatial pixel due to waveguide randomness and acoustic signal fluctuations are expected then to reduced by $\frac{1}{\sqrt{10}}$ for the low frequency data set.

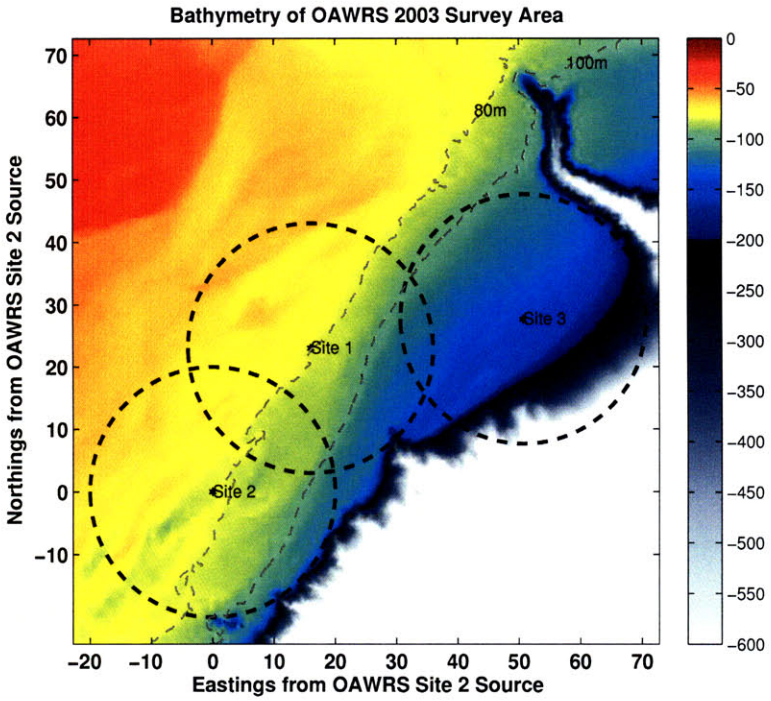

Figure A-1: The bathymetry on the New Jersey continental Shelf is shown with the black circles delimiting the three different areas surveyed by OAWRS in 2003. Both Site 1 and Site 2 sample water with typical water depths ranging between 70-100m. The Site 3 survey area encompasses in deeper waters along the continental shelf slope, with typical water depths exceeding 150m.

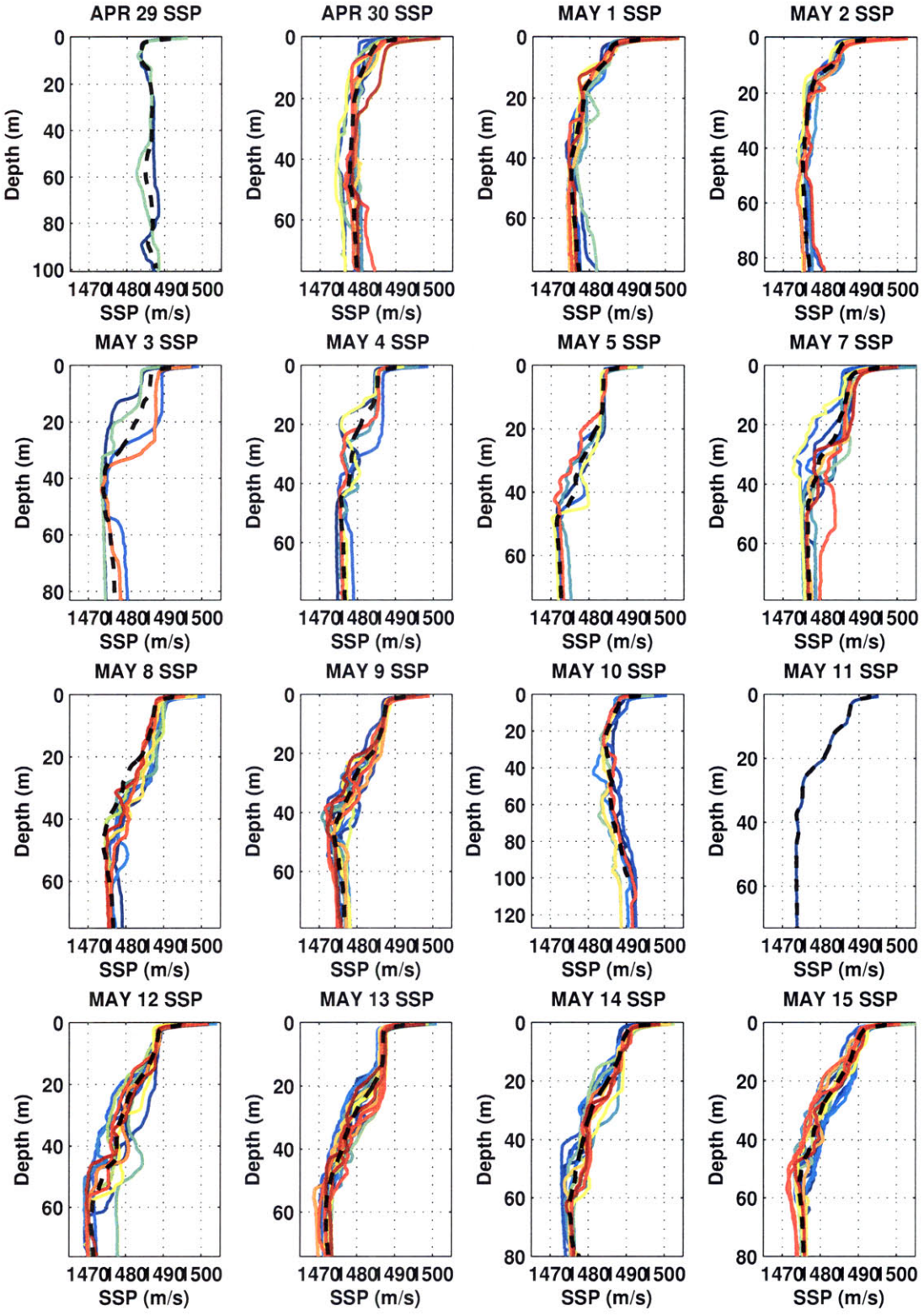

Figure A-2: Summary of the measured sound speed profiles for each experimental day. The daily mean (black dashed line), computed by averaging the measured sound speed profiles, is also shown.

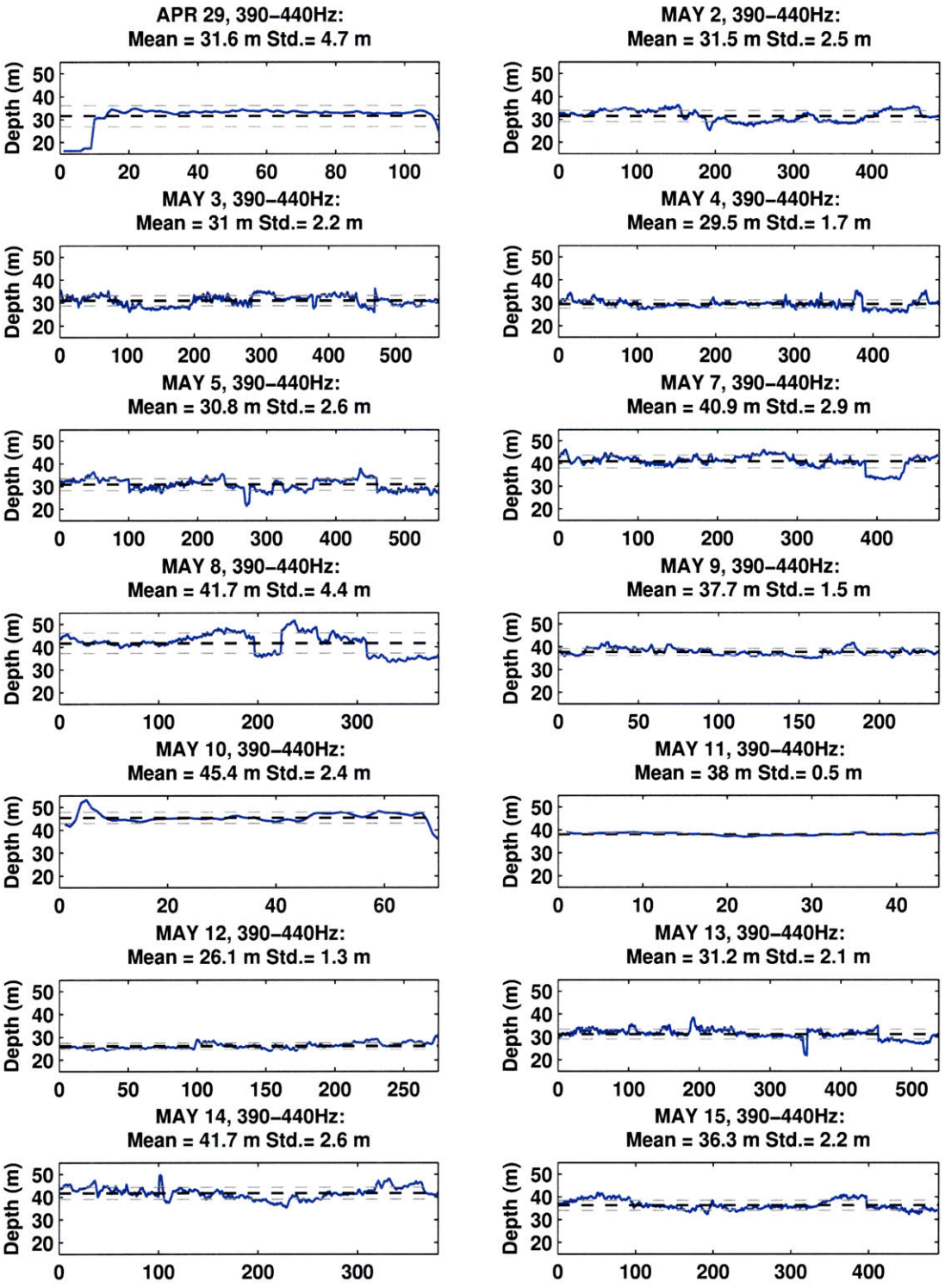

Figure A-3: Summary of the array depth at the center of the OAWRS receiver array for all WX1 (390-440Hz) transmissions on each experimental day. The mean (black line) and standard deviations (gray line) are also shown and reported. The daily standard deviation of the receiver depth was typically less 3m.

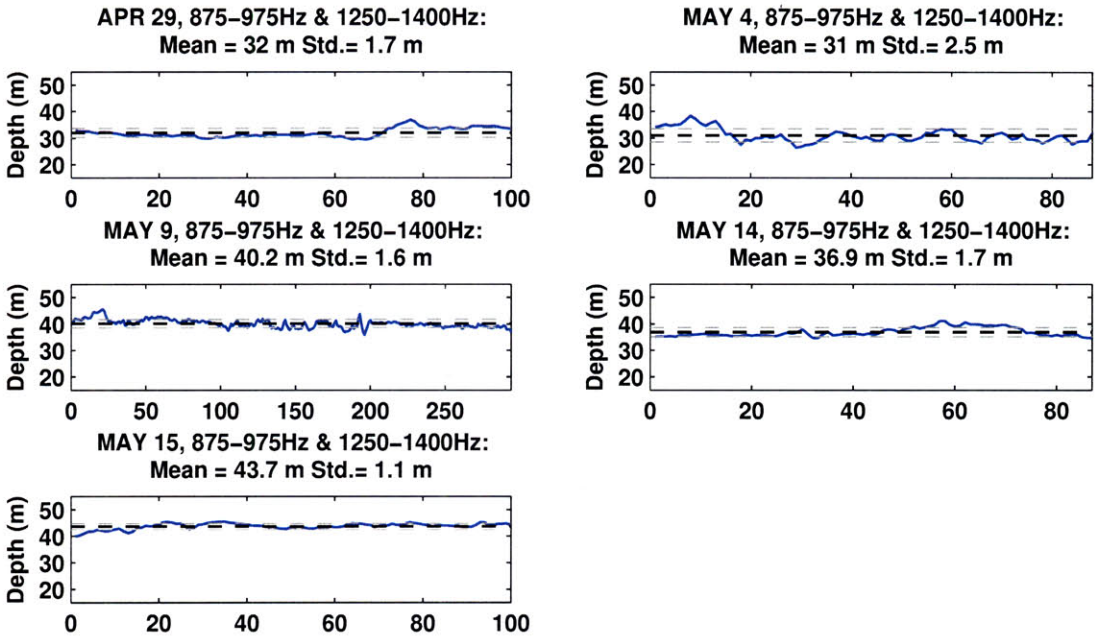

Figure A-4: Summary of the array depth at the center of the OAWRS receiver array for the simultaneous WMA (875-975Hz) and WMB (1250-1400Hz) transmissions on each experimental day. The mean (black line) and standard deviations (gray line) are also shown and reported. The daily standard deviation of the receiver depth was typically less 3m.

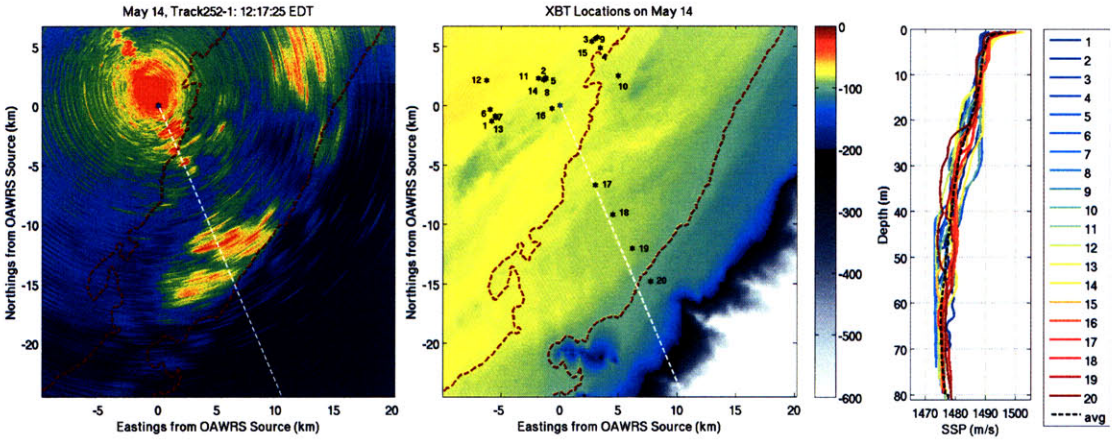

Figure A-5:

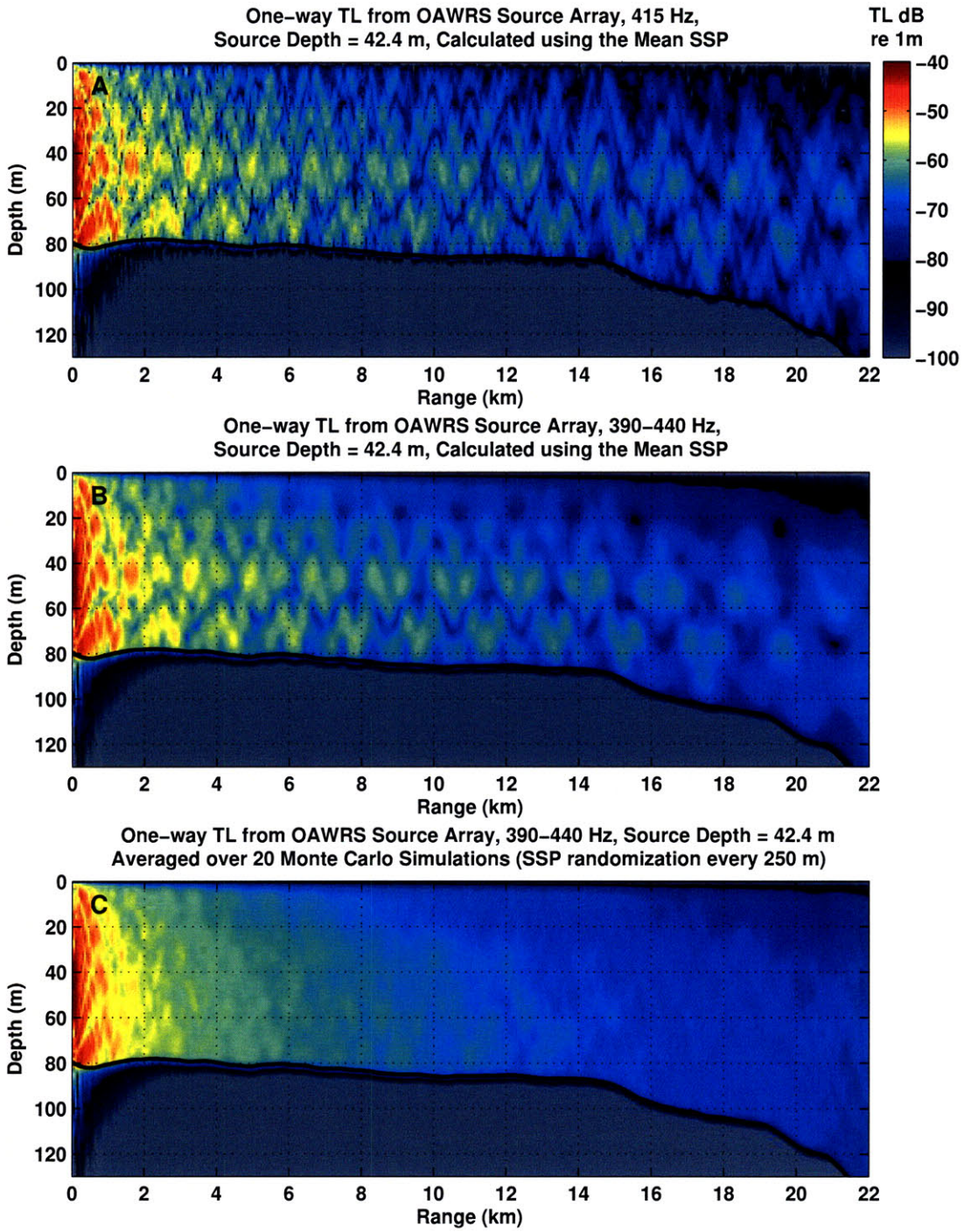
One–way TL from OAWRS Source Array, 415 Hz,
Source Depth = 42.4 m, Calculated using the Mean SSP
TL dB
re 1m
A
Depth (m)
Range (km)
One–way TL from OAWRS Source Array, 390–440 Hz,
Source Depth = 42.4 m, Calculated using the Mean SSP
B
Depth (m)
Range (km)
One–way TL from OAWRS Source Array, 390–440 Hz, Source Depth = 42.4 m
Averaged over 20 Monte Carlo Simulations (SSP randomization every 250 m)
C
Depth (m)
Range (km)

Figure A-6:

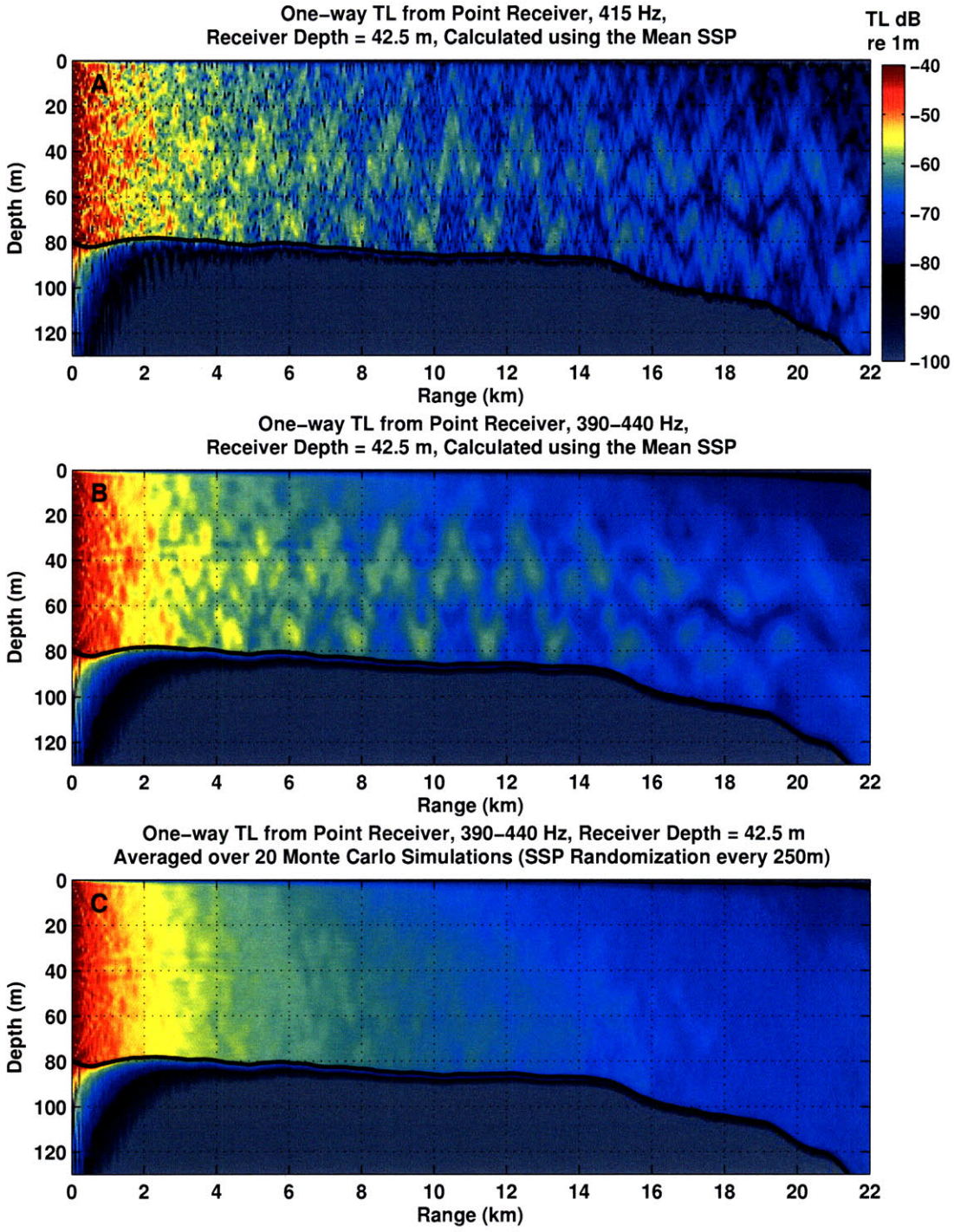
One–way TL from Point Receiver, 415 Hz,
Receiver Depth = 42.5 m, Calculated using the Mean SSP
TL dB
re 1m
A
Depth (m)
Range (km)
One–way TL from Point Receiver, 390–440 Hz,
Receiver Depth = 42.5 m, Calculated using the Mean SSP
B
Depth (m)
Range (km)
One–way TL from Point Receiver, 390–440 Hz, Receiver Depth = 42.5 m
Averaged over 20 Monte Carlo Simulations (SSP Randomization every 250m)
C
Depth (m)
Range (km)

Figure A-7:

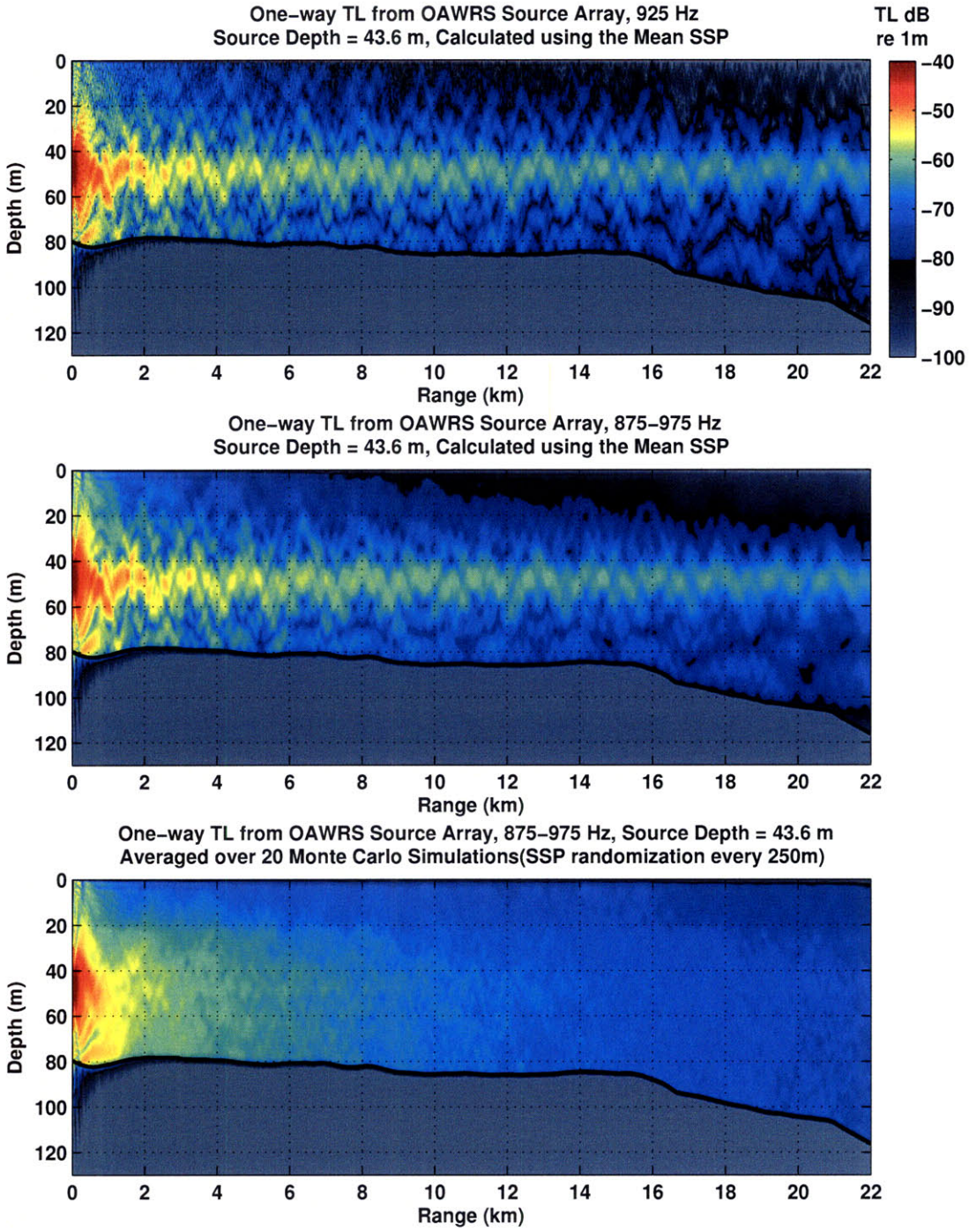
One–way TL from OAWRS Source Array, 925 Hz
Source Depth = 43.6 m, Calculated using the Mean SSP
TL dB re 1m
−40
−50
−60
−70
−80
−90
−100
Depth (m)
Range (km)
One–way TL from OAWRS Source Array, 875–975 Hz
Source Depth = 43.6 m, Calculated using the Mean SSP
Depth (m)
Range (km)
One–way TL from OAWRS Source Array, 875–975 Hz, Source Depth = 43.6 m
Averaged over 20 Monte Carlo Simulations(SSP randomization every 250m)
Depth (m)
Range (km)

Figure A-8:

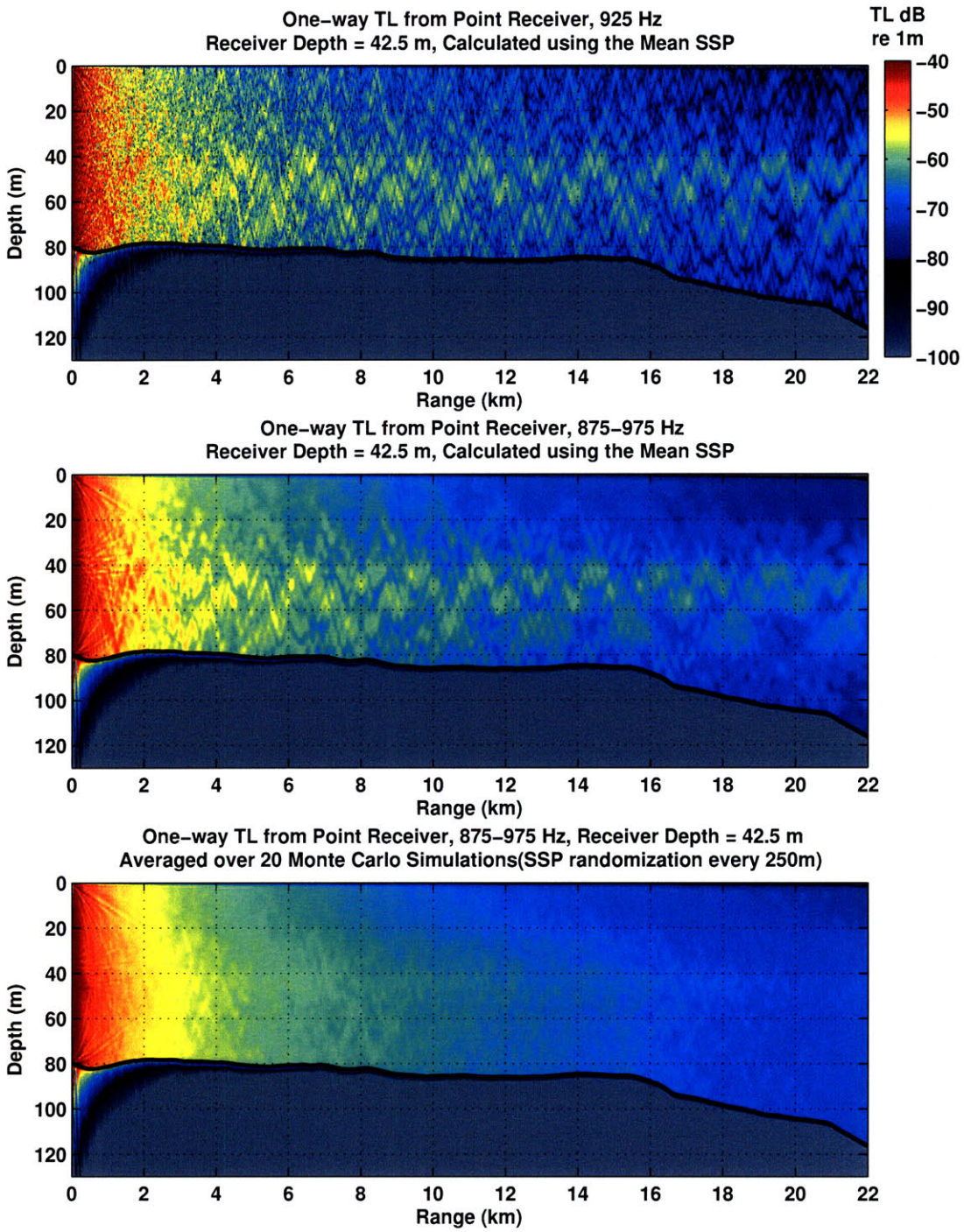
One–way TL from Point Receiver, 925 Hz
Receiver Depth = 42.5 m, Calculated using the Mean SSP
TL dB
re 1m
−40
−50
−60
−70
−80
−90
−100
Depth (m)
0
20
40
60
80
100
120
0
2
4
6
8
10
12
14
16
18
20
22
Range (km)
One–way TL from Point Receiver, 875–975 Hz
Receiver Depth = 42.5 m, Calculated using the Mean SSP
Depth (m)
Range (km)
One–way TL from Point Receiver, 875–975 Hz, Receiver Depth = 42.5 m
Averaged over 20 Monte Carlo Simulations(SSP randomization every 250m)
Depth (m)
Range (km)

Figure A-9:

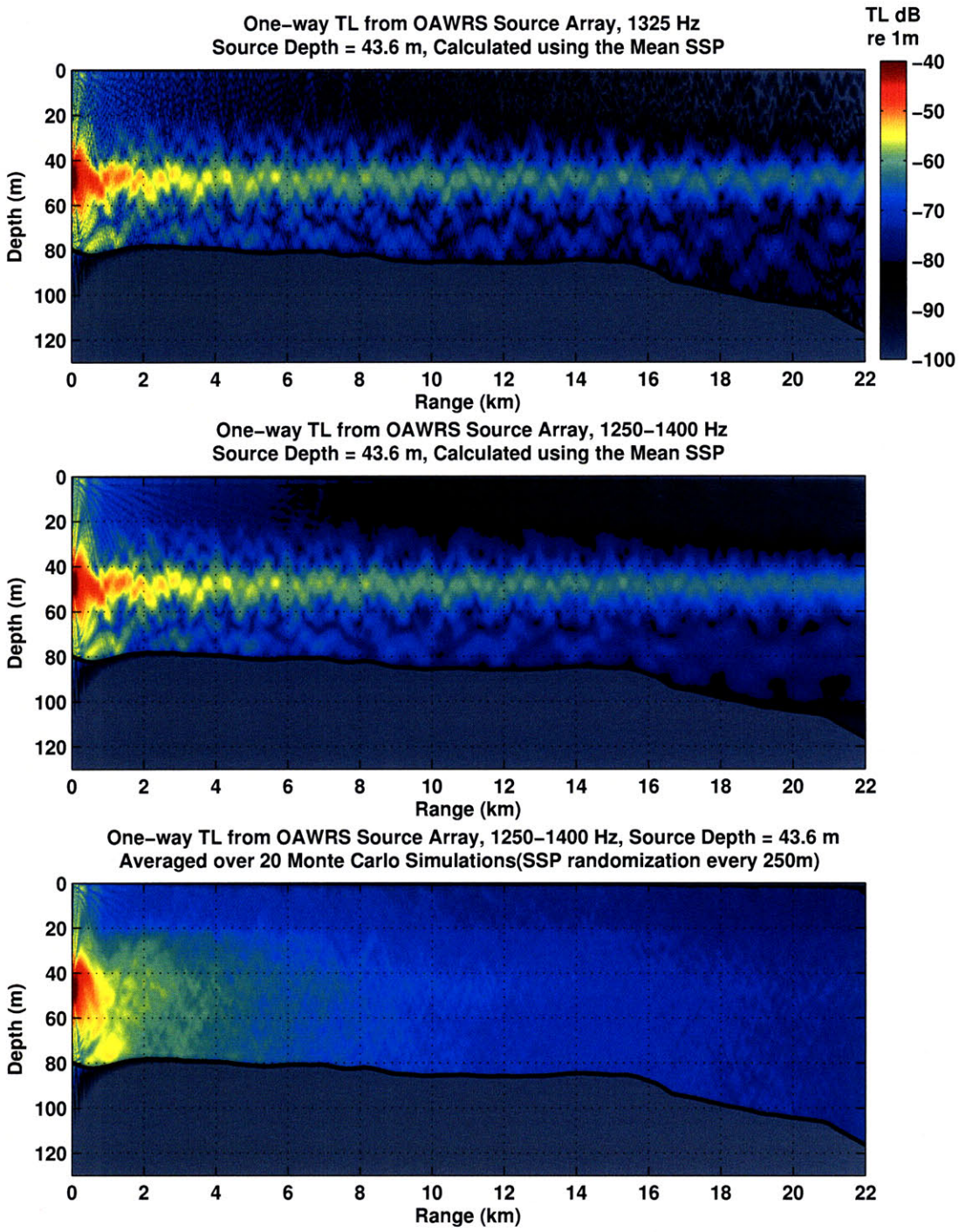
One−way TL from OAWRS Source Array, 1325 Hz
Source Depth = 43.6 m, Calculated using the Mean SSP
TL dB
re 1m
−40
−50
−60
−70
−80
−90
−100
Depth (m)
Range (km)
One−way TL from OAWRS Source Array, 1250−1400 Hz
Source Depth = 43.6 m, Calculated using the Mean SSP
Depth (m)
Range (km)
One−way TL from OAWRS Source Array, 1250−1400 Hz, Source Depth = 43.6 m
Averaged over 20 Monte Carlo Simulations(SSP randomization every 250m)
Depth (m)
Range (km)

Figure A-10:

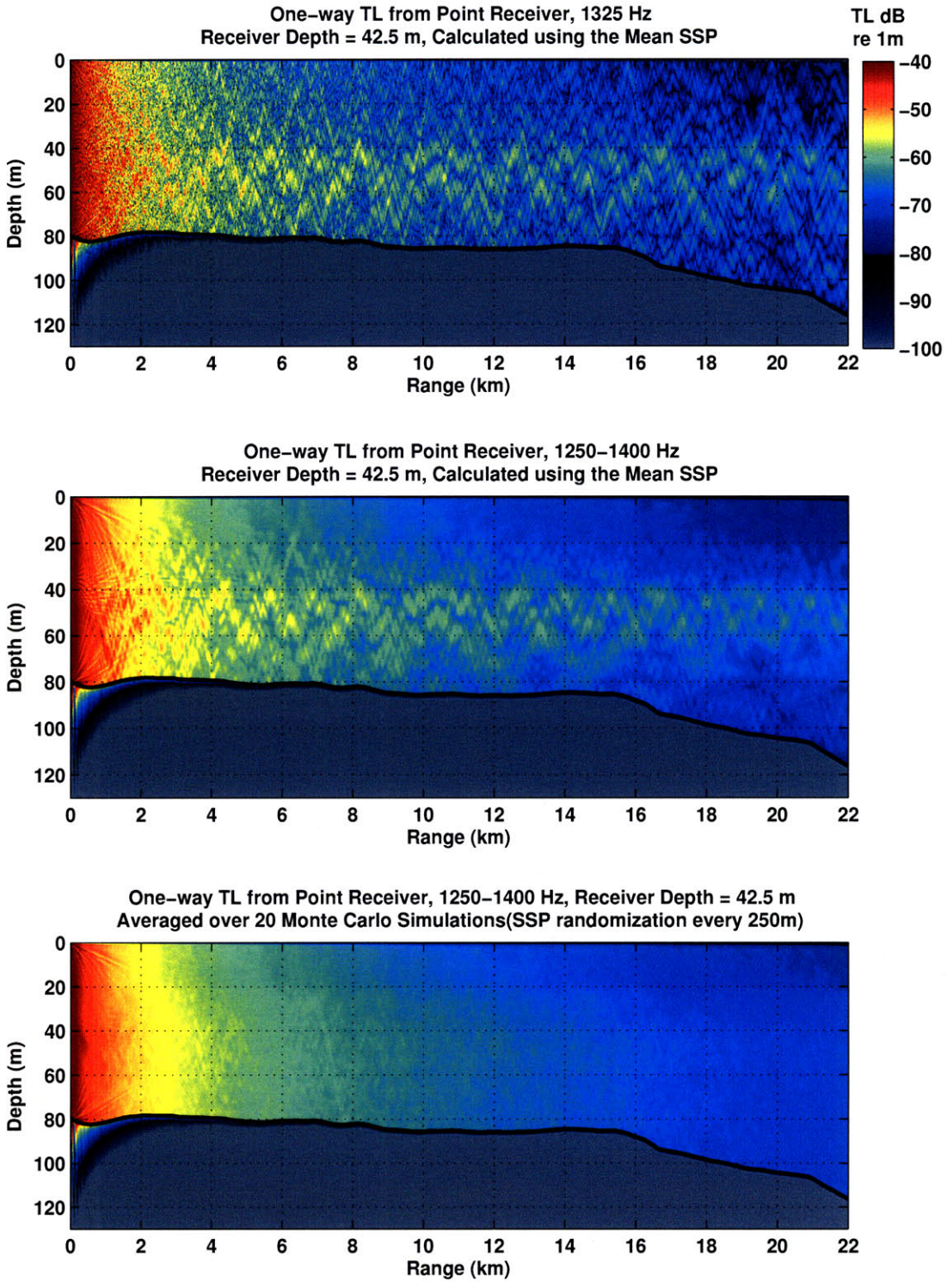
One–way TL from Point Receiver, 1325 Hz
Receiver Depth = 42.5 m, Calculated using the Mean SSP
TL dB re 1m
Depth (m)
Range (km)
One–way TL from Point Receiver, 1250–1400 Hz
Receiver Depth = 42.5 m, Calculated using the Mean SSP
Depth (m)
Range (km)
One–way TL from Point Receiver, 1250–1400 Hz, Receiver Depth = 42.5 m
Averaged over 20 Monte Carlo Simulations(SSP randomization every 250m)
Depth (m)
Range (km)

Figure A-11:

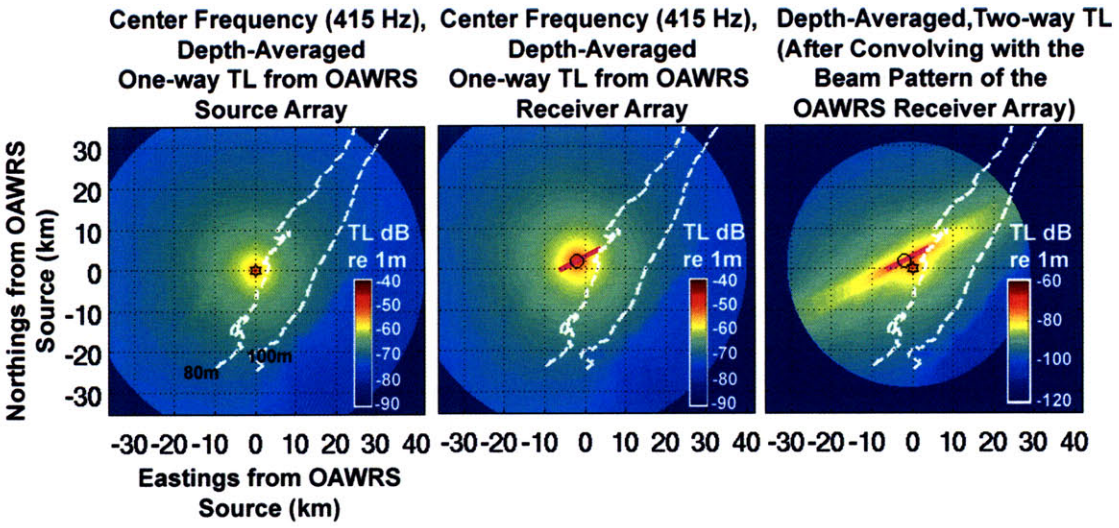

Figure A-12: Example of the OAWRS one and two-way transmission loss maps.

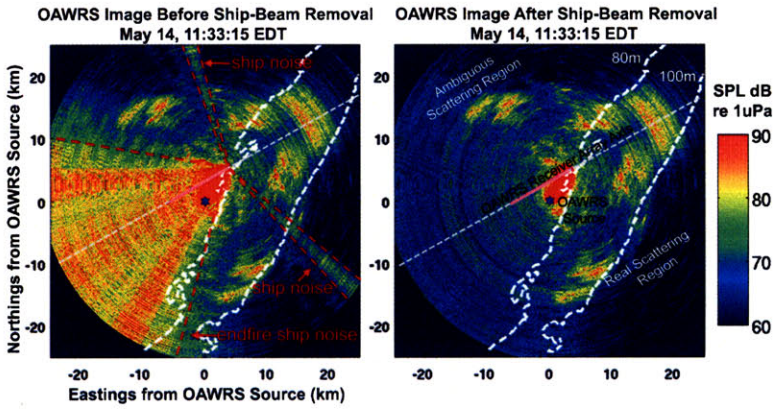

Figure A-13: Comparison of OAWRS acoustic intensity imagery before and after removing ship noise from the OAWRS receiver ship in the endfire direction and other ships operating in the vicinity of the OAWRS survey site.

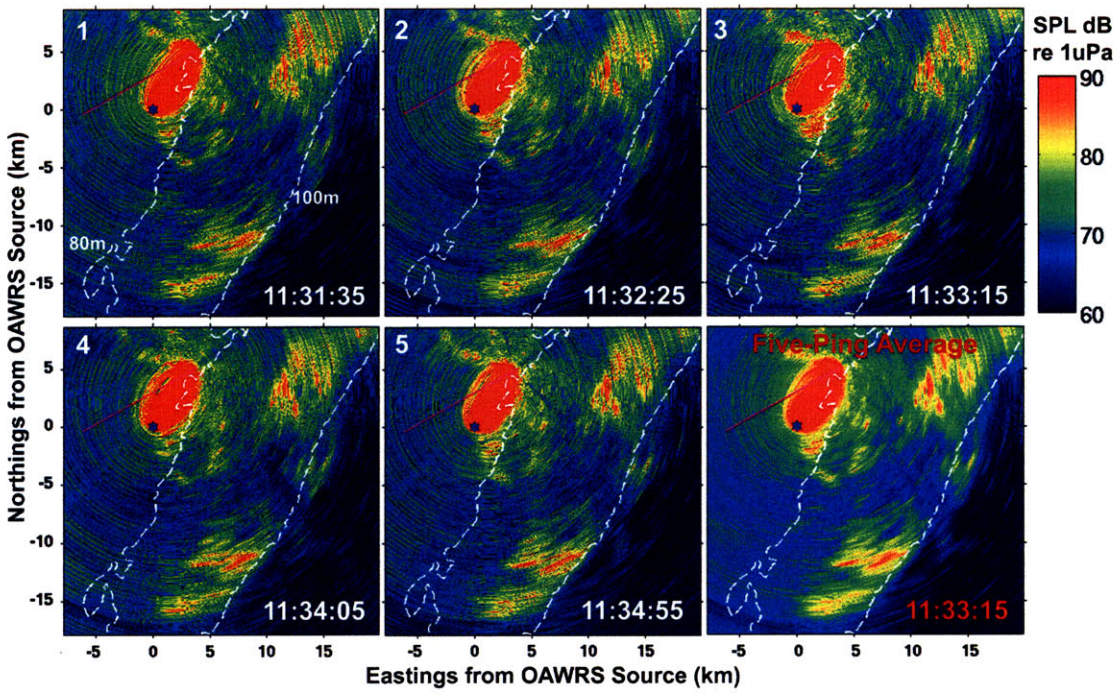

Figure A-14: Illustrative example of acoustic intensity temporal averaging. The 2D OAWRS acoustic intensity maps (390-440Hz) are incoherently averaged in time over five consecutive single ping transmissions to reduce the variability. Each individual acoustic intensity map (1-5 in the sequence) are also spatially average in range over two adjacent range cells, yielding a pixel resolution equal to 30m. The standard deviation per spatial pixel due to waveguide randomness and acoustic signal fluctuations are expected then to reduced by $\frac{1}{\sqrt{10}}$.

Appendix B

Discussion of OAWRS TS Estimation Examples for Non-Stationary OAWRS-CFFS Sampling Scenarios

During the MAE03, the OAWRS transmitted linear frequency modulated signals of 1s duration for three different frequency bands spanning roughly 400 to 1400 Hz. Here, present the analysis for the remaining, non-stationary sampling scenarios for the 390-440 Hz, 875-975 Hz, and 1250-1400 Hz OAWRS operating bands that were not discussed previously in the main text. For each sampling scenario, specific examples from MAE03 include: (i) OAWRS 2D scattering strength maps to highlight the horizontal morphology of the segment populations, (ii) corresponding range-depth profiles of the volumetric fish density measured by CFFS along the segment transect, and (iii) time series of CFFS Scattering Strength, OAWRS Scattering Strength, and the calibrated OAWRS TS.

B.1 390-440 Hz (WX1) Regime

B.1.1 Case 2A: Non-Stationary Populations within Low Density Regions of an OAWRS shoal

During MAE 03, there were 28 examples from four experiment days at Site 2 in which CFFS observed discrete, fish populations extending tens of meters within the low density, patchy regions of large, contiguous OAWRS shoals. These OAWRS shoaling regions exhibit 2D horizontal contiguity over kilometer scales as previously observed in the Case 1 Examples. The OAWRS TS estimation for the Case 2A examples were previously plotted in Fig. 3-10 (green data points) and are here described in Table B.7. The 2D OAWRS scattering strength images and range-depth profiles of volumetric fish density, highlighting the CFFS sampling segment, as well as the corresponding scattering strength time series, and calibrated OAWRS TS time series for each specific case are shown in Figs B-1-B-8.

Example	Day	Track	Segment	Time (EDT)	Number of Estimation Points	Coherence Length (Estimation Points)	Independent Samples (Coherent Cells)	$< TS_O >$ dB re $1m^2$	σ_{TS_O} dB (before averaging)	σ_{TS_O} dB (after averaging)
1	7-May	141A-2	E	12:03	13	9	1	-49	7.7	7.7
2	7-May	141A-2	F	12:06	6	6	1	-39.6	2.7	2.7
3	8-May	201-2	E	14:18	14	1	14	-42.9	3.8	1
4	14-May	252-1	D	12:00	3	3	1	-44	0.4	0.4
5	14-May	252-1	E	12:04	4	3	1	-42.2	1.4	1.4
6	14-May	252-1	F	12:06	3	3	1	-42.9	0.6	0.6
7	14-May	251-2	A	13:46	1	1	1	-41	0	0
8	14-May	251-2	B	13:49	16	8	2	-41.6	4.4	3.1
9	14-May	253-1	H	16:41	3	3	1	-42.9	0.9	0.9
10	15-May	251-4	B	7:54	12	5	2	-44.8	4.5	3.2
11	15-May	251-4	H	8:13	4	1	4	-43.8	1.2	0.6
12	15-May	251-4	I	8:15	3	1	3	-43.6	4.2	2.4
13	15-May	251-4	J	8:16	2	2	1	-43.9	1	1
14	15-May	251-4	M	8:22	2	2	1	-45.9	3.2	3.2
15	15-May	251-4	Q	8:40	1	1	1	-46.3	0	0
16	15-May	251-4	R	8:44	7	4	1	-45.4	2	2
17	15-May	251-4	T	8:46	4	2	2	-42.9	3.7	2.6
18	15-May	251-4	U	8:49	8	4	2	-43.5	2.6	1.8
19	15-May	251-4	W	8:52	3	3	1	-44	1.3	1.3
20	15-May	251-4	Y	8:59	5	1	5	-44.7	1.6	0.7
21	15-May	252-2	D	10:18	7	2	3	-43.8	4.1	2.4
22	15-May	254-1	A	12:08	2	2	1	-41.2	1.2	1.2
23	15-May	254-1	D	12:13	12	5	2	-39	3	2.1
24	15-May	254-1	E	12:20	10	4	2	-39.8	1.6	1.1
25	15-May	251-5	A	16:21	14	7	2	-41.4	3.2	2.3
26	15-May	251-5	B	16:58	2	2	1	-41.8	5.3	5.3
27	15-May	252-2	S	10:59	9	5	1	-47.1	6.8	6.8
28	15-May	252-2	T	11:02	2	1	2	-40.9	0.5	0.5

Table B.1: Table summarizing the calibrated OAWRS TS and standard deviation, as well as the standard deviation per segment after applying stationary averaging over independent coherent cells.

From Fig. 3-10 and Table B.1, we note that the mean calibrated OAWRS TS per segment are consistently lower than the calculated Case 1 global mean TS (-40 dB re $1m^2 at 415Hz$). The calibrated OAWRS TS per segment are combined to compute a global mean for the Case 2A segments . The global mean for the Case 2A segments is found to be -43 dB re $1m^2$ at the center frequency of 415 Hz.

Since the fish groupings measured by CFFS in Case 2A sampling scenarios are continuous over short distances (tens of meters), there are a lower number of identical time-space co-registration points to compute the OAWRS TS calibration. This low number of calibration points also yields lower number of independent coherent cells within each segment. Most of the segments contain 1-2 independent coherent cells, which are insufficient to significantly reduce the variability per segment. For most examples, the standard deviation per segment remains constant before (gray envelope) and after stationary averaging (black error bars) per segment in Fig. 3-10.

The OAWRS calibrated TS is consistently underestimated for these Case 2A sampling scenarios. These segments demonstrate underestimation scenarios where the CFFS sampled number density is higher than the effective number density over the corresponding OAWRS footprints, as illustrated in Fig. 3-9B. The -3dB discrepancy suggests that CFFS is sampling densities that are 50% higher than that of the effective density of the corresponding OAWRS footprints. When the populations sampled by CFFS are not statistically stationary, identically distributed over and do not fully occupy the OAWRS resolution footprint, such underestimations of OAWRS TS are likely to occur.

These low density, patchy regions often act as the adhesive which keeps the shoal intact and make up the intricate network of 2D bridges or dendrites that connect population centers within the shoal. From the range-depth profiles of volumetric fish density per segment, the CFFS-sampled fish populations can appear as a singular clump (i.e. Example 1) or a series of discrete clumps (i.e. Example 25). However, it impossible to determine whether CFFS is in fact traversing through discrete fish populations or through boundaries or vacuoles associated with larger, more contiguous populations. This is due to the limted across-transect swath (roughly 10m) of the

CFFS system. There is no way of accurately extrapolating what the 2D horizontal structure of the fish population from the CFFS range-depth profiles. The OAWRS system is able to resolve separations or vacuoles within fish populations greater than 30m in the range direction, since the range resolution is 15m for the 390-440 Hz transmission and the instantaneous imagery is averaged over 2 adjacent range cells. The OAWRS system cannot resolve separations in the cross-range direction that are smaller than the cross-range resolution at the point of observation. For example, the OAWRS cross-range resolution of OAWRS is highly dependent on the geographic location with respect to the receiver array and is typically 500m in the broadside (perpendicular to the receiver) at a a range of 10km from the receiver.

The spacing of the fish populations (roughly 50-100m) suggest that there are vacancies within the fish population contained within the corresponding OAWRS footprint that could effect the TS estimation. The presence of small vacuoles within contiguous populations can result in a lower fish density within the corresponding OAWRS footprint than the CFFS-sampled region since the entire OAWRS footprint is not occupied by fish. For these Case 2A examples, the vacant spaces between fish populations in along-transect range are rougly that of the extent of these fish populations. If these populations are representative of the spatial distribution of fish in OAWRS range and cross-range direction, it is not unlikely that only 60% of the area within corresponding OAWRS footprints are occupied by fish and the other 40% accounted for by vacancies. This is one plausible explanation of underestimation of OAWRS TS by 3dB from the established Case 1 mean of -40 dB.

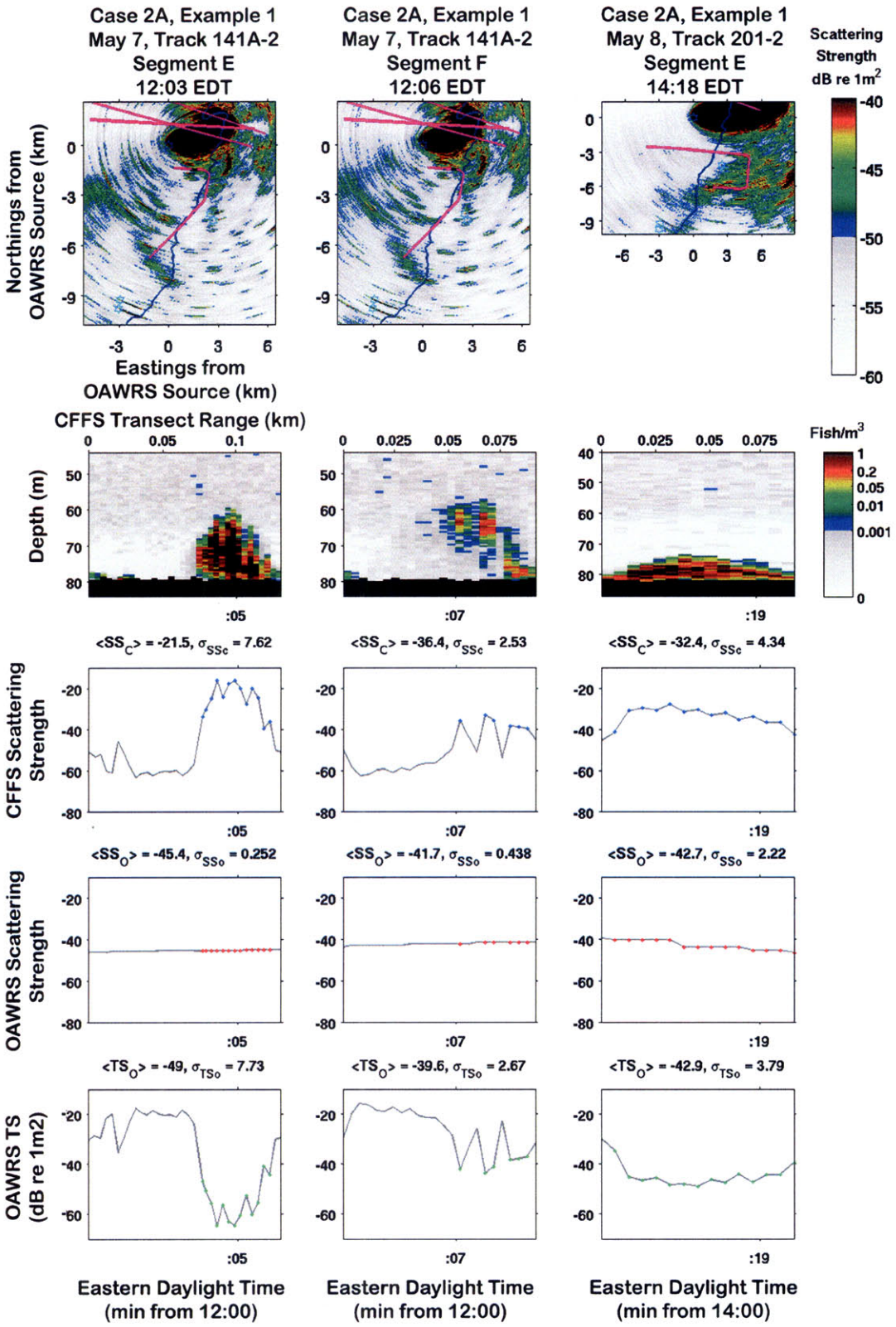

Figure B-1: Site 2, Case 2A

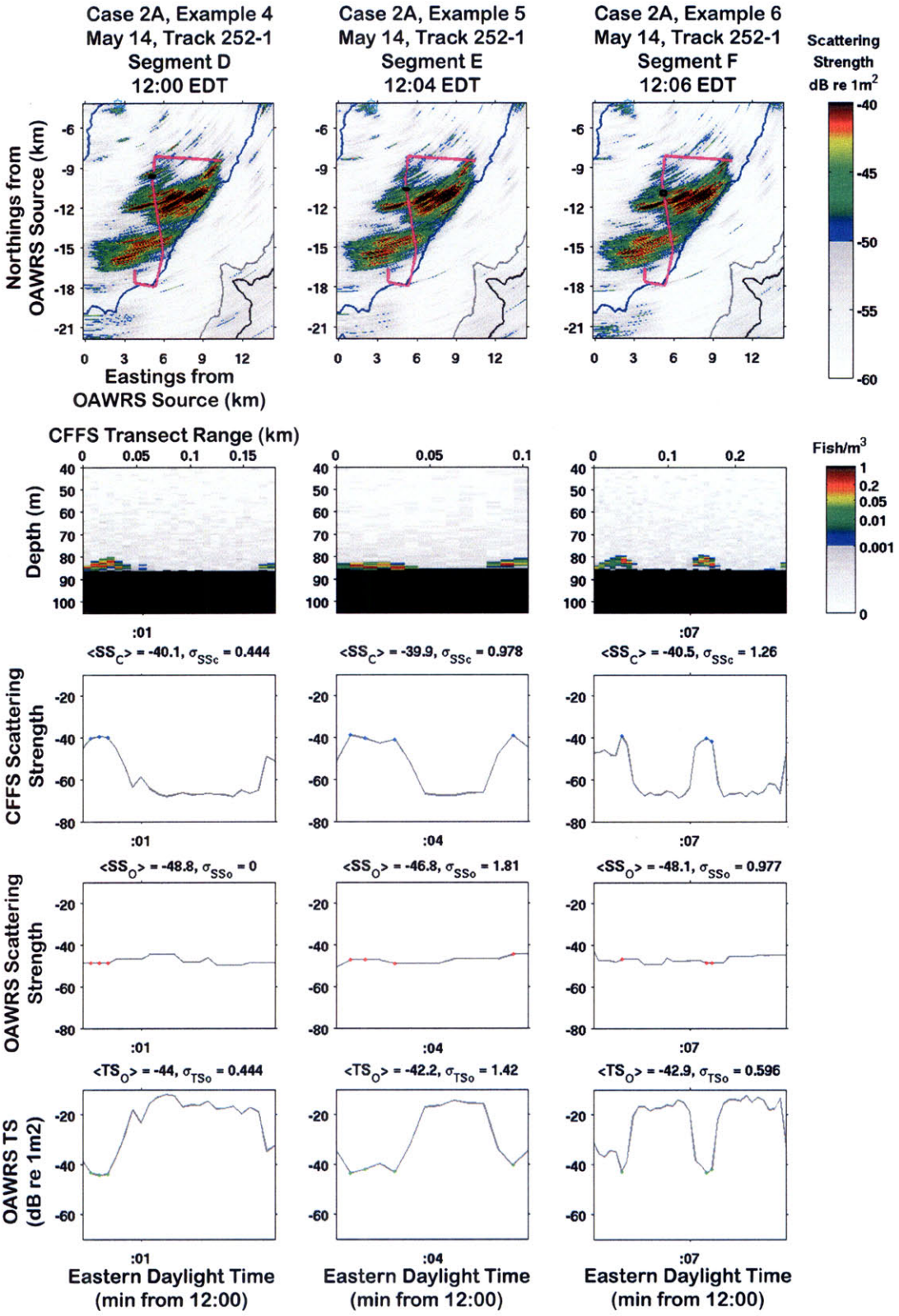

Figure B-2: Site 2, Case 2A

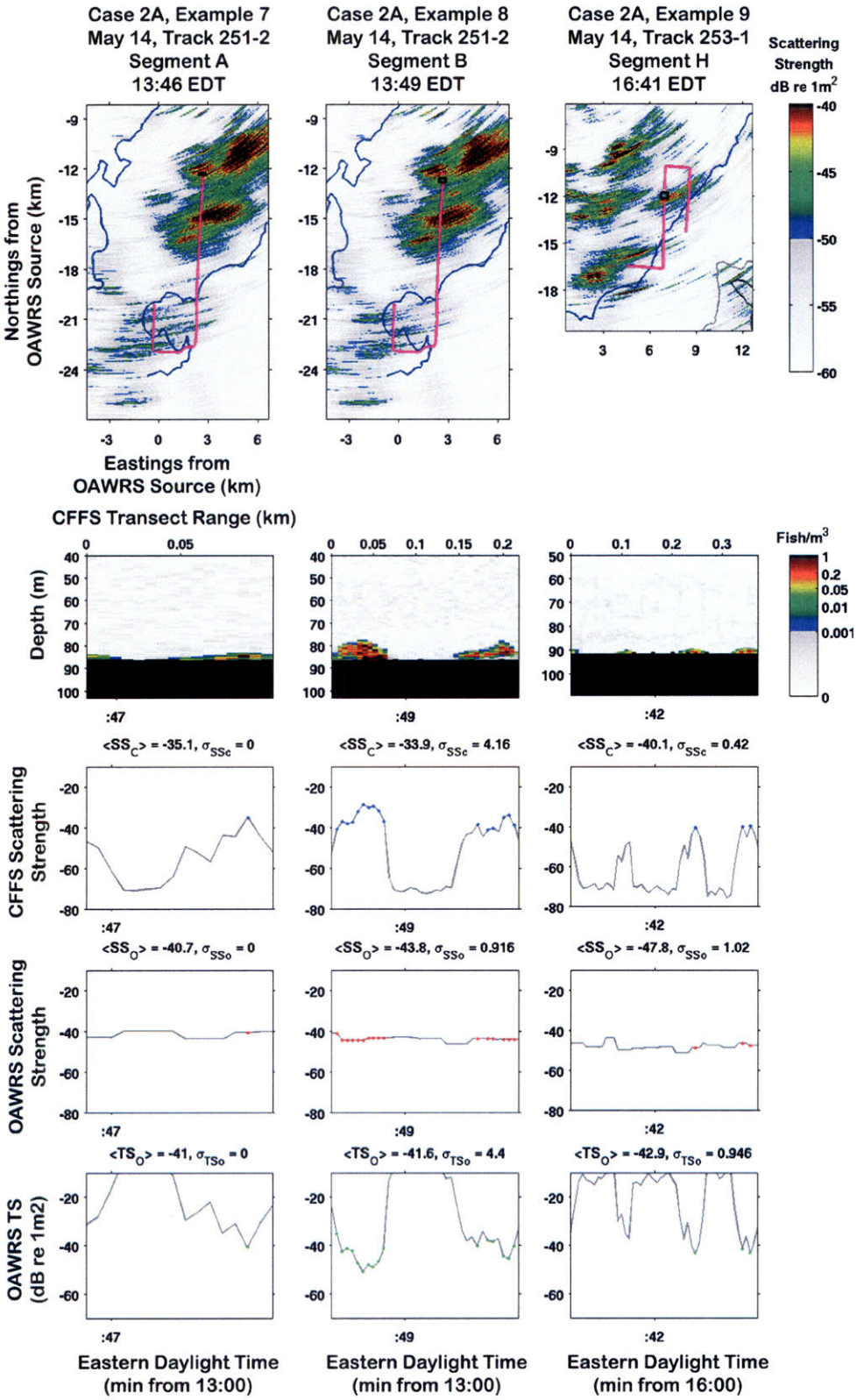

Figure B-3: Site 2, Case 2A

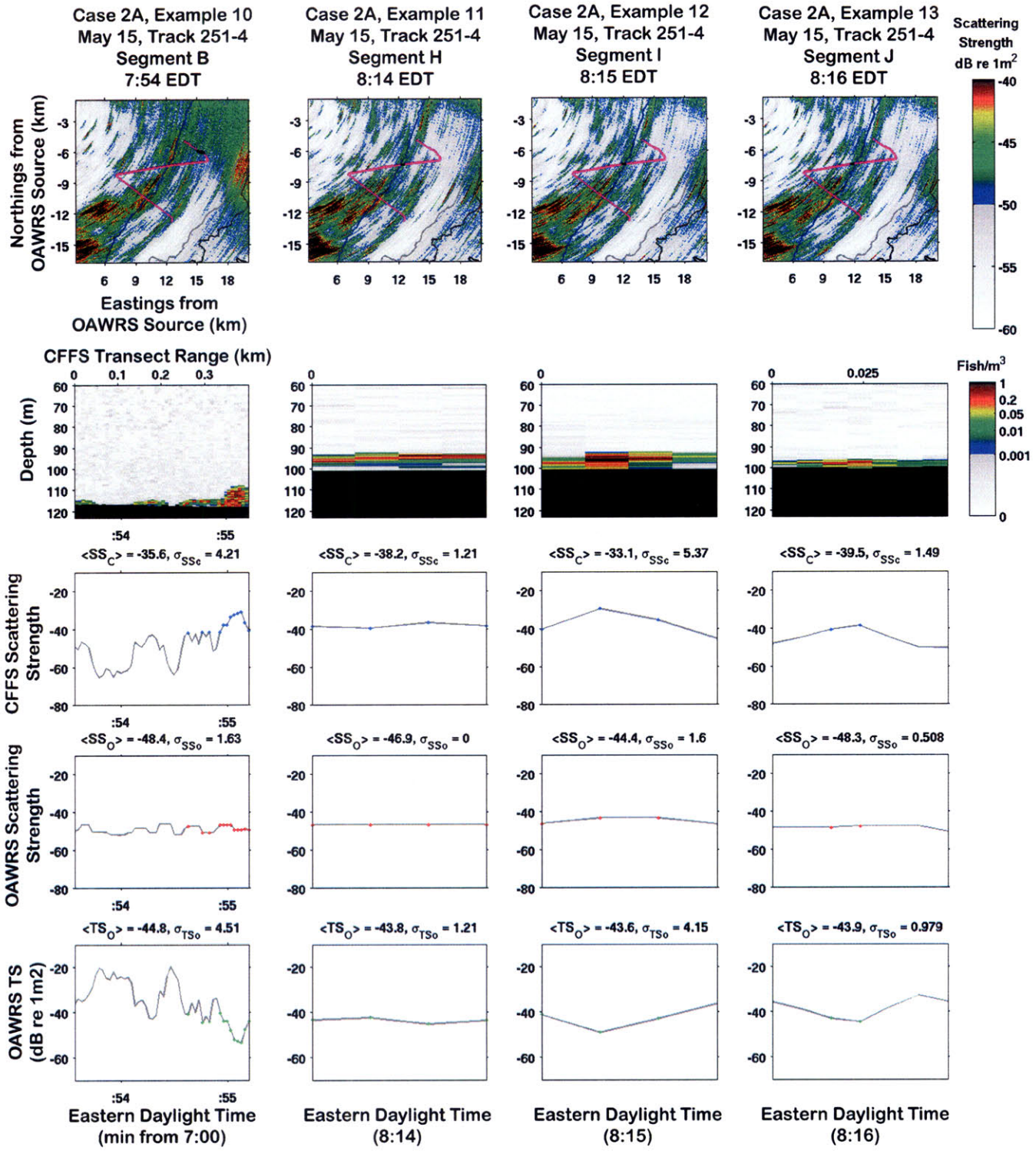

Figure B-4: Site 2, Case 2A

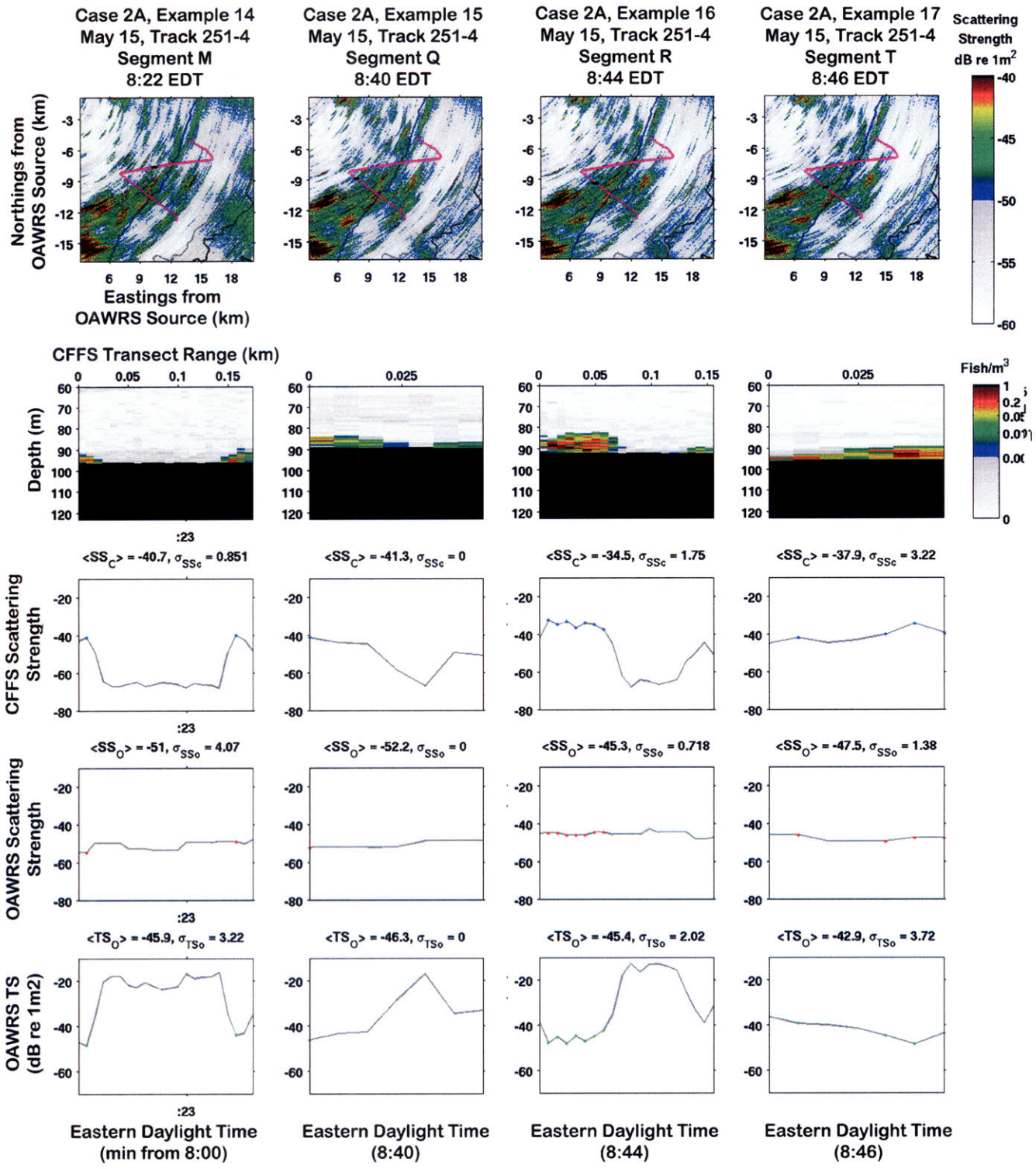

Figure B-5: Site 2, Case 2A

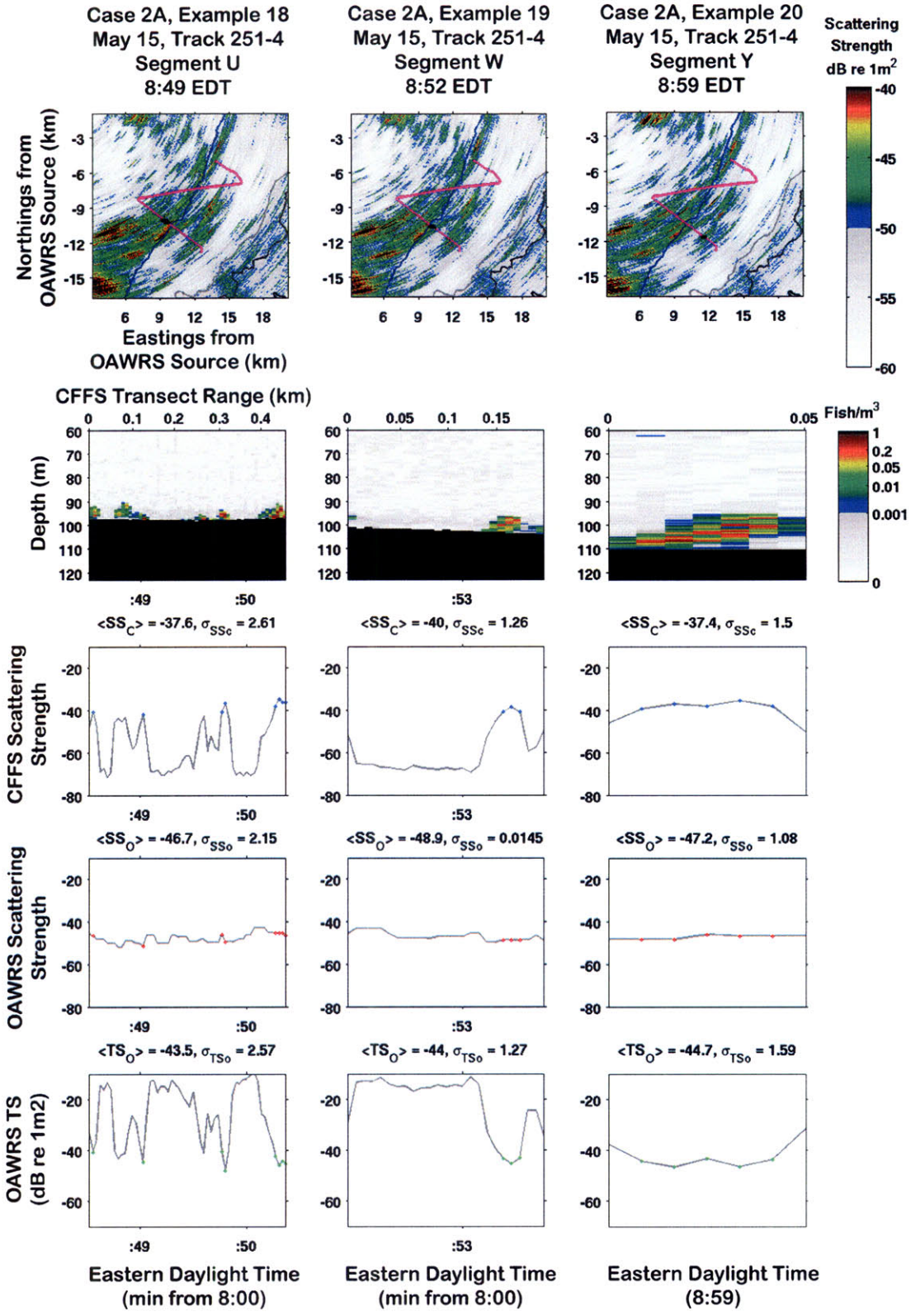

Figure B-6: Site 2, Case 2A

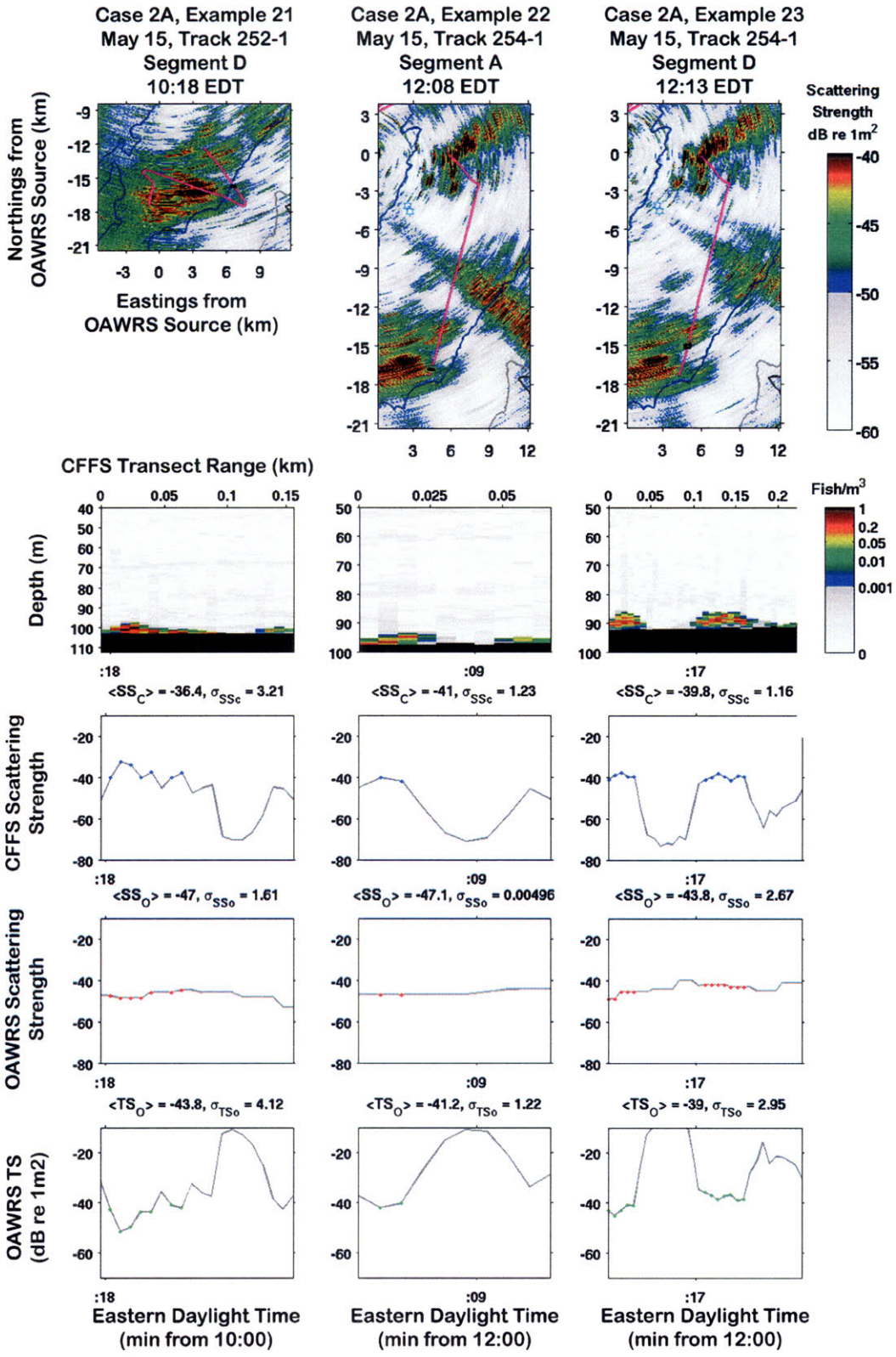

Figure B-7: Site 2, Case 2A

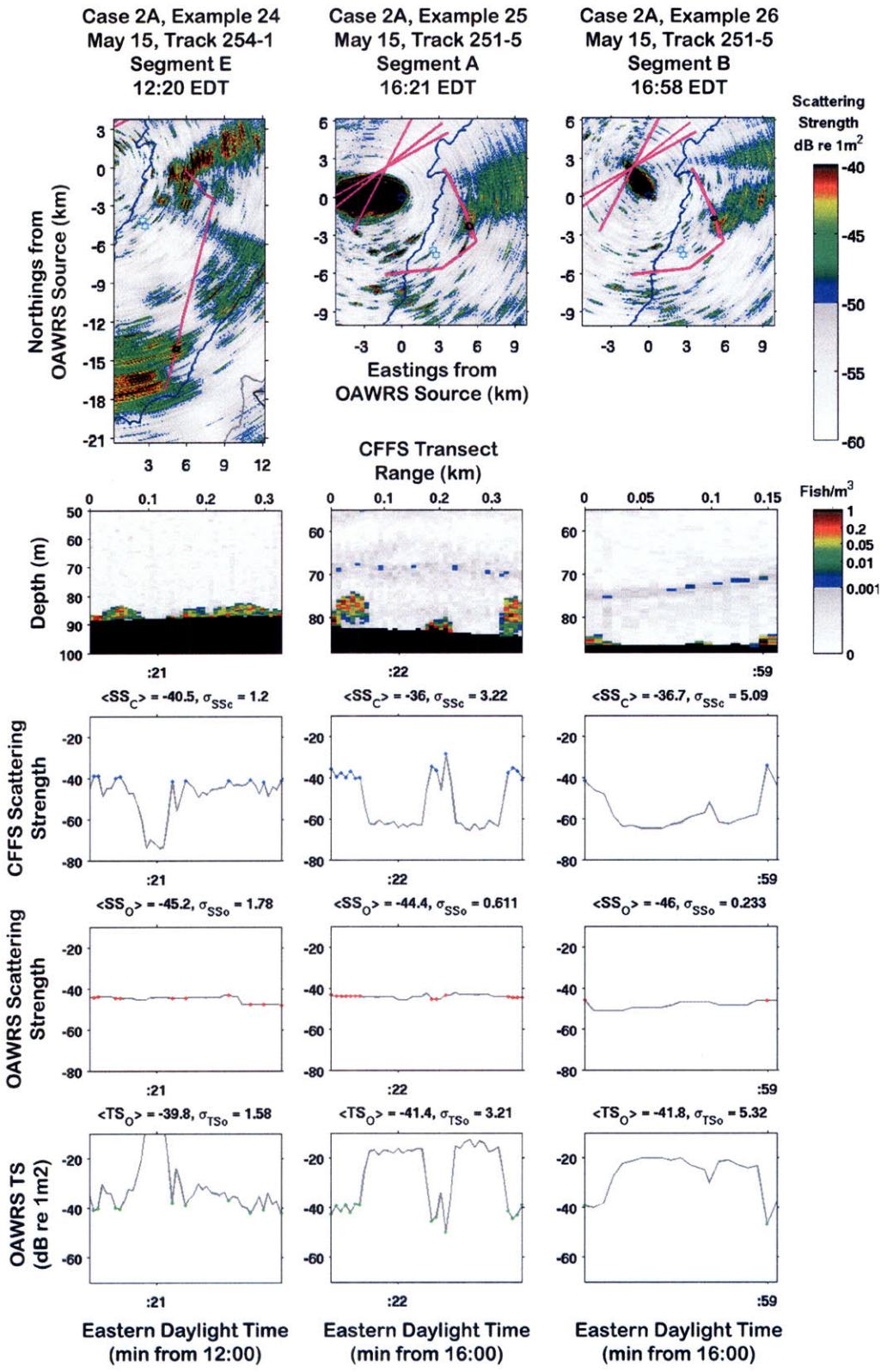

Figure B-8: Site 2, Case 2A

B.1.2 Case 2B: Non-Stationary Populations within High Density Regions in an OAWRS Shoal

Like the Case 2A sampling scenarios, the following segment examples occur when CFFS sample populations that appear as discrete groupings extending tens to a hundred meters in along-transect range within a contiguous OAWRS shoaling region. However, these segment examples demonstrate instances in which CFFS transects through dense populations centers of large, contiguous shoals. These dense nuclei comprise those regions of highest scattering density within the shoal.

Example	Day	Track	Segment	Time (EDT)	Number of Estimation Points	Coherence Length (Estimation Points)	Independent Samples (Coherent Cells)	$< TS_O >$ dB re $1m^2$	σ_{TS_O} dB (before averaging)	σ_{TS_O} dB (after averaging)
1	8-May	201-2	D	14:17	5	1	5	-36.2	3.4	3.4
2	14-May	252-1	G	12:08	13	2	6	-38.4	2.8	1.1
3	15-May	252-2	G	10:40	2	2	1	-38.3	1.5	1.5
4	15-May	252-2	H	10:42	4	3	1	-33.3	2.3	2.3
5	15-May	252-2	I	10:44	3	1	3	-34.5	2.4	2.4
6	15-May	252-2	J	10:45	1	1	1	-32.5	—	—
7	15-May	251-5	C	17:00	12	5	2	-36.8	4.5	3.2
8	15-May	252-2	K	10:52	11	1	11	-35.7	1.6	1.6
9	15-May	252-2	P	11:18	6	2	3	-36.5	0.8	0.5
10	15-May	254-1	D	12:17	12	2	6	-39	3	2.1
11	15-May	254-1	H	13:22	52	2	26	-35.8	2.6	0.5

Table B.2: Table summarizing the calibrated OAWRS TS and standard deviation, as well as the standard deviation per segment after applying stationary averaging over independent coherent cells.

For the Case 2B examples, the global mean OAWRS TS is found to be $-36 dBre1m^2$. An overestimation of OAWRS TS occurs when the CFFS sampled density is lower than that of the density contained within the corresponding OAWRS footprints. The 4 dB overestimation suggests that CFFS-sampled density is a sixth of the effective density within the corresponding OAWRS footprints. This could occur within high density regions of a shoal if CFFS misses some of the fish contained within the corresponding OAWRS footprint, as illustrated in Fig. 3-9A.

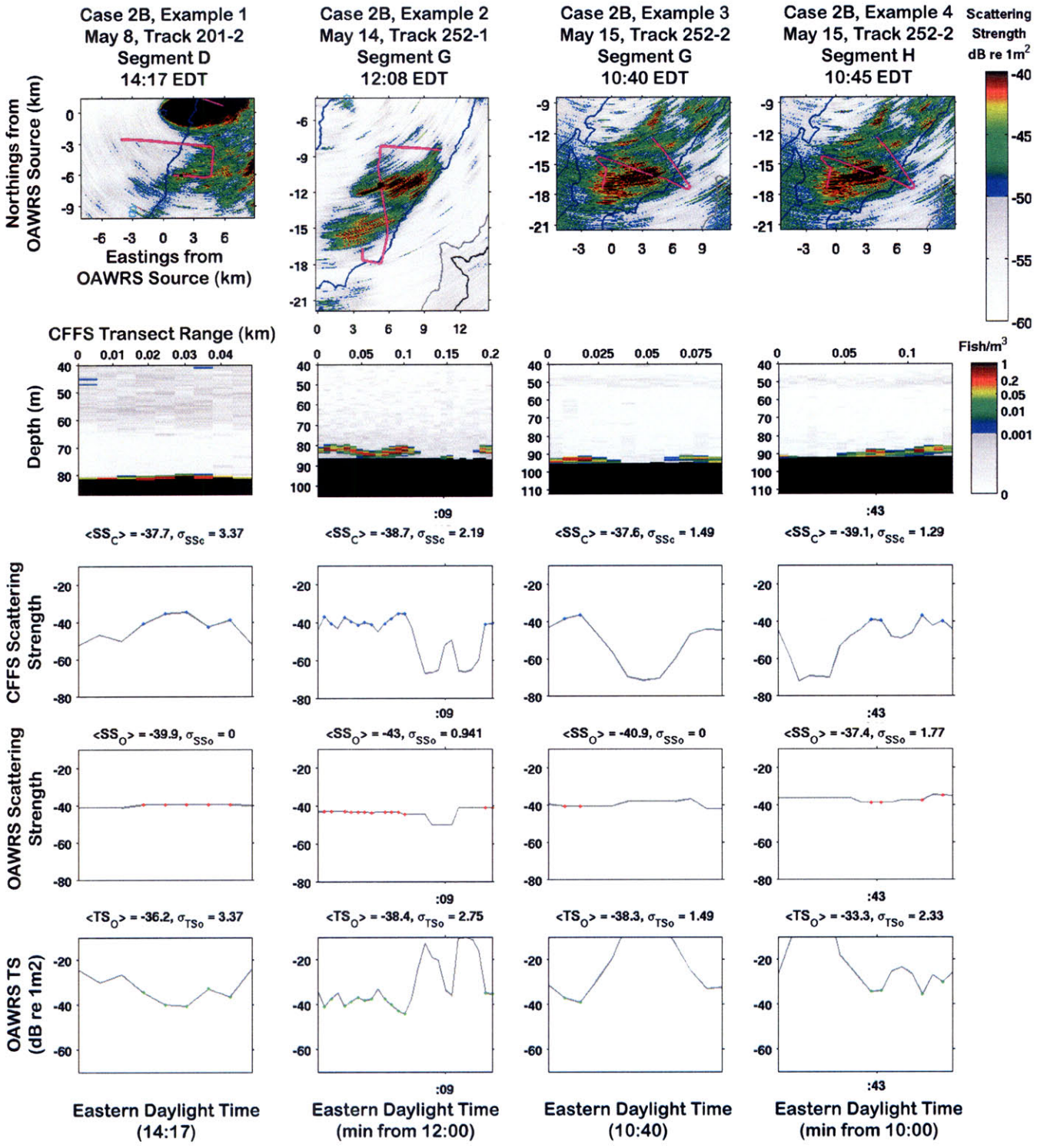

Figure B-9: Site 2, Case 2B

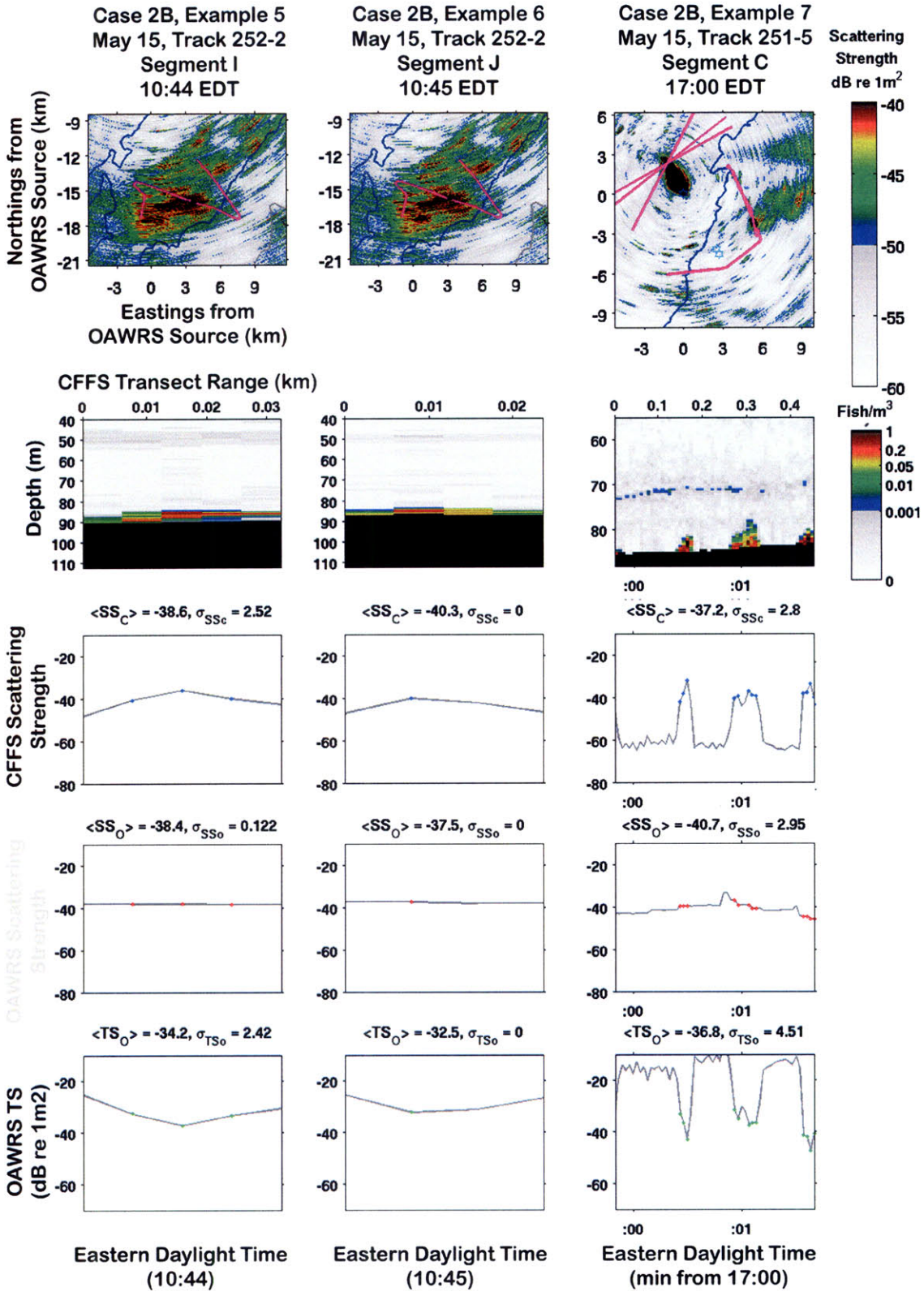

Figure B-10: Site 2, Case 2B

B.1.3 Case 2C: Non-Stationary Populations at the Boundaries of an OAWRS Shoal

For large, contiguous OAWRS shoals, the last case examined correspond to sampling scenarios where CFFS traverses through the boundary or periphery region of larger, kilometer scale shoals (Case 2C). Like the other Case 2 examples, CFFS measures small, singular groupings or a series of discrete clumps tens to a hundred meters in extent, resting in 5-10m layers off the ocean bottom.

Example	Day	Track	Segment	Time (EDT)	Number of Estimation Points	Coherence Length (Estimation Points)	Independent Samples (Coherent Cells)	$< TS_O >$ dB re $1m^2$	σ_{TS_O} dB (before averaging)	σ_{TS_O} dB (after averaging)
1	7-May	141A-2	I	12:19	3	2	1	-45.2	2.0	2.0
2	7-May	141A-2	K	12:23	4	4	1	-45.5	2.7	2.7
3	8-May	201-3	A	17:22	6	1	6	-49.7	3.4	3.4
4	8-May	202-4	B	19:33	17	7	2	-47.5	4.0	2.8
5	14-May	252-1	I	12:27	21	2	10	-49.8	2.7	0.8
6	14-May	252-1	K	12:49	4	2	2	-55.8	2.9	2.1
7	14-May	252-1	L	12:50	14	1	14	-48.7	4.9	4.9
8	14-May	253-1	I	16:45	2	2	1	-55.1	2.0	2.0
9	14-May	253-1	J	17:04	4	1	4	-51.8	2.0	2.0
10	14-May	253-1	L	17:12	2	2	1	-53.0	0.5	0.5
11	15-May	251-4	G	8:08	4	1	4	-54.1	3.6	3.6
12	15-May	251-4	K	8:17	2	1	2	-52.4	0.3	0.3
13	15-May	251-4	X	8:54	9	3	3	-49.4	2.6	1.5
14	15-May	251-4	Z	9:01	6	1	6	-48.8	4.4	4.4
15	15-May	251-4	a	9:03	15	7	2	-51.7	3.3	2.4
16	15-May	252-2	E	10:33	16	2	8	-45.5	2.7	1.0
17	15-May	252-2	N	11:09	2	2	1	-46.0	0.7	0.7
18	15-May	254-1	C	12:13	4	1	4	-51.5	2.4	2.4
19	15-May	254-1	F	13:19	20	2	10	-43.2	3	0.9

Table B.3: Table summarizing the calibrated OAWRS TS and standard deviation, as well as the standard deviation per segment after applying stationary averaging over independent coherent cells.

Example	Day	Track	Segment	Uncorrected $< TS_O >$	τ (dB)	Corrected $< TS_O >$
1	7-May	141A-2	I	-45.2	9.8	-35.4
2	7-May	141A-2	K	-45.5	7.1	-38.4
3	8-May	201-3	A	-49.7	14.4	-35.3
4	8-May	202-4	B	-47.5	2.0	-45.5
5	14-May	252-1	I	-49.8	8.4	-41.4
6	14-May	252-1	K	-55.8	14.4	-41.4
7	14-May	252-1	L	-48.7	9.4	-39.3
8	14-May	253-1	I	-55.1	15.2	-39.9
9	14-May	253-1	J	-51.8	15.0	-36.8
10	14-May	253-1	L	-53.0	12.7	-40.3
11	15-May	251-4	G	-54.1	14.2	-39.9
12	15-May	251-4	K	-52.4	12.4	-40.0
13	15-May	251-4	X	-49.4	9.6	-39.8
14	15-May	251-4	Z	-48.8	11.6	-37.2
15	15-May	251-4	a	-51.7	9.0	-42.7
16	15-May	252-2	E	-45.5	6.1	-39.4
17	15-May	252-2	N	-46.0	7.4	-38.6
18	15-May	254-1	C	-51.5	13.5	-38.0
19	15-May	254-1	F	-43.2	3.5	-39.7

Table B.4: Table summarizing the adjusted mean OAWRS TS after applying the areal correction for the Case 2C Examples.

The mean calibrated OAWRS TS per individual segments are typically between 5 to 10dB lower than the baseline (column 7 of Table B.3 and the blue diamond markers in Fig.

When the fish do not fully occupy the OAWRS areal footprint, vacancies within OAWRS footprint become important and can bias the OAWRS TS calibration by lowering the effective population density. This is due to the areal mismatch between both CFFS and OAWRS. A correction factor, τ, is calculated based on the ratio of the expected area occupied by the CFFS-sampled fish population to the area occupied by the corresponding OAWRS resolution footprints. After applying the correction factor, the corrected global mean for the Case 2C segments is found to be roughly -40 dB re $1m^2$ at 415 Hz and is consistent with the Case 1 mean.

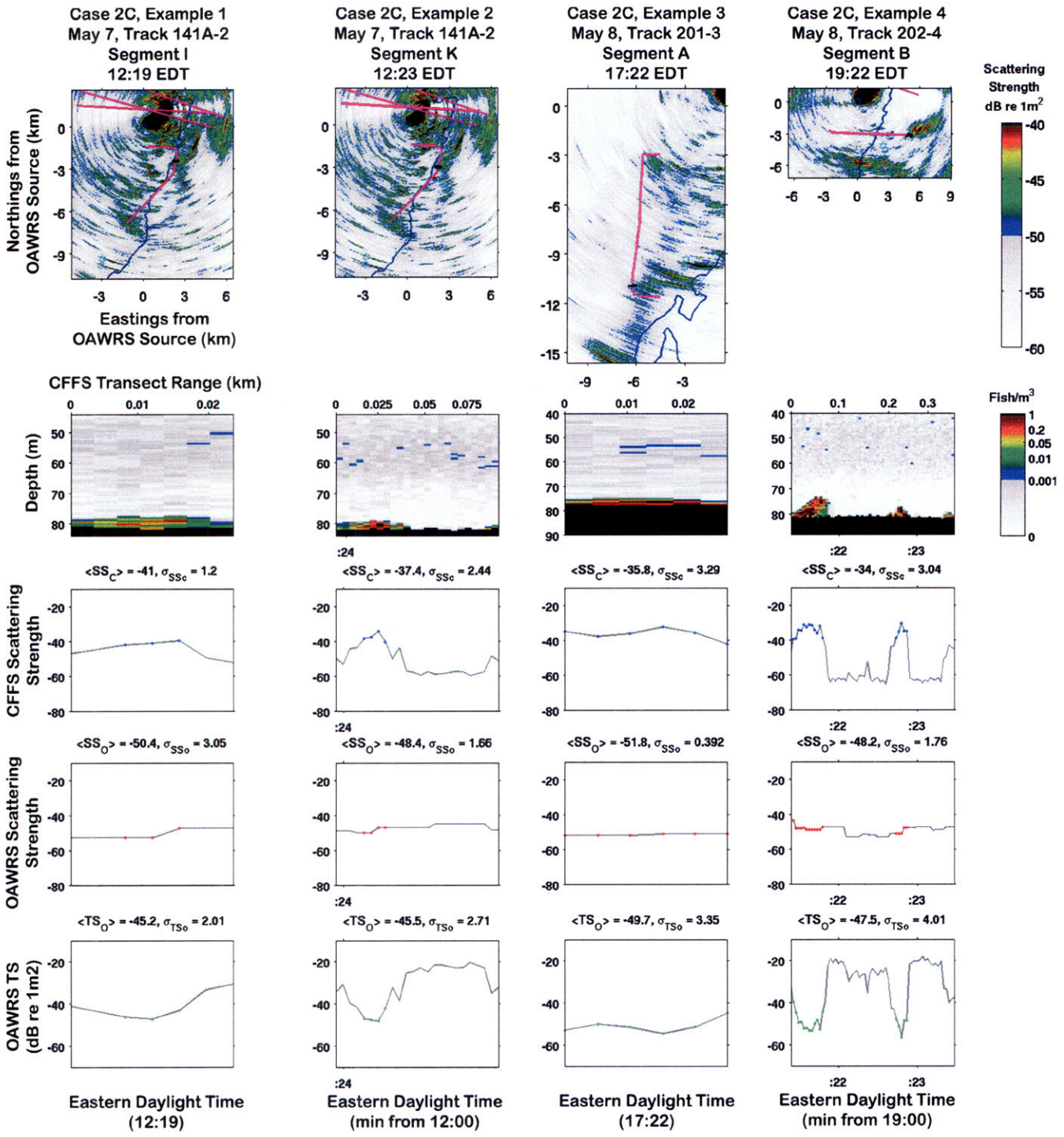

Figure B-11: Site 2, Case 2C

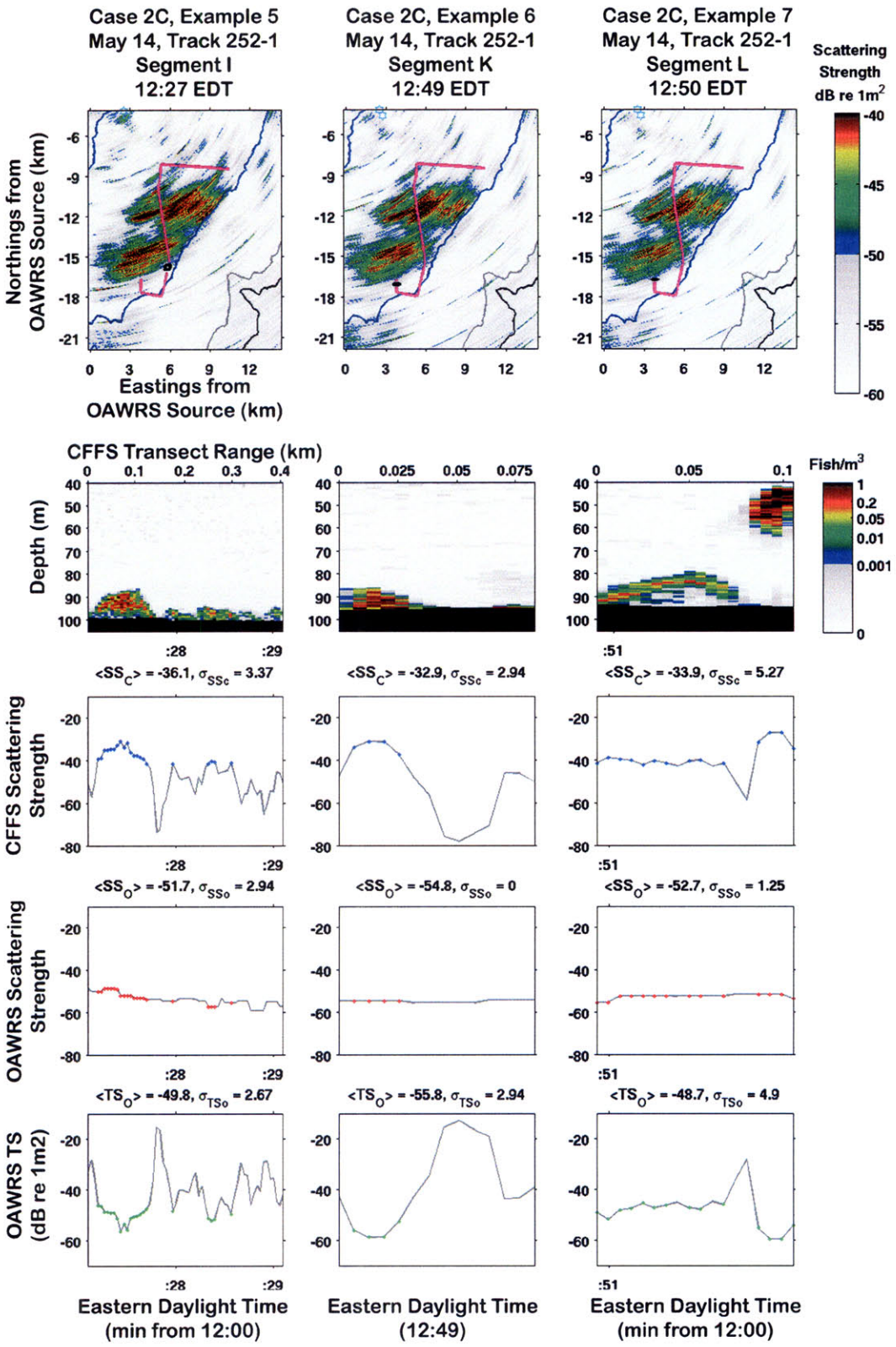

Figure B-12: Site 2, Case 2C

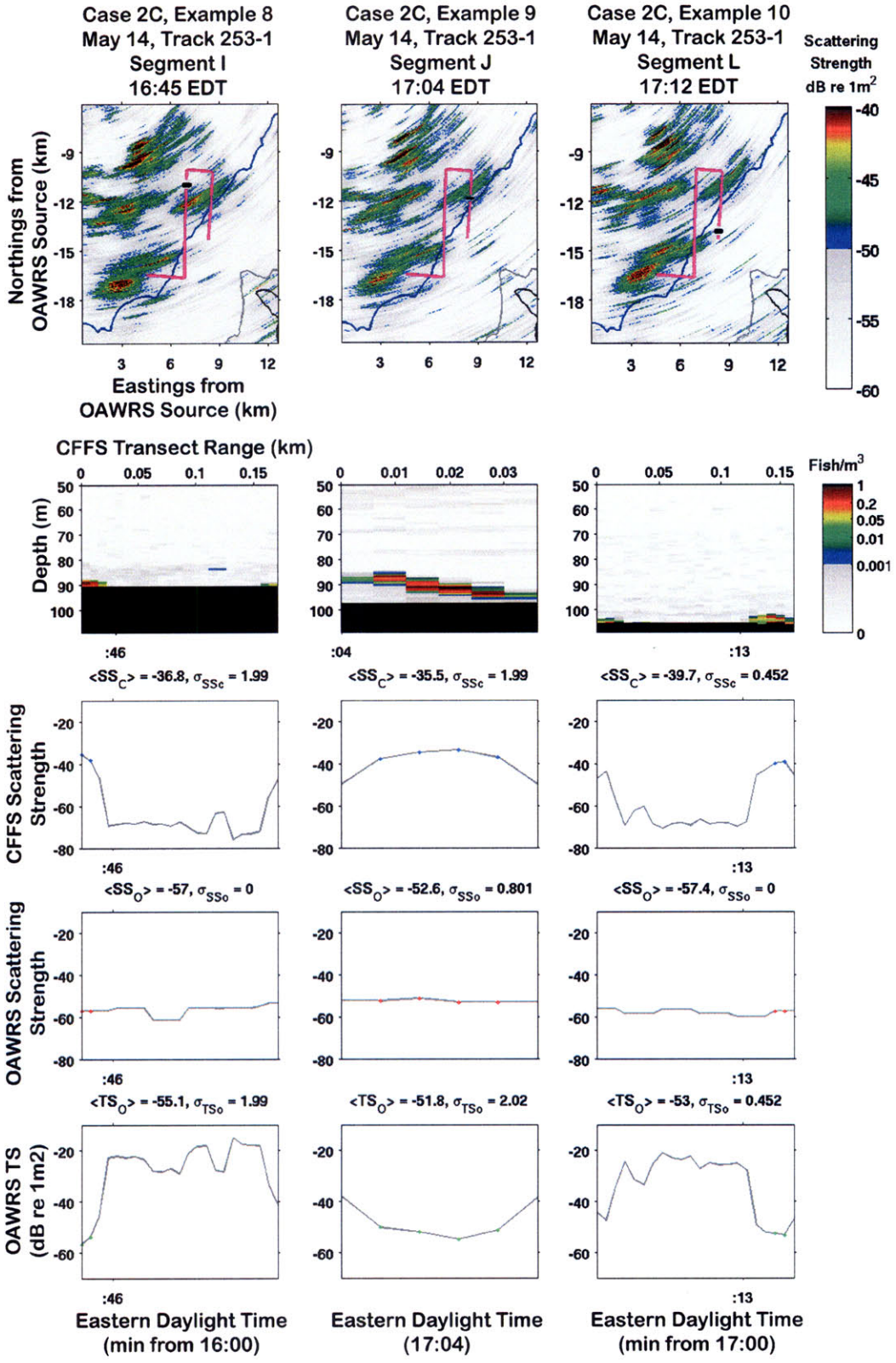

Figure B-13: Site 2, Case 2C

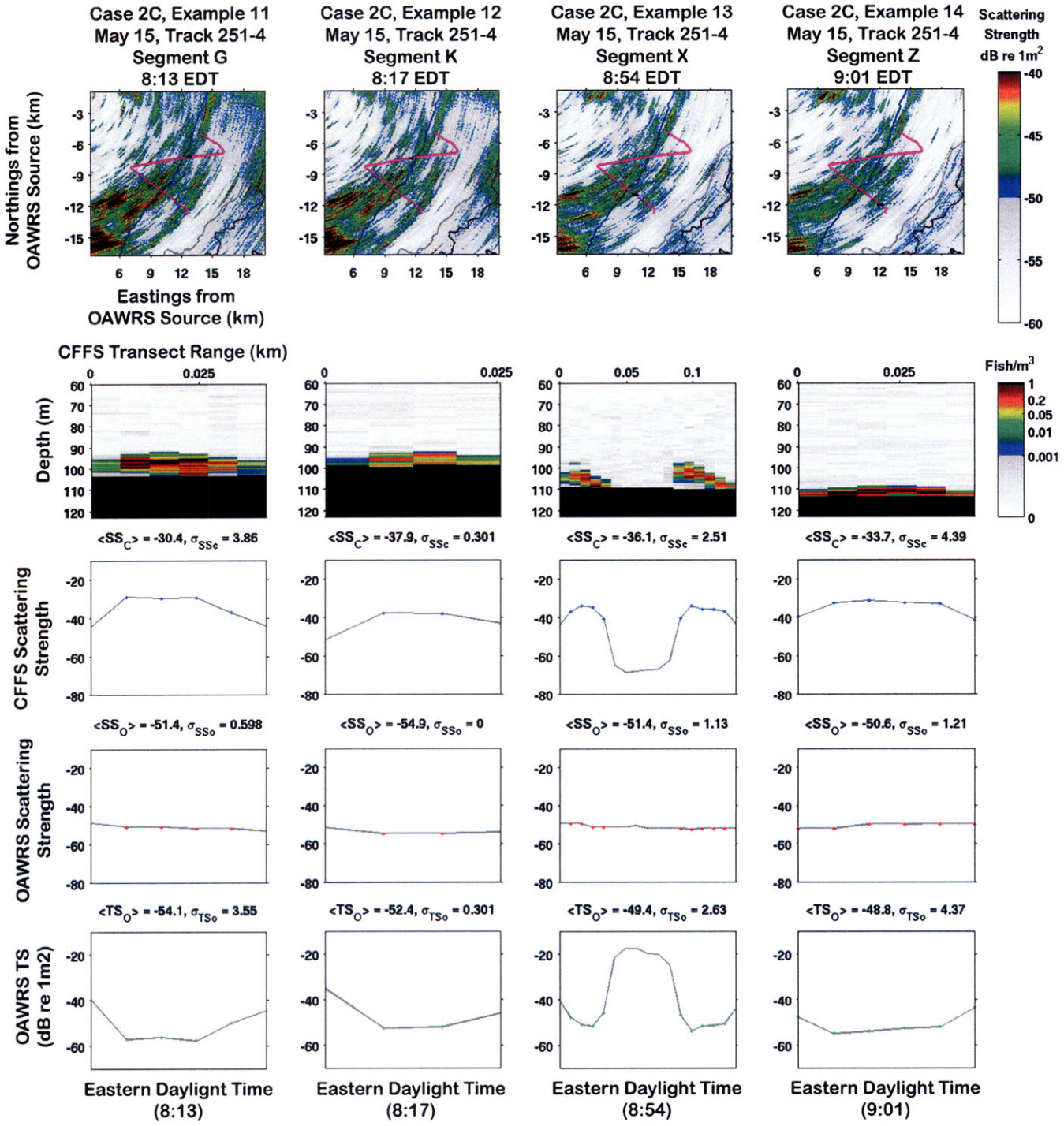

Figure B-14: Site 2, Case 2C

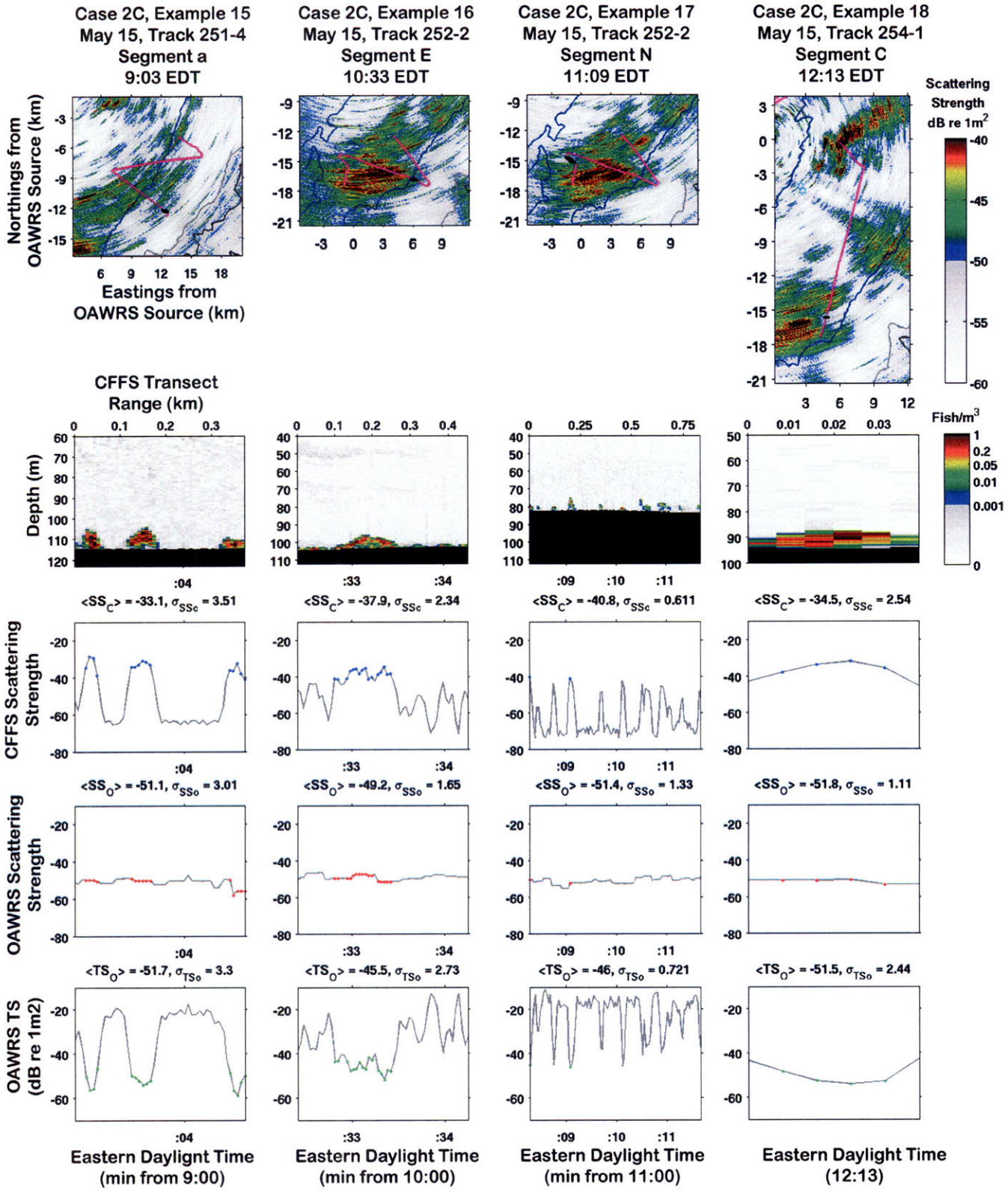

Figure B-15: Site 2, Case 2C

B.1.4 Case 3: Non-Stationary Populations within Small, Scattered Schools

Finally, the last case examined corresponds to the sampling scenario where both OAWRS and CFFS simultaneously measure small, scattered populations or schools. These populations typically extend hundreds of meters within the 2D OAWRS imagery and are observed as discrete, groupings extending tens of meters in the corresponding CFFS range-depth profiles. The small Case 3 populations can occur as compact, scattered schools or as satellite schooling populations comprising the background population surrounding larger shoals, as shown in the 2D OAWRS scattering strength maps corresponding to Examples 1 and 2 of Fig. B-16 respectively.

Example	Day	Track	Segment	Time (EDT)	Number of Estimation Points	Coherence Length (Estimation Points)	Independent Samples (Coherent Cells)	$< TS_O >$ dB re $1m^2$	σ_{TS_O} dB (before averaging)	σ_{TS_O} dB (after averaging)
1	7-May	141D-1	F	10:27	4	1	4	-54.2	5.8	5.8
2	14-May	252-1	A	11:34	1	1	1	-49.1	0.0	0.0
3	14-May	252-1	C	11:47	4	4	1	-53.1	0.7	0.7
4	14-May	253-1	B	16:13	34	3	11	-50.8	5.4	1.6
5	14-May	253-1	D	16:19	3	3	1	-51.9	1.1	1.1
6	14-May	253-1	F	16:26	2	2	1	-41.4	1.8	1.8
7	14-May	253-1	K	17:04	7	1	7	-48.0	4.4	4.4
8	15-May	251-4	L	8:19	2	1	2	-52.0	2.6	2.6
9	15-May	251-4	P	8:36	3	3	1	-49.6	0.6	0.6
10	15-May	251-4	c	9:05	3	1	3	-48.3	2.3	2.3
11	15-May	252-2	B	10:13	5	1	5	-48.2	5.3	5.3
12	14-May	253-1	G	16:39	46	5	9	-45.9	3.8	1.3

Table B.5: Table summarizing the calibrated OAWRS TS and standard deviation, as well as the standard deviation per segment after applying stationary averaging over independent coherent cells.

Example	Day	Track	Segment	Uncorrected $< TS_O >$	τ (dB)	Corrected $< TS_O >$
1	7-May	141D-1	F	-54.2	14.3	-39.9
2	14-May	252-1	A	-49.1	8.4	-40.7
3	14-May	252-1	C	-53.1	11.4	-41.7
4	14-May	253-1	B	-50.8	0.8	-50.0
5	14-May	253-1	D	-51.9	6.3	-45.6
6	14-May	253-1	F	-41.4	8.2	-33.2
7	14-May	253-1	K	-48.0	10.1	-37.9
8	15-May	251-4	L	-52.0	12.2	-39.8
9	15-May	251-4	P	-49.6	9.7	-39.9
10	15-May	251-4	c	-48.3	13.4	-34.9
11	15-May	252-2	B	-48.2	11.5	-36.7
12	14-May	253-1	G	-45.9	6.1	-39.8

Table B.6: Table summarizing the adjusted mean OAWRS TS after applying the areal correction for the Case 3 Examples.

The mean estimated OAWRS TS for all Case 3 segments are typically between 8-15dB lower than the Case 1 mean of -40 dB (column 9 of Table B.5 and the orange diamond markers in Fig.

A correction factor, similar to that of Case 2C, is found to account for the mismatch between the CFFS-sampled density and the effective density of the corresponding OAWRS footprint and the global mean after applying the correction is roughly -40 dB re $1m^2$ at 415 Hz and is consistent with the Case 1 mean.

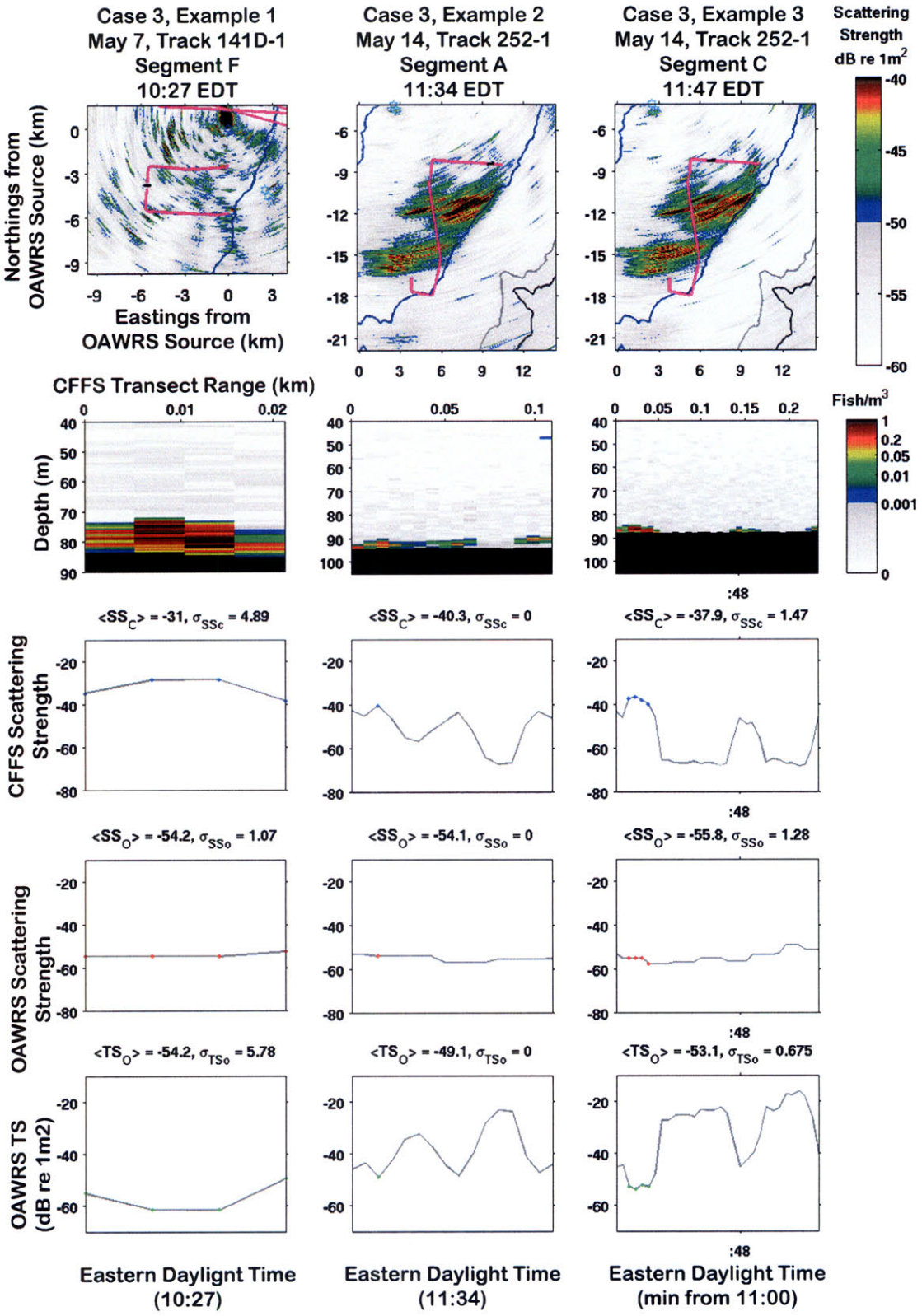

Figure B-16: Site 2, Case 3

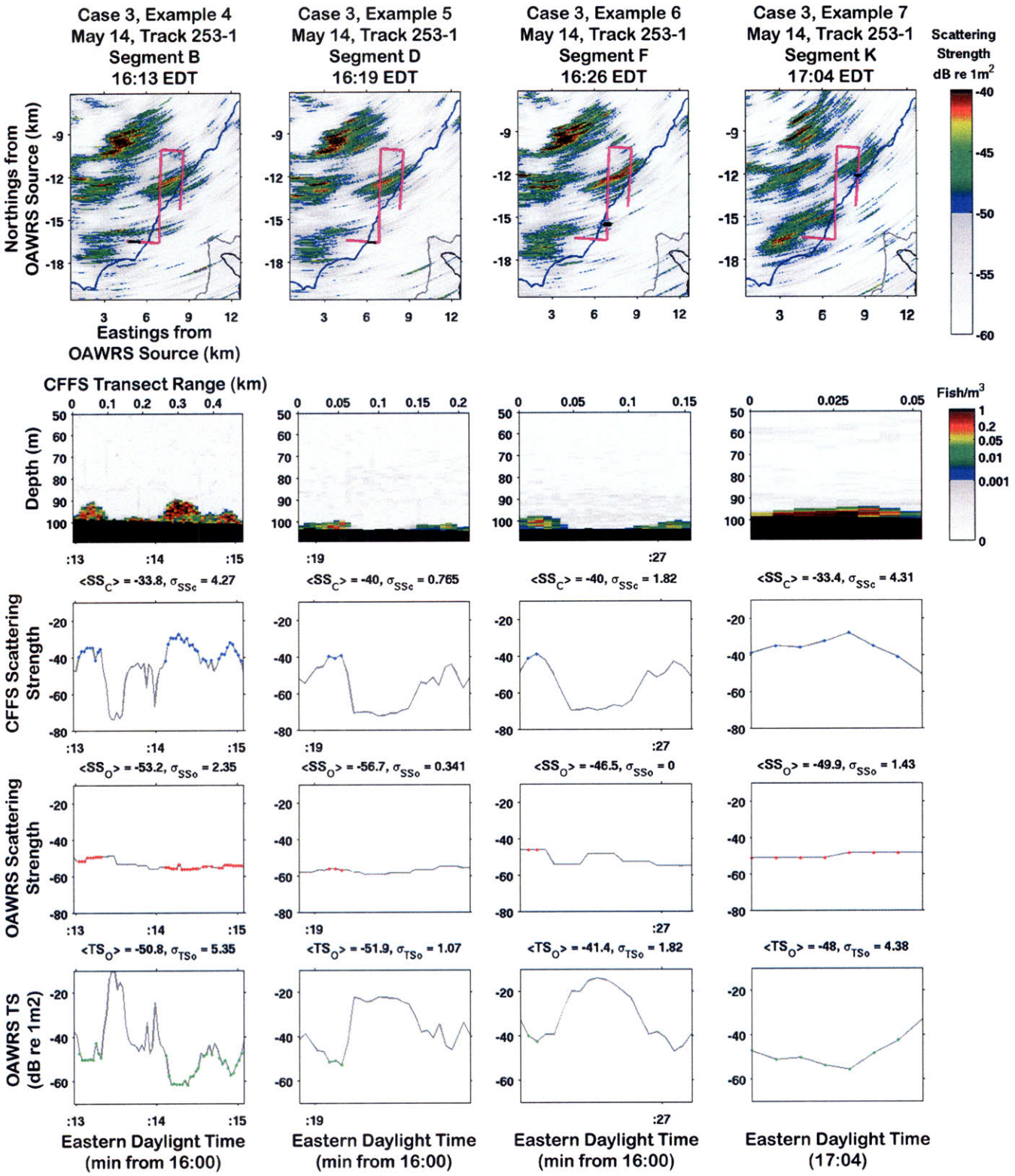

Figure B-17: Site 2, Case 2C

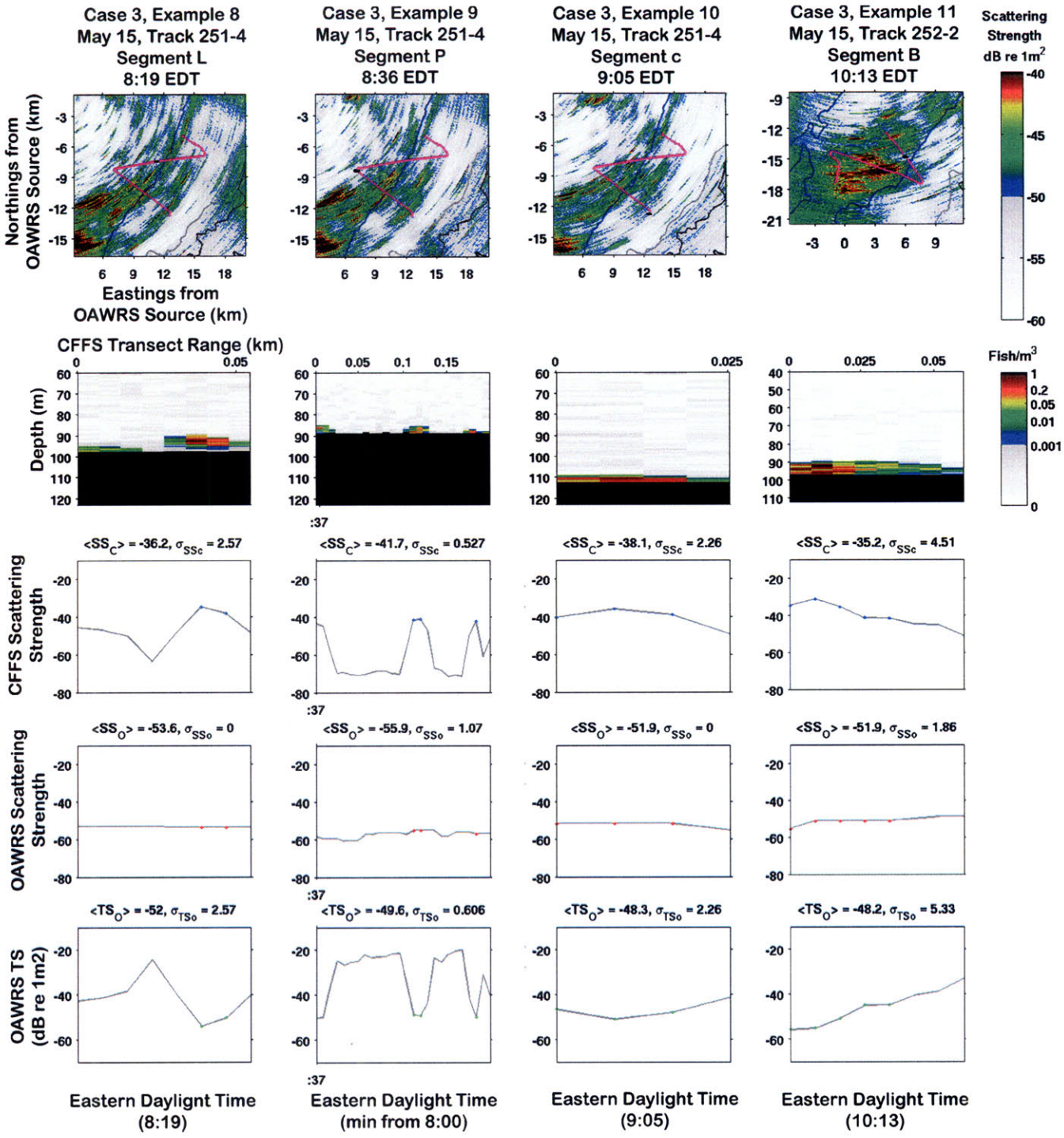

Figure B-18: Site 2, Case 2C

B.2 875-975 Hz (WMA) Regime

B.2.1 Case 2A: Non-Stationary Populations within Low Density Regions of an OAWRS shoal

Unlike the measurements at the lower frequency band (390-440 Hz), there were only four tracks from 2 days that afforded co-registration with OAWRS imaged fish populations. On May 9, there was one instance where CFFS traverses through the low density, patchy region of a shoal roughly 5km by 2km in major-minor axis extent approximately 6km southeast of the moored OAWRS source, as shown in the 2D OAWRS scattering map of Fig. B-19. The corresponding CFFS range-depth profile shows a small, compact population roughly 40m in along-transect length occupying a 7m depth layer 2m from the ocean bottom. For this population, the mean calibrated TS was found to be -34 dB re $1m^2$ at the center frequency of 925 Hz.

Example	Day	Track	Segment	Time (EDT)	Number of Estimation Points	Coherence Length (Estimation Points)	Independent Samples (Coherent Cells)	$< TS_O >$ dB re $1m^2$	σ_{TS_O} dB (before averaging)	σ_{TS_O} dB (after averaging)
1	9-May	202-6	A	12:36	10	2	5	-34.3	3.4	1.5

Table B.7: Table summarizing the calibrated OAWRS TS and standard deviation, as well as the standard deviation per segment after applying stationary averaging over independent coherent cells.

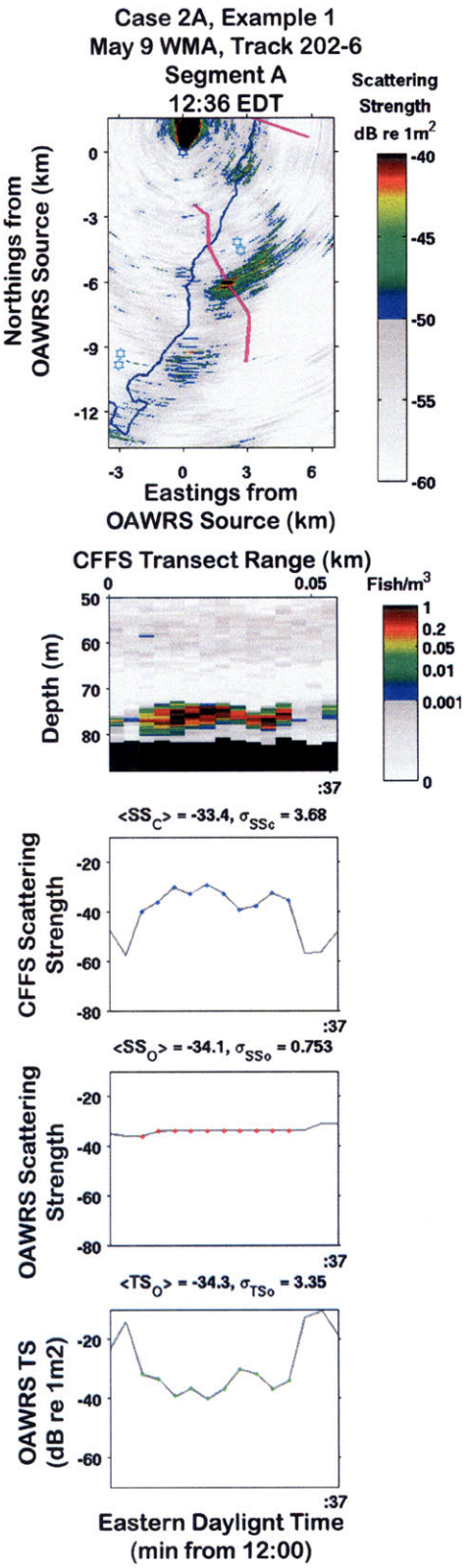

Figure B-19: Site 2, Case 2A

B.2.2 Case 2C: Non-Stationary Populations at the Boundaries of an OAWRS Shoal

Six examples are presented from the three tracks on May 9, where CFFS traverses through the periphery of OAWRS shoaling regions and measure discrete fish populations extending tens to a hundred meters in along-transect extent. The shoaling regions imaged at the high frequencies, however, are not as extensive as those consolidated shoals from May 14 and May 15 imaged with the 390-440 Hz waveform. The global mean before applying a correction factor is roughly -40dB re $1m^2$ at 925 Hz. After applying a correction factor, the corrected global mean is found to be roughly -32dB re $1m^2$ at 925 Hz.

Example	Day	Track	Segment	Time (EDT)	Number of Estimation Points	Coherence Length (Estimation Points)	Independent Samples (Coherent Cells)	$< TS_O >$ dB re $1m^2$	σ_{TS_O} dB (before averaging)	σ_{TS_O} dB (after averaging)
1	9-May	202-5	H	8:17	2	2	1	-38.5	2.7	2.7
2	9-May	202-5	I	8:19	25	25	1	-38.2	3.6	3.6
3	9-May	201-4	C	9:58	32	4	8	-41.7	5.4	1.9
4	9-May	202-6	B	12:40	9	1	9	-38.4	3.4	3.4
5	9-May	202-6	C	12:42	16	1	16	-39.5	4.6	4.6
6	9-May	202-6	D	12:44	10	3	3	-38.5	4.1	2.4

Table B.8: Table summarizing the calibrated OAWRS TS and standard deviation, as well as the standard deviation per segment after applying stationary averaging over independent coherent cells.

Example	Day	Track	Segment	Uncorrected $< TS_O >$	τ (dB)	Corrected $< TS_O >$
1	9-May	202-5	H	-38.5	13.4	-25.1
2	9-May	202-5	I	-38.2	5.6	-32.6
3	9-May	201-4	C	-41.7	5.3	-36.4
4	9-May	202-6	B	-38.4	10.1	-28.3
5	9-May	202-6	C	-39.5	8.1	-31.4
6	9-May	202-6	D	-38.5	8.3	-30.2

Table B.9: Table summarizing the adjusted mean OAWRS TS after applying the areal correction for the Case 2C Examples.

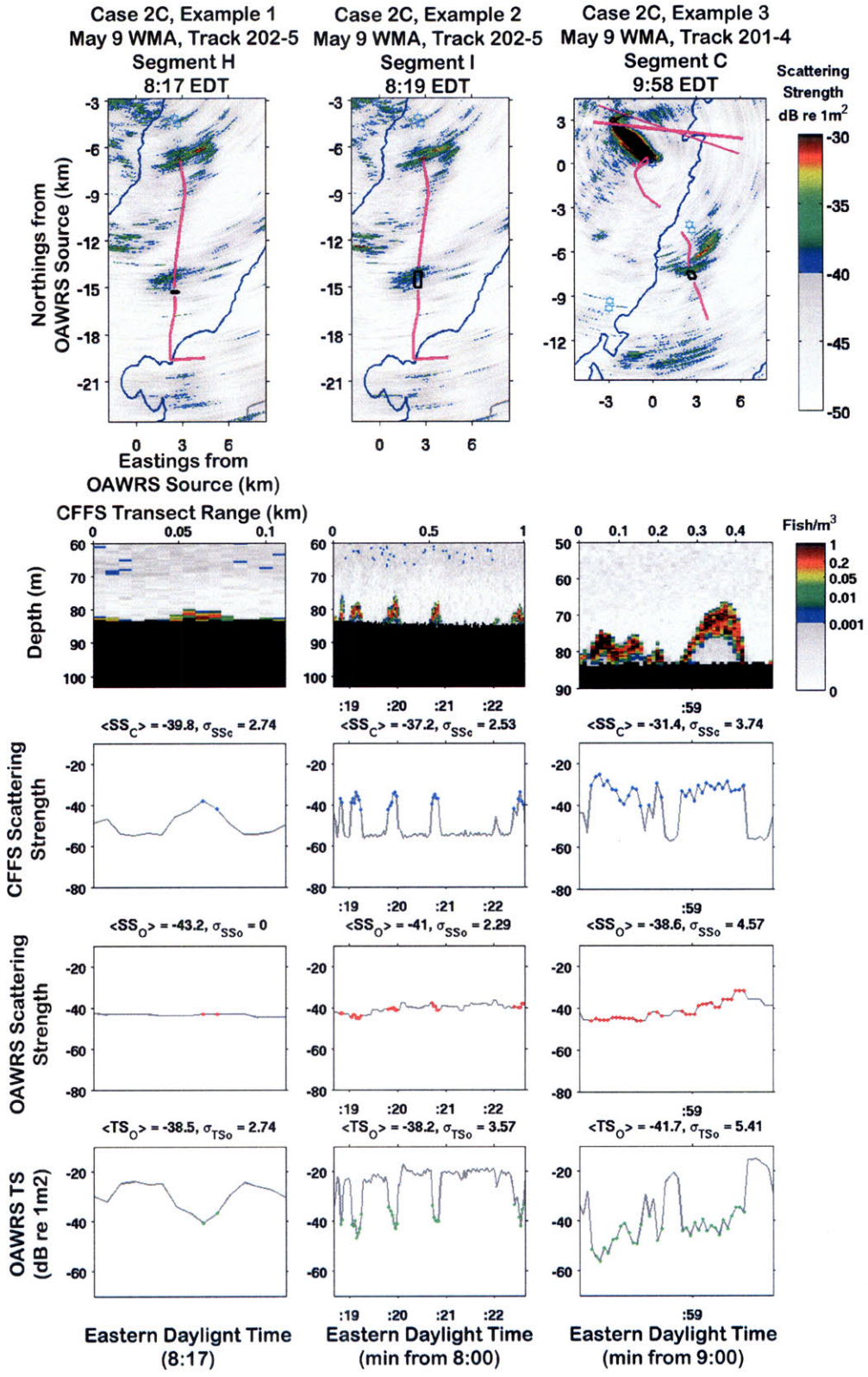

Figure B-20: Site 2, Case 2C

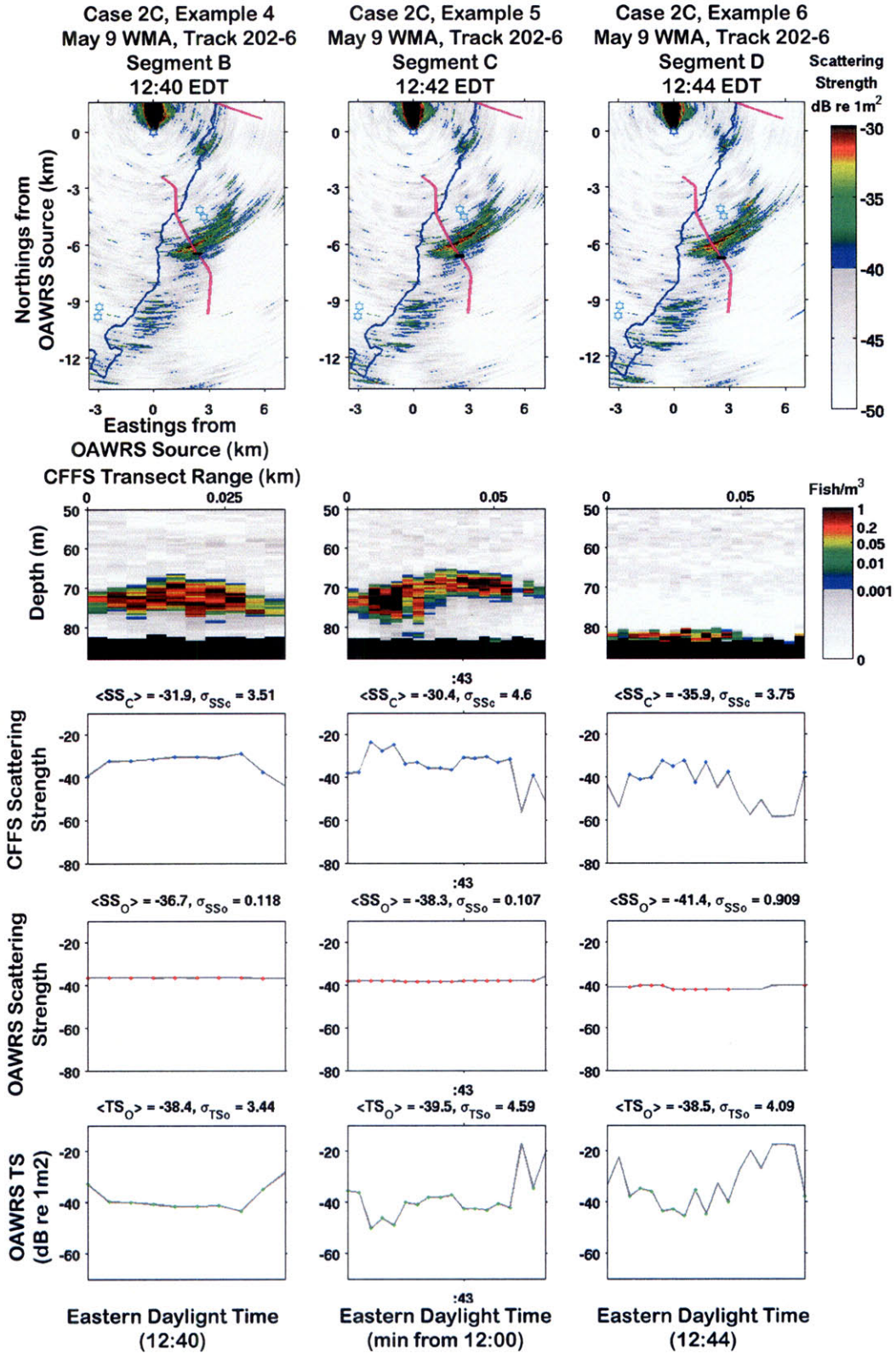

Figure B-21: Site 2, Case 2C

B.2.3 Case 3: Non-Stationary Populations within Small, Scattered Schools

On May 9 and May 15, there were three instances each where CFFS traverses through small scattered schools. The global mean before applying a correction factor is roughly -38 dB re $1m^2$ at 925 Hz on May 9 and -40 dB on May 15. After applying a correction factor, the corrected global mean is found to be -28dB re $1m^2$ at 925 Hz on May 9 and -38 dB for the May 15 schools. The corrected global mean on May 9 is consistent with the Case 2C values.

Example	Day	Track	Segment	Time (EDT)	Number of Estimation Points	Coherence Length (Estimation Points)	Independent Samples (Coherent Cells)	$< TS_O >$ dB re $1m^2$	σ_{TS_O} dB (before averaging)	σ_{TS_O} dB (after averaging)
1	9-May	202-5	L	8:42	1	1	1	-40.5	0.0	0.0
2	9-May	202-5	M	8:44	5	4	1	-36.5	2.7	2.7
3	9-May	201-4	B	9:54	2	2	1	-42.0	0.7	0.7
4	15-May	252-3	A	14:55	57	5	11	-38.9	4.4	1.3
5	15-May	252-3	B	15:00	2	2	1	-43.6	1.5	1.5
6	15-May	252-3	C	15:03	55	5	11	-42.0	2.5	0.8

Table B.10: Table summarizing the calibrated OAWRS TS and standard deviation, as well as the standard deviation per segment after applying stationary averaging over independent coherent cells.

Example	Day	Track	Segment	Uncorrected $< TS_O >$	τ (dB)	Corrected $< TS_O >$
1	9-May	202-5	L	-40.5	13.8	-26.7
2	9-May	202-5	M	-36.5	9.0	-27.5
3	9-May	201-4	B	-42.0	10.3	-31.7
4	15-May	252-3	A	-38.9	1.2	-37.7
5	15-May	252-3	B	-43.6	13.3	-30.3
6	15-May	252-3	C	-42.0	2.7	-39.3

Table B.11: Table summarizing the adjusted mean OAWRS TS after applying the areal correction for the Case 2C Examples.

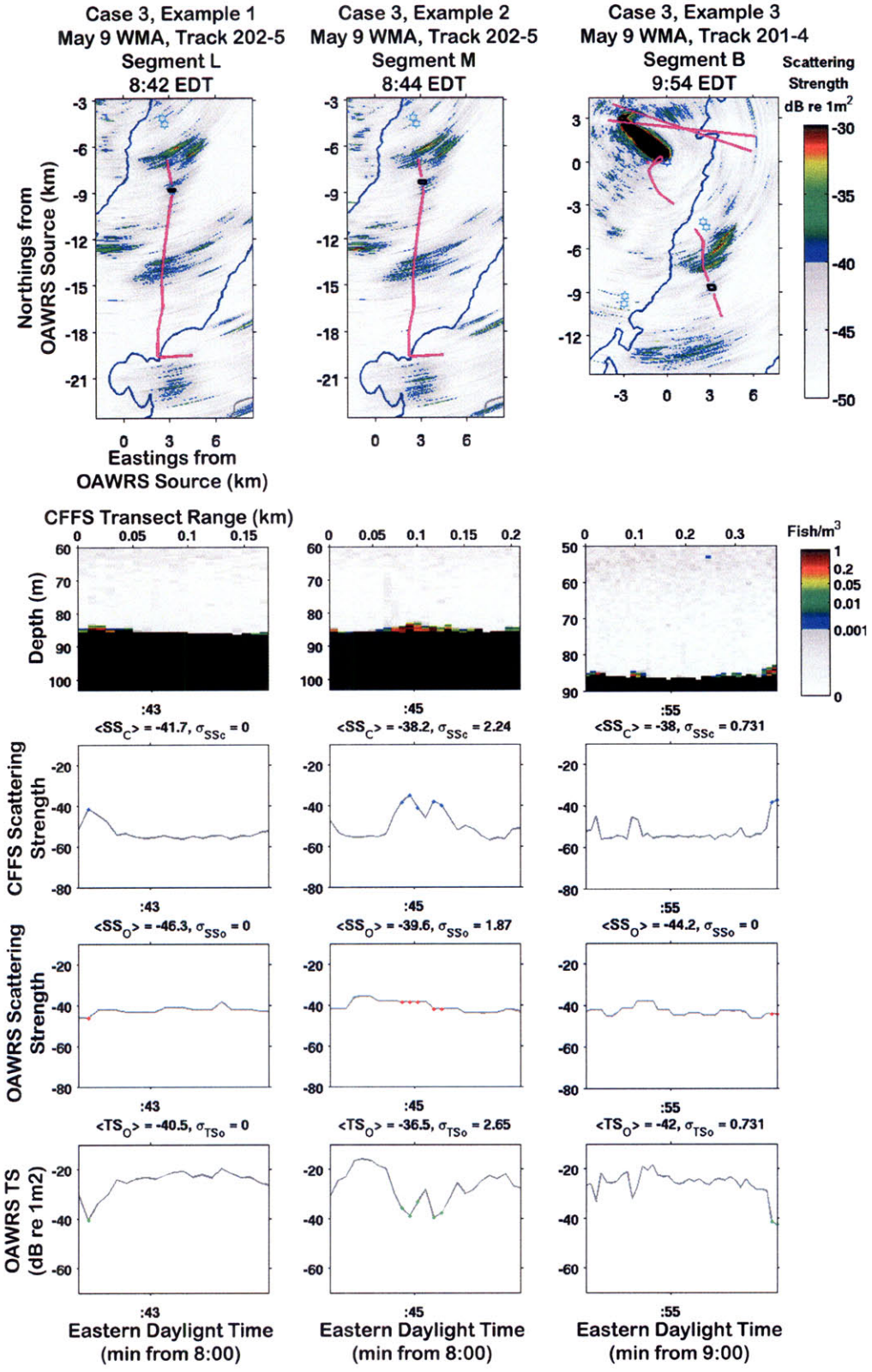

Figure B-22: Site 2, Case 2C

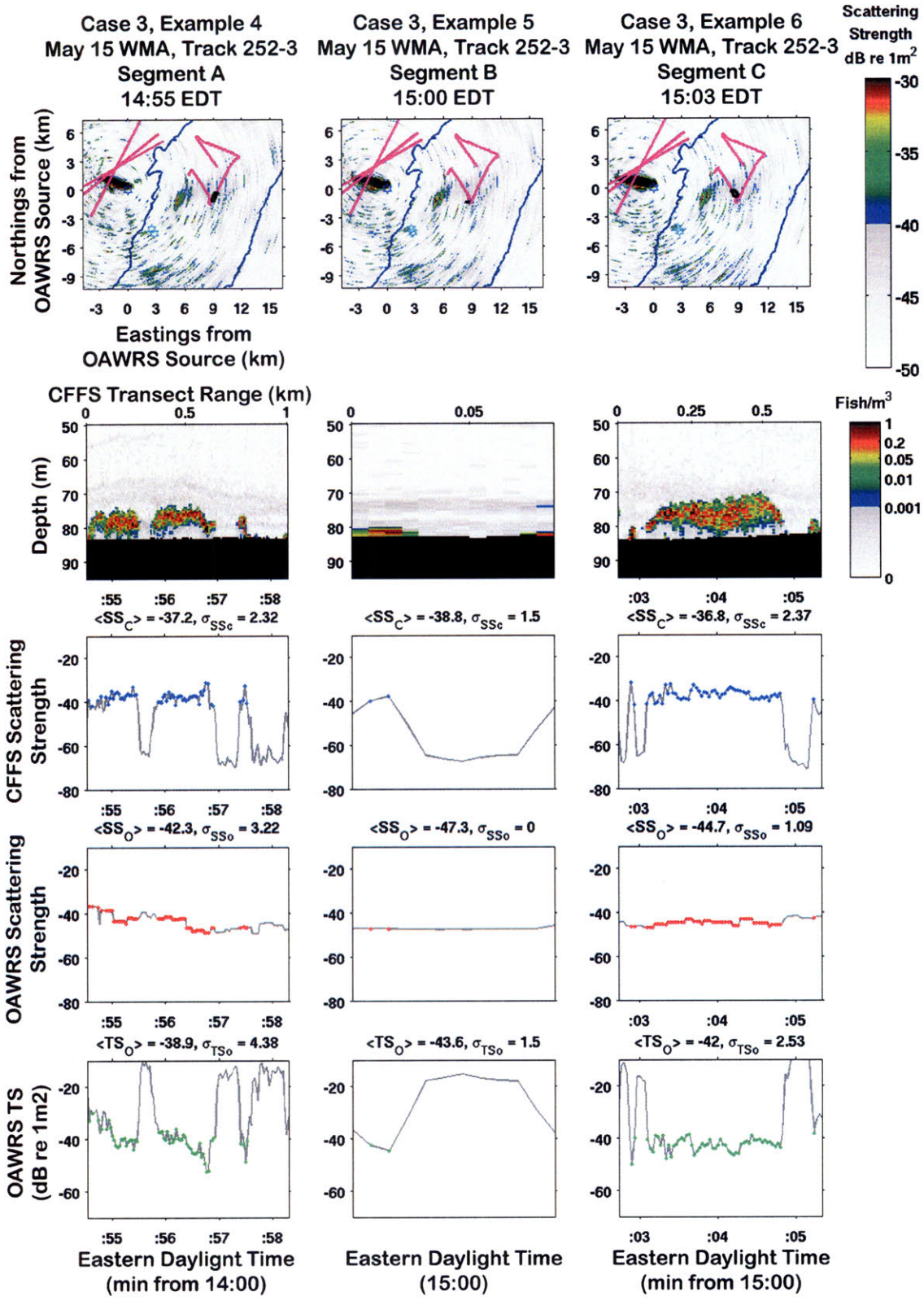

Figure B-23: Site 2, Case 2C

B.3 1250-1400 Hz (WMB)

B.3.1 Case 2A: Non-Stationary Populations within Low Density Regions of an OAWRS shoal

On May 9, there was one instance where CFFS traverses through the diffuse, patchy region of a shoal roughly 5km by 2km in major-minor axis extent approximately 6km southeast of the moored OAWRS source, as shown in the 2D OAWRS scattering map of Fig. B-19. The corresponding CFFS range-depth profile shows a small, compact population roughly 40m in along-transect length occupying a 7m depth layer 2m from the ocean bottom. For this population, the mean calibrated TS was found to be -33 dB re $1m^2$ at the center frequency of 1325 Hz.

Example	Day	Track	Segment	Time (EDT)	Number of Estimation Points	Coherence Length (Estimation Points)	Independent Samples (Coherent Cells)	$< TS_O >$ dB re $1m^2$	σ_{TS_O} dB (before averaging)	σ_{TS_O} dB (after averaging)
1	9-May	202-6	A	12:36	10	2	5	-32.8	3.1	1.4

Table B.12: Table summarizing the calibrated OAWRS TS and standard deviation, as well as the standard deviation per segment after applying stationary averaging over independent coherent cells.

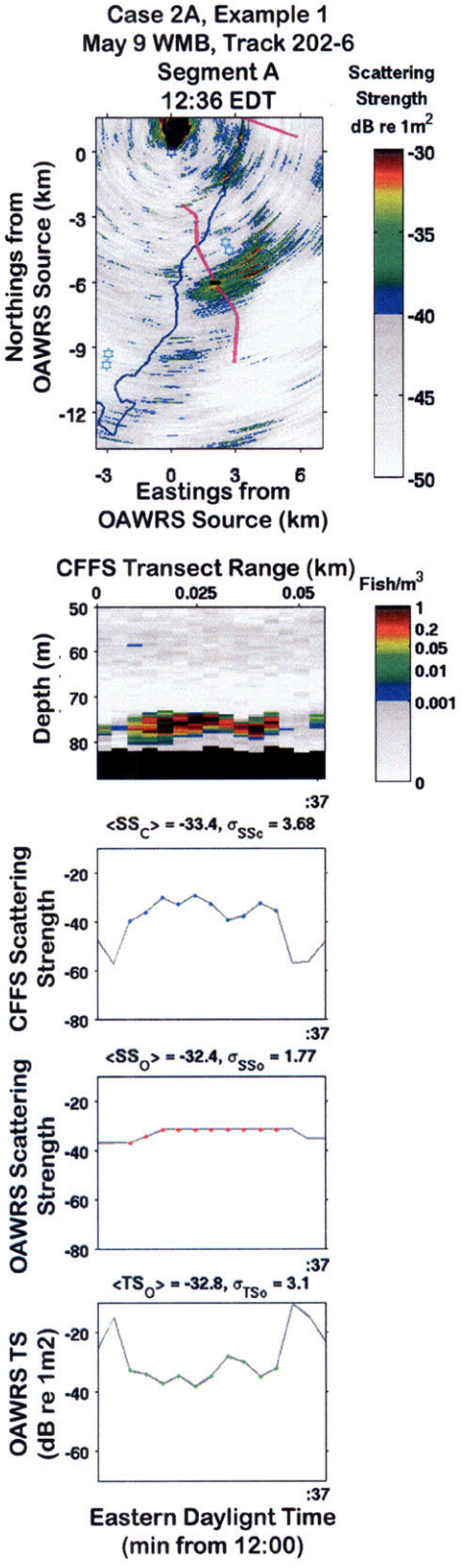

Figure B-24: Site 2, Case 2A

B.3.2 Case 2C: Non-Stationary Populations at the Boundaries of an OAWRS Shoal

The global mean before applying a correction factor is -37dB re $1m^2$ at 1325 Hz. After applying a correction factor, the corrected global mean is found to be roughly -29dB re $1m^2$ at 1325 Hz.

Example	Day	Track	Segment	Time (EDT)	Number of Estimation Points	Coherence Length (Estimation Points)	Independent Samples (Coherent Cells)	$< TS_O >$ dB re $1m^2$	σ_{TS_O} dB (before averaging)	σ_{TS_O} dB (after averaging)
1	9-May	202-5	H	8:17	2	2	1	-39.80	2.7	2.7
2	9-May	202-5	I	8:19	25	25	1	-37.90	3.0	3.0
3	9-May	201-4	C	9:58	32	4	8	-38.70	5.2	1.8
4	9-May	202-6	B	12:40	9	1	9	-38.00	3.8	3.8
5	9-May	202-6	C	12:42	16	1	16	-35.30	5.3	5.3
6	9-May	202-6	D	12:44	10	3	3	-33.90	4.2	2.4

Table B.13: Table summarizing the calibrated OAWRS TS and standard deviation, as well as the standard deviation per segment after applying stationary averaging over independent coherent cells.

Example	Day	Track	Segment	Uncorrected $< TS_O >$	τ (dB)	Corrected $< TS_O >$
1	9-May	202-5	H	-39.80	14.6	-25.2
2	9-May	202-5	I	-37.90	7.0	-30.9
3	9-May	201-4	C	-38.70	6.7	-32.0
4	9-May	202-6	B	-38.00	11.1	-26.9
5	9-May	202-6	C	-35.30	9.2	-26.1
6	9-May	202-6	D	-33.90	9.5	-24.4

Table B.14: Table summarizing the adjusted mean OAWRS TS after applying the areal correction for the Case 2C Examples.

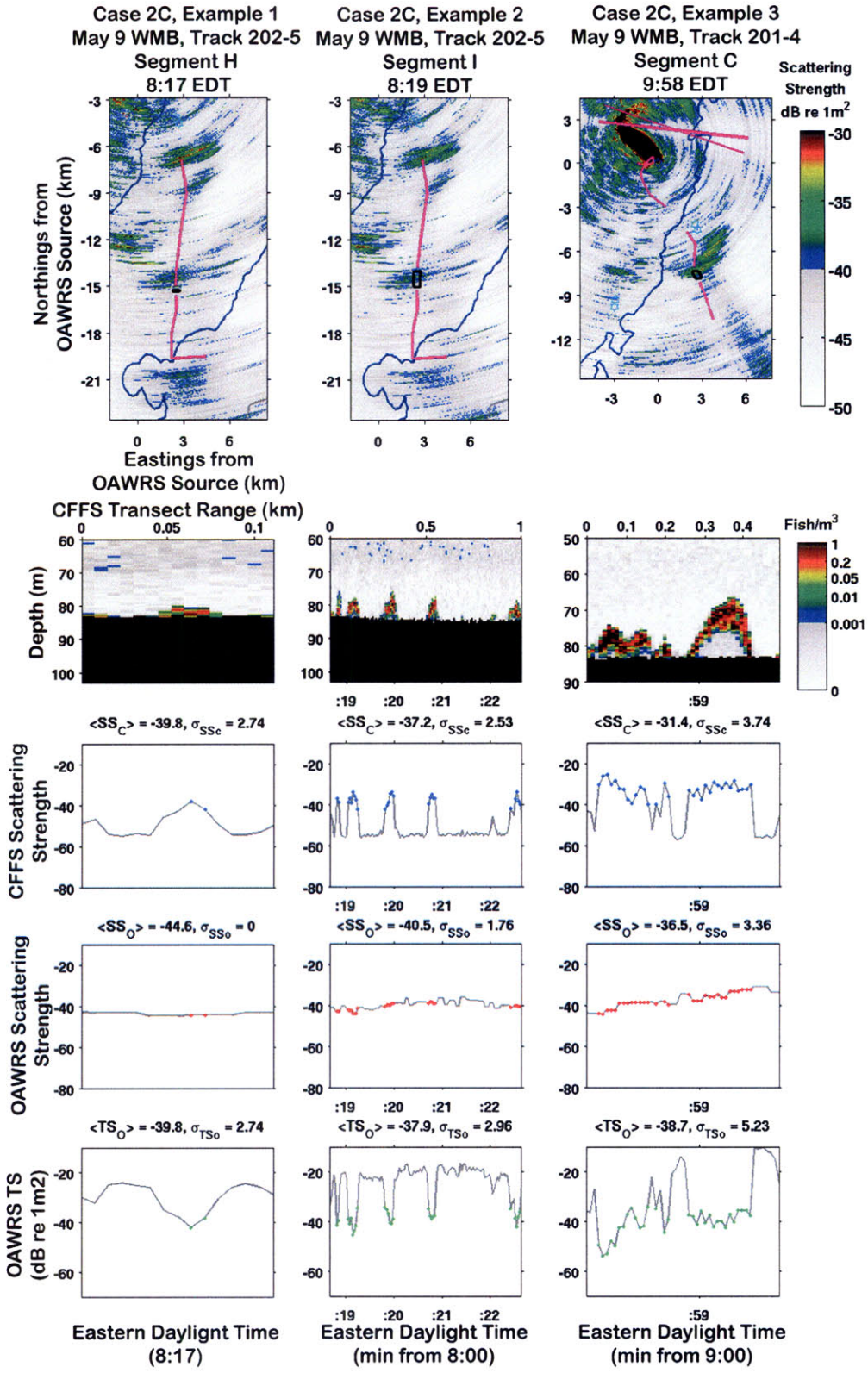

Figure B-25: Site 2, Case 2C

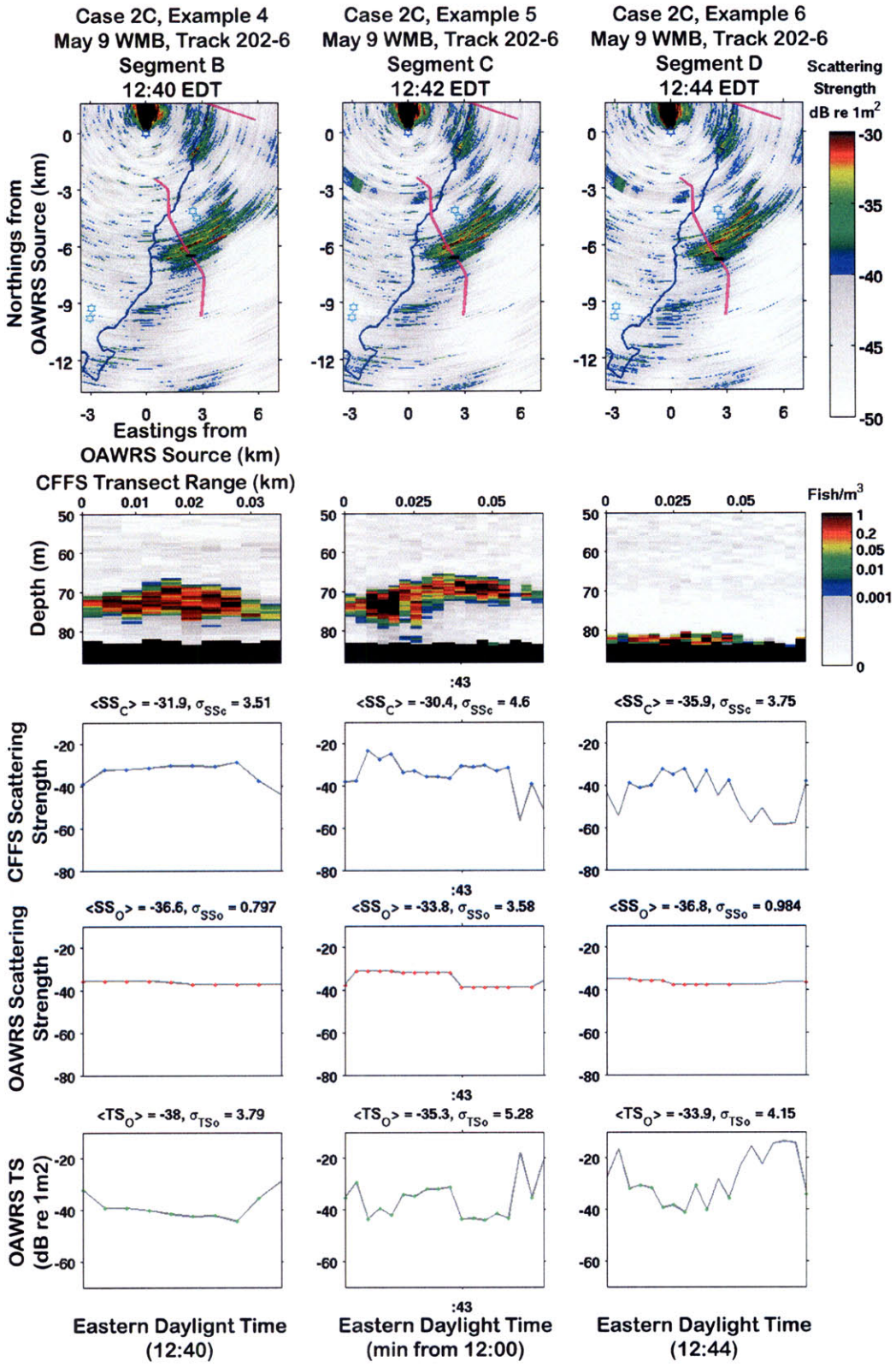

Figure B-26: Site 2, Case 2C

B.3.3 Case 3: Non-Stationary Populations within Small, Scattered Schools

On May 9 and May 15, there were three instances each where CFFS traverses through small scattered schools. The global mean before applying a correction factor is -38 dB re $1m^2$ at 1325 Hz on May 9 and -37dB on May 15. After applying a correction factor, the corrected global mean is found to be -27 dB re $1m^2$ at 1325 Hz on May 9 and -33 dB for the May 15 schools.

Example	Day	Track	Segment	Time (EDT)	Number of Estimation Points	Coherence Length (Estimation Points)	Independent Samples (Coherent Cells)	$< TS_O >$ dB re $1m^2$	σ_{TS_O} dB (before averaging)	σ_{TS_O} dB (after averaging)
1	9-May	202-5	L	8:42	1	1	1	-38.00	0.0	0.0
2	9-May	202-5	M	8:44	5	4	1	-38.20	2.3	2.3
3	9-May	201-4	B	9:54	2	2	1	-40.30	0.7	0.7
4	15-May	252-3	A	14:55	57	5	11	-37.60	3.6	1.1
5	15-May	252-3	B	15:00	2	2	1	-39.40	1.5	1.5
6	15-May	252-3	C	15:03	55	5	11	-36.40	2.9	0.9

Table B.15: Table summarizing the calibrated OAWRS TS and standard deviation, as well as the standard deviation per segment after applying stationary averaging over independent coherent cells.

Example	Day	Track	Segment	Uncorrected $< TS_O >$	τ (dB)	Corrected $< TS_O >$
1	9-May	202-5	L	-38.00	14.8	-23.2
2	9-May	202-5	M	-38.20	10.6	-27.6
3	9-May	201-4	B	-40.30	11.5	-28.8
4	15-May	252-3	A	-37.60	2.6	-35.0
5	15-May	252-3	B	-39.40	14.7	-24.7
6	15-May	252-3	C	-36.40	4.1	-32.3

Table B.16: Table summarizing the adjusted mean OAWRS TS after applying the areal correction for the Case 2C Examples.

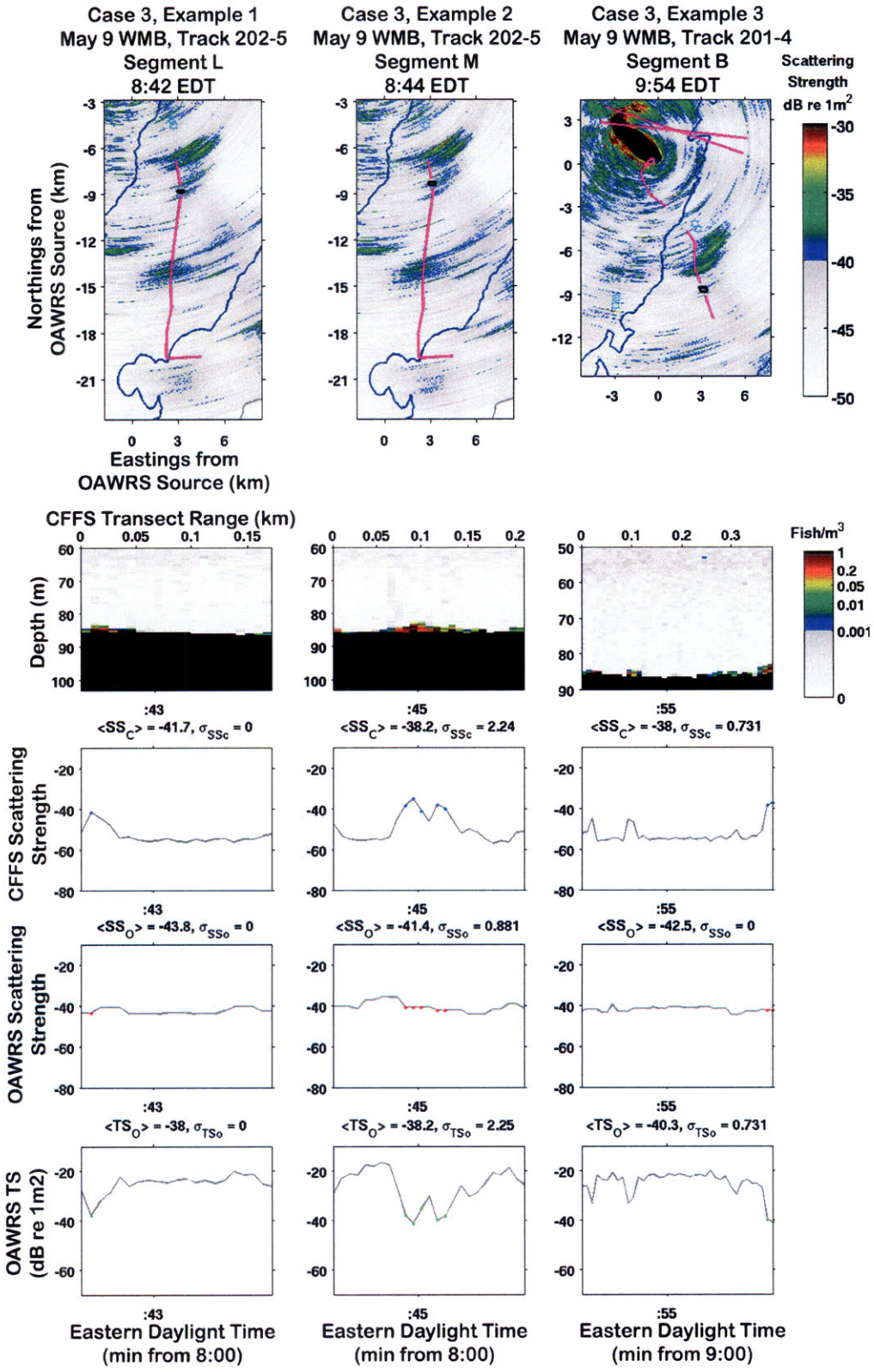

Figure B-27: Site 2, Case 2C

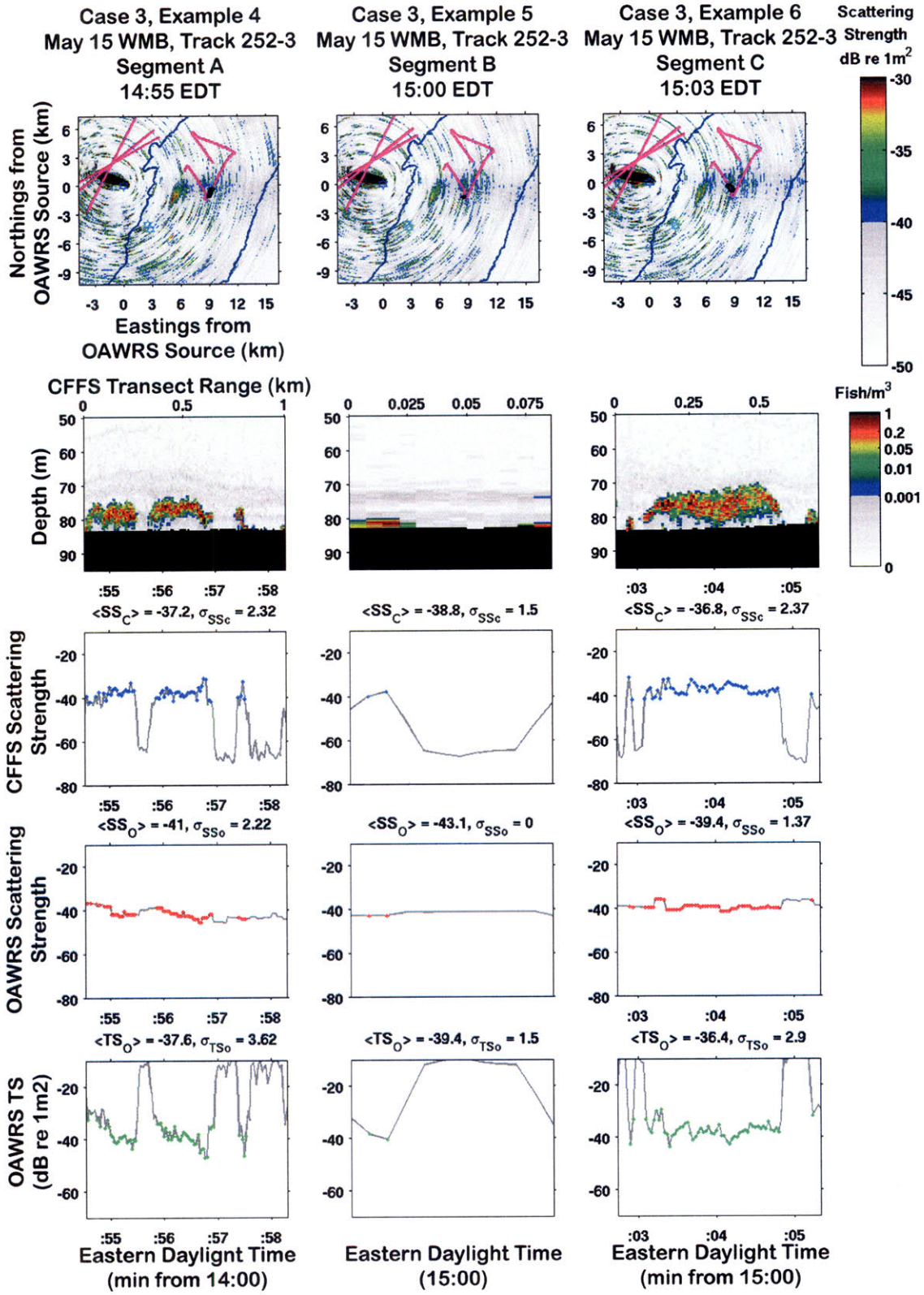

Figure B-28: Site 2, Case 2C

Appendix C

OAWRS TS Summary Tables

Example	Date	Time	Segment	Range from OAWRS Reciever (m)	Angle from OAWRS Broadside (deg)	Mean Cross Range Resolution (m)	OAWRS Range Resolution (m)	Number of Corresponding Resolution Footprints	Area of Corresponding Footprints (m^2)
1	7-May	141A-2	E	3287	38	209	15	1	3135
2	7-May	141A-2	F	2915	28	164	15	1	2460
3	8-May	201-2	E	10251	39	657	15	1	9855
4	14-May	252-1	D	13503	7	676	15	2	20280
5	14-May	252-1	E	14421	5	720	15	3	32400
6	14-May	252-1	F	14739	3	734	15	4	44040
7	14-May	251-2	A	13957	5	697	15	2	20910
8	14-May	251-2	B	14253	6	713	15	4	42780
9	14-May	253-1	H	15815	17	820	15	4	49200
10	15-May	251-4	B	20994	32	1228	15	9	165780
11	15-May	251-4	H	17303	18	904	15	1	13560
12	15-May	251-4	I	16954	15	875	15	1	13125
13	15-May	251-4	J	16724	14	856	15	2	25680
14	15-May	251-4	M	15493	9	780	15	2	23400
15	15-May	251-4	Q	14376	10	726	15	2	21780
16	15-May	251-4	R	15228	11	771	15	5	57825
17	15-May	251-4	T	15985	11	811	15	3	36495
18	15-May	251-4	U	16589	12	843	15	7	88515
19	15-May	251-4	W	17422	15	896	15	4	53760
20	15-May	251-4	Y	19016	16	982	15	4	58920
21	15-May	252-2	D	20204	11	1025	15	5	76875
22	15-May	254-1	A	17135	40	1110	15	1	16650
23	15-May	254-1	D	16172	38	1020	15	1	15300
24	15-May	254-1	E	16002	39	1027	15	4	61620
25	15-May	251-5	A	10756	45	752	15	5	56400
26	15-May	251-5	B	7597	22	409	15	2	12270

Table C.1: Table summarizing the OAWRS Resolution Parameters for the Case 2A Segments, 390-440 Hz (WX1)

Example	Date	Track	Segment	Mean Fish Density fish/m^2)	Depth Extent (m)	Bottom Depth	Longest Continuous Along-Transect Extent (m)	Transect Trajectory Angle* (deg)	Cross Range Projection (m)	Range Projection (km)	Estimated Area Occupied by fish (m^2)
1	7-May	141A-2	E	25.12	57-80	80	50	89	1	1	2945
2	7-May	141A-2	F	0.81	55-70	79	40	90	0	0	1885
3	8-May	201-2	E	0.66	72-80	81	90	90	0	0	9543
4	14-May	252-1	D	0.33	80-85	86	40	43	29	29	1885
5	14-May	252-1	E	0.35	82-85	86	40	19	38	38	1885
6	14-May	252-1	F	0.3	79-85	85	60	17	57	57	4241
7	14-May	251-2	A	1.05	82-85	85	30	35	25	25	1060
8	14-May	251-2	B	1.38	77-86	86	60	38	47	47	4241
9	14-May	253-1	H	0.33	90-92	92	50	12	49	49	2945
10	15-May	251-4	B	0.93	110-115	117	125	11	123	123	18408
11	15-May	251-4	H	0.51	92-100	101	15	56	8	8	265
12	15-May	251-4	I	1.66	92-100	100	15	55	9	9	265
13	15-May	251-4	J	0.38	97-100	100	40	53	24	24	1885
14	15-May	251-4	M	0.29	90-95	95	40	57	22	22	1885
15	15-May	251-4	Q	0.25	85-90	90	25	9	25	25	736
16	15-May	251-4	R	1.2	81-91	91	75	11	74	74	6627
17	15-May	251-4	T	0.55	90-95	95	45	9	44	44	2386
18	15-May	251-4	U	0.59	90-98	98	100	10	98	98	11781
19	15-May	251-4	W	0.34	94-100	100	50	8	50	50	2945
20	15-May	251-4	Y	0.62	95-110	110	50	7	50	50	2945
21	15-May	252-2	D	0.78	97-101	101	70	9	69	69	5773
22	15-May	254-1	A	0.27	93-97	97	25	85	2	2	736
23	15-May	254-1	D	0.35	87-92	92	50	82	7	7	2945
24	15-May	254-1	E	0.3	83-89	89	300	81	47	47	106029
25	15-May	251-5	A	0.85	75-80	83	80	26	72	72	7540
26	15-May	251-5	B	0.72	82-86	86	25	14	24	24	736

Table C.2: Table summarizing the CFFS Characterization of the Case 2A Segments, 390-440 Hz (WX1)

Example	Date	Track	Segment	Number of Estimation	$< TS_C >$ dB re	σ_{TS_C} (dB)	$< SS_C >$ dB re	σ_{SS_C} (dB)	$< SS_O >$ dB re	σ_{SS_O} (dB)	$< TS_O >$ dB re	σ_{TS_O} (dB)	σ_{TS_O} (dB)
1	7-May	141A-2	E	13	-35.5	1.2	-21.5	7.6	-45.4	0.3	-49	7.7	7.7
2	7-May	141A-2	F	6	-35.5	1.2	-36.4	2.5	-41.7	0.4	-39.6	2.7	2.7
3	8-May	201-2	E	14	-35.9	1.45	-37.7	3.4	-42.7	2.2	-42.9	3.8	1
4	14-May	252-1	D	3	-35.3	0.64	-40.1	0.4	-48.8	0.0	-44	0.4	0.4
5	14-May	252-1	E	4	-35.3	0.64	-39.9	1.0	-46.8	1.8	-42.2	1.4	1.4
6	14-May	252-1	F	3	-35.3	0.64	-40.5	1.3	-48.1	1.0	-42.9	0.6	0.6
7	14-May	251-2	A	1	-35.3	0.64	-35.1	0.0	-40.7	0.0	-41	0	0
8	14-May	251-2	B	16	-35.3	0.64	-33.9	4.2	-43.8	0.9	-41.6	4.4	3.1
9	14-May	253-1	H	3	-35.3	0.64	-40.1	0.4	-47.8	1.0	-42.9	0.9	0.9
10	15-May	251-4	B	12	-35.3	0.64	-35.6	4.2	-48.4	1.6	-44.8	4.5	3.2
11	15-May	251-4	H	4	-35.3	0.64	-38.2	1.2	-54.1	3.6	-43.8	1.2	0.6
12	15-May	251-4	I	3	-35.3	0.64	-33.1	5.4	-44.4	1.6	-43.6	4.2	2.4
13	15-May	251-4	J	2	-35.3	0.64	-39.5	1.5	-48.3	0.5	-43.9	1	1
14	15-May	251-4	M	2	-35.3	0.64	-40.7	0.9	-51	4.1	-45.9	3.2	3.2
15	15-May	251-4	Q	1	-35.3	0.64	-41.3	0.0	-52.2	0.0	-46.3	0	0
16	15-May	251-4	R	7	-35.3	0.64	-34.5	1.8	-45.3	0.7	-45.4	2	2
17	15-May	251-4	T	4	-35.3	0.64	-37.9	3.2	-47.5	1.4	-42.9	3.7	2.6
18	15-May	251-4	U	8	-35.3	0.64	-37.6	2.6	-46.7	2.2	-43.5	2.6	1.8
19	15-May	251-4	W	3	-35.3	0.64	-40	1.3	-48.9	0.0	-44	1.3	1.3
20	15-May	251-4	Y	5	-35.3	0.64	-37.4	1.5	-47.2	1.1	-44.7	1.6	0.7
21	15-May	252-2	D	7	-35.3	0.64	-36.4	3.2	-47	1.6	-43.8	4.1	2.4
22	15-May	254-1	A	2	-35.3	0.64	-41	1.2	-47.1	0.0	-41.2	1.2	1.2
23	15-May	254-1	D	12	-35.3	0.64	-39.8	1.2	-43.8	2.7	-39	3	2.1
24	15-May	254-1	E	10	-35.3	0.64	-40.5	1.2	-45.2	1.8	-39.8	1.6	1.1
25	15-May	251-5	A	14	-35.3	0.64	-36	3.2	-44.4	0.6	-41.4	3.2	2.3
26	15-May	251-5	B	2	-35.3	0.64	-36.7	5.1	-46	0.2	-41.8	5.3	5.3

Table C.3: Table summarizing the Statistical Parameters of Estimation Variabilities of the Case 2A Segments, 390-440 Hz (WX1)

Example	Date	Time	Segment	Range from OAWRS Reciever (m)	Angle from OAWRS Broadside (deg)	Mean Cross Range Resolution (m)	OAWRS Range Resolution (m)	Number of Corresponding Resolution Footprints	Area of Corresponding Footprints (m^2)
1	8-May	201-2	D	10051	38	634	15	2	19020
2	14-May	252-1	G	15118	3	753	15	3	33885
3	15-May	252-2	G	19329	11	980	15	2	29400
4	15-May	252-2	H	19039	10	960	15	4	57600
5	15-May	252-2	I	18813	12	956	15	2	28680
6	15-May	252-2	J	18490	13	944	15	2	28320
7	15-May	251-5	C	7990	18	419	15	2	12570

Table C.4: Table summarizing the OAWRS Resolution Parameters for the Case 2B Segments, 390-440 Hz (WX1)

Example	Date	Track	Segment	Mean Fish Density fish/m^2)	Depth Extent (m)	Bottom Depth	Longest Continuous Along-Transect Extent (m)	Transect Trajectory Angle* (deg)	Cross Range Projection (m)	Range Projection (km)	Estimated Area Occupied by fish (m^2)
1	8-May	201-2	D	0.66	80-81	81	30	90	0	30	1060
2	14-May	252-1	G	0.44	80-85	86	100	18	95	31	11781
3	15-May	252-2	G	0.59	90-95	95	30	44	22	21	1797
4	15-May	252-2	H	0.42	87-91	91	70	45	49	49	5773
5	15-May	252-2	I	0.47	85-90	90	32	44	23	22	1206
6	15-May	252-2	J	0.32	85-87	87	22	43	16	15	570
7	15-May	251-5	C	0.65	80-85	85	70	13	68	16	10132

Table C.5: Table summarizing the CFFS Characterization of the Case 2B Segments, 390-440 Hz (WX1)

Example	Date	Track	Segment	Number of Estimation	$< TS_C >$ dB re	σ_{TS_C} (dB)	$< SS_C >$ dB re	σ_{SS_C} (dB)	$< SS_O >$ dB re	σ_{SS_O} (dB)	$< TS_O >$ dB re	σ_{TS_O} (dB)	σ_{TS_O} (dB)
1	8-May	201-2	D	5	-35.9	1.45	-37.7	3.37	-39.9	0.0	-36.2	3.4	3.4
2	14-May	252-1	G	13	-35.3	0.64	-38.9	2.19	-43	0.9	-38.4	2.8	1.1
3	15-May	252-2	G	2	-35.3	0.64	-37.6	1.49	-40.9	0.0	-38.3	1.5	1.5
4	15-May	252-2	H	4	-35.3	0.64	-39.1	1.29	-37.4	1.8	-33.3	2.3	2.3
5	15-May	252-2	I	3	-35.3	0.64	-38.6	2.52	-38.4	0.1	-34.5	2.4	2.4
6	15-May	252-2	J	1	-35.3	0.64	-40.3	0	-37.5	0.0	-32.5	0.0	0.0
7	15-May	251-5	C	12	-35.3	0.64	-37.2	2.8	-40.7	3.0	-36.8	4.5	3.2

Table C.6: Table summarizing the Statistical Parameters of Estimation Variabilities of the Case 2B Segments, 390-440 Hz (WX1)

Example	Date	Time	Segment	Range from OAWRS Reciever (m)	Angle from OAWRS Broadside (deg)	Mean Cross Range Resolution (m)	OAWRS Range Resolution (m)	Number of Corresponding Resolution Footprints	Area of Corresponding Footprints (m^2)
1	7-May	141A-2	I	3626	6	181	15	2	5430
2	7-May	141A-2	K	4223	12	215	15	3	9675
3	8-May	201-3	A	14445	24	787	15	2	23610
4	8-May	202-4	B	5832	48	437	15	3	19665
5	14-May	252-1	I	19150	2	953	15	16	228720
6	14-May	252-1	K	19366	3	964	15	2	28920
7	14-May	252-1	L	19068	4	950	15	4	57000
8	14-May	253-1	I	15364	20	814	15	2	24420
9	14-May	253-1	J	18109	28	1016	15	3	45720
10	14-May	253-1	L	20316	28	1149	15	4	68940
11	15-May	251-4	G	17656	19	929	15	2	27870
12	15-May	251-4	K	16499	14	844	15	1	12660
13	15-May	251-4	X	18021	16	933	15	4	55980
14	15-May	251-4	Z	19653	16	1018	30	1	30540
15	15-May	251-4	a	20048	16	1038	15	5	77850
16	15-May	252-2	E	20739	9	1043	15	6	93870
17	15-May	252-2	N	15496	19	816	15	2	24480
18	15-May	254-1	C	16593	39	1067	15	1	16005

Table C.7: Table summarizing the OAWRS Resolution Parameters for the Case 2C Segments, 390-440 Hz (WX1)

Example	Date	Track	Segment	Mean Fish Density fish/m^2)	Depth Extent (m)	Bottom Depth	Longest Continuous Along-Transect Extent (m)	Transect Trajectory Angle* (deg)	Cross Range Projection (m)	Range Projection (km)	Estimated Area Occupied by fish (m^2)
1	7-May	141A-2	I	0.28	79-81	81	22	16	6	21	570
2	7-May	141A-2	K	0.65	80-82	82	40	13	9	39	1885
3	8-May	201-3	A	1.02	75-77	78	27	2	1	27	859
4	8-May	202-4	B	1.55	71-80	80	90	61	79	44	12488
5	14-May	252-1	I	0.83	87-100	100	300	40	193	230	33134
6	14-May	252-1	K	1.74	87-95	95	30	33	16	25	1060
7	14-May	252-1	L	1.38	40-92	93	70	36	41	57	6509
8	14-May	253-1	I	0.71	89-90	90	25	11	5	25	736
9	14-May	253-1	J	0.95	85-98	98	35	13	8	34	1443
10	14-May	253-1	L	0.36	100-105	105	50	13	11	49	3682
11	15-May	251-4	G	3.09	95-103	103	30	55	25	17	1060
12	15-May	251-4	K	0.55	92-100	100	25	56	21	14	736
13	15-May	251-4	X	0.83	100-110	110	60	7	7	60	6126
14	15-May	251-4	Z	1.45	110-112	112	30	8	4	30	1060
15	15-May	251-4	a	1.66	105-113	113	65	5	6	70	9808
16	15-May	252-2	E	0.55	95-102	102	100	37	60	80	23002
17	15-May	252-2	N	0.28	75-80	82	25	17	7	24	4418
18	15-May	254-1	C	1.20	88-94	94	35	82	35	5	1443

Table C.8: Table summarizing the CFFS Characterization of the Case 2C Segments, 390-440 Hz (WX1)

Example	Date	Track	Segment	Number of Estimation	$< TS_C >$ dB re	σ_{TS_C} (dB)	$< SS_C >$ dB re	σ_{SS_C} (dB)	$< SS_O >$ dB re	σ_{SS_O} (dB)	$< TS_O >$ dB re	σ_{TS_O} (dB)	σ_{TS_O} (dB)
1	7-May	141A-2	I	3	-35.5	1.2	-41.0	1.2	-50.4	3.1	-45.2	2.0	2.0
2	7-May	141A-2	K	4	-35.5	1.2	-37.4	2.4	-48.4	1.7	-45.5	2.7	2.7
3	8-May	201-3	A	6	-35.9	1.5	-35.8	3.3	-51.8	0.4	-49.7	3.4	3.4
4	8-May	202-4	B	17	-35.9	1.5	-34.0	3.0	-48.2	1.8	-47.5	4.0	2.8
5	14-May	252-1	I	21	-35.3	0.6	-36.1	3.4	-51.7	2.9	-49.8	2.7	0.8
6	14-May	252-1	K	4	-35.3	0.6	-32.9	2.9	-54.8	0.0	-55.8	2.9	2.1
7	14-May	252-1	L	14	-35.3	0.6	-33.9	5.3	-52.7	1.3	-48.7	4.9	4.9
8	14-May	253-1	I	2	-35.3	0.6	-36.8	2.0	-57.0	0.0	-55.1	2.0	2.0
9	14-May	253-1	J	4	-35.3	0.6	-35.5	2.0	-52.6	0.8	-51.8	2.0	2.0
10	14-May	253-1	L	2	-35.3	0.6	-39.7	0.5	-57.4	0.0	-53.0	0.5	0.5
11	15-May	251-4	G	4	-35.3	0.6	-30.4	3.9	-51.4	0.6	-54.1	3.6	3.6
12	15-May	251-4	K	2	-35.3	0.6	-37.9	0.3	-54.9	0.0	-52.4	0.3	0.3
13	15-May	251-4	X	9	-35.3	0.6	-36.1	2.5	-51.4	1.1	-49.4	2.6	1.5
14	15-May	251-4	Z	6	-35.3	0.6	-33.7	4.4	-50.6	1.2	-48.8	4.4	4.4
15	15-May	251-4	a	15	-35.3	0.6	-33.1	3.5	-51.1	3.0	-51.7	3.3	2.4
16	15-May	252-2	E	16	-35.3	0.6	-37.9	2.3	-49.2	1.7	-45.5	2.7	1.0
17	15-May	252-2	N	2	-35.3	0.6	-40.8	0.6	-51.4	1.3	-46.0	0.7	0.7
18	15-May	254-1	C	4	-35.3	0.6	-34.5	2.5	-51.8	1.1	-51.5	2.4	2.4

Table C.9: Table summarizing the Statistical Parameters of Estimation Variabilities of the Case 2C Segments, 390-440 Hz (WX1)

Example	Date	Time	Segment	Range from OAWRS Reciever (m)	Angle from OAWRS Broadside (deg)	Mean Cross Range Resolution (m)	OAWRS Range Resolution (m)	Number of Corresponding Resolution Footprints	Area of Corresponding Footprints (m^2)
1	7-May	141D-1	F	7442	37	462	15	2	13860
2	14-May	252-1	A	14591	5	728	15	3	32760
3	14-May	252-1	C	13169	5	658	15	2	19740
4	14-May	253-1	B	19077	2	949	15	5	71175
5	14-May	253-1	D	19367	3	964	15	1	14460
6	14-May	253-1	F	18635	7	933	15	4	55980
7	14-May	253-1	K	18394	28	1036	15	4	62160
8	15-May	251-4	L	16228	11	822	15	1	12330
9	15-May	251-4	P	13679	10	691	15	2	20730
10	15-May	251-4	c	20584	17	1074	15	1	16110
11	15-May	252-2	B	19354	15	997	15	4	59820

Table C.10: Table summarizing the OAWRS Resolution Parameters for the Case 3 Segments, 390-440 Hz (WX1)

Example	Date	Track	Segment	Mean Fish Density fish/m^2)	Depth Extent (m)	Bottom Depth	Longest Continuous Along-Transect Extent (m)	Transect Trajectory Angle* (deg)	Cross Range Projection (m)	Range Projection (km)	Estimated Area Occupied by fish (m^2)
1	7-May	141D-1	F	2.82	71-81	84	21	5	2	21	520
2	14-May	252-1	A	0.32	90-92	94	60	54	49	35	4712
3	14-May	252-1	C	0.55	85-87	87	35	59	30	18	1443
4	14-May	253-1	B	1.41	90-100	100	420	81	415	66	58905
5	14-May	253-1	D	0.34	100-102	102	50	79	49	10	3416
6	14-May	253-1	F	0.34	98-102	102	60	8	8	59	8482
7	14-May	253-1	K	1.55	95-99	99	60	16	17	58	6126
8	15-May	251-4	L	0.81	90-97	97	25	54	20	15	736
9	15-May	251-4	P	0.23	85-90	90	25	13	6	24	2209
10	15-May	251-4	c	0.52	110-112	112	25	87	25	1	736
11	15-May	252-2	B	1.02	90-97	97	60	9	9	59	4241

Table C.11: Table summarizing the CFFS Characterization of the Case 3 Segments, 390-440 Hz (WX1)

Example	Date	Track	Segment	Number of Estimation	$< TS_C >$ dB re	σ_{TS_C} (dB)	$< SS_C >$ dB re	σ_{SS_C} (dB)	$< SS_O >$ dB re	σ_{SS_O} (dB)	$< TS_O >$ dB re	σ_{TS_O} (dB)	σ_{TS_O} (dB)
1	7-May	141A-2	I	3	-35.5	1.2	-31	4.9	-54.2	1.07	-54.2	5.8	5.8
2	7-May	141A-2	K	4	-35.3	0.6	-40.3	0.0	-54.1	0	-49.1	0.0	0.0
3	8-May	201-3	A	6	-35.3	0.6	-37.9	1.5	-55.8	1.28	-53.1	0.7	0.7
4	8-May	202-4	B	17	-35.3	0.6	-33.8	4.3	-53.2	2.35	-50.8	5.4	1.6
5	14-May	252-1	I	21	-35.3	0.6	-40	0.8	-56.7	0.341	-51.9	1.1	1.1
6	14-May	252-1	K	4	-35.3	0.6	-40	1.8	-46.5	0	-41.4	1.8	1.8
7	14-May	252-1	L	14	-35.3	0.6	-33.4	4.3	-49.9	1.43	-48.0	4.4	4.4
8	14-May	253-1	I	2	-35.3	0.6	-36.2	2.6	-52.4	0.301	-52.0	2.6	2.6
9	14-May	253-1	J	4	-35.3	0.6	-41.7	0.5	-55.9	1.07	-49.6	0.6	0.6
10	14-May	253-1	L	2	-35.3	0.6	-38.1	2.3	-51.9	0	-48.3	2.3	2.3
11	15-May	251-4	G	4	-35.3	0.6	-35.2	4.5	-51.9	1.86	-48.2	5.3	5.3

Table C.12: Table summarizing the Statistical Parameters of Estimation Variabilities of the Case 3 Segments, 390-440 Hz (WX1)

Example	Date	Time	Segment	Range from OAWRS Reciever (m)	Angle from OAWRS Broadside (deg)	Mean Cross Range Resolution (m)	OAWRS Range Resolution (m)	Number of Corresponding Resolution Footprints	Area of Corresponding Footprints (m^2)
1	9-May	202-6	A	8694	26	433	7.5	4	12990

Table C.13: Table summarizing the OAWRS Resolution Parameters for the Case 2A Segments, 875-975 Hz (WMA)

Example	Date	Track	Segment	Mean Fish Density fish/m^2)	Depth Extent (m)	Bottom Depth	Longest Continuous Along-Transect Extent (m)	Transect Trajectory Angle* (deg)	Cross Range Projection (m)	Range Projection (km)	Estimated Area Occupied by fish (m^2)
1	9-May	202-6	A	1.78	72-80	81	40	45	28	28	1885

Table C.14: Table summarizing the CFFS Characterization of the Case 2A Segments, 875-975 Hz (WMA)

Example	Date	Track	Segment	Number of Estimation	$< TS_C >$ dB re	σ_{TS_C} (dB)	$< SS_C >$ dB re	σ_{SS_C} (dB)	$< SS_O >$ dB re	σ_{SS_O} (dB)	$< TS_O >$ dB re	σ_{TS_O} (dB)	σ_{TS_O} (dB)
1	9-May	202-6	A	10	-35.90	1.5	-33.4	3.7	-34.1	0.8	-34.3	3.4	1.5

Table C.15: Table summarizing the Statistical Parameters of Estimation Variabilities of the Case 2A Segments, 875-975 Hz (WMA)

Example	Date	Time	Segment	Range from OAWRS Reciever (m)	Angle from OAWRS Broadside (deg)	Mean Cross Range Resolution (m)	OAWRS Range Resolution (m)	Number of Corresponding Resolution Footprints	Area of Corresponding Footprints (m^2)
1	9-May	202-5	H	17736	21	846	7.5	5	31725
2	9-May	202-5	I	17228	23	838	7.5	17	106845
3	9-May	201-4	C	11477	32	605	7.5	42	190575
4	9-May	202-6	B	9504	29	485	7.5	3	10913
5	9-May	202-6	C	9794	30	507	7.5	5	19013
6	9-May	202-6	D	10074	32	532	7.5	5	19950

Table C.16: Table summarizing the OAWRS Resolution Parameters for the Case 2C Segments, 875-975 Hz (WMA)

Example	Date	Track	Segment	Mean Fish Density fish/m^2)	Depth Extent (m)	Bottom Depth	Longest Continuous Along-Transect Extent (m)	Transect Trajectory Angle* (deg)	Cross Range Projection (m)	Range Projection (km)	Estimated Area Occupied by fish (m^2)
1	9-May	202-5	H	0.41	80-82	82	35	17	10	33	1443
2	9-May	202-5	I	0.74	75-83	83	125	16	34	120	29452
3	9-May	201-4	C	2.82	65-82	83	350	28	164	309	55960
4	9-May	202-6	B	2.51	67-77	82	30	50	23	19	1060
5	9-May	202-6	C	3.55	65-80	82	50	48	37	33	2945
6	9-May	202-6	D	1.00	80-82	82	50	49	38	33	2945

Table C.17: Table summarizing the CFFS Characterization of the Case 2C Segments, 875-975 Hz (WMA)

Example	Date	Track	Segment	Number of Estimation	$< TS_C >$ dB re	σ_{TS_C} (dB)	$< SS_C >$ dB re	σ_{SS_C} (dB)	$< SS_O >$ dB re	σ_{SS_O} (dB)	$< TS_O >$ dB re	σ_{TS_O} (dB)	σ_{TS_O} (dB)
1	9-May	202-5	H	2	-35.9	1.5	-39.8	2.7	-43.2	0.0	-38.5	2.7	2.7
2	9-May	202-5	I	25	-35.9	1.5	-37.2	2.5	-41.0	2.3	-38.2	3.6	3.6
3	9-May	201-4	C	32	-35.9	1.5	-31.4	3.7	-38.6	4.6	-41.7	5.4	1.9
4	9-May	202-6	B	9	-35.9	1.5	-31.9	3.5	-36.7	0.1	-38.4	3.4	3.4
5	9-May	202-6	C	16	-35.9	1.5	-30.4	4.6	-38.3	0.1	-39.5	4.6	4.6
6	9-May	202-6	D	10	-35.9	1.5	-35.9	3.8	-39.5	4.6	-38.5	4.1	2.4

Table C.18: Table summarizing the Statistical Parameters of Estimation Variabilities of the Case 2C Segments, 875-975 Hz (WMA)

Example	Date	Time	Segment	Range from OAWRS Reciever (m)	Angle from OAWRS Broadside (deg)	Mean Cross Range Resolution (m)	OAWRS Range Resolution (m)	Number of Corresponding Resolution Footprints	Area of Corresponding Footprints (m^2)
1	9-May	202-5	L	13539	35	775	7.5	6	34875
2	9-May	202-5	M	13239	41	777	7.5	9	52447.5
3	9-May	201-4	B	12711	35	689	7.5	5	25837.5
4	15-May	252-3	A	12450	45	782	7.5	41	240465
5	15-May	252-3	B	12413	42	749	7.5	4	22470
6	15-May	252-3	C	12642	46	810	7.5	82	498150

Table C.19: Table summarizing the OAWRS Resolution Parameters for the Case 3 Segments, 875-975 Hz (WMA)

Example	Date	Track	Segment	Mean Fish Density fish/m^2)	Depth Extent (m)	Bottom Depth	Longest Continuous Along-Transect Extent (m)	Transect Trajectory Angle* (deg)	Cross Range Projection (m)	Range Projection (km)	Estimated Area Occupied by fish (m^2)
1	9-May	202-5	L	0.26	82-85	85	40	18	12	38	1443
2	9-May	202-5	M	0.59	82-85	85	75	26	33	67	6627
3	9-May	201-4	B	0.62	83-87	87	35	29	17	31	2386
4	15-May	252-3	A	0.65	75-82	83	625	61	547	303	182605
5	15-May	252-3	B	0.45	80-82	83	30	5	3	30	1060
6	15-May	252-3	C	0.71	70-81	83	625	11	119	614	269490

Table C.20: Table summarizing the CFFS Characterization of the Case 3 Segments, 875-975 Hz (WMA)

Example	Date	Track	Segment	Number of Estimation	$< TS_C >$ dB re	σ_{TS_C} (dB)	$< SS_C >$ dB re	σ_{SS_C} (dB)	$< SS_O >$ dB re	σ_{SS_O} (dB)	$< TS_O >$ dB re	σ_{TS_O} (dB)	σ_{TS_O} (dB)
1	9-May	202-5	L	1	-35.90	1.5	-41.70	0.0	-46.30	0.0	-40.5	0.0	0.0
2	9-May	202-5	M	5	-35.90	1.5	-38.20	2.2	-39.60	1.9	-36.5	2.7	2.7
3	9-May	201-4	B	2	-35.90	1.5	-38.00	0.7	-44.20	0.0	-42.0	0.7	0.7
4	15-May	252-3	A	57	-35.30	0.6	-37.20	2.3	-42.30	3.2	-38.9	4.4	1.3
5	15-May	252-3	B	2	-35.30	0.6	-38.80	1.5	-47.30	0.0	-43.6	1.5	1.5
6	15-May	252-3	C	55	-35.30	0.6	-36.80	2.4	-44.70	1.1	-42.0	2.5	0.8

Table C.21: Table summarizing the Statistical Parameters of Estimation Variabilities of the Case 3 Segments, 875-975 Hz (WMA)

Example	Date	Time	Segment	Range from OAWRS Reciever (m)	Angle from OAWRS Broadside (deg)	Mean Cross Range Resolution (m)	OAWRS Range Resolution (m)	Number of Corresponding Resolution Footprints	Area of Corresponding Footprints (m^2)
1	9-May	202-6	A	8694	26	604	5	5	15100

Table C.22: Table summarizing the OAWRS Resolution Parameters for the Case 2A Segments, 1250-1400 Hz (WMB)

Example	Date	Track	Segment	Mean Fish Density fish/m^2)	Depth Extent (m)	Bottom Depth	Longest Continuous Along-Transect Extent (m)	Transect Trajectory Angle* (deg)	Cross Range Projection (m)	Range Projection (km)	Estimated Area Occupied by fish (m^2)
1	9-May	202-6	A	1.78	72-80	81	40	45	28	28	1885

Table C.23: Table summarizing the CFFS Characterization of the Case 2A Segments, 1250-1400 Hz (WMB)

Example	Date	Track	Segment	Number of Estimation	$< TS_C >$ dB re	σ_{TS_C} (dB)	$< SS_C >$ dB re	σ_{SS_C} (dB)	$< SS_O >$ dB re	σ_{SS_O} (dB)	$< TS_O >$ dB re	σ_{TS_O} (dB)	σ_{TS_O} (dB)
1	9-May	202-6	A	10	-35.9	1.5	-33.4	3.7	-32.4	1.8	-32.80	3.1	1.4

Table C.24: Table summarizing the Statistical Parameters of Estimation Variabilities of the Case 2A Segments, 1250-1400 Hz (WMB)

Example	Date	Time	Segment	Range from OAWRS Reciever (m)	Angle from OAWRS Broadside (deg)	Mean Cross Range Resolution (m)	OAWRS Range Resolution (m)	Number of Corresponding Resolution Footprints	Area of Corresponding Footprints (m^2)
1	9-May	202-5	H	17736	21	1181	5	7	41335
2	9-May	202-5	I	17228	23	1170	5	25	146250
3	9-May	201-4	C	11477	32	845	5	62	261950
4	9-May	202-6	B	9504	29	677	5	4	13540
5	9-May	202-6	C	9794	30	708	5	7	24780
6	9-May	202-6	D	10074	32	743	5	7	26005

Table C.25: Table summarizing the OAWRS Resolution Parameters for the Case 2C Segments, 1250-1400 Hz (WMB)

Example	Date	Track	Segment	Mean Fish Density fish/m^2)	Depth Extent (m)	Bottom Depth	Longest Continuous Along-Transect Extent (m)	Transect Trajectory Angle* (deg)	Cross Range Projection (m)	Range Projection (km)	Estimated Area Occupied by fish (m^2)
1	9-May	202-5	H	0.41	80-82	82	35	17	10	33	1443
2	9-May	202-5	I	0.74	75-83	83	125	16	34	120	29452
3	9-May	201-4	C	2.82	65-82	83	350	28	164	309	55960
4	9-May	202-6	B	2.51	67-77	82	30	50	23	19	1060
5	9-May	202-6	C	3.55	65-80	82	50	48	37	33	2945
6	9-May	202-6	D	1.00	80-82	82	50	49	38	33	2945

Table C.26: Table summarizing the CFFS Characterization of the Case 2C Segments, 1250-1400 Hz (WMB)

Example	Date	Track	Segment	Number of Estimation	$< TS_C >$ dB re	σ_{TS_C} (dB)	$< SS_C >$ dB re	σ_{SS_C} (dB)	$< SS_O >$ dB re	σ_{SS_O} (dB)	$< TS_O >$ dB re	σ_{TS_O} (dB)	σ_{TS_O} (dB)
1	9-May	202-5	H	2	-35.9	1.5	-39.8	2.7	-44.60	0.00	-39.80	2.7	2.7
2	9-May	202-5	I	25	-35.9	1.5	-37.2	2.5	-40.50	1.76	-37.90	3.0	3.0
3	9-May	201-4	C	32	-35.9	1.5	-31.4	3.7	-36.50	3.36	-38.70	5.2	1.8
4	9-May	202-6	B	9	-35.9	1.5	-31.9	3.5	-36.60	0.80	-38.00	3.8	3.8
5	9-May	202-6	C	16	-35.9	1.5	-30.4	4.6	-33.80	3.58	-35.30	5.3	5.3
6	9-May	202-6	D	10	-35.9	1.5	-35.9	3.8	-36.80	0.98	-33.90	4.2	2.4

Table C.27: Table summarizing the Statistical Parameters of Estimation Variabilities of the Case 2C Segments, 1250-1400 Hz (WMB)

Example	Date	Time	Segment	Range from OAWRS Reciever (m)	Angle from OAWRS Broadside (deg)	Mean Cross Range Resolution (m)	OAWRS Range Resolution (m)	Number of Corresponding Resolution Footprints	Area of Corresponding Footprints (m^2)
1	9-May	202-5	L	13539	39	1082	5	8	43280
2	9-May	202-5	M	13239	41	1085	5	14	75950
3	9-May	201-4	B	12711	35	962	5	7	33670
4	15-May	252-3	A	12450	45	1092	5	61	333060
5	15-May	252-3	B	12413	42	1046	5	6	31380
6	15-May	252-3	C	12642	46	1131	5	123	695565

Table C.28: Table summarizing the OAWRS Resolution Parameters for the Case 3 Segments, 1250-1400 Hz (WMB)

Example	Date	Track	Segment	Mean Fish Density fish/m^2)	Depth Extent (m)	Bottom Depth	Longest Continuous Along-Transect Extent (m)	Transect Trajectory Angle* (deg)	Cross Range Projection (m)	Range Projection (km)	Estimated Area Occupied by fish (m^2)
1	9-May	202-5	L	0.26	82-85	85	40	18	12	38	1443
2	9-May	202-5	M	0.59	82-85	85	75	26	33	67	6627
3	9-May	201-4	B	0.62	83-87	87	35	29	17	31	2386
4	15-May	252-3	A	0.65	75-82	83	625	61	547	303	182605
5	15-May	252-3	B	0.45	80-82	83	30	5	3	30	1060
6	15-May	252-3	C	0.71	70-81	83	625	11	119	614	269490

Table C.29: Table summarizing the CFFS Characterization of the Case 3 Segments, 1250-1400 Hz (WMB)

Example	Date	Track	Segment	Number of Estimation	$< TS_C >$ dB re	σ_{TS_C} (dB)	$< SS_C >$ dB re	σ_{SS_C} (dB)	$< SS_O >$ dB re	σ_{SS_O} (dB)	$< TS_O >$ dB re	σ_{TS_O} (dB)	σ_{TS_O} (dB)
1	9-May	202-5	L	1	-35.90	1.5	-41.70	0.0	-43.80	0.0	-38.00	0.0	0.0
2	9-May	202-5	M	5	-35.90	1.5	-38.20	2.2	-41.40	0.9	-38.20	2.3	2.3
3	9-May	201-4	B	2	-35.90	1.5	-38.00	0.7	-42.50	0.0	-40.30	0.7	0.7
4	15-May	252-3	A	57	-35.30	0.6	-37.20	2.3	-41.00	2.2	-37.60	3.6	1.1
5	15-May	252-3	B	2	-35.30	0.6	-38.80	1.5	-43.10	0.0	-39.40	1.5	1.5
6	15-May	252-3	C	55	-35.30	0.6	-36.80	2.4	-39.40	1.4	-36.40	2.9	0.9

Table C.30: Table summarizing the Statistical Parameters of Estimation Variabilities of the Case 3 Segments, 1250-1400 Hz (WMB)

Appendix D

Procedure for Calculating the Areal Correction Factor,τ

For scenarios where the CFFS-measured populations do not fully occupy the corresponding OAWRS footprint, such as Case 2C and 3, a more accurate estimate of the OAWRS TS can be made by accounting for the resolution mismatch between the OAWRS and CFFS system. For such cases, CFFS measures the minimum number of fish contained within the corresponding OAWRS resolution footprints. We can rewrite the OAWRS target strength in terms of the number of fish and the estimated area occupied by the fish measured by CFFS as

$$SS_O = TS_O + 10\log_{10}(N) - 10\log_{10}(A_O) \tag{D.1}$$

$$SS_C = TS_C + 10\log_{10}(N_C) - 10\log_{10}(A_C) \tag{D.2}$$

$$TS_O = SS_O - SS_C + TS_C - 10\log_{10}\frac{A_C}{A_O} \tag{D.3}$$

$$TS_O = SS_O - SS_C + TS_C + \tau \tag{D.4}$$

where A_C is the estimated area occupied by the fish surveyed by CFFS , A_O is the area of the corresponding OAWRS resolution footprints that contain the segment of interest, and $\tau = -10\log_{10}\frac{A_C}{A_O}$, is the the correction factor to adjust the mean

OAWRS TS.

In order to practically apply this correction factor τ, some reasonable assumptions are made to approximate the actual area occupied by the fish population as measured by CFFS. This will determine the area of the corresponding resolution cells necessary to contain these measured population. For Case 2C and Case 3, where the measured populations are expected to occupy areas less than the corresponding OAWRS footprints, the correction factor can be written as a function of the spatially varying footprint of the OAWRS system, the trajectory of the CFFS system through the fish population, and the along-transect extents of the CFFS-measured population.

Though fish population heights can be determined directly from vertical extents of the corresponding echograms, estimating the horizontal dimensions are more complicated since CFFS often makes singular pass along a line transect within a population. The distance from the transect from the center of a population is unknown, but is unlikely that the transect crosses the middle of the population [89]. Consequently, the observed length of the population in the echogram trace will be less than the true diameter of the school. Though large, shoaling populations have been shown to have irregular horizontal cross-sections [44], we assume here that these smaller populations (<100m in along-transect extent), occupy circular areas in horizontal cross-section.

For a particular fish grouping, a survey track is equally likely to cross any part of fish population. The expected area occupied by a fish population is described in Appendix 5A of Ref. [89] and is given by $A_C = 3\pi l^2/8$, where l is the length of the fish population. If more than one fish grouping occurs within the segment echogram, the total area occupied by the CFFS-measured populations is the a sum of the areas of each of the contributing groupings.

The correction factor τ is highly dependent on the corresponding areal resolution footprint A_t of the bistatic OAWRS system. The OAWRS resolution footprint varies spatially as function of operating frequency, the azimuthal angle, and the range from the receiver there range.

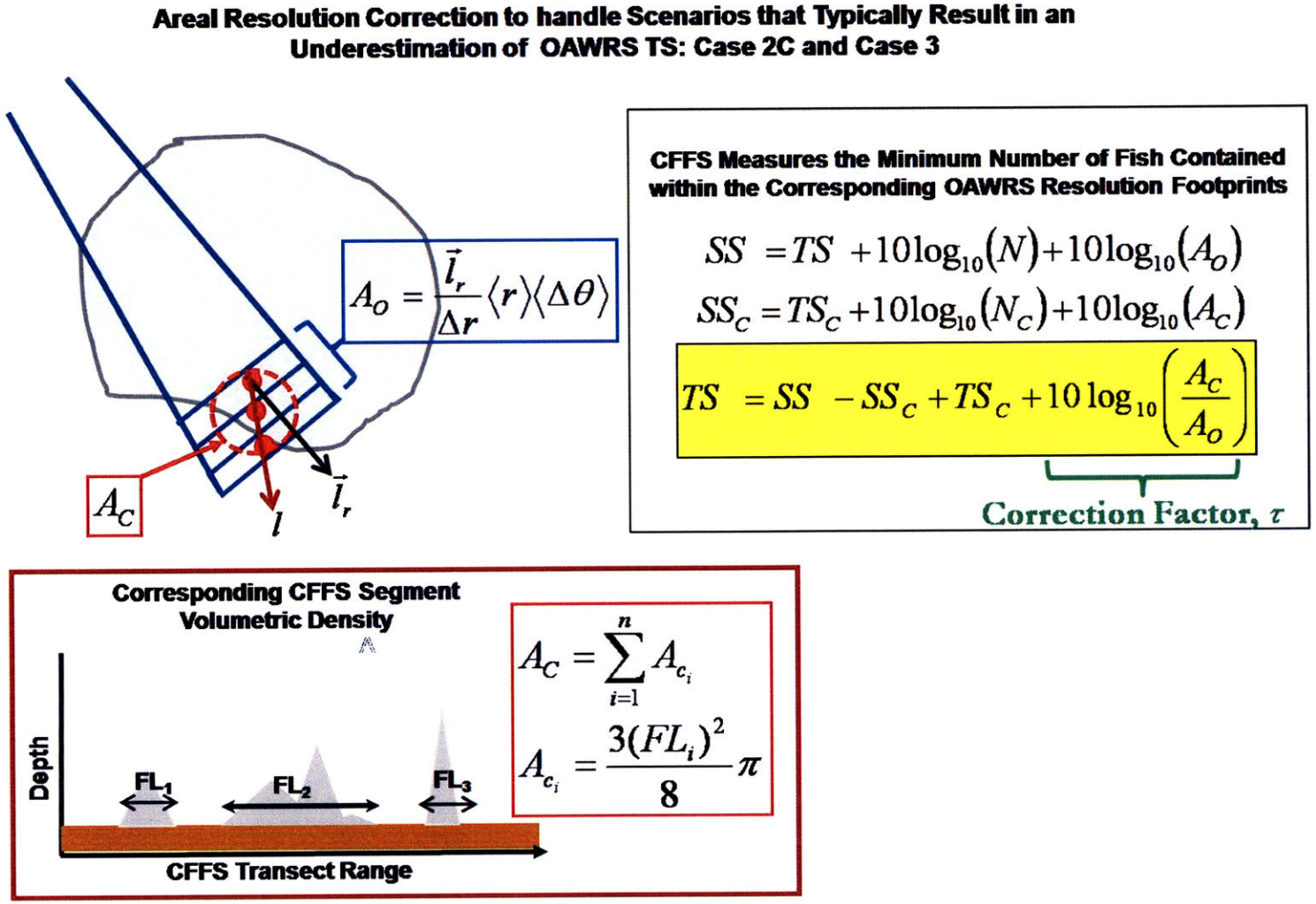

Figure D-1: Schematic detailing how we compute the correction factor, τ.

$$A_t = \Delta r(r\Delta\theta) \tag{D.5}$$

In Eq. D.5, Δr is the range resolution of the OAWRS system, r is the range of the the resolution cell from the receiver, and $\Delta(\theta)$ is the angular resolution of the system at an angle θ from broadside or perpendicular to the receiver axis. The angular resolution can be written as:

$$\Delta\theta = \eta\frac{\lambda}{L\cos\theta} \tag{D.6}$$

where λ is the acoustic wavelength, $L\cos\theta$ is the projected array length, θ is the azimuth angle or steering angle from broadside, η is the directivity weighting factor associated with the taper function. For steering angles from broadside $\theta = 0$ (perpendicular to the array) to a transitional angle θ_t near endfire (parallel to the array), Eqn. D.6 is a valid approximation of the azimuthal resolution. As θ approaches θ_t, ambiguous beamwidths tend to reach values approximately equal to that at endfire. At endfire, or parallel to the array axis, ambiguous beams completely merge yielding an approximate beamwidth described by

$$\Delta\theta_{\theta=\frac{\pi}{2}} \approx 2.6\sqrt{\frac{\lambda}{L}} \tag{D.7}$$

A receiving array with a uniform taper function has a weighting factor $\eta = 1$. We apply a Hanning spatial window function during beamforming to reduce the sidelobe levels, such that the first sidelobe is down 30dB from the main lobe. The weighting factor for a Hanning window is $eta = 1.3$. To improve the range resolution and the signal-to-additive noise ration, the LFM data for the various OAWRS operating frequency bands were match filtered with replicas of the source waveforms to give an effective range resolution $\Delta r \approx \frac{c}{2B}$ where $c = 1500$ m/s is the mean sound speed of the medium and B is the waveform bandwidth.

Table D.1 compares the OAWRS areal resolution footprint for the three OAWRS operating frequency bands. The area of the resolution cells occupied the fish school in the OAWRS system is equal to the product of the average cross-range resolution at

Waveform	Bandwidth	L in m	λ_c (m)	Δr (m)	$\Delta\theta_{\theta=0}$	$r\Delta\theta_{\theta=0}$ (m)	$\Delta\theta_{\theta=\frac{\pi}{2}}$	
WX1	390-440	94.5	3.6	15	2.8°	495	29°	5060
WM11A	875-975	47.25	1.6	7.5	2.6°	453	28°	4890
WM11B	1250-1400	23.625	1.1	5	2.7°	480	32°	5690

Table D.1: Table comparing the range resolution and the cross-range resolution (at the center frequency) at broadside and endfire at a range of 10km from the OAWRS receiver.

location of the CFFS fish grouping measurement and number of range cells spanned by the along-transect extent projected in the OAWRS range direction, $A_O = \frac{l_{\vec{r}}}{\Delta r} r\Delta\theta\rangle$.

Appendix E

Appendix: Analysis of the NOAA/NEFSC Annual Spring Trawl in the New Jersey Continental Shelf March-April 2003

During the OAWRS 2003 survey of the New Jersey Continental, both OAWRS and CFFS simultaneously measured shoaling fish populations. Unfortunately, simultaneous trawls were not available during this field experiment to directly identify the species composition and length frequency of the fish within the observed shoals. In this appendix, we analyze biological samples from 24 relevant stations during the 2003 National Oceanographic and Atmospheric Agency (NOAA) annual spring bottom trawl of the US East Coast (reference bottom trawl and Mike Jech personal communication) in order to identify candidate species and fish length classes that could have comprised the major constituent of the OAWRS 2003 shoals. The biological samples from the NOAA survey were collected within the same geographic vicinity one month prior to the OAWRS survey. Note that a similar analysis was done by

Nero and Love to identify possible biological scatterers that could have contributed to strong scattering regions in the same geographic region during the Acoustic Clutter Reconnaissance Experiment and Boundary Characterization Experiment in April-May 2001, where simultaneous measures by independent trawls were also unavailable [74]. Nero and Love concentrated their analysis to the continental shelf environment bounded by the 50m and 200m bathymetric contours in an area roughly bounded by 37.5°N, 75°W; 40°N,75°W; 40°N, 71.5°W; and 37.5°N, 71.5°W. Stations chosen for this analysis are chosed within this same area of interest.

The Northeast Fisheries Science Center (NEFSC), a branch of NOAA Fisheries, conducts annual spring bottom trawl surveys to sample coastal and continental-shelf marine populations inhabiting the US East Coast (between Cape Cod, MA and Cape Hatteras, NC). The NOAA ship Delaware II conducted the 2003 survey from March 5, 2003 - April 27, 2003; spending March 3-March 27 between the latitudes of interest for this analysis. Both trawl samplings and measurements from a national-fisheries-standard, 38kHz echosounder were made of the sampled fish populations.

We collate species information from the trawl stations shown in E-1 and identify the most abundant demersal and pelagic fish species found at these stations, as shown in the pie charts in E-1. Abundant pelagic (open water),swimbladder-bearing species include: Atlantic Herring and other herring-like species (alewife, American shad, blueback herring). Abundant demersal, or bottom-dwelling, species include: hake (spotted, white, silver, red), scup and black sea bass. The only abundant pelagic, non-swimbladder-bearing species is butterfish, while Atlantic mackerel and spiny dogfish constitute the most abundant demersal, non-swimbladder-bearing species. Swimbladder-berring species contain an air-filled organ for buoyancy regulation. Swimbladder-bearing fish are expected to dominate the scattering within fish shoals of mixed compositions since this air-filled organ acts as a strong reflector of sound. Atlantic herring comprises the major composition of swimbladder-bearing species in the geographic vicinity since it accounts for roughly 30% of the cumulative catch at the stations. Black sea bass and scup each contribute 23% and 25% respectively, while hake and other herring make up the remaining 22% of the total catch.

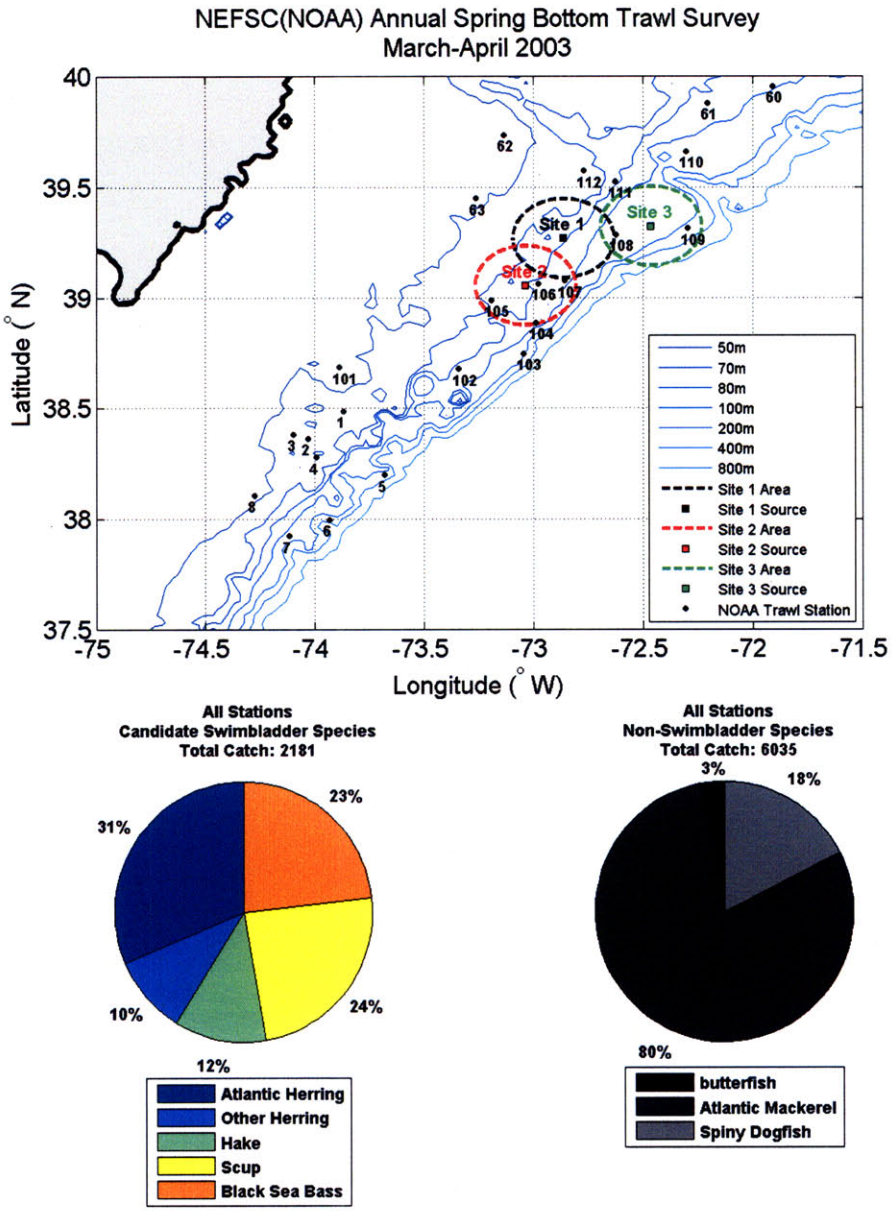

Figure E-1: The areas surveyed by OAWRS during MAE03 are delimited (broken-lined circles). Regions of very large fish shoals observed at Site 2 (red circle) on May 14 and May 15, 2003 by OAWRS were found between the 80-100m contour southeast of the Site 2 source (red square). The 2003 NEFSC Spring Bottom Trawl Sampling Stations used in this analysis are labeled and marked (black circles). The choice of stations are consistent with the same geographic bounding box used for a similar analysis done by Nero and Love in 2001 [74]. Catches were compiled from each of the stations to identify from the most abundant swimbladder-bearing and non-swimbladder-bearing fish species found in the region of interest. The percentage of catch for swimbladder-bearing fish (colored pie chart) and non-swimbladder-bearing fish (grayscale pie cart) are also shown. Bathymetric contours are also shown for geographic reference.

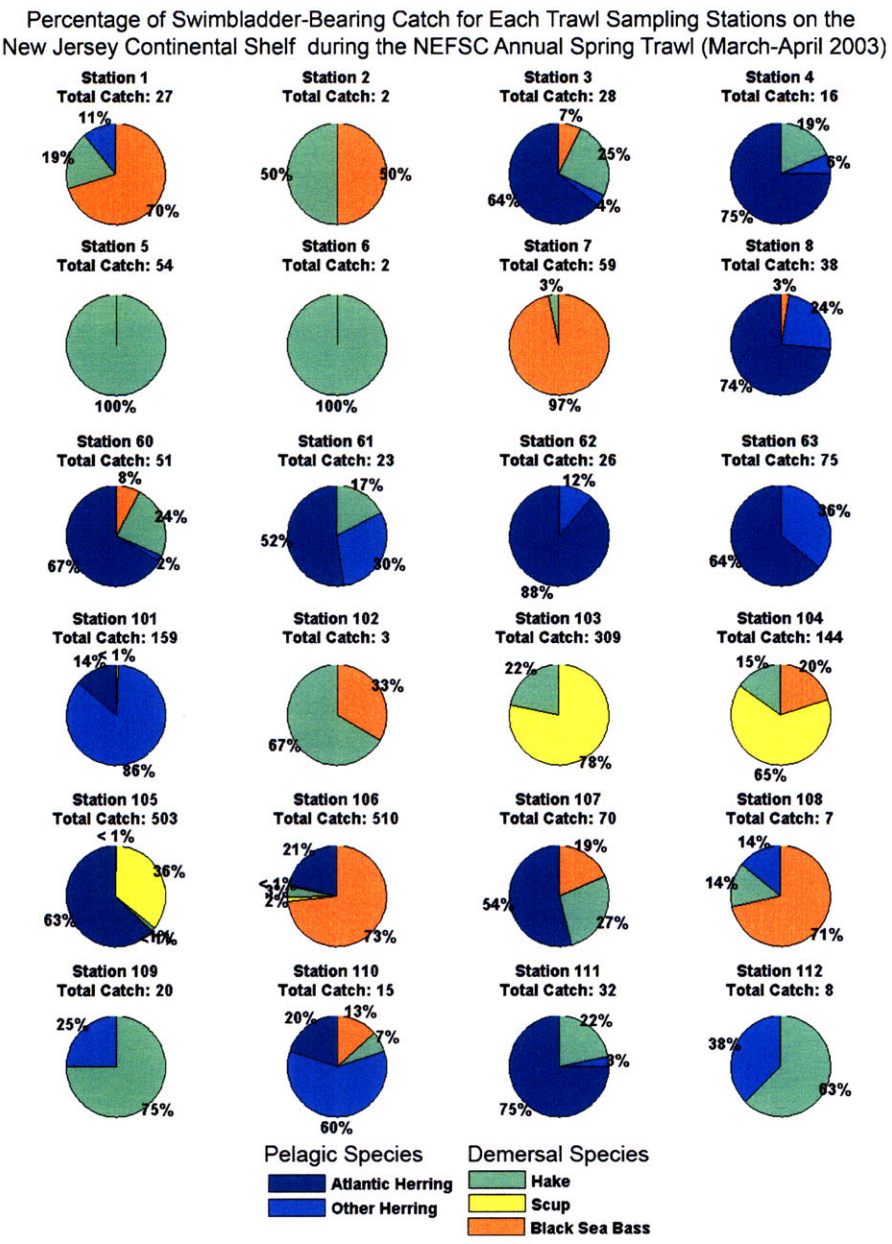

Figure E-2: Percentage of catch corresponding to the most abundant swimbladder bearing species for each station of interest

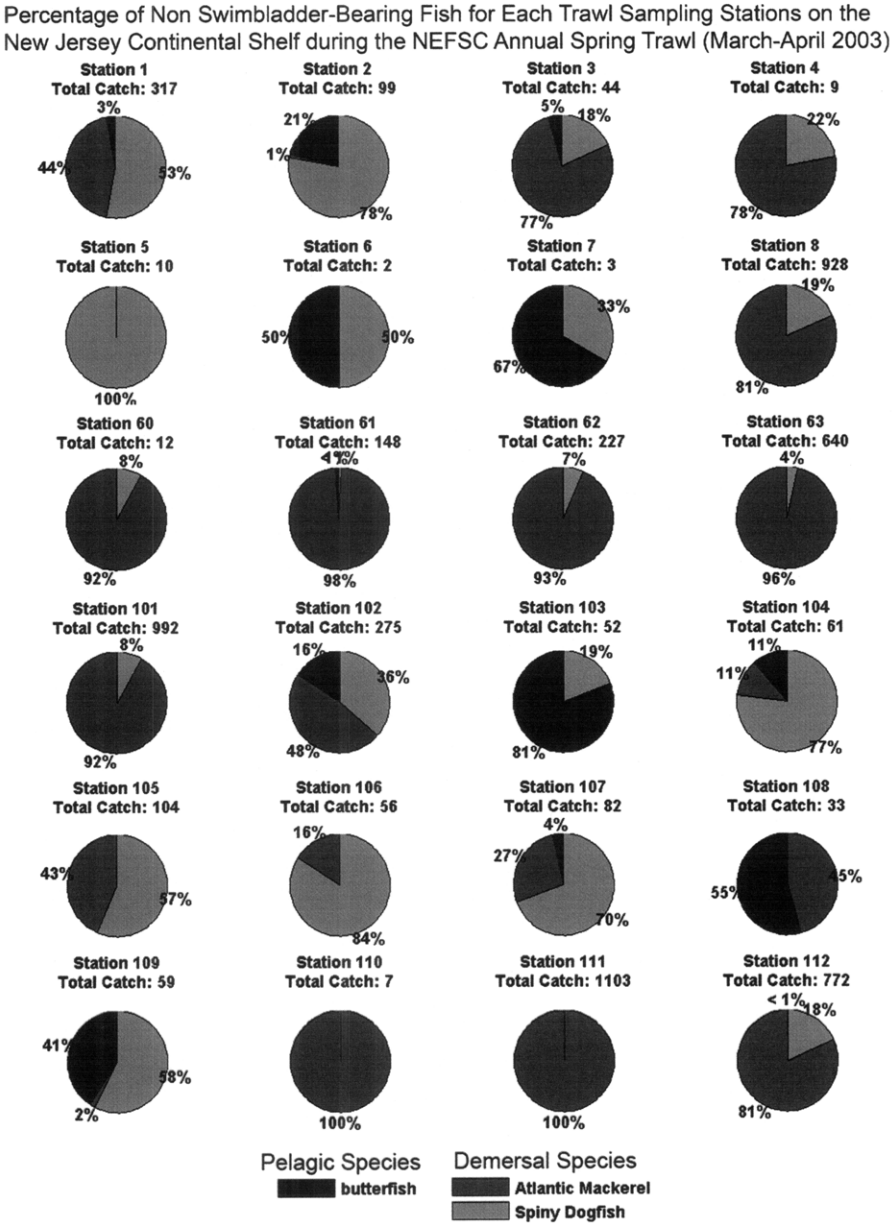

Figure E-3: Percentage of catch corresponding to the most abundant swimbladder bearing species for each station of interest

Catch percentages for abundant swimbladder and non-swimbladder fish species at each trawl station are summarized inE-2 and E-3, respectively.

Histograms summarizing the length frequency distribution for swimbladder and non-swimbladder bearing species from all trawl stations are shown in ?? and ??, respectively. The compiled length frequency associated with the sweimbladder-bearing species exhibits a bi-modal distribution due to the smaller length contributions from scup and larger length contributions from Atlantic herring, other herring, hake, and black sea bass. Though the mean length for swimbladder-bearing fish is found to be 24 cm with a standard deviation of 5.8 cm, the herring, black sea bass, and hake have slightly larger means ranging between 24-27 cm. The compiled length frequency associated with the non-swimbladder-bearing species is also bi-modal, with smaller lengths associated with butterfish and Atlantic mackerel and the much larger lengths associated with dogfish. The length frequency distribution per station for swimbladder-bearing fish and nonswimbladder-bearing fish are also shown in E-6 through E-15.

The need for simultaneous trawl sampling during hydroacoustic surveys of marine populations is pertinent in order pin species composition of the sampled scatterers. It is likely that the scattering within the OAWRS-imaged shoals in 2003 were dominated by swimbladder-bearing fish with length ranges between 24-27 cm. Atlantic herring are expected to be the dominant species contribution of these shoals since they comprise the majority of the trawl catch. The km-long extents of the shoals in the simultaneous CFFS echograms are also point to Atlantic herring as the dominant contribution, since the other demersal species are not known to shoal so extensively. Also, black sea bass, scup, alewife and blueback herring are expected to begin seasonal migration to inshore coastal waters during the time of the OAWRS 2003 survey. It is possible that hake of similar length could have intermingled with the herring schools, since fish of similar length class are known to shoal together. However, Atlantic herring are known to exercise phenotypical selection when shoaling and typically tend to associate with other herring-like fish. The homogeneity of the OAWRS 2003 echograms indicate a uniformity of scattering do not indicate contamination by other

larger interspersed species. The presence of larger fish species would also contradict the stationarity of the 2003 OAWRS and CFFS scattering measurements.

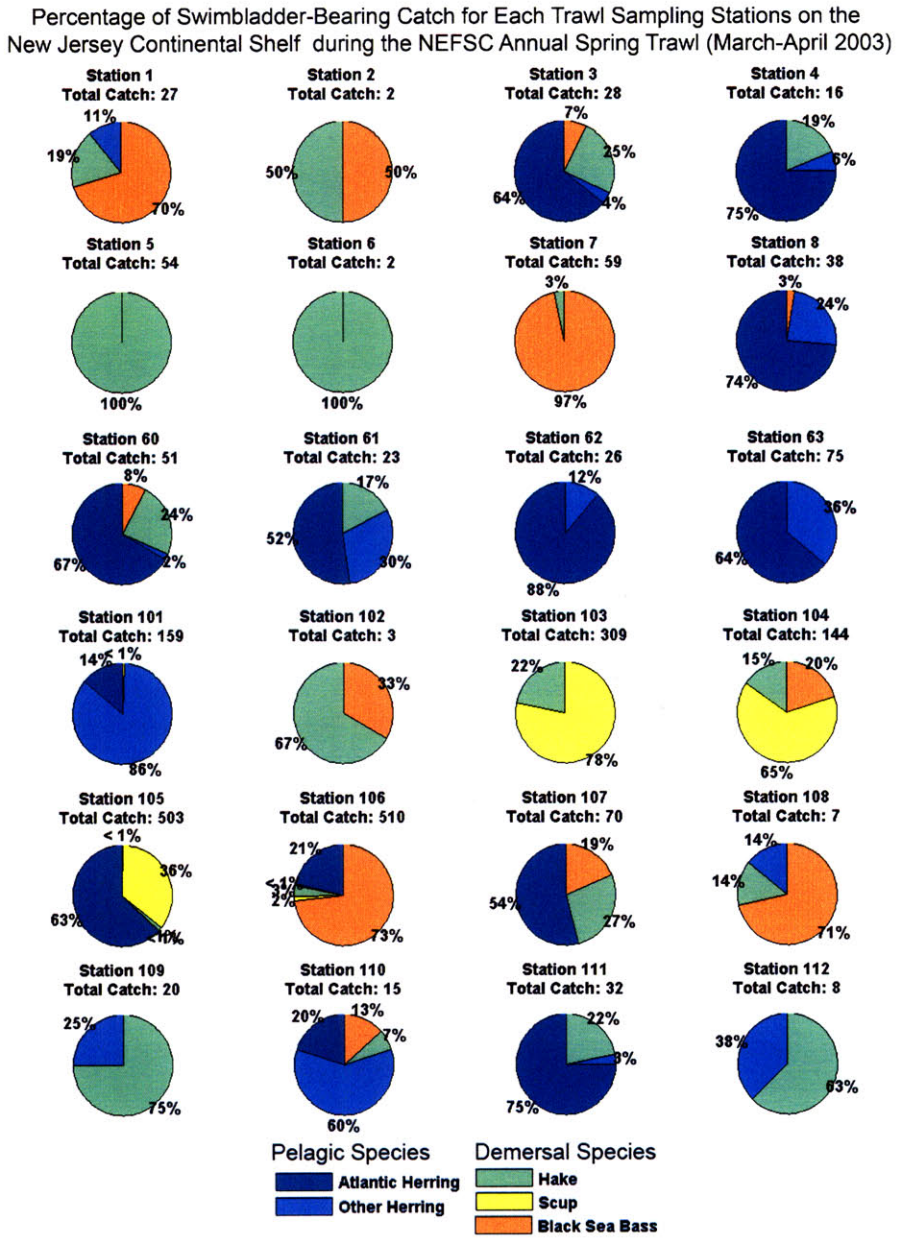

Figure E-4: Cumulative fork length frequency distribution corresponding to the most abundant swimbladder bearing species compiled from all stations.

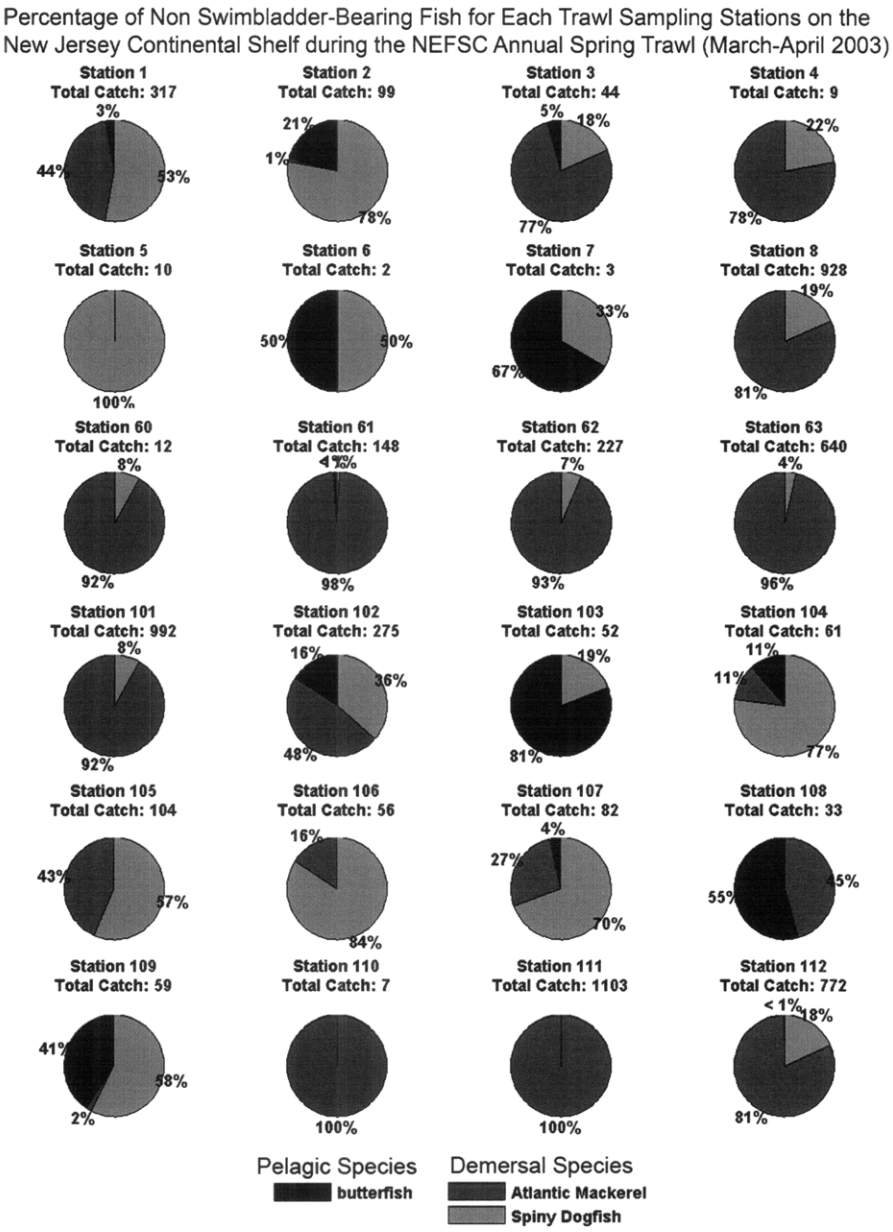

Figure E-5: Cumulative fork length frequency distribution corresponding to the most abundant non swimbladder-bearing species compiled from all stations.

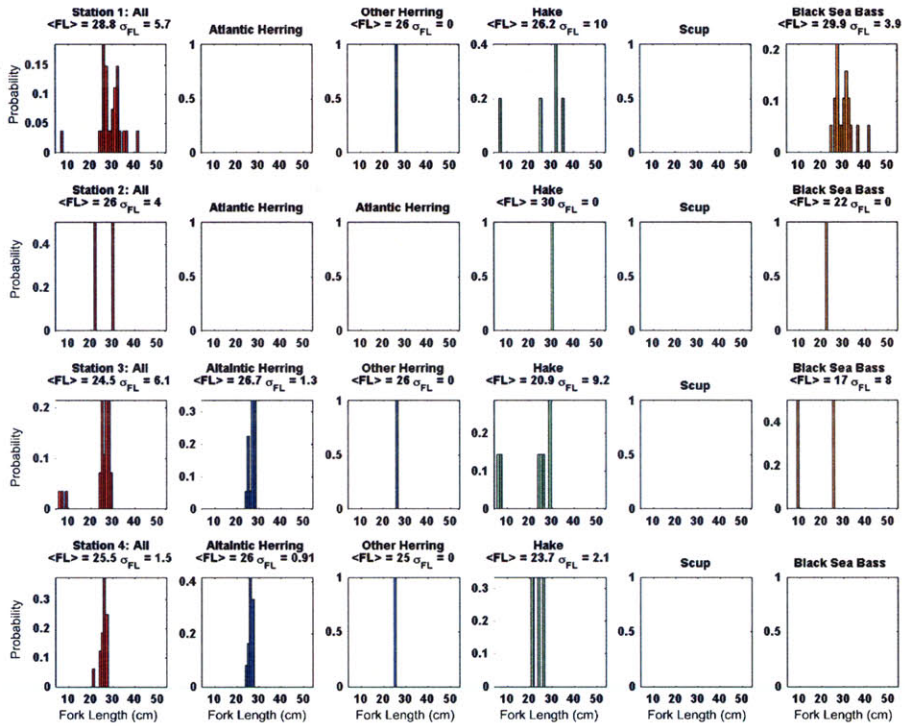

Figure E-6: Stations 1-4: Fork length frequency distribution corresponding to swimbladder-bearing species for each station.

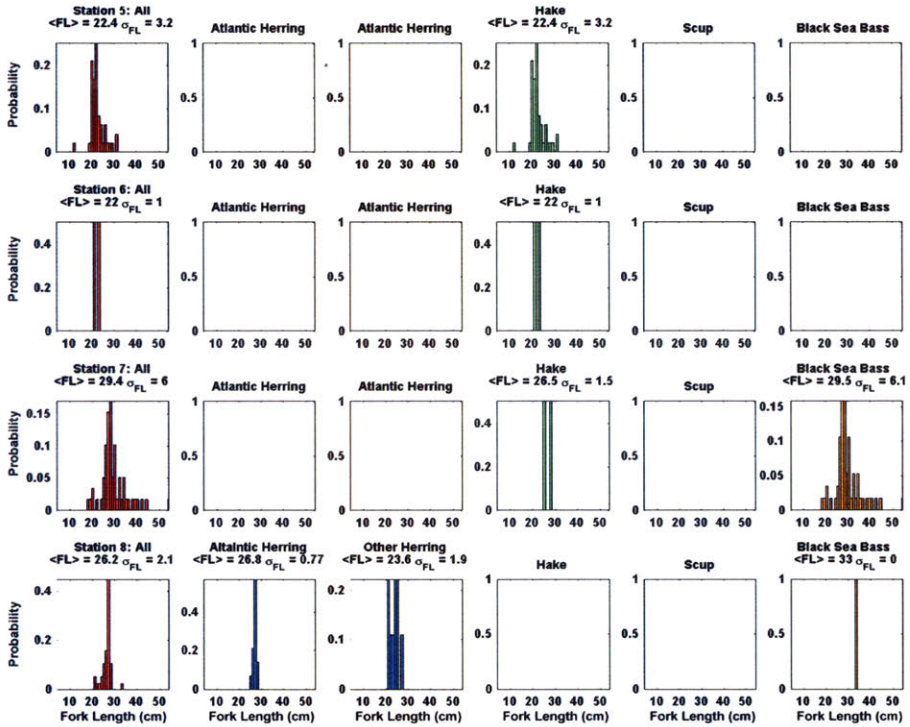

Figure E-7: Stations 5-8: Fork length frequency distribution corresponding to swimbladder-bearing species for each station.

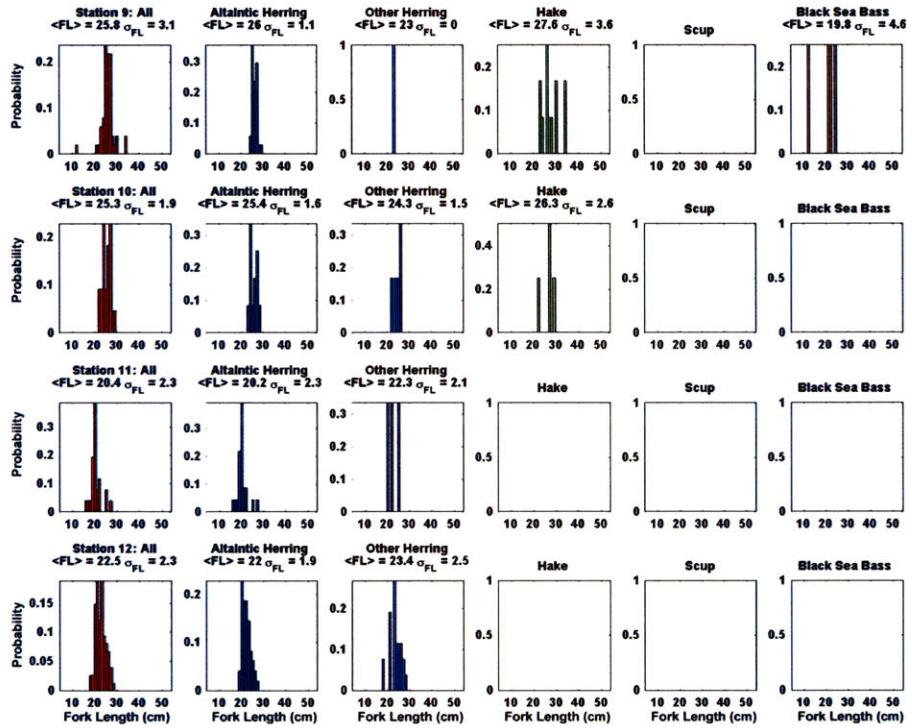

Figure E-8: Stations 9-12: Fork length frequency distribution corresponding to swimbladder-bearing species for each station.

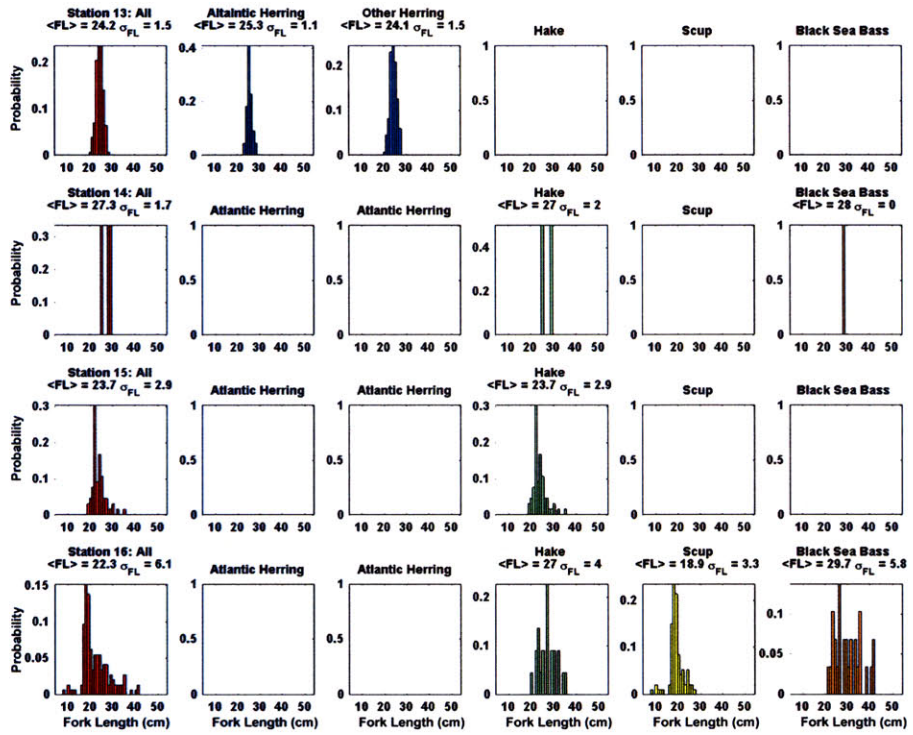

Figure E-9: Stations 13-16: Fork length frequency distribution corresponding to swimbladder-bearing species for each station.

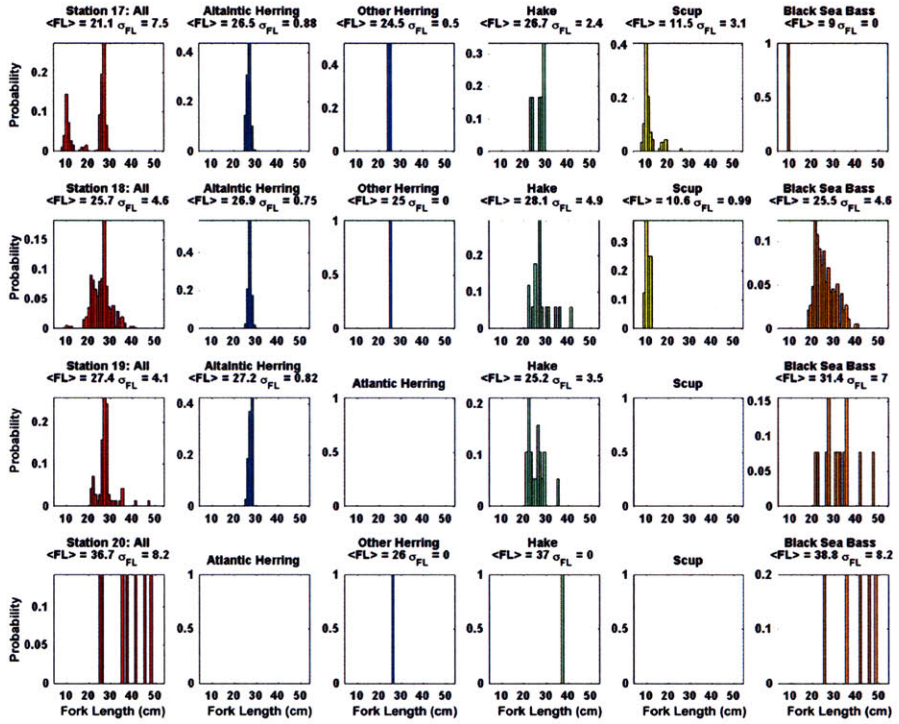

Figure E-10: Stations 17-20: Fork length frequency distribution corresponding to swimbladder-bearing species for each station.

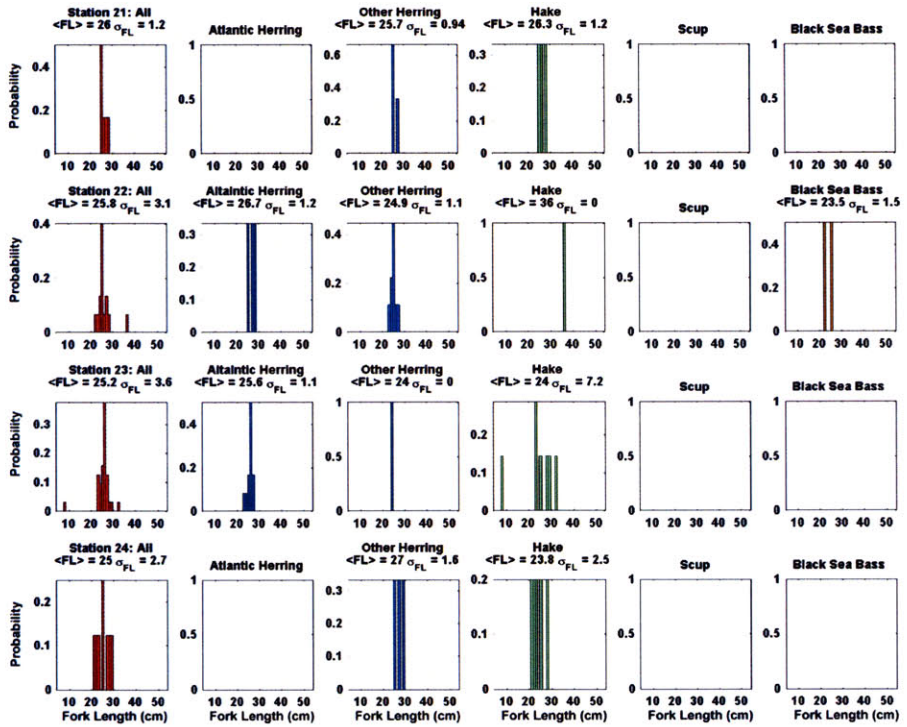

Figure E-11: Stations 21-24: Fork length frequency distribution corresponding to swimbladder-bearing species for each station.

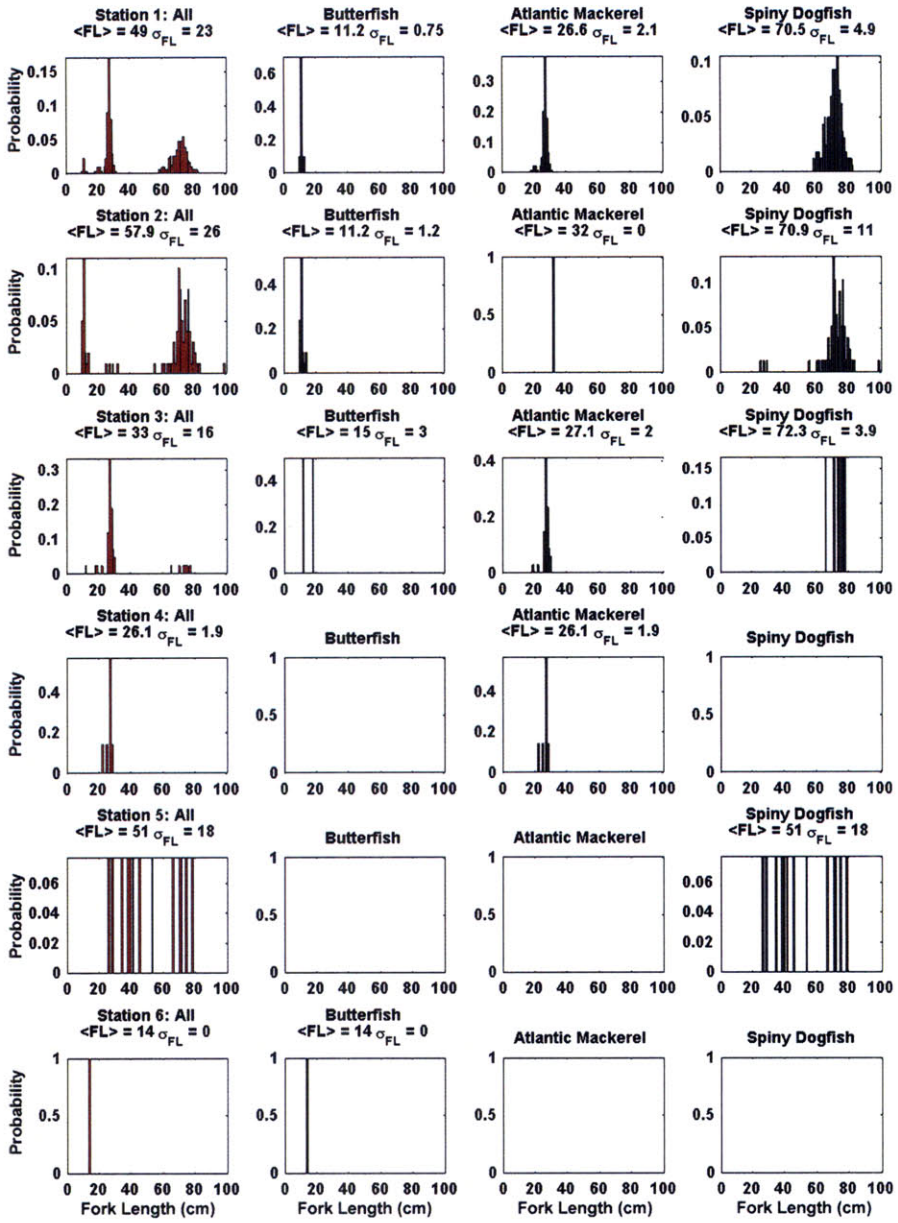

Figure E-12: Fork length frequency distribution corresponding to non-swimbladder-bearing species for each station.

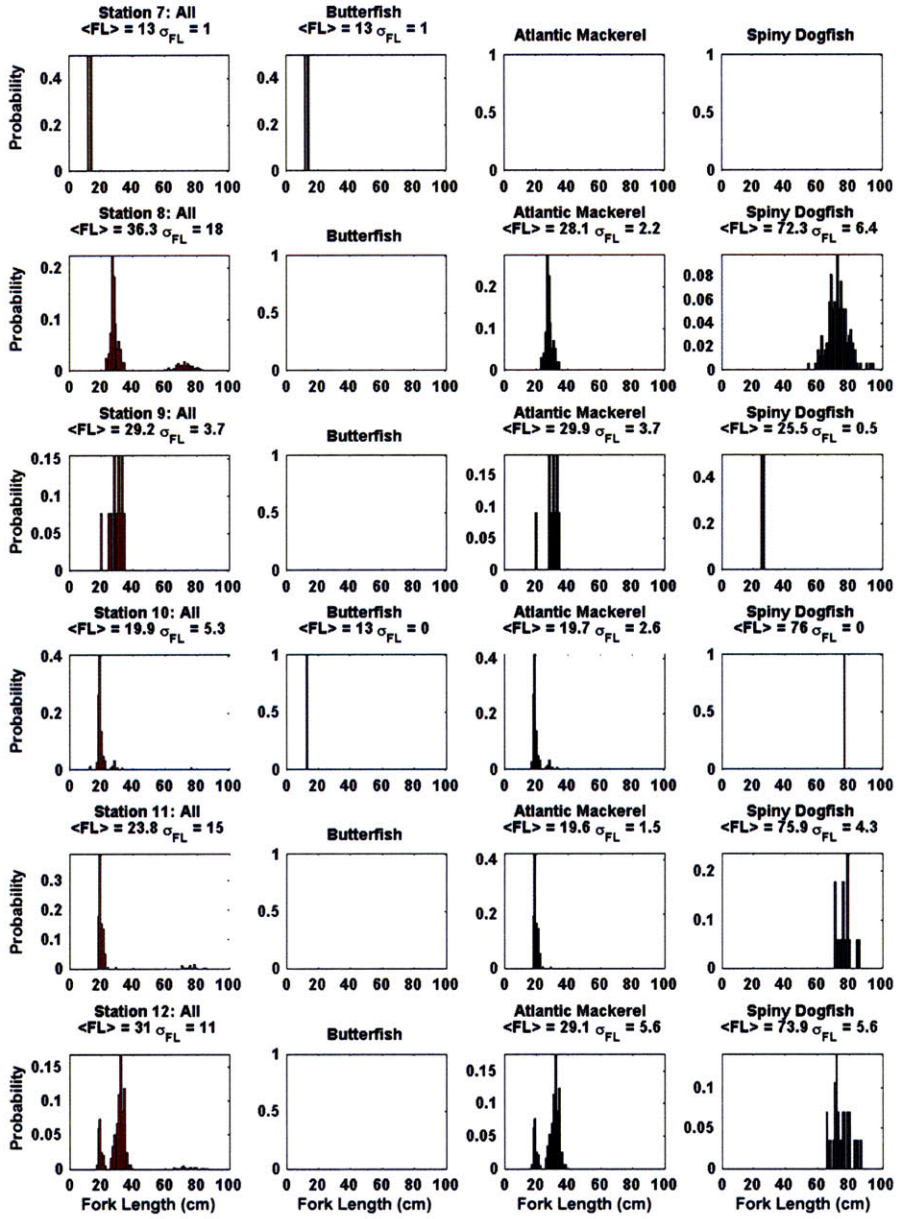

Figure E-13: Fork length frequency distribution corresponding to non-swimbladder-bearing species for each station.

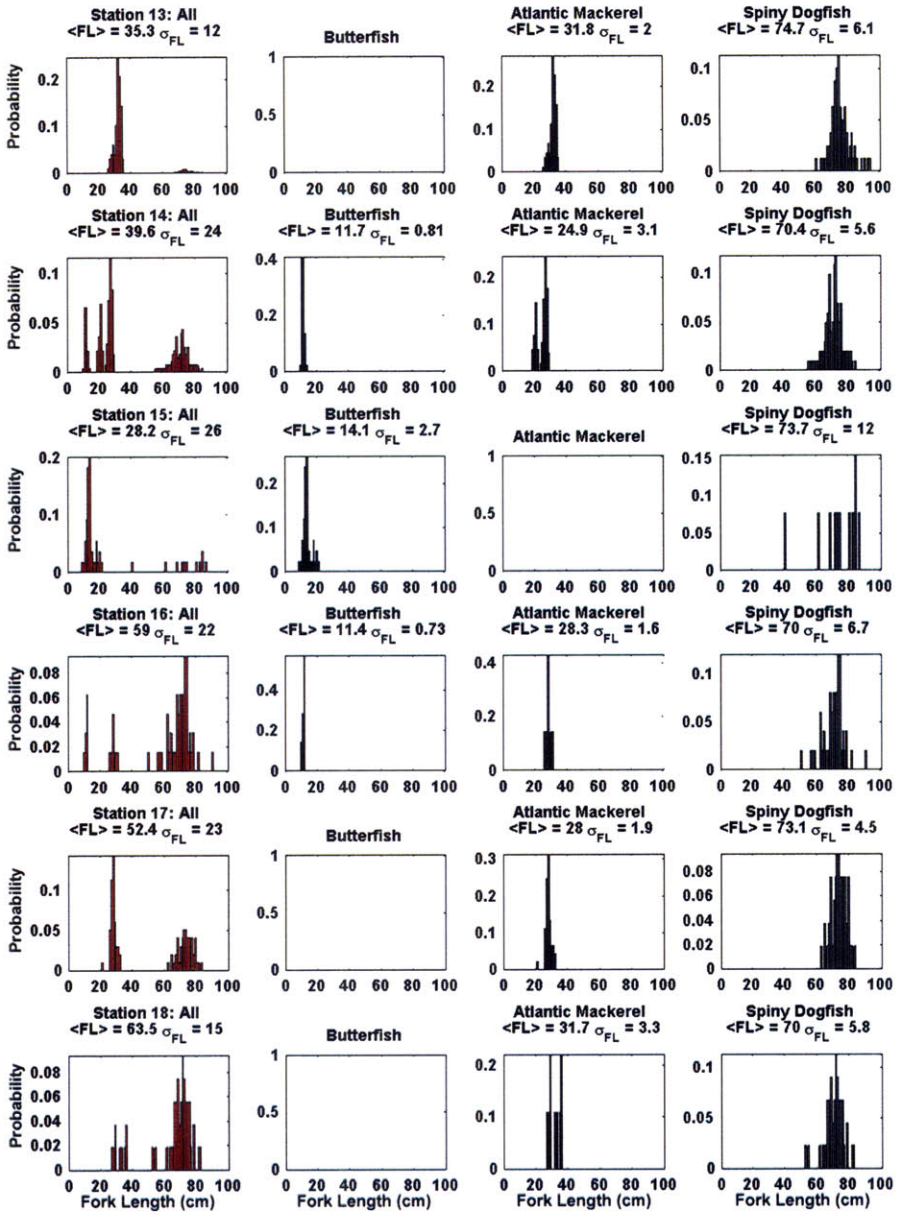

Figure E-14: Fork length frequency distribution corresponding to non-swimbladder-bearing species for each station.

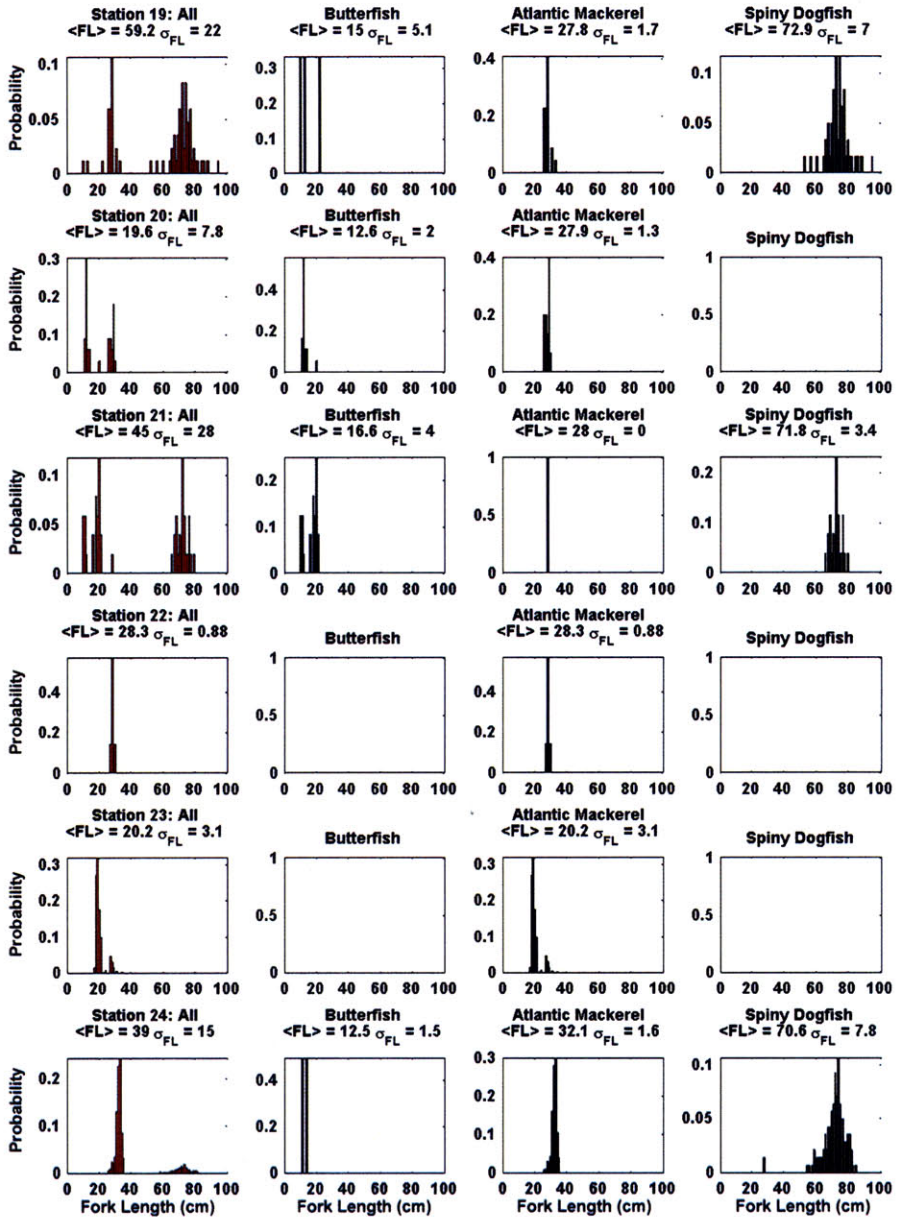

Figure E-15: Fork length frequency distribution corresponding to non-swimbladder-bearing species for each station.

List of Figures

List of Tables

Bibliography

[1] V. C. Anderson. J. acoust. soc. am., 1967.

[2] I. B. Andreeva. Scattering of sound by air bladders of fish in deep sound-scattering ocean layers. *Akust. Zh.*, 10:20–24, 1964. English translation in Soviet Phys.-Acoust. 10: 17-20.

[3] I. B. Andreeva. Acoustical characteristics of sonic scattering layers in ocean. In *Proc. 5th Intern. Congr. on Acoustics, Liege*, page 1A: paper E68, 1965.

[4] I. B. Andreeva and Y. G. Chindonova. On the nature of sound-scattering layers. *Okeanologiya*, 1:112–124, 1964.

[5] R. Balls. Herring fishing with the echometer. *J. Cons. Perm. Int. Explor. Mer.*, 15:193–206, 1948.

[6] R. Balls. Environmental changes in herring behavior : a theory of light avoidance, as suggested by echo-sounding observations in the north sea. *J. Cons. Explor. Mer.*, 17:274–298, 1951.

[7] E. G. Barham. Science, 1966.

[8] L. M. Brekhovskikh and Y. P. Lysanov. *Fundamentals of Ocean Acoustics.* Springer, New York, 3 edition, 2003.

[9] W. S. Burdic. *Underwater acoustic system analysis.* Prentice Hall, New Jersey, 1991.

[10] T. R. Chen. Mean, variance and temporal coherence of the 3d field forward propagated through random inhomogeneities in continental shelf and deep ocean waveguides. ph.d. thesis (in preperation). dept. of mechanical and ocean engineering, 2008.

[11] C. S. Chia, N. C. Makris, and L. T. Fialkowski. A comparison of bistatic scattering from two geologically distinct abyssal hills,. *J. Acoust. Soc. Am.*, 108:2053–2070, 2000.

[12] National Defence Research Committee. *Physics of sound in the sea.* Peninsula, Los Altos, 1989.

[13] Council and European Parliament. Fisheries and poverty reduction, http://europa.edu/scadplus/leg/en/lvb/r12512.htm, November 8, 2000.

[14] P. G. Fernades D.N. MacLennan and J. Dalen. A consistent approach to definitions and symbols in fisheries acoustics. *ICES J.Mar.Sci.*, 50:365–369, 2002.

[15] O. Dragesund and S. Olsen. On the possibility of estimating year-class strength by measuring echo-abundance of 0-group fish. *FiskDir. Skr. Ser. Havunders*, 13:47–75, 1965.

[16] G. E. Duvall and R. J. Christensen. Stratification of sound scatterers in the ocean. *J. Acoust. Soc. Am.*, 18:254, 1946.

[17] I. Dyer. Fundamentals and application of underwater sound. MIT Ocean Engineering 13.851 course notes.

[18] I. Dyer. J. acoust. soc. am., 1970.

[19] C. F. Eyring et al. Reverberation in the sea. *J. Acoust. Soc. Am.*, 20:462–475, 1948.

[20] Croft et al. When fish shoals meet: Outcomes for evolution and fisheries. *Fish. Fish.*, 4:138–146, 2003.

[21] Cury et al. The functioning of marine ecosystems, reykjavik conference on responsible fisheries in the marine ecosystem, fao, Accessed 26 Feb, ftp://ftp.fao.org/fi/document/reykjavik/pdf/07Cury.pdf.

[22] D. A. Hancock et al, editor. *Developing and Sustaining World Fisheries Resources: The State of Science and Management, Proceedings of the 2nd World Fisheries Congress.* Commonwealth Scientific and Industrial Research Organization Publishing, Collingwood, Victoria, Australia, 1997.

[23] D.T. Symonds et al. Fish schools are the dominant cause of long-range active sonar clutter in the new jersey continental shelf: Quantitative correlations. *J. Acoust. Soc. Am.*, 114:2375, 2003.

[24] Farmer et al. Intermediate range fish detection with a 12khz sidescan sonar,. *J. Acoust. Soc. Am.*, 106:2481–2490, 1999.

[25] G. Hempel et al. *Large Marine Ecosystems of the World: Trends in Exploitation, Protection and Research.* Elsevier Science, Amsterdam, The Netherlands, 2003.

[26] Gerlotto et al. From two dimensions to three: the use of multibeam sonar for a new approach in fisheries acoustics. *Can. J. Fish. Aquat. Sci.*, 58:6–12, 1999.

[27] J. B. Hersey et al. Sound-scattering spectra of deep scattering layers in the western north atlantic ocean. *Deep-Sea Res.*, 8:196–210, 1962.

[28] J.B.C. Jackson et al. Historical overfishing and the recent collapse of coastal ecosystems. *Science*, 293:629–637, 2001.

[29] M. Andrews et al. Broadband transmission statistics and match filter degradation in the new jersey continental shelf waveguide. *submitted to J. Acoust. Soc. Am.*, 2008.

[30] M. Andrews et al. High-resolution population density imaging of random scatterers through cross-spectral coherence in matched filted variance. *submitted to IEEE Geoscience Remote Sensing Letters*, 2008.

[31] Mackinson et al. Bioeconomics and catchability: Fish and fisheries' behavior during stock collapse. *Fish. Res.*, 31:11–17, 1997.

[32] N. C. Makris et al. Fish population and behavior revealed by instantaneous continental shelf-scale imaging. *Science*, 311:660–663, 2006.

[33] N. C. Makris et al. Fish population and behavior revealed by instantaneous continental shelf-scale imaging, supporting online material. http://www.sciencemag.org/cgi/content/full/sci;311/576/660/dc1. *Science*, 311:660–663, 2006.

[34] O. A. Misund et al. Int. council explor. sea j. mar. sci., 1998.

[35] P. Ratilal et al. Long range acoustic imaging of the continental shelf environment: The acoustic clutter reconnaissance experiment 2001. *J. Acoust. Soc. Am.*, 117:1977–1998, 2005.

[36] Rusby et al. An experimental survey of a herring fishery by long-range sonar. *Mar. Biol.*, 22:271–292, 1973.

[37] S. Jagannathan et al. Ocean acoustic waveguide remote sensing (oawrs) of marine ecosystems. *submitted to Marine Ecology Progress Series*, 2008.

[38] Sherman et al. *Large Marine Ecosystems:Patterns, Processes, and Yields.* AAAS Press, Washington DC, 1990.

[39] Sherman et al. *Large Marine Ecosystems.* AAAS Press, Washington DC, 1993.

[40] Sherman et al. *Large Marine Ecosystems of the North Atlantic: Changing States and Sustainability.* Elsevier Science, Amsterdam, The Netherlands, 2002.

[41] T. R. Chen et al. Mean and variance of the forward field propagated through three-dimensional random internal waves in a continental-shelf waveguide. *J. Acoust. Soc. Am.*, 118:3560–3574, 2005.

[42] R. A. Fisher. *Statistical Methods and Scientific Inference.* Hafner, New York, 1956.

[43] United Nations Food and Fishery Resources Division Agriculture Orgnaization (FAO), Rome (IT). *Review of the state of world marine fishery resources.* FAO, Rome, Italy, 2005.

[44] P. Freon and O. A. Misund. *Dynamics of Pelagic Fish Distribution and Behavior: Effects on Fisheries and Stock Assessment, Fishing News Books.* Blackwell Publishing, Oxford, 1999.

[45] J. W. Goodman. *Statistical Optics.* John Wiley, New York, 1985.

[46] J. B. Hersey and R. H. Backus. Sound scattering by marine organisms. In M. N. Hill, editor, *The Sea, Vol. 1*, chapter 13. Interscience Publications, New York, 1962.

[47] John K. Horne. Acoustic approaches to remote species identification. *Fisheries Oceanography*, 9:356–371, 2000.

[48] I. Huse and E. Onea. Tilt angle distribution and swimming speed of overwintering norwegian spring spawning herring. *ICES J. Mar. Sci.*, 53:863–873, 1996.

[49] et al. I.D. Richardson, D.H. Cushing. Echo sounding experiments in the barents sea. *Fishery Investigations*, 22:55, 1959.

[50] J.D. Issacs and R.A. Schwatzlose. Migrant sound scatterers: Interaction with the sea flor. *Science*, pages 1810–1813, 150.

[51] F. B. Jensen, W. A. Kuperman, M. B. Porter, and H. Schmidt. *Computational Ocean Acoustics.* American Institute of Physics, New York, 1994.

[52] S. M. Kay. *Fundamentals of Statistical signal Processing: Estimation Theory*, volume 1. Prentice-Hall, Upper Saddle River, 1993.

[53] K. Kimura. On the detection of fish-groups by an acoustic method. *J. Imp. Fish. Inst., Tokyo*, 24:41–45, 1929.

[54] L. E. Kinsler, A. R. Frey, A. B. Coppens, and J. V. Sanders. *Fundamentals of acoustics.* John Wiley, New York, 1982.

[55] Y. Lai. Massachusetts institute of technology, 2004.

[56] W. C. Leggett. Annu. rev. ecol. syst., 1977.

[57] R. H. Love. Dorsal-aspect target strength of an individual fish. *J. Acoust. Soc. Am.*, 49:816–823, 1971.

[58] R. H. Love. A comparison of volume scattering strength data with model calculations based on quasisynoptically collected fishery data. *J. Acoust. Soc. Am.*, 94:2255–2268, 1993.

[59] N. C. Makris. A foundation fo logarithmic measures of fluctuating intensity in pattern recognition. *Opt. Lett.*, 20:2012, 1995.

[60] N. C. Makris. The effect of saturated tranmission scintillation on ocean acoustic intensity measurements. *J. Acoust. Soc. Am.*, 100:769–783, 1996.

[61] N. C. Makris, L. Z. Avelino, and R. Menis. Deterministic reveberation from ocean ridges. *J. Acoust. Soc. Am.*, 97:3547–3574, 1995.

[62] N. C. Makris and C. S. Chia. The bi-azimuthal scattering distribution of an abyssal hill. *J. Acoust. Soc. Am.*, 106:2491–2512, 1999.

[63] N. C. Makris and P. Ratilal. Validity of the sonar equation and babinet's principle for object scattering in a shallow water waveguide. *J. Acoust. Soc. Am.*, 106:2158, 1999.

[64] N. C. Makris and P. Ratilal. A unified model for reverberation and submerged object scattering in a stratified ocean waveguide. *J. Acoust. Soc. Am.*, 109:909–941, 2001.

[65] N.C. Makris, Office of Naval Research Initial Report: Geological Clutter Acoustics Experiment, April 27 to May 5, 2001.

[66] N.C. Makris, Office of Naval Research Initial Report: Main Acoustics Experiment, April 24 to May 24, 2003.

[67] J. R. Marshall and R. P. Chapman. Reverberation from a deep scattering layer measured with explosive sound sources. *J. Acoust. Soc. Am.*, 36:164–167, 1964.

[68] N. B. Marshall. Bathypelagic fishes as sound scatterers in the ocean. *J. Mar. Res.*, 10:1–17, 1951.

[69] H. Medwin and C. Clay. *Fundamentals of Acoustical Oceanography.* Academic Press, Boston, 1998.

[70] O. A. Misund. Underwater acoustics in marine fisheries and fisheries research. *Fish. Biol. Fish.*, 7:1–34, 1997.

[71] R.B. Mitson and R.J. Wood. An automatic method of counting fish echos. *J. Cons. Int. Explor. Mer*, 26:282–91, 1962.

[72] R.A. Myers and B. Worm. Rapid worldwide depletion of predatory fish communities. *Nature*, 423:280–283, 2003.

[73] R. Nero. personal communication, 2002.

[74] R. Nero and R. Love. Estimation of low frequency scattering from fish schools on the continental shelf off new jersey. *Naval Research Laboratory: Acoustic Simulation, Measurements, and Tactics Branch. Stennis Space Center, MS: NRL/MR/7180-03-8723*, pages 1–10, November 10,2003.

[75] R. Nero and C. H. Thompson. Fish scattering during boundary characterization 2001. *Proceedings of Geoclutter and Boundary Characterization 2001, Acoustic Interaction with the Seabed, Workshop held at DREA, Canada 2–3 October, 2001, Defence R. and D. Canada, Technical Memorandum, DREA TM 2001–185*, pages 39–42, October 2001.

[76] R.W. Nero and M.E. Huster. Low-frequency acoustic imaging of pacific salmnon on the high seas. *Can. J. Fish. Aquat. Sci.*, 53:2513–2523, 1996.

[77] C. B. Officer. *Introduction to the Theory of Sound Transmission.* McGraw-Hill, New York, 1958.

[78] T. J. Pitcher, 2001.

[79] T. J. Pitcher and J. Parrish. *The Behavior of Teleost Fishes.* Chapman and Hall, London, 1993.

[80] MIT Press. Mit article: Can we save our oceans?, Accessed 26 Feb, http://web.mit.edu/12.000/www/m2011/finalpresentation/.

[81] R. W. Raitt. Sound scatterers in the sea. *J. Mar. Res.*, 7:393–409, 1948.

[82] P. Ratilal. *Remote Sensing of Submerged Objects and Geomorphology in Continental Shelf Waters with Acoustic Waveguide Scattering.* PhD thesis, Massachusetts Institute of Technology, 2002.

[83] P. Ratilal and N.C. Makris. Mean and covariance of the forward field propagated through a stratified ocean waveguide with three-dimensional random inhomogeneities. *J. Acoust. Soc. Am.*, 118:3532–3559, 2005.

[84] G. A. Rose. Cod spawning on a migration highway in the north-west atlantic. *Nature*, 366:458, 1993.

[85] C.H. Thompson R.W. Nero and J.M. Jech. In-situ acoustic estimates of the swimbladder volume of atlantic herring. *ICES Journal of Marine Science*, 61:323–337, 2004.

[86] M. Scherbino and M.D. Truskanov. Determination of fish concentration by means of acoustic apparatus. *ICES CM 1966/F:3*, page 6, 1966.

[87] NOAA/National Marine Fisheries Service. Resource survey reports.http://www.nmfs.noaa.gov, 1999-2007.

[88] W. Siebert. *Circuits, signals and systems.* The MIT Press, Cambridge, Massachusetts, 1986.

[89] J. Simmonds and D. MacLennan. *Fisheries Acoustics: Theory and Practice.* Blackwell Science Ltd., Oxford UK, 2005.

[90] O.R. Smith, 1947.

[91] O. Sund. Echo sounding in fishery research. *Nature*, 135:953, 1935.

[92] BBN Technologies. The passive acoustic reflector. New London, Conneticut.

[93] A.L. Tester, 1943.

[94] D.S. Tungate. Echo-sounder surveys in the autumn of 1956. *Fisheries Investigations, Series 2*, 12:3–17, 1958.

[95] R. J. Urick. *Principles of Underwater Sound.* McGraw Hill, New York, 1983.

[96] D. Weston. Sound propagation in the presence of bladder fish. In V. M. Alberts, editor, *Underwater Acoustics, Vol. 2*, pages 55–88. Plenum Press, New York, 1967.

[97] D. Weston and J. Revie. Fish echoes on a long-range sonar display. *J. Sound Vib.*, 17:105–112, 1971.